

**TAILORING CELLULOSE NANOCRYSTAL,  
POLYMER AND SURFACTANT INTERACTIONS  
FOR GELS, EMULSIONS, AND FOAMS**

**TAILORING CELLULOSE NANOCRYSTAL,  
POLYMER AND SURFACTANT INTERACTIONS  
FOR GELS, EMULSIONS, AND FOAMS**

A Thesis

Submitted to the School of Graduate Studies

in Partial Fulfillment of the Requirements

for the Degree

Doctor of Philosophy

McMaster University

© Copyright by Zhen Hu, January 2015

DOCTOR OF PHILOSOPHY (2015)

(Chemical Engineering)

McMaster University

Hamilton, Ontario

TITLE: Tailoring Cellulose Nanocrystal, Polymer and  
Surfactant Interactions for Gels, Emulsions, and Foams

AUTHOR: Zhen Hu

B.Eng. (Tianjin University)

M.A.Sc (McMaster University)

SUPERVISORS: Professor Robert H. Pelton

Professor Emily D. Cranston

NUMBER OF PAGES: ix, 141

## Abstract

This thesis describes the investigation of the properties of cellulose nanocrystals (CNCs) in water and at interfaces in the presence of different water-soluble polymers and surfactants. The potential of producing hydrogels, emulsions, and foams using both CNCs and surfactants and polymers is extensively explored herein.

Interactions between CNCs and polymers were studied by measuring adsorption of polymers on CNC-coated surface in quartz crystal microbalance with dissipation monitoring (QCM-D) and surface plasmon resonance (SPR) instruments. Hydroxyethyl cellulose, hydroxypropyl guar, and locust bean gum adsorbed onto CNC-coated surfaces, whereas dextran did not adsorb. Gelation of CNC dilute dispersions was found for the samples added with adsorbing polymers, whereas the introduction of non-adsorbing polymers showed no such change of rheological behaviors of CNC dilute dispersions. The further addition of negative surfactant SDS or non-ionic surfactant Triton X-100 disrupted the gels whereas cationic surfactant CTAB did not. These behaviors illustrate the complexities associated with including CNC dispersions in formulated water-based products where polymers and surfactants are commonly used as well.

The adsorption of cationic surfactants on CNC particle surfaces and the associated change of CNC hydrophobicity were investigated. Surfactant-modified CNCs were then employed as emulsifying agents to determine the effects of stabilizing oil-water interface with CNCs after surfactant addition. Emulsion stability was substantially enhanced with the introduction of surfactants. Based on the chemistry of cationic surfactants, and the extent CNC surface hydrophobicity increases after surfactant binding, either oil-in-water or water-in-oil emulsions were successfully produced. This *in situ* surfactant adsorption method thus offers a simple way of modifying surface hydrophobicity of CNCs and allows fine tuning of CNC-based emulsion properties.

Adsorbing polymers were used together with CNCs to prepare stable emulsions. The introduction of polymers facilitated the production of emulsion droplets with enhanced stability and smaller diameters. Both polymer-coated CNCs and the extra polymers partitioned at the interface and worked as the emulsifiers in a synergistic manner, leading to a reduction in CNC coverage on the emulsion droplet surfaces. Furthermore, reversible thermogelation of the emulsion was obtained when thermosensitive polymers were added. No noticeable emulsion coalescence occurred after multiple cycles of heating and cooling treatments of the emulsion gels. Freeze-drying and air-drying of these emulsion gels produced oil powders containing oil content as high as 94 wt. %.

Finally, highly stable wet foams were successfully produced using CNCs and the water-soluble polymer, methyl cellulose. The effect of CNC and methyl cellulose concentration on the stability of air-water interfaces was elucidated. Both foamability and foam stability were greatly improved by adding CNCs to methyl cellulose solutions. The CNC particles helped to retain

fluid in the films and plateau borders between bubbles, increasing bulk viscosity, and impeding water drainage. We also demonstrated that adding various monomers to CNCs- methyl cellulose wet foams did not lead to noticeable foam breaking. The successful production of macroporous structures with tailored chemistry and properties was achieved by subsequent polymerization of the monomers added to the foam.

## Acknowledgements

First of all, I would like to express my deep appreciation for my supervisors, Dr. Robert H. Pelton and Dr. Emily D. Cranston, for their kind guidance and constant support through the years. Their great motivation and encouragement inspired me to not only try out new ideas but also dig into the fundamental scientific questions behind every project I worked on during this long journey of PhD here in McMaster. I am truly grateful for all the opportunities and challenges I had in both Pelton lab and Cranston lab.

I would also like to thank my advisory committee for their instruction, suggestions and discussions. I would like to acknowledge Dr. John D. Brennan and Dr. Alex Adronov for their very insightful thoughts and guidance in many aspects of this work, especially at the early stage of this PhD work. Dr. Jose Moran-Mirabal and Dr. Todd Hoare are also acknowledged for allowing me to use their instruments. Dr. Glynis de Silveira, Ms. Marcia Reid and Ms. Marine Timeleck are thanked for SEM, TEM and confocal microscopy support.

I also would also like to acknowledge all the current and previous group members from both Dr. Pelton and Dr. Cranston groups for their encouragement and support. The valuable discussion and instrument training from Dr. Zuohe Wang, Dr. Yuguo Cui, Dr. Jingyun Wang, Dr. Songtao Yang and Dr. Tiffany Abitbol are greatly appreciated. Last but not least, I am also thankful for several excellent undergraduate students, Robin Ng, Jaclyn Obermeyer, Sarah Ballinger, Tyler Patten and Richard Xu, for their hard work and contributions.

I would like to thank our lab manager Mr. Doug Keller, administrator Ms. Sally Watson, Ms. Kathy Goodram, Ms. Lynn Falkiner, Ms. Cathie Roberts, Mr. Paul Gatt, Ms. Justyna Derkach and Mr. Dan Wright for their administrative assistant and technical support.

I acknowledge NSERC for research funding support through CREATE Biointerfaces training program grant. Without the funding, none of this work would be possible.

Very special thanks are given to my family members, my friends, and my roommates. Without their relentless support and constant encouragement, this graduate school experience would be much harder.

# Table of Contents

|   |      |
|---|------|
| Abstract .....  | iii  |
| Acknowledgements .....  | v    |
| Abbreviations .....   | viii |
| Chapter 1 Introduction .....  | 1    |
| 1.1 Literature Review .....   | 1    |
| 1.1.1 Cellulose .....   | 1    |
| 1.1.2 Cellulose Derivatization .....  | 2    |
| 1.1.3 Nanocellulose .....   | 4    |
| 1.1.3.1 Microfibrillated Cellulose .....  | 4    |
| 1.1.3.2 Bacterial Nanocellulose .....   | 6    |
| 1.1.3.3 Cellulose Nanocrystals .....  | 6    |
| 1.1.4 Hydrogels .....   | 9    |
| 1.1.4.1 Nanocomposite Hydrogels .....   | 9    |
| 1.1.4.2 CNC Physical Hydrogels .....  | 10   |
| 1.1.4.3 CNC Chemical Hydrogels .....  | 11   |
| .....   | 12   |
| 1.1.5 Pickering Emulsions .....   | 12   |
| 1.1.6 CNC Pickering Emulsions .....   | 17   |
| 1.1.7 CNC Wet Foams .....   | 18   |
| 1.1.8 CNC Solid Foams .....   | 21   |
| 1.2 Objectives .....  | 22   |
| 1.3 Thesis outline .....  | 23   |
| References .....  | 25   |
| Chapter 2 Tuning Cellulose Nanocrystal Gelation with Polysaccharides and Surfactants .....                                      | 38   |
| Appendix: Supporting Information for Chapter 2 .....  | 48   |
| Chapter 3 Surfactant-enhanced Cellulose Nanocrystal Pickering Emulsions .....   | 69   |
| Appendix: Supporting Information for Chapter 3 .....  | 80   |
| Chapter 4 Synergistic Stabilization of Emulsions and Emulsion Gels with Water-soluble Polymers and Cellulose Nanocrystals ..... | 83   |
| Abstract .....  | 84   |

|   |     |
|---|-----|
| 4.1 Introduction .....  | 84  |
| 4.2 Experimental Section .....  | 86  |
| 4.3 Results .....   | 89  |
| 4.4 Discussion .....  | 101 |
| 4.5 Conclusions .....   | 103 |
| References .....  | 104 |
| Appendix: Supporting Information for Chapter 4.....   | 107 |
| Chapter 5 Preparation and Templating Properties of Stable Foams of Cellulose Nanocrystals and Methyl Cellulose..... | 113 |
| Abstract .....  | 114 |
| 5.1 Introduction .....  | 114 |
| 5.2 Experimental Section .....  | 116 |
| 5.3 Results .....   | 119 |
| 5.4 Discussion .....  | 128 |
| 5.5 Conclusions .....   | 131 |
| References .....  | 132 |
| Appendix: Supporting Information for Chapter 5.....   | 135 |
| Chapter 6 Concluding Remarks .....  | 140 |

## Abbreviations

|       |   |
|-------|---|
| AM    | acrylamide  |
| AIBN  | azobisisobutyronitrile                                  |
| CLSM  | confocal laser scanning microscopy                      |
| CNCs  | cellulose nanocrystals                                  |
| CTAB  | cetyl trimethylammonium bromide                         |
| DEX   | dextran   |
| DLS   | dynamic light scattering                                |
| DMAB  | didecyldimethylammonium bromide                         |
| DS    | degree of substitution                                  |
| DTAF  | dichlorotriazinyl aminofluorescein                      |
| HEC   | hydroxyethyl cellulose                                  |
| HEMA  | hydroxyethylmethacrylate                                |
| HEPES | 4-(2-hydroxyethyl)-1-piperazineethanesulfonic acid      |
| HPG   | hydroxypropyl guar                                      |
| LBG   | locust bean gum   |
| MBA   | N,N'-methylenebisacrylamide                             |
| MC    | methyl cellulose  |
| MS    | molar substitution                                      |
| PEGDA | polyethylene glycol diacrylate                          |
| POM   | polarized optical microscopy                            |
| QCM-D | quartz crystal microbalance with dissipation monitoring |
| SDS   | sodium dodecyl sulfate                                  |
| SEM   | scanning electron microscopy                            |

|              |   |
|--------------|---|
| SPR          | surface plasmon resonance                   |
| TEM          | transmission electron microscopy            |
| TEMPO        | (2,2,6,6-tetramethylpiperidin-1-yl)oxidanyl |
| Triton X-100 | polyoxyethylene octyl phenyl ether          |

## Chapter 1 Introduction

### 1.1 Literature Review

#### 1.1.1 Cellulose

Cellulose is the most abundant natural polymer on earth as it constitutes about half of all biomass, with an annual production of estimated to be  $10^{11}$  tons per year.<sup>1</sup> It is isolated mainly from higher plants but also from bacteria (e.g. *Acetobacter xylinum*), animals (e.g. tunicate), and marine plants (e.g. algae). Cellulose is defined as long polymer chains of cellobiose, which consists of  $\beta$ -D-anhydro-glucopyranose units (AGU units) covalently bonded together by the linkage between the C1 anomeric carbon and the C4 oxygen atom.<sup>2-4</sup> The chain is directionally asymmetric, with a hemiacetal unit (the reducing end) on one end and a pendant hydroxyl group (the nominal nonreducing end) on the other terminus (Figure 1.1). The chair conformation of the sugar units and the equatorial positioning of the hydroxyl groups promote the formation of hydrogen bonds within the chains. The intramolecular and intermolecular hydrogen bonds and van der Waals interactions give rise to a highly crystalline extended structure that is entirely insoluble in water and most other common solvents.<sup>5</sup>

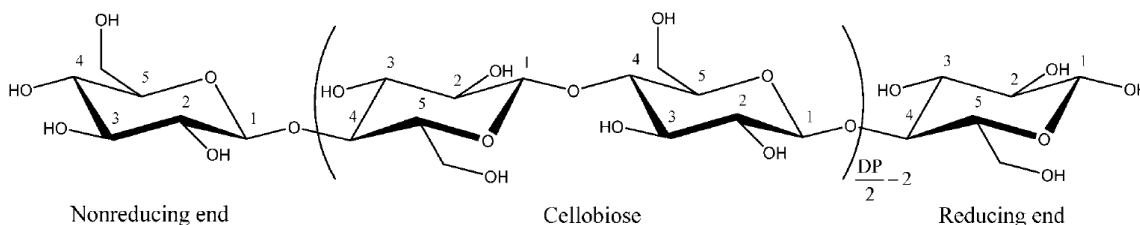


Figure 1.1. The chemical structure of cellulose. The repeat unit is called “cellobiose” which is composed of two  $\beta$  (1 $\rightarrow$ 4) linked D-glucose units. (Figure reproduced from Ref.<sup>4</sup>)

In nature, cellulose does not occur as an isolated individual molecule, but it is found as fibrous units assembled from approximately 36 individual cellulose molecules.<sup>4</sup> These fibrous units, known as elementary fibrils, pack into larger units called microfibrils that display cross dimensions ranging from 2 to 20 nm, depending on the source of celluloses. These microfibrils are then in turn assembled into the cellulose fibers. The amorphous regions are distributed as chain dislocations on segments along the elementary fibril where the microfibrils are distorted by internal strain in the fiber and proceed to tilt and twist.<sup>6</sup> The ordered regions, on the other hand, are crystalline as a result of tight packing of cellulose chains. The hydrogen-bonding network and molecular orientation in cellulose can vary widely, which can give rise to cellulose polymorphs or allomorphs. Six interconvertible crystalline allomorphs of cellulose, namely, I, II, III<sub>I</sub>, III<sub>II</sub>, IV<sub>I</sub>, and IV<sub>II</sub>, have been identified.<sup>7</sup> The crystal structure of native celluloses is cellulose

I, whereas non-native celluloses (i.e. regenerated or derivatized) have different H-bonding patterns and the potential for anti-parallel chain orientations such as II, III<sub>II</sub> and IV<sub>II</sub>. The relative amounts of crystalline cellulose and amorphous cellulose are origin dependent. Cotton is almost entirely composed of pure cellulose (~95%) whereas the cellulose in woody plants is closely associated with lignin and hemicelluloses (i.e. polysaccharides containing other sugars and sugar derivatives) and only makes up ~42% of the cell wall.<sup>3</sup>

Cellulose has been traditionally used in the form of wood and plant fibers as an energy source, building materials, and clothing.<sup>2</sup> To produce novel types of cellulose-based materials, the controlled physical and/or chemical modification of the cellulose structure is necessary. Therefore, cellulose esters and cellulose ethers as well as cellulose regenerates were developed.<sup>3,8</sup> The large-scale industrial production of cellulose esters and ethers facilitated application of cellulose in coatings, films, membranes, pharmaceuticals, and foodstuffs. The reaction of cellulose with nitric acid to form cellulose nitrate was carried out by the Hyatt Manufacturing Company in 1870 to produce celluloid, the very first thermoplastic polymer material.<sup>3</sup> Regenerated cellulose filaments were fabricated by spinning a solution of cellulose in a mixture of copper hydroxide and aqueous ammonia.<sup>3</sup> Dissolving pulp with aqueous sodium hydroxide and carbon disulfide produced a solution of cellulose xanthate that could be used to produce the rayon fiber and cellophane.<sup>3,9</sup>

### 1.1.2 Cellulose Derivatization

Cellulose is amenable to chemical derivatization due to the presence of three hydroxyl groups in each glucose residue.<sup>9</sup> The chemical modification of cellulose and its derivatives has been performed under both homogeneous and heterogeneous conditions.<sup>7-8</sup> Homogeneous derivatization involves dissolution or, at least, by the swelling of cellulose in the reaction medium and modification of the entire cellulose chains. This remains extremely challenging as a result of the limited solubility of cellulose in common solvents. Ionic liquids as the “green” reaction media for homogeneous derivatization of cellulose have drawn much attention in recent years.<sup>10</sup> Heterogeneous methods, on the other hand, refer to situations where cellulose is not dissolved in the reaction medium so the reaction occurs at the interface between the solid and liquid phase giving rise to only surface modification.<sup>9</sup> They are the actually applied ones in the industrial production of most commercial cellulose derivatives. The reactivity of the three hydroxyl groups under heterogeneous methods can be affected by their inherent chemical reactivity as well as the steric effects due to the supramolecular structure of cellulose. For example, it has been found that the primary alcohol group can react ten times faster than the other two secondary alcohol groups for esterification.

The industrial history of the chemical modification of cellulose to impart new properties can be tracked back to 1870 with the production of the first thermoplastic cellulose-based material “celluloid”, which involves the plasticization of cellulose nitrate with camphor. Cellulose nitrate was formed by nitrating cellulose through exposure to nitric acid in the presence of sulfuric acid,

phosphoric acid or acetic acid.<sup>9</sup> There are other commercially important cellulose esters such as cellulose acetate, cellulose acetate propionate, and cellulose acetate butyrate.<sup>2, 11</sup> These cellulose esters have long played an important role in applications such as coatings, biodegradable plastics, composites and laminates, optical films, and membranes and related separation media. The use of etherification reaction provides another useful chemical modification of cellulose. Some commercially important cellulose ethers are hydroxyalkyl celluloses, methyl cellulose, and carboxymethyl cellulose. These cellulose ethers are water-soluble polymers and they have played an important role in a host of applications, from construction products, ceramics and paints to foods, cosmetics and pharmaceuticals.

Cellulose ethers can be prepared by treating alkali cellulose with a number of various reagents including alkyl or aryl halides, alkene oxides, and unsaturated compounds activated by electron-attracting groups.<sup>11</sup> For example hydroxyethyl cellulose (HEC) and methyl cellulose (MC) can be prepared by the action of ethylene oxides and methyl chlorides, respectively, on cellulose that has been treated with alkali. Cellulose ethers can be either soluble in organic or aqueous media, but for the context of this thesis, only water-soluble cellulose ethers will be discussed.

Commercial cellulose ethers are normally graded based on the chemical nature of the substituent, the degree of substitution (DS) or molar substitution (MS), and solution viscosity.<sup>11</sup> The DS denotes the average number of alcoholic groups substituted per anhydroglucose unit, and can thus vary between 0 and 3. Since etherification reactions generate new reactive sites that are capable of chain branching, the extent of reaction or MS is used occasionally. MS is defined as the moles of reagent combined per mole of anhydroglucose. Therefore, the ratio of MS to DS is a measure of the average length of the hydroxyalkyl chain. These cellulose ethers are relatively amphiphilic as a result of chemical grafting of hydrophobic alkyl chains.

Hydroxyethyl cellulose (HEC), a non-ionic water-soluble cellulose ether, is prepared by nucleophilic ring opening of ethylene oxide, by the hydroxyl anions on the anhydroglucose ring of cellulose.<sup>11</sup> Due to good thickening, dispersing, emulsifying, film-forming, and water-retention properties, HEC has been widely used in cosmetic products, pharmaceutical preparations, polymerization processes, oil exploitation, coatings, building, food, textile, papermaking, emulsions, paints and other industrial applications.

Methylcellulose (MC) has the most straightforward chemical composition among cellulose derivatives with a partial replacement of hydroxyl groups with methoxy moieties. The balance between hydrophilic hydroxyl and hydrophobic methoxy groups determines the aqueous solubility of the polymer. If the DS is too low, sufficient hydrogen bonds remain that this MC is still insoluble, whereas MC with a high DS is hydrophobic and is also insoluble in water.<sup>12-16</sup> Therefore, the commercial products usually have an intermediate DS, ca. 1.7-2.0.

Commercial MC is a heterogeneous polymer consisting of highly substituted zones called “hydrophobic zones” and less substituted ones called “hydrophilic zones. MC exhibits lower

critical solution temperature (LCST) phase behavior in aqueous systems; at low temperature the polymer is readily soluble in water, whereas sufficiently concentrated solutions gel above the LCST. Depending on the degree of substitution, heating rate, and polymer concentration, the sol-gel transition generally resides in the range of 50-60 °C.<sup>13-14</sup> At low temperatures, the water-polymer interactions are stronger than the polymer-polymer interactions and “cagelike” water structures surrounding the hydrophobic methoxyl groups were formed, leading to MC solubilization in water. Upon heating, the MC molecules lose part of their affinity to the surrounding water and there is an entropically favored release of bound and structured water, leading to exposure of the hydrophobic regions and polymer chain association into fibrils of about 14 nm. This fibrillation is observed as a sol-gel transition with considerably increased storage modulus ( $G'$ ) values as well as an increase in turbidity. Commercial MC is sold under a variety of trade names and is used as a thickener and emulsifier in various food and cosmetic products.

### 1.1.3 Nanocellulose

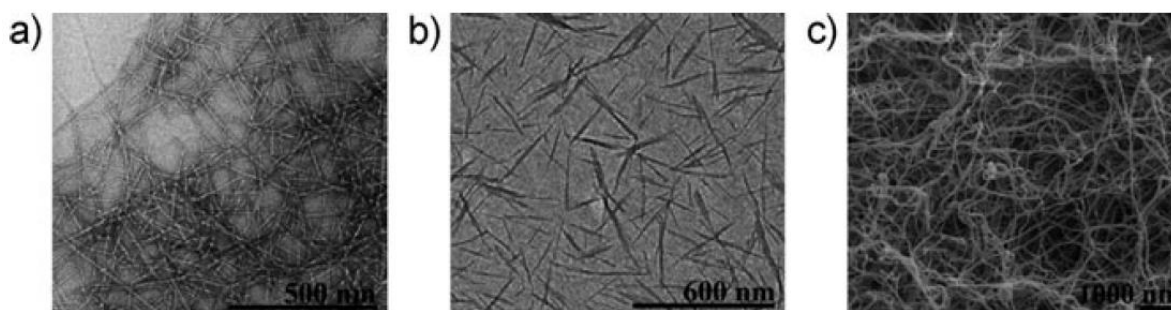
Nanocellulose is a term referring to nano-structured cellulosic materials with one dimension in the nanometer range.<sup>17</sup> Currently, the isolation, characterization, and search for applications of novel forms of nanocellulose are generating much activity. Nanocellulose can be extracted from forest and agricultural residues using top-down methods involving enzymatic/chemical/physical strategies or produced via bottom-up routes using certain types of bacteria. Based on their sources, dimensions, function, and preparation methods, nanocelluloses may be classified into three main subcategories of microfibrillated cellulose (MFC), cellulose nanocrystals (CNCs), and bacterial nanocellulose (BNC) (Table 1.1). CNCs have also been referred to in the literature as cellulose nanowhiskers or nanocrystalline cellulose (NCC), and MFC is also sometimes called nanofibrillated cellulose (NFC) or cellulose nanofibrils (CNF). Typical structures of these cellulose types on the nanoscale can be seen in the transmission electron micrographs in Figure 1.2.

#### 1.1.3.1 Microfibrillated Cellulose

Microfibrillated cellulose may be isolated from the cellulosic fibers using mechanical shearing forces to rip the larger fibers apart into nanofibers. Produced through mechanically induced destructuring strategy, MFC is composed of both crystalline and amorphous regions. Different mechanical treatment procedures have been reported to prepare MFC. They typically involve high-pressure homogenization and/or grinding. However, this process is responsible for the high energy consumption over 25000 kWh per ton in the production of MFC as a result of the required multiple passes through the homogenizers.<sup>18-19</sup> Pre-treatments are therefore used to address this problem. Different pre-treatments such as mechanical cutting, acid hydrolysis, enzymatic degradation, and the introduction of charged groups through carboxymethylation or 2,2,6,6-tetramethylpiperidine-1-oxyl (TEMPO)-mediated oxidation have been proposed to facilitate this homogenization process and thus decrease the energy consumption.<sup>20-24</sup>

Table 1.1. The family of nanocellulose materials. (Figure reproduced from Ref.<sup>17</sup>)

| Type of nanocellulose            | Synonyms   | Typical sources   | Formation and average size  |
|----------------------------------|--|---|---|
| microfibrillated cellulose (MFC) | nanofibrils, microfibrils, microfibrillated cellulose                                    | wood, sugar beet, potato tuber, hemp, flax  | high pressure homogenizer<br>diameter: 5-60 nm<br>length: several micrometers   |
| cellulose nanocrystals (CNCs),   | nanocrystalline cellulose (NCC), crystallites, whiskers, rodlike cellulose microcrystals | wood, cotton, hemp, flax, wheat straw, mulberry bark, ramie, Avicel, tunicin, algae, bacteria | acid hydrolysis<br>diameter: 5-70 nm<br>length: 100-250 nm (from plant celluloses); 100 nm to several micrometers (from celluloses of tunicates, algae, bacteria) |
| bacterial nanocellulose (BNC)    | bacterial cellulose, microbial cellulose, biocellulose                                   | low-molecular-weight sugars and alcohols  | bacterial synthesis<br>diameter: 20-100 nm; different types of nanofiber networks   |

Figure 1.2. Transmission electron micrographs of a) MFC<sup>23</sup> and b) CNCs;<sup>25</sup> c) scanning electron micrograph of BNC.<sup>26</sup> (Figure reproduced from Ref.<sup>17</sup>)

Typical lateral dimensions of MFC are 20-60 nm and longitudinal dimension is in a wide range, typically several micrometers. Therefore, each MFC fibril is composed of 10-50 microfibrils if we consider that the microfibrils have a 2-10-nm-thick fibrous cellulose structure.<sup>27</sup> In addition, the aspect ratio (length/diameter) of MFC is very high, which endows it with a low percolation threshold and a very good ability to form a rigid network. MFC aqueous suspensions are pseudo-plastic and display the shear-thinning property of gels or fluids that are viscous (thick) under normal conditions, but flow and become less viscous (thin) when sheared.<sup>21, 27</sup> Due to its rheological behavior, MFC is being investigated as rheological modifiers that possess potential applications in food, cosmetic, pharmaceutical, and oil recovery industries. The shear-thinning behavior is of importance in industrial processing and particularly in coating applications.

Due to the good film-forming properties of MFC, Berglund and coworkers formed cellulose nanopapers by dewatering MFC through a vacuum-filtration method.<sup>28</sup> The films were tough, as judged from the high strain to failure observed. Syverud *et al.* used MFC as a surface layer (0-8% of total basis weight) on base paper and observed that the strength of the paper sheets significantly increased whereas their air permeability dramatically reduced.<sup>29</sup> In addition to papermaking applications, MFC has been used as reinforcement in composite materials. It has been reported that MFC films impregnated with an epoxy resin give transparent composites with excellent thermal conductivity.<sup>30</sup> Furthermore, efforts are being made to use MFC-reinforced starch foams for packaging applications as a replacement for polystyrene-based foams.<sup>31</sup> Compared to conventional wood-based pulp fibers, the nanosized fibrils enable reinforcement of the thin cell walls in the starch foam. By using various freeze-drying techniques, MFC-based aerogels were successfully produced and used as porous templates.<sup>32</sup> As a result of its non-toxicity and tunable hydrophilicity, MFC has been used in emulsions and drug tablets.<sup>33</sup>

### **1.1.3.2 Bacterial Nanocellulose**

The biosynthesis of cellulose takes place not only in plants, but also in bacteria, with *Acetobacter* spp. strains being one of the most common. Bacterial nanocellulose, also called bacterial cellulose, microbial cellulose, or biocellulose, is produced by the respective bacteria strains in response to specific environmental conditions.<sup>34-35</sup> The aerobic bacteria, such as acetic acid bacteria of the genus *Gluconacetobacter*, are cultivated in common aqueous nutrient media with low-molecular weight carbon and nitrogen sources, forming highly porous nanofiber network structures (fiber diameter: 20-100 nm) with culture medium filling the voids. Unlike MFC and CNCs isolated from cellulose sources, BNC is excreted by bacteria as exopolysaccharide through biotechnological assembly processes from nutrient media. The molar mass, molar mass distribution, and the supramolecular structure of BNC can be controlled by selecting the substrates, cultivation conditions, various additives, and bacterial strain. Although identical to cellulose from plant origins in terms of molecular formula, BNC is very pure cellulose with a high degree of polymerization (DP values of 2000-8000), high crystallinity (60-90%), and good mechanical properties.<sup>36-38</sup> As a result of the nanostructured network and morphological similarities with collagen, BNC has been extensively tested for cell immobilization, cell migration, production of extracellular matrices, and other medical applications.<sup>17</sup> Previous *in vitro* and *in vivo* evaluation showed that the BNC implants elicited no foreign-body reaction. In addition, fibrosis, capsule formation, or giant cells were not detected around the implants, and connective tissue was nicely integrated with the BNC implants. BNC-based membranes were also functionalized with platinum nanoparticles and multiwalled carbon nanotubes to produce electrocatalytic and electrically conductive materials, respectively.<sup>39-40</sup>

### **1.1.3.3 Cellulose Nanocrystals**

The dislocations or defects in native cellulose disrupt the crystalline ordering of the microfibril chains, leading to formation of disorder (i.e. amorphous) regions. Cellulose nanocrystals (CNCs),

rigid rod-like particles with widths of a few nanometers and lengths between 100 nm and several micrometers, are produced by the removal of amorphous sections of a purified cellulose source by acid hydrolysis, often followed by ultrasonic treatment (Figure 1.3).<sup>4</sup> This procedure was first developed in 1949 by Rånby in Sweden, and later modified in Canada.<sup>41-43</sup> Dimensions of the liberated cellulose nanocrystals depend strongly on the hydrolysis conditions, cellulose sources and their crystallinity. Cotton and wood yield a narrow distribution of highly crystalline (90% crystallinity) rod-like particles (width: 5-10 nm, length: 100-300 nm), whereas other sources like bacteria, algae, and tunicin produce nanocrystals with larger size distributions and dimensions comparable to those of MFC (width: 5-60 nm, length: 100 nm to several micrometers).<sup>44-50</sup> Figure 1.4 shows the dimensions of CNCs from different cellulose sources.

The surface functionality of CNCs depends on the mineral acid used in the hydrolysis. Particles are uncharged and colloidally unstable if prepared with hydrochloric acid (HCl), whereas sulfuric acid (H<sub>2</sub>SO<sub>4</sub>) hydrolysis results in more negatively charged and electrostatically stabilized particles due to the sulfate ester groups introduced onto the surface of the crystallites during reaction.<sup>51-52</sup> Phosphoric acid hydrolysis generates crystals with good dispersibility in polar solvents as a result of surface phosphate groups.<sup>53</sup> Interestingly, the difference in surface functionalization also causes the phosphorylated CNCs to display a much higher thermal stability than the sulfated CNCs. Ammonium persulfate oxidation can also produce CNCs with similar dimensions and crystallinity, but with carboxylic acid groups on the surface instead of sulfate ester groups.<sup>54</sup> The dimensions and surface charge densities of CNCs were also found to depend on the duration of the hydrolysis, whereby a longer reaction time produced shorter crystals with greater surface charge densities. The commonly employed recipe in our lab uses temperature of 45 °C, 64 wt. % sulfuric acid, 45 minute reaction times and acid to cellulose ratios of 17.5 mL/g.<sup>48, 55</sup>

Similar to other colloidally stable dispersions of rod-like particles, CNC suspensions of sufficiently high concentrations undergo spontaneous phase separation into a lower anisotropic phase and an upper isotropic phase.<sup>56-57</sup> Within the anisotropic phase, the rod-like CNCs form a chiral nematic (cholesteric) liquid crystal with the alignment of CNCs in each layer slightly rotated with respect to adjacent layers.<sup>58</sup> A left-handed, cholesteric pitch can be observed between crossed polarizers, where the spacing between lines within the characteristic fingerprint texture gives half the pitch. The isotropic-to-anisotropic phase transition which occurs upon increasing the concentration is attributed to higher packing entropy compared with the disordered phase as a result of favorably excluded volume interactions.<sup>59</sup> In the biphasic concentration range, the isotropic and chiral nematic phases are in equilibrium. As the concentration of CNCs is further increased, the whole suspension becomes liquid crystalline.<sup>51</sup> The isotropic-to-anisotropic equilibrium is sensitive to the nature and density of the charges on the surface of CNCs as well as the presence of electrolytes in the suspension.<sup>57</sup> Non-adsorbing polymers can also induce an entropic phase separation of aqueous suspensions of sulfated CNCs to an isotropic phase.<sup>60-61</sup>

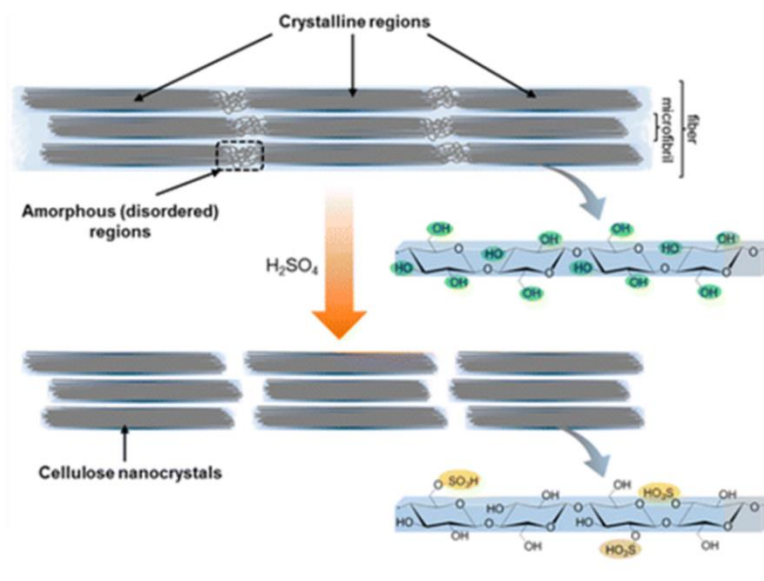


Figure 1.3. Schematic diagram illustrating the sulfuric acid hydrolysis of cellulose to produce sulfated CNCs. (Figure reproduced from Ref.<sup>62</sup>)

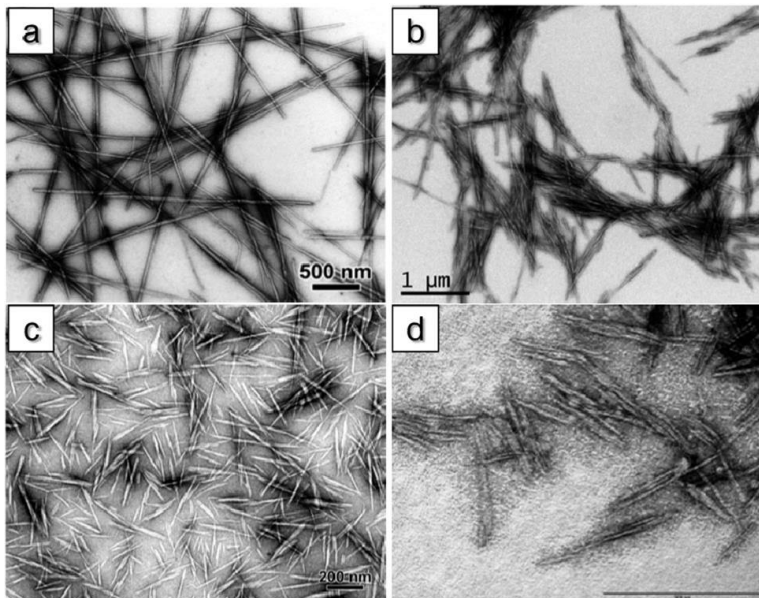


Figure 1.4. Transmission electron micrographs of dried dispersion of CNCs derived from a) tunicate,<sup>63</sup> b) bacterial,<sup>64</sup> c) ramie,<sup>65</sup> and d) sisal.<sup>47</sup> (Figure adapted from Ref.<sup>4</sup>)

Due to their appealing intrinsic properties such as nanoscale dimensions, high surface area, unique morphology, low density, and mechanical strength, CNCs have been extensively employed as reinforcing agents in nanocomposites.<sup>66</sup> Casting evaporation has been the main technique of transferring CNCs from aqueous dispersion into an organic polymer matrix. Good dispersibility of CNCs in the polymer matrix, as well as in the processing solvent, is critical for significant mechanical reinforcement.<sup>66</sup> Capadona *et al.* reported another versatile processing approach of forming a three-dimensional template through self-assembly of individualized CNCs and then backfilling the template with a polymer of choice.<sup>67</sup> Twin screw extrusion has also been used to prepare CNC-based nanocomposites in both conventional thermoplastic polymer matrices and biodegradable polymers, such as polylactic acid.<sup>68</sup>

### 1.1.4 Hydrogels

Hydrogels are usually referred to as polymer networks extensively swollen with water that exhibit no flow in the steady-state. They sometimes are found as colloidal gels in which water is the dispersion medium.<sup>69</sup> They can be good candidates for various applications ranging from biomedicine to daily chemicals, such as drug delivery systems, biosensors, and superabsorbent in diapers.<sup>70</sup> In general, polymeric hydrogels can be classified as physical and chemical hydrogels based on the nature of crosslinking.<sup>71</sup> In physical hydrogels, individual polymer chains are held together via transient interactions such as ionic interactions, hydrogen bonds, metal–ligand coordination, host–guest complexation, and hydrophobic associations.<sup>72-79</sup> Although physical gels do not possess permanent network structures and are more susceptible to shearing by mechanical forces, their dynamic features can be regarded as advantageous characteristics because they impart sensitivity and reversible gelation of the hydrogels to environmental stimuli. In contrast, chemical hydrogels consist of chains that are interconnected by permanent non-reversible bonds, which often make gels brittle and fragile and unable to withstand large deformations.<sup>80</sup>

#### 1.1.4.1 Nanocomposite Hydrogels

In general, nanocomposite hydrogels may be defined as cross-linked networks swollen with water in the presence of nanoparticles or nanostructures.<sup>81-82</sup> The cross-linking can be obtained through physical and/or chemical interactions. The nanoparticles can be used to either chemically cross-link the hydrogel as particulate cross-linker, to adsorb or attach polymer chains, or to add new functionalities to the hydrogel by simple entrapment within the hydrogel network. In addition to mechanical reinforcement, the introduction of nanoparticles to hydrogel network can also impart responsiveness to optical, thermal, barrier, magnetic, and electric stimulations, which lead to applications in optics, sensors, actuators, electronics, separation devices, and drug delivery.<sup>83</sup>

Previous studies focused on mechanical reinforcement of nanocomposite hydrogels using nanoparticles such as laponite, silica, hydroxyapatite, carbon nanotube, and superparamagnetic

iron oxide.<sup>84-88</sup> Due to the favourable properties of CNCs, such as nanoscale dimensions, high aspect ratio and Young's modulus, hydrophilicity, biocompatibility, and facile surface functionalization, a large body of recent work has focused on reinforcing hydrogels with CNCs and investigating the role of interfacial layer between CNCs and hydrogel matrix on the mechanical reinforcement.

#### ***1.1.4.2 CNC Physical Hydrogels***

The viscosity and moduli of CNC suspensions increases steeply with concentration and two critical values can be observed, namely, the overlap and the gelation concentration, which depend strongly on the aspect ratio of the nanocrystals.<sup>89-91</sup> The thickening effect provided by the presence of CNCs in aqueous dispersions is attributed to the network formation due to particle entanglements and physical crosslinking upon increasing particle concentration. These hydrogels are self-standing and anisotropic alignment of the CNCs can be confirmed using cross polarized lenses. Shear thinning is also observed for CNC suspensions as a result of the axis alignment of CNCs parallel to the flow direction. The balance of attractive forces (van der Waals forces and hydrogen bonding) and repulsive forces (electrostatics) between CNC particles can be tuned by changing the degree of protonation of the CNC surface functional groups. For example, sulfated, carboxylated and aminated CNCs can be protonated or deprotonated by changing the pH and gel formation can be fine controlled by destabilizing the colloidal suspensions, i.e., by reducing the surface charge density and thus the repulsive forces between particles.

Another common route to modify the rheological properties of CNC suspensions involves the addition of polymers.<sup>92</sup> Depending on the nature of the particle-polymer interactions, enhanced stability or flocculation of the suspensions can be observed.<sup>93-95</sup> Flocculation due to bridging by adsorption of polymers on particle surfaces or depletion by nonadsorbing polymers induces formation of viscoelastic gels. Mckee *et al.*<sup>96</sup> demonstrated a particularly facile and scalable fabrication process for tunable all-cellulose thermoresponsive gels incorporating a mixture of CNCs physically bound together by methylcellulose (Figure 1.5).

In addition, CNCs have been incorporated as fillers to reinforce polymer hydrogels with no covalent attachment to the hydrogel networks. For instance, Yang *et al.*<sup>97</sup> found that the elastic component and the capacity to dampen deformation stress was enhanced by increasing the interface between CNCs and *in situ* polymerized poly(acrylic acid) chains. Abitbol *et al.*<sup>98</sup> obtained structural reinforcement and a decrease of crystallinity for hydrogel samples by loading CNCs into polyvinyl alcohol (PVA) hydrogels through repeated freeze-thaw processing, suggesting the improved interaction between CNCs and PVA. Lin *et al.*<sup>99</sup> reported that when  $\beta$ -cyclodextrin ( $\beta$ -CD) grafted CNCs are mixed with Pluronic polymer, supramolecular hydrogels can be obtained as a result of the *in situ* host-guest inclusion interaction. Although surface modification of CNCs or polymerization of the hydrogel matrix around the CNCs was required for the successful gel formation, no permanent covalent bonds between CNCs and the polymer

networks were present to produce the nanocomposite hydrogels. Therefore, the examples described above are still defined as CNC physical hydrogels in this thesis.

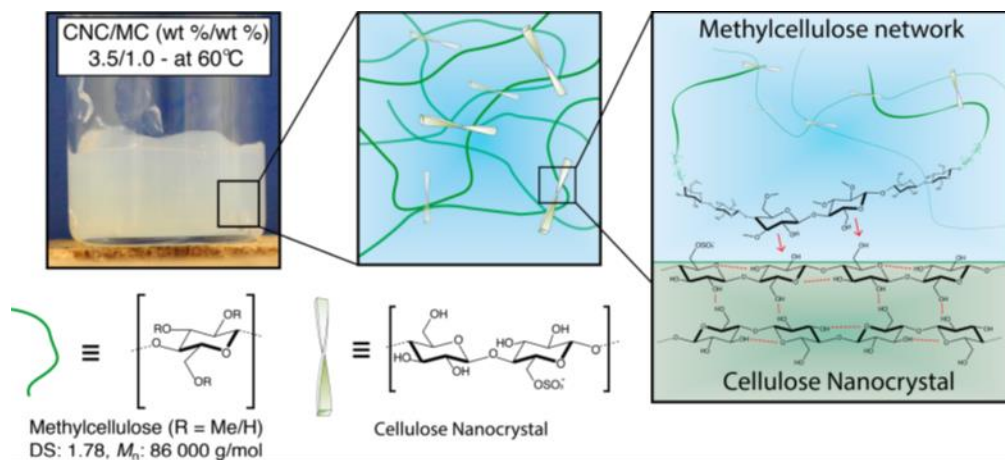


Figure 1.5. Photograph showing gelation in a cellulose nanocrystals and methylcellulose mixture at 60 °C. Also included is a schematic representation of the nanocomposite hydrogel. The suggested adsorption of MC on CNC is indicated by red arrows. (Figure adapted from Ref.<sup>96</sup>)

#### 1.1.4.3 CNC Chemical Hydrogels

In most demonstrations of nanocomposite hydrogels reinforced with CNCs, the particles are physically entrapped within the gel matrix to yield the mechanical enhancing effects. Some other works have instead used CNCs with particular surface modifications as both nanofillers and particulate cross-linker to achieve the reinforcement. Recently, Yang *et al.*<sup>100</sup> prepared a series of nanocomposite hydrogels through *in situ* grafting of poly(*N,N*-dimethylacrylamide) (PDMA) chains on CNC surfaces. The CNC–polymer interfacial interactions consist of reversible physical interactions and stable covalent bonds: the CNCs functionalized with a silane coupling agent act as particulate anchors to covalently graft PDMA, and the interpenetrated PDMA shells entangle to form reversible physical networks. The same research group also prepared cellulose nanocrystal-poly(acrylamide) (CNC-PAM) composite hydrogels with a double network combining a permanent network through chemical cross-links and a transient network by surface adsorption.<sup>101</sup> They suggested that attractive physical interactions in the network increased the fracture strength of the hydrogels via reversible adsorption–desorption processes on the CNC surface. Dash *et al.*<sup>102</sup> obtained gelatin-based hydrogels employing the reaction between aldehyde groups on the surface of oxidized CNCs and amine groups on gelatin. Similarly, Yang *et al.*<sup>103</sup> prepared injectable hydrogels based on the hydrazone bond formation between aldehyde-functionalized CNCs and hydrazide-modified polymers (Figure 1.6). The CNC nanocomposite hydrogels exhibited dimensional stability in 60 day swelling experiments and showed no significant cytotoxicity to 3T3 fibroblasts in an MTT assay, implying their potential biomedical

applications where longer term dimensional stability and enhanced mechanical strength are desirable.<sup>103</sup>

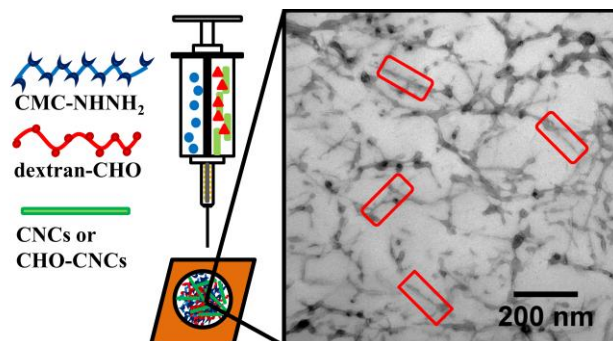


Figure 1.6. Schematic representation of injectable hydrogels reinforced with CNCs, prepared using a double-barrel syringe. The cross-linking hydrogel components include hydrazide-functionalized carboxymethyl cellulose, aldehyde-functionalized dextran, and either unmodified CNCs or aldehyde-modified CNCs. Transmission electron micrograph of CNC-reinforced hydrogel with 0.25 wt % loading implies the incorporation of CNCs in the hydrogel network, where individual CNC crosslink points are highlighted by the red boxes. (Figure reproduced from Ref. <sup>103</sup>)

### 1.1.5 Pickering Emulsions

An emulsion is a mixture of immiscible liquids, usually oil and water, with one liquid dispersed in the continuous liquid phase. It is well known that low molar mass surfactants and surface-active polymers are commonly employed as emulsifiers in the preparation of emulsions. Colloidal particles with intermediate wettability can function in similar ways to surfactants by adsorbing at oil-water interfaces and stabilizing emulsion droplets.<sup>104-108</sup> So-called Pickering emulsions are found in many formulated products such as food, pharmaceutical, household cleaning, and personal care products.

While traditional emulsions are stabilized by amphiphilic surfactant molecules, more recently Pickering emulsions have garnered significant interest. Inorganic or petrochemical-based particles of silica, clay, calcium carbonate, hematite, polystyrene,  $\text{Fe}_3\text{O}_4$  particles, and microgels, which range in size from nanometers to micrometers, can all act as emulsifiers.<sup>109-115</sup> Interestingly, small changes in the chemical composition of the liquids and/or particles, salt concentration, pH, temperature, and particle shape, lead to major changes in emulsion properties and rich physicochemical phenomena.<sup>116-120</sup>

The type and stability of emulsions stabilized by surfactants is dominated by the hydrophile-lipophile balance (HLB), however, colloidal particles in Pickering emulsions do not have to be

amphiphilic to adsorb at the oil-water interface.<sup>106, 120</sup> Instead, particles with partial wettability in both immiscible liquid phases will partition preferentially at the interface and can be extremely stable to coalescence depending on the particle size, shape, concentration, degree of particle aggregation and wettability.<sup>105, 120-121</sup> Additionally, while conventional surfactants are typically used to lower oil-water interfacial tension, Pickering emulsions with micrometer sized droplets are often formed with a relatively small reduction of interfacial tension.<sup>122-124</sup>

The conventional model for Pickering emulsions assumes the formation of a densely packed particle layer at the oil–water interface, which prevents droplet coalescence by a steric barrier mechanism.<sup>104, 125</sup> The magnitude of the steric barrier is controlled by the energy required to remove a spherical particle from the oil–water interface ( $\Delta E$ ) which is a function of the three-phase contact angle of the particle ( $\theta_{ow}$ ), and can be calculated according to equation 1:

$$\Delta E = \pi r^2 \gamma_{ow} (1 - |\cos \theta_{ow}|)^2 \quad [1]$$

where  $r$  is the radius of the particle, and  $\gamma_{ow}$  is the oil-water interfacial tension.<sup>126-128</sup> This energy is considerably large (on the order of  $10^5 k_B T$  for a 100 nm particle) at contact angles around  $90^\circ$ .<sup>112, 119, 129</sup> Therefore, once a partially wettable particle is at the oil-water interface, it will not leave spontaneously. Furthermore, Pickering emulsions are stabilized due to the mechanical barrier which slows Oswald ripening (coalescence) and the high viscosity of the continuous phase which slows creaming/sedimentation.<sup>120</sup>

In the case of spherical hydrophilic particles which adsorb to interfaces (oil-water or air-water), the three-phase contact angle  $\theta$  measured in the aqueous phase is normally  $< 90^\circ$  and a larger fraction of the particle resides in water than in the non-polar phase. For hydrophobic particles,  $\theta$  is generally greater than  $90^\circ$  and the particle resides more in oil or air than in water. By analogy with surfactant molecules, the monolayers of particles will curve such that the larger area of the particle surface remains on the external side, leading to oil-in-water (o/w) emulsions or aqueous foams when  $\theta < 90^\circ$  and water-in-oil (w/o) emulsions and aerosols when  $\theta > 90^\circ$  (Figure 1.7).<sup>106, 130</sup>

In many commercial products, both surface-active molecules and particulate emulsifiers are used to optimize emulsion characteristics. The role of surface-active molecules in providing enhanced stability of particle-stabilized emulsion is reported to be threefold: (1) to lower the interfacial tension to favor droplet formation, (2) to change particle contact angle and hydrophobicity and (3) to induce flocculation of the solid particles in the continuous phase.<sup>127, 131</sup> Adsorption of surfactants on nanoparticles competes with the adsorption of surfactant at the oil-water interface.<sup>132</sup> For example, loss of surfactant to an oppositely charged particle's surface lowers the amount of free surfactant that may adsorb at the oil–water interface, which may raise the interfacial tension.<sup>133-135</sup> On the contrary, like-charged particles and surfactants often show a decrease in interfacial tension as surfactant is driven to the interface because it is repelled by the suspended particles.<sup>136-137</sup>

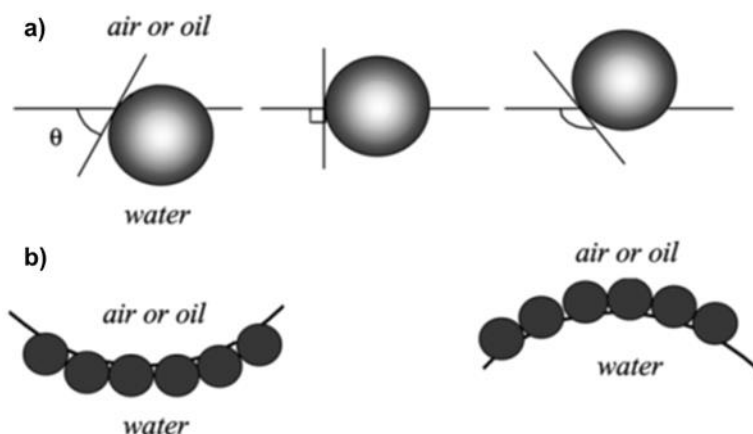


Figure 1.7. a) Schematic representation of small spherical particles at a planar fluid-water interface for a contact angle (measured through the aqueous phase) less than  $90^\circ$  (left), equal to  $90^\circ$  (center) and greater than  $90^\circ$  (right); b) Corresponding probable positioning of particles at a curved fluid-water interface. For  $\theta < 90^\circ$ , Pickering aqueous o/w emulsions or foams may form (left). For  $\theta > 90^\circ$ , Pickering w/o emulsions or aerosols may form (right). (Figure adapted from Ref.<sup>106</sup>)

In addition to varying the charge on surfactant headgroups, Binks and co-workers have extensively studied the effect of varying the amphiphile tail length and concentration to tune the interactions between surface-active molecules and particles, which led to more controlled and stable emulsions. For instance, double phase inversions (o/w [1] to w/o to o/w [2]) have been observed in Pickering emulsions containing silica or calcium carbonate nanoparticles with added surfactant.<sup>111, 138-140</sup> The inversions are attributed to the adsorption of oppositely charged surfactant at the particle surface which changes the particle wettability (Figure 1.8). The contact angle of the particles at the planar oil-water interface has been measured directly using freeze-fracture shadow-casting cryo-scanning electron microscopy, which allowed single-particle contact angle measurements of high accuracy.<sup>139</sup> It is shown that upon increasing surfactant concentration, particles undergo a hydrophilic–hydrophobic–hydrophilic transition that closely corresponds to the double phase inversion observed in the emulsions. Surfactants that can pack densely on the particle surface or that have long (or multiple) alkyl tails easily lead to more hydrophobic particles at low surfactant concentration which then become hydrophilic again at high surfactant concentration due to surfactant bilayer adsorption (or maybe more precisely admicelle aggregates adsorbed on the nanoparticle surfaces).

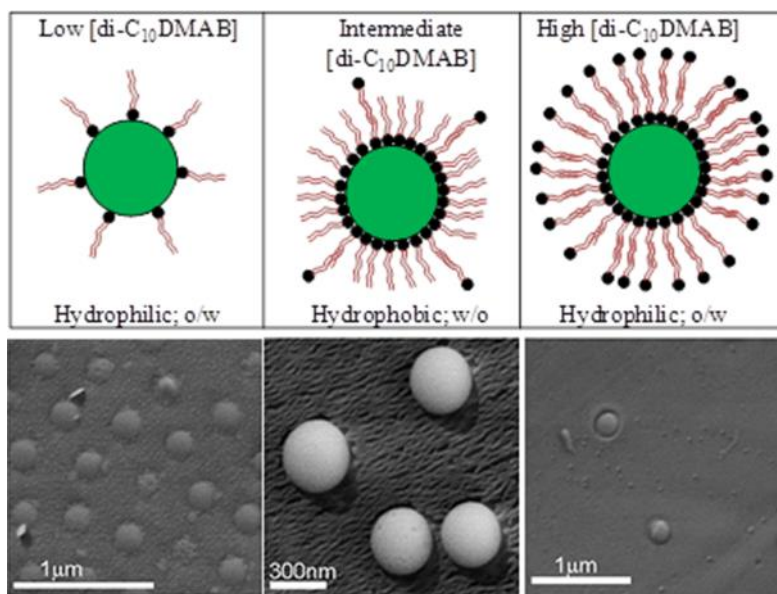


Figure 1.8. Schematic representations (top) of the effect of surfactant concentration on the adsorption of surfactant on particle surfaces and its influence on particle wettability and emulsion type; freeze-fracture shadow-casting cryo-scanning electron microscopy images (bottom) of the interfacial silica nanoparticles in the presence of increasing amount of surfactants. (Figure reproduced from Ref.<sup>139</sup>)

Because surfactant adsorption on particles is readily reversible and polymer adsorption is essentially an irreversible process, high molecular weight polymers have been used to more permanently tune the interfacial properties of particles. Saleh *et al.*<sup>141</sup> found that physisorbed layers of amphiphilic PMAA-block-PMMA-block-PSS triblock copolymers improved the colloidal stability of iron nanoparticles in water, drove them to adsorb at the oil/water interface, and formed a highly stable emulsion (Figure 1.9). Adsorbing surface-active polymers onto nanoparticles makes the nanoparticles efficient emulsifiers; concentrations as low as 0.04 wt. % are sufficient to stabilize emulsions for many months. Similarly, Feng *et al.*<sup>142</sup> observed that salt-bridge interactions between carboxylic acid groups of single-walled carbon nanotubes (SWCNTs) and amine groups on amine-terminated polystyrene drove the assembly of SWCNTs to the oil/water interface. In addition to adsorbing polymers onto nanoparticles to produce efficient emulsifiers, Saigal *et al.*<sup>143</sup> obtained highly stable xylene-in-water and cyclohexane-in-water emulsions at extremely low particle concentrations by using silica nanoparticles with poly(2-(dimethylamino)ethyl methacrylate) brushes grafted from their surfaces (SiO<sub>2</sub>-PDMAEMA) as the emulsifying agent. Interestingly, these emulsions were thermally responsive, rapidly breaking upon increasing the temperature above the critical flocculation temperature of the SiO<sub>2</sub>-PDMAEMA particles in water.

The enhanced emulsification effectiveness of polymer-adsorbed or polymer-grafted nanoparticles relative to that of bare particles is attributed to the surface activity of polymer chains.<sup>143</sup> Whereas bare particles often do not reduce interfacial tension significantly, adsorbed/grafted polymer chains are normally surface-active and capable of partitioning to the oil/water interface to decrease the interfacial tension.<sup>123</sup> In addition to lowering the interfacial tension, swollen polymer brushes on nanoparticles between two approaching emulsion droplets may inhibit droplet coalescence via steric or electrosteric repulsive forces. Compared to soluble polymers or surfactants used as emulsifiers, complete removal of one polymer-coated nanoparticle from the oil/water interface would require the simultaneous removal of many additional polymer chains that are adsorbed or grafted to the same nanoparticle.

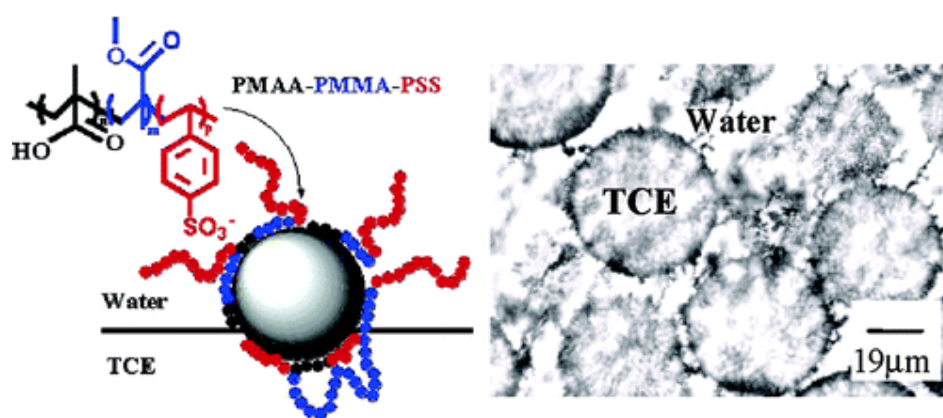


Figure 1.9. Schematic representation (left) of polymer-modified iron nanoparticle partitioning at oil/water interface; optical micrograph (right) of o/w emulsion droplets stabilized by polymer-modified iron nanoparticles. (Figure reproduced from Ref.<sup>141</sup>)

In all of these experiments, the particles were modified with surfactants prior to the formation of emulsions. Addition of surfactants to a particle-stabilized emulsion, however, led to complicated emulsion behavior. Binks *et al.*<sup>132</sup> observed a coalescence induced increase in emulsion droplet size after the addition of nonionic surfactant C<sub>12</sub>E<sub>7</sub> to tricaprilyn-in-water emulsions stabilized by surface modified silica particles. Vashisth *et al.*<sup>144</sup> studied the effect of adding sodium dodecyl sulfate (SDS) to dodecane-in-water emulsions stabilized by fumed silica particles and found that SDS displaces nanoparticles from the interface. Similarly, Whitby *et al.*<sup>145</sup> noticed that the rate and extent of creaming and flocculation of the drops were enhanced upon diluting emulsions stabilized by silica particles in SDS solutions. They attributed it to a significant drop in the oil/water interfacial tension upon addition of surfactant due to its preferential adsorption at the oil/water interface.

### 1.1.6 CNC Pickering Emulsions

In many applications, non-toxic and biocompatible colloidal particles derived from biomass are preferred, making starch,<sup>146-147</sup> chitin,<sup>148-149</sup> and cellulose particles (microcrystalline cellulose,<sup>150-151</sup> MFC,<sup>152-153</sup> CNCs,<sup>154-156</sup> BNC,<sup>157-158</sup> and cellulose derivatives<sup>159</sup>) more suitable. Various fibrillated cellulose materials have been successfully used as emulsifiers.<sup>33, 160-161</sup> However, fibrillated cellulose has the drawback of producing emulsion droplet networks rather than individual droplets as a result of their high aspect ratio. Therefore, shorter and well-defined cellulose particles such as CNCs appear to be excellent candidates for interfacial stabilization in a more controlled manner.<sup>154, 162</sup> Capron and co-workers showed that the aspect ratio of CNCs directly influences the coverage ratio of CNCs on the surface of emulsion droplets giving rise, on the one hand to a dense organization (surface coverage >80%) with short CNCs from cotton and on the other hand to an interconnected network of low covered droplets (40%) when longer nanocrystals from bacterial cellulose are used (Figure 1.10).<sup>154</sup>

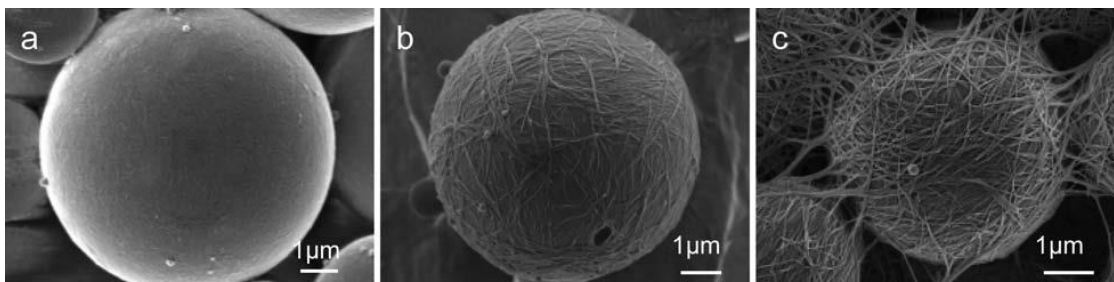


Figure 1.10. Scanning electron micrographs of polymerized styrene-water emulsions stabilized by a) cotton cellulose nanocrystals, b) bacterial cellulose nanocrystals, and c) *Cladophora* cellulose nanocrystals. (Figure reproduced from Ref.<sup>154</sup>)

The surface charge density of CNCs has been shown to play a major role in how well CNCs stabilize the oil/water interface. Kalashnikova *et al.*<sup>162</sup> found that CNCs with a surface charge density above  $0.03 \text{ e/nm}^2$  were not able to efficiently stabilize the interface, whereas a decreasing surface charge density led to stable emulsions. The surface charge reduction can be readily achieved by a desulfation process or by screening charge repulsions. The authors suggested that although being globally hydrophilic, CNCs possess hydrophobic edges, which enable the formation of stable oil-in-water emulsions.<sup>162</sup>

The hydrophobicity of cellulose nanoparticles can be increased by using agents such as silanes or alkylamines to facilitate the stabilization of water-in-oil (w/o) emulsions.<sup>33, 163</sup> However, the hydrophobization process typically involves multiple steps of surface modification and purification. In addition, some CNC surface chemistries are detrimental to some specific applications. For instance, hydrophobization of cellulose particles by silylation is not suitable for fuel emulsions because the silicon atom may poison the exhaust catalyst. Therefore, *in situ* surface modification of cellulosic nanomaterials using surfactants is highly desirable.<sup>164</sup> Emulsions stabilized by the combination of both colloidal particles and surfactants allow for

emulsion properties to be finely tuned, requiring relatively small amounts of both stabilizers due to particle-surfactant synergy. Due to rising environmental, health and safety concerns regarding a number of synthetic surfactants, stabilizing emulsions using CNCs and less surfactant is considered favorable. Replacing conventional surfactants with natural amphiphilic molecules or biocompatible surface-active polymers should also be beneficial for some applications where low-toxicity is highly desired.

Functional materials based on CNC emulsions have attracted a great deal of attention in recent years due to their wide range of applications. Tasset *et al.*<sup>165</sup> prepared lightweight cellulose foams by freeze-drying o/w emulsions stabilized with CNCs. The same research group also produced high-internal-phase emulsion “gels” by making CNC-stabilized emulsions with equal parts oil and water and then slowly increasing the oil content (Figure 1.11).<sup>155</sup> In another literature example, Nypelö *et al.*<sup>166</sup> reported production of hybrid CNC magneto-responsive microbeads and microcapsules by using CNC Pickering emulsion as media. Such hybrid systems can be used for application in colloidal stabilization, concentration, separation, sorption, and delivery, among others. Li *et al.*<sup>167</sup> used electrospinning of CNCs/poly(lactic acid) w/o emulsions to prepare composite ultrafine fibers. In these fibers, CNCs were aligned along the core (in the core-shell fibers), or on the wall (in the hollow fibers) and acted as nucleating agent influencing PLA crystallinity, and improved the strength and stiffness of the electrospun composite fibers.

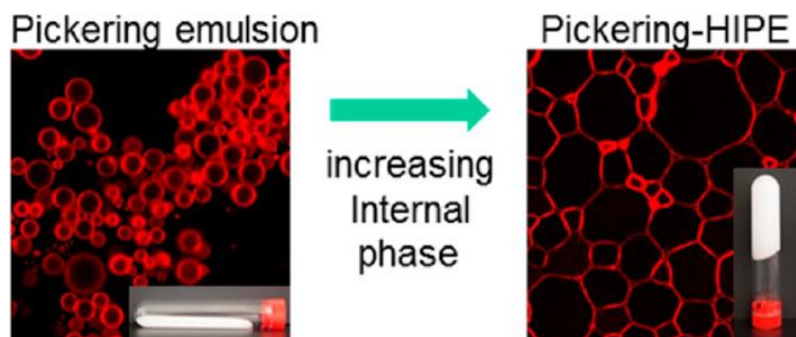


Figure 1.11. Confocal laser scanning microscopy images of emulsions stabilized by cotton CNCs containing increasing amounts of hexadecane stained with BODIPY (inset images showing the gel formation at high oil volume fraction). (Figure adapted from Ref.<sup>155</sup>)

### 1.1.7 CNC Wet Foams

Foams occur in mixtures of immiscible fluids in which a vapor phase is dispersed as millimeter-sized bubbles in the continuous phase of a liquid.<sup>168</sup> Surfactants and proteins are the most widely used foaming agents in a range of areas including the detergent, food, and cosmetic industries,

and yet it appears that they may possess certain deficiencies when long-term foam stability is required. There have been a number of publications in recent years investigating colloidal particles as stabilizers for foams which are stable for months or years.<sup>106, 169-170</sup> The detailed mechanisms of foam stabilization using particles are still under debate. It is generally accepted that drainage of the intervening fluid between air bubbles followed by the close approach of bubble surfaces and bubble coalescence can occur, resulting in foam collapse, loss of gas and foam structure and texture. In addition, gas diffusion from smaller to larger bubbles as a result of differences in Laplace pressure, leading to coarsening of the foams. The effect is called disproportionation, and is analogous to Ostwald ripening in emulsions. Together, drainage, coalescence and coarsening lead to foam instability.

Similar to the stabilization of emulsions, the key to the air bubble stabilizing mechanism by particles is that, if the surface energy (or contact angle) of the particles with the aqueous phase is in the correct range, then the adsorption energy per particle can be up to several thousand  $kT$ , making it almost impossible to force particles off of the interface.<sup>169</sup> Partially hydrophobic silica nanoparticles have been used as the sole stabilizer of air bubbles; the foams were completely stable to collapse, coalescence, and disproportionation.<sup>110, 171-172</sup> Although a detailed picture of the particle film stabilizing the bubbles is far from clear, the particles tend to become highly aggregated in the aqueous phase and at the air-water interface.

The well-documented flotation process involves the attachment of mineral particles to air bubbles by adding to the slurry surface-active molecules as frothing agents and collectors. Recently, Yang et al.<sup>173-176</sup> provided an excellent example of using particles to stabilize air bubbles and improve flotation efficiency. The hydrophobic nanoparticles were adsorbed onto much larger, hydrophilic mineral particle surfaces to facilitate attachment to air bubbles in flotation.

Compared to the body of work describing particle-stabilized oil-in-water and water-in-oil emulsions, up to now there have been relatively few studies of the stabilization of foams by particles. In addition to silica particles, other colloidal particles such as clay platelets,<sup>177</sup> iron particles,<sup>178</sup> metal oxide nanoparticles,<sup>179</sup> polymer latex,<sup>180</sup>  $\text{CaCO}_3$  rods,<sup>181</sup> and (non CNC) cellulose particles,<sup>182-184</sup> have been employed as the stabilizing agents. Surface modification of the particles is normally required to tune the hydrophobicity by chemical functionalization of the surface. An easier and more versatile approach to modify the wettability of the particles is the *in situ* adsorption of amphiphilic molecules onto the particle surface.<sup>185-186</sup> By changing the surfactant concentration, the attachment of surfactant-decorated particles to air-water interface can be readily adjusted. It has been determined that foams are most stable when particles are strongly flocculated corresponding to them possessing a low charge, being maximally hydrophobic and containing a monolayer of adsorbed surfactant.

While most forms of nanocellulose have been demonstrated to be capable of stabilizing emulsions without the use of additional surfactants, this has not been shown for foams. Lam *et*

*al.*<sup>130</sup> suggested a few reasons why the stabilization of oil-water interfaces is easier than air-water interfaces: (1) The air-water interfacial tension is higher than that at oil-water interface, leading to larger capillary pressures in the foam films than emulsion films; (2) The density difference between the dispersed and continuous phases is higher in foams than in emulsions, driving more enhanced phase separation in the former; (3) The solubility and diffusivity of a gas in H<sub>2</sub>O is normally higher than that of the typical emulsion oil phase in H<sub>2</sub>O, causing easier foam destabilization than emulsion destabilization. Relatively hydrophilic particles can stabilize o/w emulsions, but they may not be hydrophobic efficient in stabilizing foams. Hunter *et al.*<sup>104</sup> presented a detailed comparison of the particle properties necessary for foam stabilization compared to emulsion stabilization.

Most nanocellulose materials by themselves do not have strong interfacial activity to produce stable foams, however amphiphilic behavior can be imparted by either physical adsorption of amphiphilic molecules or by chemical surface modification. For instance, aqueous foams stabilized with up to 1 wt.% nanofibrillated cellulose were prepared by adsorbing positively charged octylamine on the surface of the fibrils.<sup>184</sup> Careful removal of the water through freeze-drying resulted in highly porous, lightweight cellulose foams (pore size ~ 300–500 μm). In this work, NFC particles were “brought to the interface” by the octylamine.

Some other researchers also reported generating cellulose-based foams, but these cellulose particles were mostly on a micrometer size-scale. Al-Qararah *et al.*<sup>187</sup> foamed Kraft fibers from wood pulp in the presence of SDS to generate foams containing cellulose fibers. However, they found that the fibers were not adsorbed at the interface. Hydrophobic cellulose microparticles of hypromellose phthalate have been formed *in situ* by a liquid-liquid dispersion technique and used to create foams that were stable for months (Figure 1.12).<sup>183</sup> The short-term and long-term stabilization of interfaces strongly depended on the cellulose particle concentration. Micrometer-sized hydrophobic cellulose particles were also made through precipitation of ethyl cellulose onto Tencel and combined with caseins or whey proteins to give significant improvements in stability of bubbles. The complexes formed using hydrophobic cellulose particles and caseins or whey proteins gave significant improvements in stability of foams and bubbles to coalescence and disproportionation compared to either component alone.<sup>182</sup> Jin *et al.*<sup>188</sup> also reported that super stable aqueous foams with various bubble sizes were stabilized by food grade colloidal ethyl cellulose particles. However, to the best of our knowledge, no example of aqueous foams comprised of CNCs alone or in combination with amphiphilic molecules exists yet in the literature.

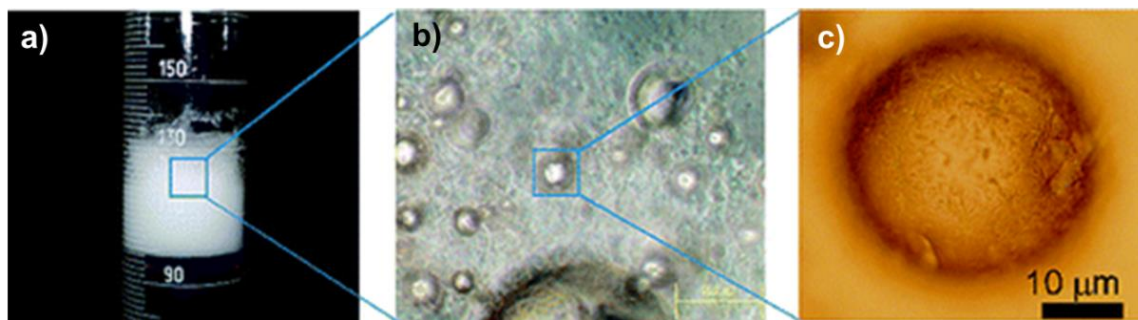


Figure 1.12. a) Appearance of the foams stabilized by hydrophobic cellulose microparticles of hypromellose phthalate; b) and c) Optical micrographs of wet foam. (Figure reproduced from Ref.<sup>183</sup>)

### 1.1.8 CNC Solid Foams

Polymeric foams are utilized in a range of applications such as mechanical dampeners, solid supports for catalysis and separations, immobilization of enzymes and proteins, thermal and acoustic insulating materials, and medical devices.<sup>189-190</sup> Macroporous polymer foams have been produced by dispersion of a gaseous phase in a fluid polymer phase, thermally induced phase separation, hydrocarbon templating, and emulsion templating.<sup>189-195</sup> Emulsion templating has become a very active research area for the production of macroporous polymers with tailored porosity and pore structure. In order to fabricate polymeric foams with high porosity, high internal phase emulsions (HIPEs) are normally utilized as templates, which is often defined as a concentrated emulsion with a minimum internal phase volume ratio of 74 %.<sup>193</sup> Both surfactants<sup>196-197</sup> and particles<sup>198</sup> have been used as the stabilizers to create water-in-monomer emulsions and subsequent polymerization of the monomer phase and removal of dispersed water phase lead to emulsion templated macroporous polymeric foams. The prepared macroporous polymers are often termed poly-HIPEs. Various types of poly-HIPEs have been synthesized using different solid particles as stabilizers, including silica nanoparticles, titania particles, iron oxide nanoparticles, microgels, carbon nanotubes, and graphene oxide.<sup>157, 199-203</sup> However, to the best of our knowledge, no poly-HIPEs have been produced by using CNCs as the particulate stabilizers.

Tasset *et al.*<sup>165</sup> reported another versatile method of preparing lightweight cellular foams by freeze-drying o/w emulsions stabilized by CNCs. The foams exhibited cell sizes similar to the droplets of the starting emulsion as a result of the robustness of the starting emulsion drops to withstand centrifugation and freeze drying without collapsing. Further functionalization of the foams was achieved by addition of positively charged chitosan, whereas addition of negatively charged alginate promoted coalescence leading to a networked porous structure with no defined pore shape. To avoid using oil to prepare emulsions and freeze-drying to produce porous foams,

Cervin *et al.*<sup>184</sup> introduced the production of a lightweight and strong porous cellulose foam by air drying aqueous foams stabilized with surface-modified NFC. However, the inability to readily tailor the surface functionality, structural and mechanical properties of the cellulosic foams produced by these methods have been a motivation for researchers to design new ways of making macroporous foams using nanocellulose materials.

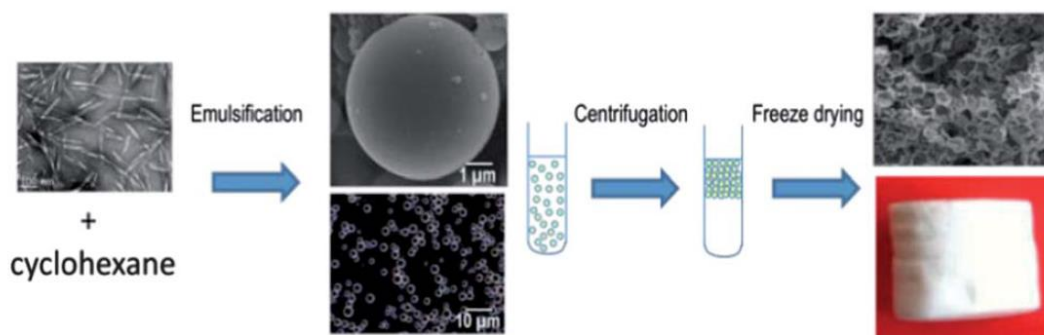


Figure 1.13. Schematic representation of the preparation of o/w emulsion stabilized by CNCs, subsequent concentration by centrifugation, and freeze-drying to prepare CNC macroporous foam. (Figure adapted from Ref.<sup>165</sup>)

## 1.2 Objectives

As new, green, and sustainable materials, CNCs are currently being evaluated in a variety of applications, including as reinforcing agents in nanocomposites, as stabilizers for emulsions and foams, and as templating materials. Most of these formulated chemical products in food, cosmetics, and biomedical industries, are complex mixtures of particulate materials and surfactants and polymers. However, there is a lack of understanding of the relationship between CNC, surfactant and polymer interactions and the properties of these components in solution and at interfaces. Before this work was initiated, the majority of work in the literature was focused on studying the properties of CNCs in aqueous systems and oil-water interfaces in the absence of any other surface-active components. The overall objective of this thesis is to investigate the properties of CNCs in solution and at interfaces in the presence of different water-soluble surfactants and polymers. The potential of producing hydrogels, emulsions, and foams using CNCs and surfactants and polymers is also explored herein. The specific goals of this work are summarized below:

1. To understand the influence of water-soluble polymers and surfactants on the rheological and gelation behavior of CNC dispersions at high ionic strength. The results can provide industries with generic design rules for formulating aqueous products with CNCs.

2. To investigate the effect of cationic surfactants and non-ionic polymers on the properties of Pickering emulsions stabilized by CNCs. Through this work, a better understanding of tuning emulsion type, emulsion droplet size, and emulsion stability was achieved, which could pave the way for developing emulsion-based products incorporating CNCs. In addition, the exploration of producing emulsion gels and oil solids using CNCs may lead to interesting applications in various industries.
3. To determine the effects of adding CNCs to polymeric foaming agents on foamability and foam stability. Furthermore, fabrication of polymeric macroporous solid foams by using CNC-based aqueous foams as the templates, was also studied. The research findings in this work may offer some insights into the design of both aqueous and solid foams in a wide range of applications.

### 1.3 Thesis outline

*Chapter 1: Introduction.* This chapter presents a thorough background of this project as well as the relevant literature and research objectives. The thesis outline is also listed in this chapter.

*Chapter 2: Tuning cellulose nanocrystal gelation with polysaccharides and surfactants.* This chapter studies the adsorption of non-ionic polysaccharides on CNCs and correlates the adsorption behavior with gelation of CNCs upon addition of these polysaccharides. An increased effective volume fraction mechanism was proposed to explain the gelation of dilute CNC suspensions after adsorbing polysaccharides on the CNC surfaces. The effect of adding surfactants to gels made by CNCs and polysaccharides was also investigated. This work has been published in *Langmuir*.<sup>204</sup>

*Chapter 3. Surfactant-enhanced cellulose nanocrystal Pickering emulsions.* This chapter evaluates the tailoring of Pickering emulsions stabilized by CNCs through addition of cationic surfactants with different chemical structures and concentrations. The change in CNC wettability from surfactant adsorption was directly linked to emulsion properties; adding surfactant generally increased hydrophobicity of CNCs, enhanced the emulsion stability, decreased the droplet size, and controlled the dispersed phase of CNC Pickering emulsions. A double phase inversion, from o/w to w/o and back to o/w, was observed for emulsions with CNCs and increasing amounts of double-tailed surfactants. This work has been published in *Journal of Colloid and Interface Science*.<sup>164</sup>

*Chapter 4. Synergistic Stabilization of Emulsions and Emulsion Gels with Water-soluble Polymers and Cellulose Nanocrystals.* This chapter reports the production of stable emulsions with tunable droplet sizes by using CNCs and water-soluble non-ionic polymers. The co-stabilization of oil-water interfaces with both CNCs and polymers was suggested. Temperature-induced gelation of the emulsions stabilized by CNCs in the presence of polymers was demonstrated. In addition, freeze-drying of the emulsion gels led to production of oil solids with oil content as high as 94 wt.%. This chapter is in preparation for publication.

*Chapter 5. Preparation and Templating Properties of Stable Wet Foams of Cellulose Nanocrystals and Methyl Cellulose.* This chapter describes the production and characterization of stable aqueous foams based on CNCs and methyl cellulose. The foamability, foam stability, and water drainage of foams with CNCs at various loadings were examined to investigate the effect of adding CNCs. The production of macroporous composite solid foams with tunable properties using aqueous foams based on CNCs and methyl cellulose as the templating materials was also demonstrated. This chapter is in preparation for publication.

*Chapter 6: Concluding remarks.* This chapter summarizes the major contributions of this study.

## References

- (1) Kaplan, D. L. *Biopolymers from Renewable Resources*. Springer: Berlin, **1998**, pp. **1-29**.
- (2) Klemm, D.; Heublein, B.; Fink, H.-P.; Bohn, A. Cellulose: Fascinating Biopolymer and Sustainable Raw Material. *Angewandte Chemie International Edition* **2005**, *44* (22), 3358-3393.
- (3) Young, R. *Cellulose structure modification and hydrolysis*. Wiley: New York, **1986**.
- (4) Habibi, Y.; Lucia, L. A.; Rojas, O. J. Cellulose Nanocrystals: Chemistry, Self-Assembly, and Applications. *Chemical Reviews* **2010**, *110* (6), 3479-3500.
- (5) Wang, H.; Gurau, G.; Rogers, R. D. Ionic liquid processing of cellulose. *Chemical Society Reviews* **2012**, *41* (4), 1519-1537.
- (6) Rowland, S. P.; Roberts, E. J. The nature of accessible surfaces in the microstructure of cotton cellulose. *Journal of Polymer Science Part A-1: Polymer Chemistry* **1972**, *10* (8), 2447-2461.
- (7) Preston, R. D. *Natural Celluloses*. In *Cellulose: Structure, Modification and Hydrolysis*. John Wiley & Sons: New York, **1986**.
- (8) Akira, I. *Chemical modification of cellulose*. . Marcel Dekker: New York, **2001**, pp. **599-626**.
- (9) Hiatt, G. D. R., W. J., B. Esters. *Cellulose and Cellulose Derivatives*. Wiley: New York, **1971**; Vol. V, pp 741-784.
- (10) Heinze, T.; Schwikal, K.; Barthel, S. Ionic Liquids as Reaction Medium in Cellulose Functionalization. *Macromolecular Bioscience* **2005**, *5* (6), 520-525.
- (11) Edgar, K. J.; Buchanan, C. M.; Debenham, J. S.; Rundquist, P. A.; Seiler, B. D.; Shelton, M. C.; Tindall, D. Advances in cellulose ester performance and application. *Progress in Polymer Science* **2001**, *26* (9), 1605-1688.
- (12) Hirrien, M.; Chevillard, C.; Desbrières, J.; Axelos, M. A. V.; Rinaudo, M. Thermogelation of methylcelluloses: new evidence for understanding the gelation mechanism. *Polymer* **1998**, *39* (25), 6251-6259.
- (13) Kobayashi, K.; Huang, C.-i.; Lodge, T. P. Thermoreversible Gelation of Aqueous Methylcellulose Solutions. *Macromolecules* **1999**, *32* (21), 7070-7077.
- (14) Arvidson, S. A.; Lott, J. R.; McAllister, J. W.; Zhang, J.; Bates, F. S.; Lodge, T. P.; Sammler, R. L.; Li, Y.; Brackhagen, M. Interplay of Phase Separation and Thermoreversible Gelation in Aqueous Methylcellulose Solutions. *Macromolecules* **2012**, *46* (1), 300-309.
- (15) Lott, J. R.; McAllister, J. W.; Wasbrough, M.; Sammler, R. L.; Bates, F. S.; Lodge, T. P. Fibrillar Structure in Aqueous Methylcellulose Solutions and Gels. *Macromolecules* **2013**, *46* (24), 9760-9771.
- (16) Lott, J. R.; McAllister, J. W.; Arvidson, S. A.; Bates, F. S.; Lodge, T. P. Fibrillar Structure of Methylcellulose Hydrogels. *Biomacromolecules* **2013**, *14* (8), 2484-2488.
- (17) Klemm, D.; Kramer, F.; Moritz, S.; Lindstrom, T.; Ankerfors, M.; Gray, D.; Dorris, A. Nanocelluloses: A New Family of Nature-Based Materials. *Angewandte Chemie-International Edition* **2011**, *50* (24), 5438-5466.
- (18) Zimmermann, T.; Bordeanu, N.; Strub, E. Properties of nanofibrillated cellulose from different raw materials and its reinforcement potential. *Carbohydrate Polymers* **2010**, *79* (4), 1086-1093.

- 
- (19) Nakagaito, A. N.; Yano, H. The effect of morphological changes from pulp fiber towards nano-scale fibrillated cellulose on the mechanical properties of high-strength plant fiber based composites. *Appl Phys A* **2004**, *78* (4), 547-552.
  - (20) Boldizar, A.; Klason, C.; Kubát, J.; Näslund, P.; Sáha, P. Prehydrolyzed Cellulose as Reinforcing Filler for Thermoplastics. *International Journal of Polymeric Materials and Polymeric Biomaterials* **1987**, *11* (4), 229-262.
  - (21) Pääkkö, M.; Ankerfors, M.; Kosonen, H.; Nykänen, A.; Ahola, S.; Österberg, M.; Ruokolainen, J.; Laine, J.; Larsson, P. T.; Ikkala, O.; Lindström, T. Enzymatic Hydrolysis Combined with Mechanical Shearing and High-Pressure Homogenization for Nanoscale Cellulose Fibrils and Strong Gels. *Biomacromolecules* **2007**, *8* (6), 1934-1941.
  - (22) Henriksson, M.; Henriksson, G.; Berglund, L. A.; Lindström, T. An environmentally friendly method for enzyme-assisted preparation of microfibrillated cellulose (MFC) nanofibers. *European Polymer Journal* **2007**, *43* (8), 3434-3441.
  - (23) Wågberg, L.; Decher, G.; Norgren, M.; Lindström, T.; Ankerfors, M.; Axnäs, K. The build-up of polyelectrolyte multilayers of microfibrillated cellulose and cationic polyelectrolytes. *Langmuir* **2008**, *24* (3), 784-795.
  - (24) Isogai, A.; Saito, T.; Fukuzumi, H. TEMPO-oxidized cellulose nanofibers. *Nanoscale* **2011**, *3* (1), 71-85.
  - (25) Fleming, K.; Gray, D.; Prasannan, S.; Matthews, S. Cellulose Crystallites: A New and Robust Liquid Crystalline Medium for the Measurement of Residual Dipolar Couplings. *Journal of the American Chemical Society* **2000**, *122* (21), 5224-5225.
  - (26) Nakagaito, A. N.; Iwamoto, S.; Yano, H. Bacterial cellulose: the ultimate nano-scalar cellulose morphology for the production of high-strength composites. *Appl Phys A* **2005**, *80* (1), 93-97.
  - (27) Lavoine, N.; Desloges, I.; Dufresne, A.; Bras, J. Microfibrillated cellulose – Its barrier properties and applications in cellulosic materials: A review. *Carbohydrate Polymers* **2012**, *90* (2), 735-764.
  - (28) Henriksson, M.; Berglund, L. A.; Isaksson, P.; Lindström, T.; Nishino, T. Cellulose Nanopaper Structures of High Toughness. *Biomacromolecules* **2008**, *9* (6), 1579-1585.
  - (29) Syverud, K.; Stenius, P. Strength and barrier properties of MFC films. *Cellulose* **2009**, *16* (1), 75-85.
  - (30) Shimazaki, Y.; Miyazaki, Y.; Takezawa, Y.; Nogi, M.; Abe, K.; Ifuku, S.; Yano, H. Excellent Thermal Conductivity of Transparent Cellulose Nanofiber/Epoxy Resin Nanocomposites. *Biomacromolecules* **2007**, *8* (9), 2976-2978.
  - (31) Svagan, A. J.; Samir, M. A. S. A.; Berglund, L. A. Biomimetic Foams of High Mechanical Performance Based on Nanostructured Cell Walls Reinforced by Native Cellulose Nanofibrils. *Advanced Materials* **2008**, *20* (7), 1263-1269.
  - (32) Paakko, M.; Vapaavuori, J.; Silvennoinen, R.; Kosonen, H.; Ankerfors, M.; Lindstrom, T.; Berglund, L. A.; Ikkala, O. Long and entangled native cellulose I nanofibers allow flexible aerogels and hierarchically porous templates for functionalities. *Soft Matter* **2008**, *4* (12), 2492-2499.
  - (33) Andresen, M.; Stenius, P. Water-in-oil Emulsions Stabilized by Hydrophobized Microfibrillated Cellulose. *Journal of Dispersion Science and Technology* **2007**, *28* (6), 837-844.

- 
- (34) Son, H.-J.; Heo, M.-S.; Kim, Y.-G.; Lee, S.-J. Optimization of fermentation conditions for the production of bacterial cellulose by a newly isolated *Acetobacter*. *Biotechnology and Applied Biochemistry* **2001**, *33* (1), 1-5.
- (35) Ross, P.; Mayer, R.; Benziman, M. CELLULOSE BIOSYNTHESIS AND FUNCTION IN BACTERIA. *Microbiological Reviews* **1991**, *55* (1), 35-58.
- (36) Mohite, B. V.; Patil, S. V. A novel biomaterial: bacterial cellulose and its new era applications. *Biotechnology and Applied Biochemistry* **2014**, *61* (2), 101-110.
- (37) Huang, Y.; Zhu, C. L.; Yang, J. Z.; Nie, Y.; Chen, C. T.; Sun, D. P. Recent advances in bacterial cellulose. *Cellulose* **2014**, *21* (1), 1-30.
- (38) Lin, S. P.; Calvar, I. L.; Catchmark, J. M.; Liu, J. R.; Demirci, A.; Cheng, K. C. Biosynthesis, production and applications of bacterial cellulose. *Cellulose* **2013**, *20* (5), 2191-2219.
- (39) Si, W.; Lei, W.; Zhang, Y.; Xia, M.; Wang, F.; Hao, Q. Electrodeposition of graphene oxide doped poly(3,4-ethylenedioxythiophene) film and its electrochemical sensing of catechol and hydroquinone. *Electrochimica Acta* **2012**, *85* (0), 295-301.
- (40) Yoon, S. H.; Jin, H.-J.; Kook, M.-C.; Pyun, Y. R. Electrically Conductive Bacterial Cellulose by Incorporation of Carbon Nanotubes. *Biomacromolecules* **2006**, *7* (4), 1280-1284.
- (41) Ranby, B. G. Fibrous macromolecular systems. Cellulose and muscle. The colloidal properties of cellulose micelles. *Discussions of the Faraday Society* **1951**, *11* (0), 158-164.
- (42) Revol, J. F. On the cross-sectional shape of cellulose crystallites in *Valonia ventricosa*. *Carbohydrate Polymers* **1982**, *2* (2), 123-134.
- (43) Hanley, S. J.; Giasson, J.; Revol, J.-F.; Gray, D. G. Atomic force microscopy of cellulose microfibrils: comparison with transmission electron microscopy. *Polymer* **1992**, *33* (21), 4639-4642.
- (44) de Souza Lima, M. M.; Borsali, R. Static and Dynamic Light Scattering from Polyelectrolyte Microcrystal Cellulose†. *Langmuir* **2002**, *18* (4), 992-996.
- (45) Anglès, M. N.; Dufresne, A. Plasticized Starch/Tunicin Whiskers Nanocomposite Materials. 2. Mechanical Behavior. *Macromolecules* **2001**, *34* (9), 2921-2931.
- (46) Hirai, A.; Inui, O.; Horii, F.; Tsuji, M. Phase Separation Behavior in Aqueous Suspensions of Bacterial Cellulose Nanocrystals Prepared by Sulfuric Acid Treatment. *Langmuir* **2008**, *25* (1), 497-502.
- (47) Garcia de Rodriguez, N. L.; Thielemans, W.; Dufresne, A. Sisal cellulose whiskers reinforced polyvinyl acetate nanocomposites. *Cellulose* **2006**, *13* (3), 261-270.
- (48) Dong, X.; Revol, J.-F.; Gray, D. Effect of microcrystallite preparation conditions on the formation of colloid crystals of cellulose. *Cellulose* **1998**, *5* (1), 19-32.
- (49) Siqueira, G.; Bras, J.; Dufresne, A. Cellulose Whiskers versus Microfibrils: Influence of the Nature of the Nanoparticle and its Surface Functionalization on the Thermal and Mechanical Properties of Nanocomposites. *Biomacromolecules* **2008**, *10* (2), 425-432.
- (50) Elazzouzi-Hafraoui, S.; Nishiyama, Y.; Putaux, J.-L.; Heux, L.; Dubreuil, F.; Rochas, C. The Shape and Size Distribution of Crystalline Nanoparticles Prepared by Acid Hydrolysis of Native Cellulose. *Biomacromolecules* **2008**, *9* (1), 57-65.
- (51) Beck-Candanedo, S.; Roman, M.; Gray, D. G. Effect of Reaction Conditions on the Properties and Behavior of Wood Cellulose Nanocrystal Suspensions. *Biomacromolecules* **2005**, *6* (2), 1048-1054.

- 
- (52) Araki, J.; Wada, M.; Kuga, S.; Okano, T. Flow properties of microcrystalline cellulose suspension prepared by acid treatment of native cellulose. *Colloids and Surfaces A: Physicochemical and Engineering Aspects* **1998**, *142* (1), 75-82.
- (53) Camarero Espinosa, S.; Kuhnt, T.; Foster, E. J.; Weder, C. Isolation of Thermally Stable Cellulose Nanocrystals by Phosphoric Acid Hydrolysis. *Biomacromolecules* **2013**, *14* (4), 1223-1230.
- (54) Leung, A. C. W.; Hrapovic, S.; Lam, E.; Liu, Y.; Male, K. B.; Mahmoud, K. A.; Luong, J. H. T. Characteristics and Properties of Carboxylated Cellulose Nanocrystals Prepared from a Novel One-Step Procedure. *Small* **2011**, *7* (3), 302-305.
- (55) Kan, K. H. M.; Li, J.; Wijesekera, K.; Cranston, E. D. Polymer-Grafted Cellulose Nanocrystals as pH-Responsive Reversible Flocculants. *Biomacromolecules* **2013**, *14* (9), 3130-3139.
- (56) Dong, X. M.; Kimura, T.; Revol, J.-F.; Gray, D. G. Effects of Ionic Strength on the Isotropic-Chiral Nematic Phase Transition of Suspensions of Cellulose Crystallites. *Langmuir* **1996**, *12* (8), 2076-2082.
- (57) Araki, J.; Kuga, S. Effect of Trace Electrolyte on Liquid Crystal Type of Cellulose Microcrystals. *Langmuir* **2001**, *17* (15), 4493-4496.
- (58) Marchessault, R. H.; Morehead, F. F.; Walter, N. M. Liquid Crystal Systems from Fibrillar Polysaccharides. *Nature* **1959**, *184* (4686), 632-633.
- (59) Onsager, L. THE EFFECTS OF SHAPE ON THE INTERACTION OF COLLOIDAL PARTICLES. *Annals of the New York Academy of Sciences* **1949**, *51* (4), 627-659.
- (60) Beck-Candanedo, S.; Viet, D.; Gray, D. G. Triphase Equilibria in Cellulose Nanocrystal Suspensions Containing Neutral and Charged Macromolecules. *Macromolecules* **2007**, *40* (9), 3429-3436.
- (61) Beck-Candanedo, S.; Viet, D.; Gray, D. G. Induced Phase Separation in Low-Ionic-Strength Cellulose Nanocrystal Suspensions Containing High-Molecular-Weight Blue Dextrans. *Langmuir* **2006**, *22* (21), 8690-8695.
- (62) Domingues, R. M. A.; Gomes, M. E.; Reis, R. L. The Potential of Cellulose Nanocrystals in Tissue Engineering Strategies. *Biomacromolecules* **2014**, *15* (7), 2327-2346.
- (63) Elazzouzi-Hafraoui, S.; Nishiyama, Y.; Putaux, J.-L.; Heux, L.; Dubreuil, F.; Rochas, C. The Shape and Size Distribution of Crystalline Nanoparticles Prepared by Acid Hydrolysis of Native Cellulose. *Biomacromolecules* **2007**, *9* (1), 57-65.
- (64) Roman, M.; Winter, W. T. Effect of Sulfate Groups from Sulfuric Acid Hydrolysis on the Thermal Degradation Behavior of Bacterial Cellulose. *Biomacromolecules* **2004**, *5* (5), 1671-1677.
- (65) Habibi, Y.; Goffin, A.-L.; Schiltz, N.; Duquesne, E.; Dubois, P.; Dufresne, A. Bionanocomposites based on poly([varepsilon]-caprolactone)-grafted cellulose nanocrystals by ring-opening polymerization. *Journal of Materials Chemistry* **2008**, *18* (41), 5002-5010.
- (66) Azizi Samir, M. A. S.; Alloin, F.; Sanchez, J.-Y.; El Kissi, N.; Dufresne, A. Preparation of Cellulose Whiskers Reinforced Nanocomposites from an Organic Medium Suspension. *Macromolecules* **2004**, *37* (4), 1386-1393.
- (67) Capadona, J. R.; Shanmuganathan, K.; Tyler, D. J.; Rowan, S. J.; Weder, C. Stimuli-Responsive Polymer Nanocomposites Inspired by the Sea Cucumber Dermis. *Science* **2008**, *319* (5868), 1370-1374.

- 
- (68) Bengtsson, M.; Baillif, M. L.; Oksman, K. Extrusion and mechanical properties of highly filled cellulose fibre–polypropylene composites. *Composites Part A: Applied Science and Manufacturing* **2007**, *38* (8), 1922-1931.
- (69) Ahmed, E. M. Hydrogel: Preparation, characterization, and applications. *Journal of Advanced Research* (0).
- (70) Kopecek, J. Polymer chemistry: Swell gels. *Nature* **2002**, *417* (6887), 388-391.
- (71) Hennink, W. E.; van Nostrum, C. F. Novel crosslinking methods to design hydrogels. *Advanced Drug Delivery Reviews* **2002**, *54* (1), 13-36.
- (72) Wang, Y.; Zhou, L.; Sun, G.; Xue, J.; Jia, Z.; Zhu, X.; Yan, D. Construction of different supramolecular polymer systems by combining the host–guest and hydrogen-bonding interactions. *Journal of Polymer Science Part B: Polymer Physics* **2008**, *46* (12), 1114-1120.
- (73) van de Manacker, F.; van der Pot, M.; Vermonden, T.; van Nostrum, C. F.; Hennink, W. E. Self-Assembling Hydrogels Based on  $\beta$ -Cyclodextrin/Cholesterol Inclusion Complexes. *Macromolecules* **2008**, *41* (5), 1766-1773.
- (74) de Jong, S. J.; De Smedt, S. C.; Wahls, M. W. C.; Demeester, J.; Kettenes-van den Bosch, J. J.; Hennink, W. E. Novel Self-assembled Hydrogels by Stereocomplex Formation in Aqueous Solution of Enantiomeric Lactic Acid Oligomers Grafted To Dextran. *Macromolecules* **2000**, *33* (10), 3680-3686.
- (75) Hunt, J. N.; Feldman, K. E.; Lynd, N. A.; Deek, J.; Campos, L. M.; Spruell, J. M.; Hernandez, B. M.; Kramer, E. J.; Hawker, C. J. Tunable, High Modulus Hydrogels Driven by Ionic Coacervation. *Advanced Materials* **2011**, *23* (20), 2327-2331.
- (76) Tuncaboylu, D. C.; Sari, M.; Oppermann, W.; Okay, O. Tough and Self-Healing Hydrogels Formed via Hydrophobic Interactions. *Macromolecules* **2011**, *44* (12), 4997-5005.
- (77) Wang, Q.; Mynar, J. L.; Yoshida, M.; Lee, E.; Lee, M.; Okuro, K.; Kinbara, K.; Aida, T. High-water-content mouldable hydrogels by mixing clay and a dendritic molecular binder. *Nature* **2010**, *463* (7279), 339-343.
- (78) Henderson, K. J.; Zhou, T. C.; Otim, K. J.; Shull, K. R. Ionically Cross-Linked Triblock Copolymer Hydrogels with High Strength. *Macromolecules* **2010**, *43* (14), 6193-6201.
- (79) Song, G.; Zhang, L.; He, C.; Fang, D.-C.; Whitten, P. G.; Wang, H. Facile Fabrication of Tough Hydrogels Physically Cross-Linked by Strong Cooperative Hydrogen Bonding. *Macromolecules* **2013**, *46* (18), 7423-7435.
- (80) Sun, J.-Y.; Zhao, X.; Illeperuma, W. R. K.; Chaudhuri, O.; Oh, K. H.; Mooney, D. J.; Vlassak, J. J.; Suo, Z. Highly stretchable and tough hydrogels. *Nature* **2012**, *489* (7414), 133-136.
- (81) Schexnailder, P.; Schmidt, G. Nanocomposite polymer hydrogels. *Colloid Polym Sci* **2009**, *287* (1), 1-11.
- (82) Haraguchi, K. Nanocomposite hydrogels. *Current Opinion in Solid State and Materials Science* **2007**, *11* (3–4), 47-54.
- (83) Gaharwar, A. K.; Peppas, N. A.; Khademhosseini, A. Nanocomposite hydrogels for biomedical applications. *Biotechnology and Bioengineering* **2014**, *111* (3), 441-453.
- (84) Agrawal, S. K.; Sanabria-DeLong, N.; Tew, G. N.; Bhatia, S. R. Nanoparticle-Reinforced Associative Network Hydrogels. *Langmuir* **2008**, *24* (22), 13148-13154.
- (85) Wang, Q.; Hou, R.; Cheng, Y.; Fu, J. Super-tough double-network hydrogels reinforced by covalently compositing with silica-nanoparticles. *Soft Matter* **2012**, *8* (22), 6048-6056.

- 
- (86) Gaharwar, A. K.; Dammu, S. A.; Canter, J. M.; Wu, C.-J.; Schmidt, G. Highly Extensible, Tough, and Elastomeric Nanocomposite Hydrogels from Poly(ethylene glycol) and Hydroxyapatite Nanoparticles. *Biomacromolecules* **2011**, *12* (5), 1641-1650.
- (87) Campbell, S. B.; Patenaude, M.; Hoare, T. Injectable Superparamagnets: Highly Elastic and Degradable Poly(N-isopropylacrylamide)–Superparamagnetic Iron Oxide Nanoparticle (SPION) Composite Hydrogels. *Biomacromolecules* **2013**, *14* (3), 644-653.
- (88) Shin, S. R.; Jung, S. M.; Zalabany, M.; Kim, K.; Zorlutuna, P.; Kim, S. b.; Nikkhah, M.; Khabiry, M.; Azize, M.; Kong, J.; Wan, K.-t.; Palacios, T.; Dokmeci, M. R.; Bae, H.; Tang, X.; Khademhosseini, A. Carbon-Nanotube-Embedded Hydrogel Sheets for Engineering Cardiac Constructs and Bioactuators. *ACS Nano* **2013**, *7* (3), 2369-2380.
- (89) Liu, D.; Chen, X.; Yue, Y.; Chen, M.; Wu, Q. Structure and rheology of nanocrystalline cellulose. *Carbohydrate Polymers* **2011**, *84* (1), 316-322.
- (90) Ureña-Benavides, E. E.; Ao, G.; Davis, V. A.; Kitchens, C. L. Rheology and Phase Behavior of Lyotropic Cellulose Nanocrystal Suspensions. *Macromolecules* **2011**, *44* (22), 8990-8998.
- (91) Shafiei-Sabet, S.; Hamad, W. Y.; Hatzikiriakos, S. G. Rheology of Nanocrystalline Cellulose Aqueous Suspensions. *Langmuir* **2012**, *28* (49), 17124-17133.
- (92) Boluk, Y.; Zhao, L.; Incani, V. Dispersions of Nanocrystalline Cellulose in Aqueous Polymer Solutions: Structure Formation of Colloidal Rods. *Langmuir* **2012**, *28* (14), 6114-6123.
- (93) Fler, G. J.; Scheutjens, J. M. H. M.; Stuart, M. A. C. Theoretical progress in polymer adsorption, steric stabilization and flocculation. *Colloids and Surfaces* **1988**, *31* (0), 1-29.
- (94) Fler, G. J. Polymers at interfaces and in colloidal dispersions. *Advances in Colloid and Interface Science* **2010**, *159* (2), 99-116.
- (95) Tadros, T. F. Industrial applications of dispersions. *Advances in Colloid and Interface Science* **1993**, *46* (0), 1-47.
- (96) McKee, J. R.; Hietala, S.; Seitsonen, J.; Laine, J.; Kontturi, E.; Ikkala, O. Thermoresponsive Nanocellulose Hydrogels with Tunable Mechanical Properties. *ACS Macro Letters* **2014**, *3* (3), 266-270.
- (97) Yang, J.; Zhao, J.-J.; Xu, F.; Sun, R.-C. Revealing Strong Nanocomposite Hydrogels Reinforced by Cellulose Nanocrystals: Insight into Morphologies and Interactions. *ACS Appl. Mater. Interfaces* **2013**, *5* (24), 12960-12967.
- (98) Abitbol, T.; Johnstone, T.; Quinn, T. M.; Gray, D. G. Reinforcement with cellulose nanocrystals of poly(vinyl alcohol) hydrogels prepared by cyclic freezing and thawing. *Soft Matter* **2011**, *7* (6), 2373-2379.
- (99) Lin, N.; Dufresne, A. Supramolecular Hydrogels from In Situ Host–Guest Inclusion between Chemically Modified Cellulose Nanocrystals and Cyclodextrin. *Biomacromolecules* **2013**, *14* (3), 871-880.
- (100) Yang, J.; Han, C.-r.; Xu, F.; Sun, R.-c. Simple approach to reinforce hydrogels with cellulose nanocrystals. *Nanoscale* **2014**, *6* (11), 5934-5943.
- (101) Yang, J.; Han, C.-R.; Zhang, X.-M.; Xu, F.; Sun, R.-C. Cellulose Nanocrystals Mechanical Reinforcement in Composite Hydrogels with Multiple Cross-Links: Correlations between Dissipation Properties and Deformation Mechanisms. *Macromolecules* **2014**, *47* (12), 4077-4086.

- 
- (102) Dash, R.; Foston, M.; Ragauskas, A. J. Improving the mechanical and thermal properties of gelatin hydrogels cross-linked by cellulose nanowhiskers. *Carbohydrate Polymers* **2013**, *91* (2), 638-645.
- (103) Yang, X.; Bakaic, E.; Hoare, T.; Cranston, E. D. Injectable Polysaccharide Hydrogels Reinforced with Cellulose Nanocrystals: Morphology, Rheology, Degradation, and Cytotoxicity. *Biomacromolecules* **2013**, *14* (12), 4447-4455.
- (104) Hunter, T. N.; Pugh, R. J.; Franks, G. V.; Jameson, G. J. The role of particles in stabilising foams and emulsions. *Advances in Colloid and Interface Science* **2008**, *137* (2), 57-81.
- (105) Aveyard, R.; Binks, B. P.; Clint, J. H. Emulsions stabilised solely by colloidal particles. *Advances in Colloid and Interface Science* **2003**, *100*, 503-546.
- (106) Binks, B. P. Particles as surfactants—similarities and differences. *Current Opinion in Colloid & Interface Science* **2002**, *7* (1-2), 21-41.
- (107) Pickering, S. U. Emulsions. *J. Chem. Soc.* **1907**, *91*, 2001-2021.
- (108) Ramsden, W. Separation of Solids in the Surface-Layers of Solutions and 'Suspensions' (Observations on Surface-Membranes, Bubbles, Emulsions, and Mechanical Coagulation). -- Preliminary Account. *Proceedings of the Royal Society of London* **1903**, *72* (477-486), 156-164.
- (109) Ashby, N. P.; Binks, B. P. Pickering emulsions stabilised by Laponite clay particles. *Physical Chemistry Chemical Physics* **2000**, *2* (24), 5640-5646.
- (110) Binks, B. P.; Horozov, T. S. Aqueous Foams Stabilized Solely by Silica Nanoparticles. *Angewandte Chemie International Edition* **2005**, *44* (24), 3722-3725.
- (111) Cui, Z. G.; Cui, C. F.; Zhu, Y.; Binks, B. P. Multiple Phase Inversion of Emulsions Stabilized by in Situ Surface Activation of CaCO<sub>3</sub> Nanoparticles via Adsorption of Fatty Acids. *Langmuir* **2012**, *28* (1), 314-320.
- (112) de Folter Julius, W. J.; Hutter Eline, M.; Castillo Sonja, I. R.; Klop Kira, E.; Philipse Albert, P.; Kegel Willem, K. Particle shape anisotropy in pickering emulsions: cubes and peanuts. *Langmuir* **2014**, *30* (4), 955-64.
- (113) He, X.; Ge, X.; Liu, H.; Zhou, H.; Zhang, Z. Self-assembly of latex particles at droplet interface to prepare monodisperse emulsion droplets. *Colloids and Surfaces A: Physicochemical and Engineering Aspects* **2007**, *301*, 80-84.
- (114) Qiao, X.; Zhou, J.; Binks, B. P.; Gong, X.; Sun, K. Magnetorheological behavior of Pickering emulsions stabilized by surface-modified Fe<sub>3</sub>O<sub>4</sub> nanoparticles. *Colloids and Surfaces A: Physicochemical and Engineering Aspects* **2012**, *412* (0), 20-28.
- (115) Ngai, T.; Auweter, H.; Behrens, S. H. Environmental Responsiveness of Microgel Particles and Particle-Stabilized Emulsions. *Macromolecules* **2006**, *39*, 8171-8177.
- (116) Zhang, J.; Li, L.; Wang, J.; Sun, H.; Xu, J.; Sun, D. Double Inversion of Emulsions Induced by Salt Concentration. *Langmuir* **2012**, *28* (17), 6769-6775.
- (117) Binks, B. P.; Duncumb, B.; Murakami, R. Effect of pH and Salt Concentration on the Phase Inversion of Particle-Stabilized Foams. *Langmuir* **2007**, *23* (18), 9143-9146.
- (118) Shinoda, K.; Moriyama, N.; Hattori, K. The correlation between the hydrophile-lipophile balance of nonionic surfactants, the temperature and the stability of polyethylene-water suspensions. *Journal of Colloid and Interface Science* **1969**, *30* (2), 270-271.
- (119) Binks, B. P.; Fletcher, P. D. I.; Holt, B. L.; Parker, J.; Beaussoubre, P.; Wong, K. Drop sizes and particle coverage in emulsions stabilised solely by silica nanoparticles of irregular shape. *Physical Chemistry Chemical Physics* **2010**, *12* (38), 11967-11974.

- 
- (120) Aveyard, R.; Binks, B. P.; Clint, J. H. Emulsions stabilised solely by colloidal particles. *Advances in Colloid and Interface Science* **2003**, *100–102*, 503-546.
- (121) Binks, B. P.; Lumsdon, S. O. Influence of Particle Wettability on the Type and Stability of Surfactant-Free Emulsions†. *Langmuir* **2000**, *16* (23), 8622-8631.
- (122) Wang, W.; Zhou, Z.; Nandakumar, K.; Xu, Z.; Masliyah, J. H. Effect of charged colloidal particles on adsorption of surfactants at oil–water interface. *Journal of Colloid and Interface Science* **2004**, *274* (2), 625-630.
- (123) Saleh, N.; Sarbu, T.; Sirk, K.; Lowry, G. V.; Matyjaszewski, K.; Tilton, R. D. Oil-in-Water Emulsions Stabilized by Highly Charged Polyelectrolyte-Grafted Silica Nanoparticles†. *Langmuir* **2005**, *21* (22), 9873-9878.
- (124) Vignati, E.; Piazza, R.; Lockhart, T. P. Pickering Emulsions: Interfacial Tension, Colloidal Layer Morphology, and Trapped-Particle Motion. *Langmuir* **2003**, *19* (17), 6650-6656.
- (125) Binks, B. P.; Horozov, T. S.; Bergström, L.; Fernández-Toledano, J. C.; Moncho-Jordá, A.; Martínez-López, F.; Hidalgo-Álvarez, R.; Goedel, W. A.; Fuller, G. G.; Stancik, E. J.; Melle, S.; Lopetinsky, R. J. G.; Masliyah, J. H.; Xu, Z.; Velikov, K. P.; Velev, O. D.; Dickinson, E.; Nguyen, A. V.; Jameson, G. J.; Pugh, R. J.; Denkov, N. D.; Marinova, K. G.; Babcsán, N.; Banhart, J. *Colloidal Particles at Liquid Interfaces*. Cambridge University Press: Cambridge, **2008**; p 520.
- (126) Levine, S.; Bowen, B. D.; Partridge, S. J. Stabilization of emulsions by fine particles I. Partitioning of particles between continuous phase and oil/water interface. *Colloids and Surfaces* **1989**, *38* (2), 325-343.
- (127) Ghouchi Eskandar, N.; Simovic, S.; Prestidge, C. A. Synergistic effect of silica nanoparticles and charged surfactants in the formation and stability of submicron oil-in-water emulsions. *Physical Chemistry Chemical Physics* **2007**, *9* (48), 6426-6434.
- (128) Pichot, R.; Spyropoulos, F.; Norton, I. T. O/W emulsions stabilised by both low molecular weight surfactants and colloidal particles: The effect of surfactant type and concentration. *Journal of Colloid and Interface Science* **2010**, *352* (1), 128-135.
- (129) Katepalli, H.; John, V. T.; Bose, A. The Response of Carbon Black Stabilized Oil-in-Water Emulsions to the Addition of Surfactant Solutions. *Langmuir* **2013**, *29* (23), 6790-6797.
- (130) Lam, S.; Velikov, K. P.; Velev, O. D. Pickering stabilization of foams and emulsions with particles of biological origin. *Current Opinion in Colloid & Interface Science* (0).
- (131) Midmore, B. R. Synergy between silica and polyoxyethylene surfactants in the formation of O/W emulsions. *Colloids and Surfaces A: Physicochemical and Engineering Aspects* **1998**, *145* (1–3), 133-143.
- (132) Binks, B. P.; Desforges, A.; Duff, D. G. Synergistic Stabilization of Emulsions by a Mixture of Surface-Active Nanoparticles and Surfactant. *Langmuir* **2006**, *23* (3), 1098-1106.
- (133) Binks, B. P.; Rodrigues, J. A. Enhanced Stabilization of Emulsions Due to Surfactant-Induced Nanoparticle Flocculation. *Langmuir* **2007**, *23* (14), 7436-7439.
- (134) Akartuna, I.; Studart, A. R.; Tervoort, E.; Gonzenbach, U. T.; Gauckler, L. J. Stabilization of Oil-in-Water Emulsions by Colloidal Particles Modified with Short Amphiphiles. *Langmuir* **2008**, *24* (14), 7161-7168.
- (135) Lan, Q.; Yang, F.; Zhang, S.; Liu, S.; Xu, H.; Sun, D. Synergistic effect of silica nanoparticle and cetyltrimethyl ammonium bromide on the stabilization of O/W

- emulsions. *Colloids and Surfaces a-Physicochemical and Engineering Aspects* **2007**, *302* (1-3), 126-135.
- (136) Ma, H.; Luo, M.; Dai, L. L. Influences of surfactant and nanoparticle assembly on effective interfacial tensions. *Physical Chemistry Chemical Physics* **2008**, *10* (16), 2207-2213.
- (137) Luo, M.; Song, Y.; Dai, L. L. Heterogeneous or competitive self-assembly of surfactants and nanoparticles at liquid-liquid interfaces. *Molecular Simulation* **2009**, *35* (10-11), 773-784.
- (138) Binks, B. P.; Rodrigues, J. A. Double inversion of emulsions by using nanoparticles and a di-chain surfactant. *Angewandte Chemie, International Edition* **2007**, *46* (28), 5389-5392.
- (139) Binks, B. P.; Isa, L.; Tyowua, A. T. Direct Measurement of Contact Angles of Silica Particles in Relation to Double Inversion of Pickering Emulsions. *Langmuir* **2013**, *29* (16), 4923-4927.
- (140) Cui, Z. G.; Yang, L. L.; Cui, Y. Z.; Binks, B. P. Effects of Surfactant Structure on the Phase Inversion of Emulsions Stabilized by Mixtures of Silica Nanoparticles and Cationic Surfactant. *Langmuir* **2010**, *26* (7), 4717-4724.
- (141) Saleh, N.; Phenrat, T.; Sirk, K.; Dufour, B.; Ok, J.; Sarbu, T.; Matyjaszewski, K.; Tilton, R. D.; Lowry, G. V. Adsorbed Triblock Copolymers Deliver Reactive Iron Nanoparticles to the Oil/Water Interface. *Nano Letters* **2005**, *5* (12), 2489-2494.
- (142) Feng, T.; Hoagland, D. A.; Russell, T. P. Assembly of Acid-Functionalized Single-Walled Carbon Nanotubes at Oil/Water Interfaces. *Langmuir* **2014**, *30* (4), 1072-1079.
- (143) Saigal, T.; Dong, H.; Matyjaszewski, K.; Tilton, R. R. D. *Langmuir* **2010**, *26*, 15200.
- (144) Vashisth, C.; Whitby, C. P.; Fornasiero, D.; Ralston, J. Interfacial displacement of nanoparticles by surfactant molecules in emulsions. *Journal of Colloid and Interface Science* **2010**, *349* (2), 537-543.
- (145) Whitby, C. P.; Fornasiero, D.; Ralston, J. Effect of adding anionic surfactant on the stability of Pickering emulsions. *Journal of Colloid and Interface Science* **2009**, *329* (1), 173-181.
- (146) Tan, Y.; Xu, K.; Niu, C.; Liu, C.; Li, Y.; Wang, P.; Binks, B. P. Triglyceride-water emulsions stabilised by starch-based nanoparticles. *Food Hydrocolloids* **2014**, *36* (0), 70-75.
- (147) Nilsson, L.; Bergenståhl, B. Emulsification and Adsorption Properties of Hydrophobically Modified Potato and Barley Starch. *Journal of Agricultural and Food Chemistry* **2007**, *55* (4), 1469-1474.
- (148) Perrin, E.; Bizot, H.; Cathala, B.; Capron, I. Chitin Nanocrystals for Pickering High Internal Phase Emulsions. *Biomacromolecules* **2014**, *15* (10), 3766-3771.
- (149) Tzoumaki, M. V.; Moschakis, T.; Kiosseoglou, V.; Biliaderis, C. G. Oil-in-water emulsions stabilized by chitin nanocrystal particles. *Food Hydrocolloids* **2011**, *25* (6), 1521-1529.
- (150) Kargar, M.; Fayazmanesh, K.; Alavi, M.; Spyropoulos, F.; Norton, I. T. Investigation into the potential ability of Pickering emulsions (food-grade particles) to enhance the oxidative stability of oil-in-water emulsions. *Journal of Colloid and Interface Science* **2012**, *366* (1), 209-215.
- (151) Oza, K. P.; Frank, S. G. Microcrystalline cellulose stabilized emulsions. *J. Dispersion Sci. Technol.* **1986**, *7* (5), 543-561.

- (152) Lif, A.; Stensrad, P.; Syverud, K.; Nyden, M.; Holmberg, K. Fischer Tropsch diesel emulsions stabilised by microfibrillated cellulose and non ionic surfactants. *Journal of Colloid and Interface Science* **2010**, *352* (2), 585-592.
- (153) Khanari, K.; Syverud, K.; Chinga-Carrasco, G.; Paso, K.; Stenius, P. Structure of nanofibrillated cellulose layers at the o/w interface. *Journal of Colloid and Interface Science* **2011**, *356* (1), 58-62.
- (154) Kalashnikova, I.; Bizot, H.; Bertoncini, P.; Cathala, B.; Capron, I. Cellulosic Nanorods of Various Aspect Ratios for Oil in Water Pickering Emulsions. *Soft Matter* **2013**, *9* (3), 952-959.
- (155) Capron, I.; Cathala, B. Surfactant-Free High Internal Phase Emulsions Stabilized by Cellulose Nanocrystals. *Biomacromolecules* **2013**, *14* (2), 291-296.
- (156) Kalashnikova, I.; Bizot, H.; Cathala, B.; Capron, I. New Pickering Emulsions Stabilized by Bacterial Cellulose Nanocrystals. *Langmuir* **2011**, *27* (12), 7471-7479.
- (157) Lee, K.-Y.; Blaker, J. J.; Murakami, R.; Heng, J. Y. Y.; Bismarck, A. Phase Behavior of Medium and High Internal Phase Water-in-Oil Emulsions Stabilized Solely by Hydrophobized Bacterial Cellulose Nanofibrils. *Langmuir* **2013**, *30* (2), 452-460.
- (158) Blaker, J. J.; Lee, K.-Y.; Li, X.; Menner, A.; Bismarck, A. Renewable nanocomposite polymer foams synthesized from Pickering emulsion templates. *Green Chemistry* **2009**, *11* (9), 1321-1326.
- (159) Wege, H. A.; Kim, S.; Paunov, V. N.; Zhong, Q.; Velev, O. D. Long-Term Stabilization of Foams and Emulsions with In-Situ Formed Microparticles from Hydrophobic Cellulose. *Langmuir* **2008**, *24* (17), 9245-9253.
- (160) Ougiya, H.; Watanabe, K.; Morinaga, Y.; Yoshinaga, F. Emulsion-stabilizing Effect of Bacterial Cellulose. *Bioscience, Biotechnology, and Biochemistry* **1997**, *61* (9), 1541-1545.
- (161) Oza, K. P.; Frank, S. G. MICROCRYSTALLINE CELLULOSE STABILIZED EMULSIONS. *Journal of Dispersion Science and Technology* **1986**, *7* (5), 543-561.
- (162) Kalashnikova, I.; Bizot, H.; Cathala, B.; Capron, I. Modulation of Cellulose Nanocrystals Amphiphilic Properties to Stabilize Oil/Water Interface. *Biomacromolecules* **2011**, *13* (1), 267-275.
- (163) Lif, A.; Stenstad, P.; Syverud, K.; Nydén, M.; Holmberg, K. Fischer-Tropsch diesel emulsions stabilised by microfibrillated cellulose and nonionic surfactants. *Journal of Colloid and Interface Science* **2010**, *352* (2), 585-592.
- (164) Hu, Z.; Ballinger, S.; Pelton, R.; Cranston, E. D. Surfactant-enhanced cellulose nanocrystal Pickering emulsions. *Journal of Colloid and Interface Science* **2015**, *439* (0), 139-148.
- (165) Tasset, S.; Cathala, B.; Bizot, H.; Capron, I. Versatile cellular foams derived from CNC-stabilized Pickering emulsions. *RSC Adv.* **2014**, *4* (2), 893-898.
- (166) Nypelö, T.; Rodriguez-Abreu, C.; Kolen'ko, Y. V.; Rivas, J.; Rojas, O. J. Microbeads and Hollow Microcapsules Obtained by Self-Assembly of Pickering Magneto-Responsive Cellulose Nanocrystals. *ACS Appl. Mater. Interfaces* **2014**, *6* (19), 16851-16858.
- (167) Li, Y.; Ko, F. K.; Hamad, W. Y. Effects of Emulsion Droplet Size on the Structure of Electrospun Ultrafine Biocomposite Fibers with Cellulose Nanocrystals. *Biomacromolecules* **2013**, *14* (11), 3801-3807.

- 
- (168) Exerowa, D. K., P. M. *Foams and Foam Films*. Elsevier: Amsterdam, **1997**.
- (169) Murray, B. S.; Ettelaie, R. Foam stability: proteins and nanoparticles. *Current Opinion in Colloid & Interface Science* **2004**, *9* (5), 314-320.
- (170) Horozov, T. S. Foams and foam films stabilised by solid particles. *Current Opinion in Colloid & Interface Science* **2008**, *13* (3), 134-140.
- (171) Du, Z.; Bilbao-Montoya, M. P.; Binks, B. P.; Dickinson, E.; Ettelaie, R.; Murray, B. S. Outstanding Stability of Particle-Stabilized Bubbles. *Langmuir* **2003**, *19* (8), 3106-3108.
- (172) Dickinson, E.; Ettelaie, R.; Kostakis, T.; Murray, B. S. Factors Controlling the Formation and Stability of Air Bubbles Stabilized by Partially Hydrophobic Silica Nanoparticles. *Langmuir* **2004**, *20* (20), 8517-8525.
- (173) Yang, S.; Razavizadeh, B. B. M.; Pelton, R.; Bruin, G. Nanoparticle Flotation Collectors—The Influence of Particle Softness. *ACS Appl. Mater. Interfaces* **2013**, *5* (11), 4836-4842.
- (174) Yang, S.; Pelton, R.; Montgomery, M.; Cui, Y. Nanoparticle Flotation Collectors III: The Role of Nanoparticle Diameter. *ACS Appl. Mater. Interfaces* **2012**, *4* (9), 4882-4890.
- (175) Yang, S.; Pelton, R. Nanoparticle Flotation Collectors II: The Role of Nanoparticle Hydrophobicity. *Langmuir* **2011**, *27* (18), 11409-11415.
- (176) Yang, S.; Pelton, R.; Raegen, A.; Montgomery, M.; Dalnoki-Veress, K. Nanoparticle Flotation Collectors: Mechanisms Behind a New Technology. *Langmuir* **2011**, *27* (17), 10438-10446.
- (177) Guevara, J. S.; Mejia, A. F.; Shuai, M.; Chang, Y.-W.; Mannan, M. S.; Cheng, Z. Stabilization of Pickering foams by high-aspect-ratio nano-sheets. *Soft Matter* **2013**, *9* (4), 1327-1336.
- (178) Lam, S.; Blanco, E.; Smoukov, S. K.; Velikov, K. P.; Veleev, O. D. Magnetically Responsive Pickering Foams. *Journal of the American Chemical Society* **2011**, *133* (35), 13856-13859.
- (179) Pugh, R. J. Foaming in Chemical Surfactant Free Aqueous Dispersions of Anatase (Titanium Dioxide) Particles. *Langmuir* **2007**, *23* (15), 7972-7980.
- (180) Fujii, S.; Iddon, P. D.; Ryan, A. J.; Armes, S. P. Aqueous Particulate Foams Stabilized Solely with Polymer Latex Particles. *Langmuir* **2006**, *22* (18), 7512-7520.
- (181) Zhou, W.; Cao, J.; Liu, W.; Stoyanov, S. How Rigid Rods Self-Assemble at Curved Surfaces. *Angewandte Chemie International Edition* **2009**, *48* (2), 378-381.
- (182) Murray, B. S.; Durga, K.; de Groot, P. W. N.; Kakoulli, A.; Stoyanov, S. D. Preparation and Characterization of the Foam-Stabilizing Properties of Cellulose–Ethyl Cellulose Complexes for Use in Foods. *Journal of Agricultural and Food Chemistry* **2011**, *59* (24), 13277-13288.
- (183) Wege, H. A.; Kim, S.; Paunv, V. N.; Zhong, Q.; Veleev, O. D. Long-term stabilization of foams and emulsions with in-situ formed microparticles from hydrophobic cellulose. *Langmuir* **2008**, *24*, 9245-9253.
- (184) Cervin, N. T.; Andersson, L.; Ng, J. B. S.; Olin, P.; Bergström, L.; Wågberg, L. Lightweight and Strong Cellulose Materials Made from Aqueous Foams Stabilized by Nanofibrillated Cellulose. *Biomacromolecules* **2012**, *14* (2), 503-511.
- (185) Maestro, A.; Rio, E.; Drenckhan, W.; Langevin, D.; Salonen, A. Foams stabilised by mixtures of nanoparticles and oppositely charged surfactants: relationship between bubble shrinkage and foam coarsening. *Soft Matter* **2014**, *10* (36), 6975-6983.

- 
- (186) Binks, B. P.; Kirkland, M.; Rodrigues, J. A. Origin of stabilisation of aqueous foams in nanoparticle-surfactant mixtures. *Soft Matter* **2008**, *4* (12), 2373-2382.
- (187) Al-Qararah, A. M.; Hjelt, T.; Koponen, A.; Harlin, A.; Ketoja, J. A. Bubble size and air content of wet fibre foams in axial mixing with macro-instabilities. *Colloids and Surfaces A: Physicochemical and Engineering Aspects* **2013**, *436* (0), 1130-1139.
- (188) Jin, H.; Zhou, W.; Cao, J.; Stoyanov, S. D.; Blijdenstein, T. B. J.; de Groot, P. W. N.; Arnaudov, L. N.; Pelan, E. G. Super stable foams stabilized by colloidal ethyl cellulose particles. *Soft Matter* **2012**, *8* (7), 2194-2205.
- (189) Shastri, V. P.; Martin, I.; Langer, R. Macroporous polymer foams by hydrocarbon templating. *Proceedings of the National Academy of Sciences* **2000**, *97* (5), 1970-1975.
- (190) Gibson, L. A., M. *Cellular Solids: Structure and Properties*. Pergamon: Oxford, **1997**.
- (191) Mihai, M.; Huneault, M. A.; Favis, B. D.; Li, H. Extrusion Foaming of Semi-Crystalline PLA and PLA/Thermoplastic Starch Blends. *Macromolecular Bioscience* **2007**, *7* (7), 907-920.
- (192) Blaker, J. J.; Maquet, V.; Jérôme, R.; Boccaccini, A. R.; Nazhat, S. N. Mechanical properties of highly porous PDLLA/Bioglass® composite foams as scaffolds for bone tissue engineering. *Acta Biomaterialia* **2005**, *1* (6), 643-652.
- (193) Cameron, N. R. High internal phase emulsion templating as a route to well-defined porous polymers. *Polymer* **2005**, *46* (5), 1439-1449.
- (194) Kimmins, S. D.; Cameron, N. R. Functional Porous Polymers by Emulsion Templating: Recent Advances. *Advanced Functional Materials* **2011**, *21* (2), 211-225.
- (195) Wu, D.; Xu, F.; Sun, B.; Fu, R.; He, H.; Matyjaszewski, K. Design and Preparation of Porous Polymers. *Chemical Reviews* **2012**, *112* (7), 3959-4015.
- (196) Menner, A.; Haibach, K.; Powell, R.; Bismarck, A. Tough reinforced open porous polymer foams via concentrated emulsion templating. *Polymer* **2006**, *47* (22), 7628-7635.
- (197) Barbetta, A.; Cameron, N. R. Morphology and Surface Area of Emulsion-Derived (PolyHIPE) Solid Foams Prepared with Oil-Phase Soluble Porogenic Solvents: Span 80 as Surfactant. *Macromolecules* **2004**, *37* (9), 3188-3201.
- (198) Menner, A.; Ikem, V.; Salgueiro, M.; Shaffer, M. S. P.; Bismarck, A. High internal phase emulsion templates solely stabilised by functionalised titania nanoparticles. *Chemical Communications* **2007**, (41), 4274-4276.
- (199) Ikem, V. O.; Menner, A.; Bismarck, A. High Internal Phase Emulsions Stabilized Solely by Functionalized Silica Particles. *Angewandte Chemie International Edition* **2008**, *47* (43), 8277-8279.
- (200) Menner, A.; Verdejo, R.; Shaffer, M.; Bismarck, A. Particle-Stabilized Surfactant-Free Medium Internal Phase Emulsions as Templates for Porous Nanocomposite Materials: poly-Pickering-Foams. *Langmuir* **2007**, *23* (5), 2398-2403.
- (201) Colver, P. J.; Bon, S. A. F. Cellular Polymer Monoliths Made via Pickering High Internal Phase Emulsions. *Chemistry of Materials* **2007**, *19* (7), 1537-1539.
- (202) Vílchez, A.; Rodríguez-Abreu, C.; Esquena, J.; Menner, A.; Bismarck, A. Macroporous Polymers Obtained in Highly Concentrated Emulsions Stabilized Solely with Magnetic Nanoparticles. *Langmuir* **2011**, *27* (21), 13342-13352.
- (203) Ikem, V. O.; Menner, A.; Bismarck, A. High-Porosity Macroporous Polymers Synthesized from Titania-Particle-Stabilized Medium and High Internal Phase Emulsions. *Langmuir* **2010**, *26* (11), 8836-8841.

- (204) Hu, Z.; Cranston, E. D.; Ng, R.; Pelton, R. Tuning Cellulose Nanocrystal Gelation with Polysaccharides and Surfactants. *Langmuir* **2014**, *30*, 2684-2692.

## **Chapter 2 Tuning Cellulose Nanocrystal Gelation with Polysaccharides and Surfactants**

In chapter 2, all experiments were conducted by myself with assistance from Robin Ng (undergraduate student). Dr. Robert Pelton aided in the modelling of volume fraction increase and gelation after polymer adsorption. The paper was initially drafted by myself, and edited later to final version by Dr. Robert Pelton and Dr. Emily D. Cranston. This chapter has been published in *Langmuir*, 2014, 30 (10), pp 2684–2692. Copyright © 2014 American Chemical Society.

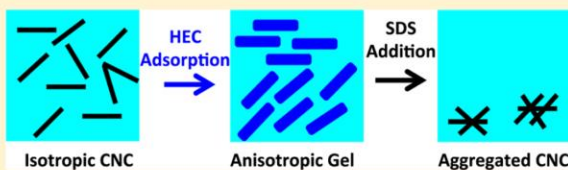
## Tuning Cellulose Nanocrystal Gelation with Polysaccharides and Surfactants

Zhen Hu, Emily D. Cranston, Robin Ng, and Robert Pelton\*

Department of Chemical Engineering, McMaster University, Hamilton, Canada L8S 4L71

### Supporting Information

**ABSTRACT:** Gelation of cellulose nanocrystal (CNC) dispersions was measured as a function of the presence of four nonionic polysaccharides. Addition of hydroxyethyl cellulose (HEC), hydroxypropyl guar (HPG), or locust bean gum (LBG) to CNC dispersions induced the gelation of dilute CNC dispersions, whereas dextran (DEX) did not. These behaviors correlated with adsorption tendencies; HEC, HPG, and LBG adsorbed onto CNC-coated quartz crystal microbalance sensors, whereas DEX did not adsorb. We propose that the adsorbing polysaccharides greatly increased the effective volume fraction of dilute CNC dispersions, driving more of the nanocrystals into anisotropic domains. SDS and Triton X-100 addition disrupted HEC–CNC gels whereas CTAB did not. Surface plasmon resonance measurements with CNC-coated sensors showed that SDS and Triton X-100 partially removed adsorbed HEC, whereas CTAB did not. These behaviors illustrate the complexities associated with including CNC dispersions in formulated products: low CNC contents can induce spectacular changes in rheology; however, surfactants and soluble polymers may promote gel formation or induce CNC coagulation.



### INTRODUCTION

Although cellulose nanocrystals (CNC) were first reported in 1949,<sup>1</sup> only now is CNC entering the marketplace in commercial scale quantities. Also called nanocrystalline cellulose or cellulose whiskers, CNC particles are stiff colloidal sized rods, approximately  $100 \times 10 \times 10 \text{ nm}^{3,2,3}$ . Aqueous CNC suspensions can be colloidally stable in water because of surface charged sulfate half-ester, carboxylate, or phosphate ester groups,<sup>4</sup> depending on the CNC preparation method. As a new, green, and sustainable material, CNC is currently being evaluated in a variety of applications, including as reinforcing materials in nanocomposites,<sup>5</sup> as stabilizers for emulsions and foams,<sup>6</sup> and as components of drilling fluids.<sup>7</sup> The recent patent literature is rich with descriptions of many other potential applications, many of which exploit the intrinsic thickening and gelation properties of small rod-shaped particles. However, most formulated chemical products, including food and cosmetics, are complex mixtures of surfactants and polymers in relatively high ionic strength solutions. Herein we set out initial results describing the influence of nonionic, water-soluble polymers on the rheological and gelation behaviors of CNC dispersions at high ionic strength. In addition, we show that surfactants alter the behavior of CNC–polymer mixtures. Our ultimate goal is to develop generic design rules for CNC-containing formulations. The following paragraphs summarize the relevant literature.

**CNC Phase Behavior.** Colloidal stability has a profound influence on CNC dispersion behavior. Colloidally unstable CNC particles adhere upon contact giving precipitates with dilute dispersions and a space filling gel floc for concentrated dispersions. Sulfated CNC particles are electrostatically

stabilized by high surface charge densities of approximately 1 charge group for every 10 surface anhydroglucose units.<sup>8</sup> The critical coagulation concentration of NaCl for sulfated CNC<sup>9–11</sup> and for much longer nanofibrillated cellulose<sup>12</sup> is in the range 10–50 mM, whereas Araki<sup>13</sup> reported aggregation of carboxylated CNC between 100 and 500 mM NaCl.

Colloidally stable dispersions of rod-shaped particles undergo isotropic phase-to-isotropic phase + anisotropic phase transitions at low volume fractions, behaviors predicted by Onsager,<sup>14</sup> Flory,<sup>15</sup> and others.<sup>16</sup> Dong et al. published a detailed study of the phase compositions as functions of electrolyte concentration and counterion type.<sup>17,18</sup> Because they found that the major features of their experimental results were captured with SLO (Stroobants, Lekkerkerker, Odijk) theory,<sup>16,19</sup> we show some of the model's predictions in Figure 1 as plots of the volume fractions of the anisotropic (presumed to be nematic) phase,  $\phi_a$ , as functions of the overall CNC concentration. The model parameters, including  $1/\kappa$ , the Debye length, and  $D_e$ , the effective diameter of the CNC rods, are shown in the Figure. The biphasic regions sits between two CNC concentrations;  $C_1$  is the CNC concentration corresponding to the isotropic phase-to-isotropic phase + anisotropic phase transition, and  $C_2$  is the total CNC concentration at which the isotropic phase disappears. For the middle curve in Figure 1, the biphasic (isotropic + anisotropic) region falls in the narrow CNC concentration range between  $C_1 = 36 \text{ g/L}$  and  $C_2 = 47 \text{ g/L}$ .

**Received:** December 30, 2013

**Revised:** February 16, 2014

**Published:** February 23, 2014

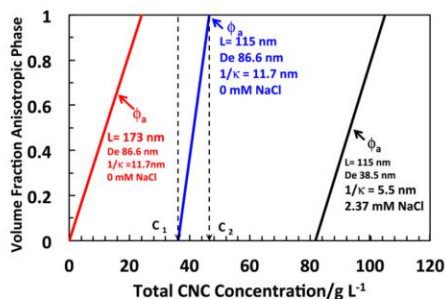


**Figure 1.** Schematic illustration of CNC phase behaviors modeled by SLO theory.<sup>16,19</sup> Parameters for the two  $L = 115$  nm curves were taken directly from Table 2 of Dong et al.<sup>17</sup>  $L$  is the nanocrystals length,  $De$  is the nanocrystals effective width, and  $1/\kappa$  is the Debye length.

Comparison of the three cases in Figure 1 illustrates two important variables controlling phase behavior. Salt addition lowered the effective diameter of the nanocrystals,  $De$ , shifting the biphasic region to higher concentrations and broadening the range of the biphasic region. By contrast, the SLO model predicts that lengthening the CNC particles by 50% shifts the biphasic region to a much lower CNC concentration, while increasing the width of the biphasic region.

We emphasize that the simulated phase behaviors in Figure 1 are approximate—Dong et al.<sup>17,18</sup> showed that CNC concentrations are not constant in the biphasic regions. Furthermore, Wierenga and Philipse<sup>20</sup> make the interesting point that rod suspensions are often present as unstable glasses if the rods have insufficient mobility to form the thermodynamically favored mixed phases.

CNC is a promising additive for aqueous formulations because low concentrations can give large increases in viscosities.<sup>9,21–24</sup> Our focus is on the interplay of water-soluble polymers and surfactants with CNC rheology and gel formation. The first publications describing CNC were from Gray's group and described interactions with water-soluble polymers dextran (DEX) and dye-labeled dextran.<sup>25–27</sup> Neither dextran nor the labeled dextran adsorbed onto the sulfated CNC surfaces. Furthermore, nonionic dextran did not influence the phase behavior of anisotropic suspensions (i.e., CNC concentrations  $> C_2$ ). By contrast, dextran labeled with ionic dyes shifted  $C_2$  to higher values, giving a coexisting isotropic phase. Some combinations of nonionic dextran and labeled ionic dextran gave two isotropic phases in equilibrium with the anisotropic phase.

Boluk<sup>28</sup> reported dynamic viscosity measurements of dilute CNC suspensions in hydroxyethyl cellulose (HEC) or carboxymethyl cellulose (CMC) solutions. HEC is a popular thickener for formulated chemical products because the polymer does not interact strongly with surfactants<sup>29</sup> and tends not to adsorb onto surfactant-coated surfaces.<sup>30</sup> They found that CNC greatly increased the viscosity of HEC solutions to the point of giving very weak gels. On the basis of isothermal titration calorimetry results, it was proposed that HEC did not adsorb onto CNC surfaces and that increased viscosities were due to depletion induced attractive interactions between CNC particles.

Surfactants are present in most formulated chemical products. Although not classical surfactants, Beck-Candanedo reported the influence of ionic dyes on the phase behavior of completely anisotropic dispersions (i.e., CNC concentration  $>$

$C_2$ ).<sup>31</sup> Cationic and other cellulose adsorptive dyes had no influence on the phase behavior, whereas dyes that remained in solution caused the formation of a coexisting isotropic phase. In other words,  $C_2$  was shifted to much higher CNC concentrations upon introduction of nonadsorbing soluble dyes. Tam's group reported cationic surfactant interactions with both sulfated CNC particles<sup>32</sup> and with CNC particles with grafted polypropylene glycol oligomers.<sup>33</sup> They showed that cationic surfactant strongly binds to sulfated CNC particles; low surfactant dosages caused aggregation whereas colloidal stable cationic CNC particles were obtained with high dosages. Finally, we have found no publications describing the properties of CNC suspensions in mixtures of surfactants with water-soluble polymers—a common situation with formulated products. Herein we report results of an initial investigation that shows the critical feature is whether or not the polysaccharides adsorb onto CNC surfaces.

## EXPERIMENTAL SECTION

**Materials and Methods.** Hydroxypropyl guar (HPG,  $2.5 \times 10^6$  Da, degree of substitution (DS) of 0.36) was obtained from Alcon Laboratories (Fort Worth, TX). Sigma-Aldrich provided hydroxyethyl celluloses: HEC250 MW = 250 kDa, DS = 1, and molar substitution (MS) = 2; HEC720 MW = 720 kDa, DS n/a, and MS = 2.5; and, HEC1300 MW = 1300 kDa, DS n/a, and MS = 2.5. Locust beam gum (LBG, 310 kDa), dextran (DEX, 2000 kDa), sodium dodecyl sulfate (SDS), cetyltrimethylammonium bromide (CTAB), poly(ethylene glycol) *p*-(1,1,3,3-tetramethylbutyl)phenyl ether (Triton X-100), HEPES (4-(2-hydroxyethyl)-1-piperazineethanesulfonic acid) buffer, TEMPO (2,2,6,6-tetramethylpiperidin-1-yl)oxidanyl, sodium bromide, and sodium hypochlorite (NaClO, available chlorine, 10–15%) were all obtained from Sigma-Aldrich. The water used in all solutions was deionized and further purified with a Barnstead Nanopure Diamond system (Thermo Scientific, Asheville, NC).

**Sulfuric Acid Hydrolysis of Cellulose.** Following Revol et al., CNC was prepared by sulfuric acid hydrolysis of cotton from cotton filter aid (Whatman ashless filter aid, GE Healthcare Canada, Mississauga, Canada).<sup>3</sup> 40 g of the filter aid was treated with 700 mL of 64 wt % sulfuric acid (Fischer Scientific) at 45 °C for 45 min with constant stirring (mechanical stirrer) in a water bath. Immediately following the acid hydrolysis, the suspension was diluted 10-fold with water to quench the reaction. The suspension was centrifuged at 6000 rpm for 10 min four times to concentrate the cellulose and to remove excess aqueous acid. The precipitate was then rinsed, centrifuged, and dialyzed against water for 2 weeks until the pH of external dialysis reservoir stabilized. The suspension was sonicated in continuous mode for 30 min (Sonifier 450, Branson Ultrasonics, Danbury, CT) at 50% output while cooling in an ice bath to prevent overheating in order to unhinge any loosely bound CNC particles. Dowex Marathon C hydrogen-form resin (Sigma-Aldrich) was introduced to the cellulose suspension for 48 h and then removed by filtering through hardened ashless filter paper (Whatman 541). The resultant aqueous suspension was approximately 1 wt % cellulose, and the concentration was increased by evaporation at ambient conditions. The surface charge density of CNC was calculated to be  $0.16 \pm 0.02$  mequiv/g as measured by conductometric titration, with average crystal dimensions of  $128 \times 7$  nm from transmission electron microscopy (TEM) images. A small amount of toluene (50  $\mu$ L per 1 L of suspension) was added to the cellulose suspension to avoid bacterial growth.

**Hydrochloric Acid Hydrolysis of Cellulose and TEMPO Oxidation.** 10 g of the cotton filter aid was hydrolyzed with 2.5 M HCl at 70 °C for 2 h as described by Kalashnikova et al.<sup>6</sup> Acid was removed by successive centrifugations at 6000 rpm for 10 min and redispersion of the solid materials in purified water until pH was above 5. The resultant precipitate was then dialyzed against water for 2 weeks to remove any remaining contaminants, deionized by mixing with mixed bed ion-exchange resin, and concentrated to constitute the stock suspension, which was used to prepare oxidized cellulose

nanocrystals. Oxidation experiments were carried out as previously published with minor modifications.<sup>34</sup> 10 mg of TEMPO and 200 mg of sodium bromide were added while magnetically stirring the cellulose suspension (60 mL of 1 wt %) that had previously been sonicated for 3 min. The TEMPO-mediated oxidation of the cellulose nanocrystals was initiated by slowly adding 4.9 mL of NaClO over 20 min at room temperature under stirring. The reaction pH was maintained constant at 10 by adding 1 M NaOH solution until the pH was stable, indicating that the reaction was finished. About 5 mL of methanol was then added to quench the extra oxidant. After adjusting the pH to 7 by adding 1 M HCl, the TEMPO-oxidized product was rinsed with purified water by centrifugation and further purified by dialysis against water for a week. The carboxylic content in the oxidized cellulose nanocrystals, with average dimensions of  $119 \times 8$  nm from TEM images, was determined to be  $0.20 \pm 0.04$  mequiv/g by conductometric titration.

**Conductometric Titration.** Titrations were performed using a Burivar-12 automatic buret (ManTech Associates) as described previously on both sulfated and carboxylated CNC to determine the charge content of the suspensions. 50 g portions of 0.5 wt % CNC suspensions in 1 mM KCl was titrated using slow base-into-acid titrations (30 min/unit pH).

**Electrophoretic Mobility.** Electrophoretic mobility values were measured using a ZetaPlus analyzer (Brookhaven Instruments Corp.) operating in phase analysis light scattering mode. A total of 10 runs (each composed of 15 cycles) were conducted; the experimental uncertainties represent the standard error of the mean of the replicate runs. The CNC and polymer concentrations were kept 0.4 wt % and 1 g/L, respectively. SDS, CTAB, and Triton X-100 were later added to CNC suspensions that had been previously mixed with polymer solutions and concentrations of the surfactants were kept 10, 2, and 2 mM, respectively.

**Dynamic Light Scattering.** Measurement were made using a Brookhaven BI-APD dynamic light scattering apparatus with a detector angle of  $90^\circ$ . A Melles Griot HeNe operating at a wavelength of 633 nm was used as the light source. The scattering intensity was between 100 and 250 kcps for all measurements. Each sample was measured for three runs with 3 min for each run. The results were analyzed using a BI-9000AT digital autocorrelator, version 6.1 (Brookhaven Instruments Corp.), and the CONTIN statistical method was used to calculate the particle size distribution.

**Preparation of CNC-Coated Sensors.**  $\text{TiO}_2$  SPR sensors (Bionavis) and silica QCM-D sensors (Q-Sense AB) were cleaned by dipping in ethanol, rinsing with purified water, and drying with nitrogen gas followed by UV/ozone treatment for 15 min. The silica QCM-D sensors were spin-coated at 3000 rpm for 60 s, with a layer of 1.0 g/L polyvinylamine (PVAm),  $M_w = 45$  kDa (BASF, Ludwigshafen, Germany) as the adhesive layer. Excess, unadsorbed PVAm was removed by washing with water. Next, the CNC suspension (2 wt %) was spin-coated onto the substrates at 3000 rpm for 60 s. To ensure that the spin-coated films did not desorb in water, they were heat-treated in an oven at  $80^\circ\text{C}$  for 2 h, rinsed with purified water, and dried with  $\text{N}_2$  gas. Some CNC desorption was observed with shorter (15 min) heating times. The same procedure was followed to spin-coat  $\text{TiO}_2$  SPR sensors with a CNC film. However, the adhesive layer of PVAm was not required for coating on the cationic  $\text{TiO}_2$  SPR sensors.

**Quartz Crystal Microbalance with Dissipation Monitoring (QCM-D).** Adsorption measurements were performed with an E4 QCM-D instrument from Q-Sense AB (Sweden) where the third, fifth, and seventh overtones were recorded. QCM-D measures the damping of the crystal oscillation (the dissipation factor  $D$ ) in addition to the frequency shift ( $\Delta f$ ) of a quartz crystal sensor in contact with an adsorbing medium. All the data were normalized to the fundamental frequency by dividing the result with the overtone number (3). Before the adsorption experiments, all CNC-coated QCM-D sensors were soaked in purified water overnight. All experiments were performed at  $23^\circ\text{C}$ , using HEPES buffer solutions (150 mM, pH 7.4).

For each adsorption experiment, the sequence of injections was identical: (1) an aqueous solution of HEPES buffer was injected at a constant flow rate of  $150 \mu\text{L}/\text{min}$  until the baseline frequency shift was

less than 0.5 Hz over 10 min; (2) the 1 g/L hydroxyethyl cellulose (HEC), hydroxypropyl guar (HPG), locust bean gum (LBG), or dextran (DEX) in HEPES buffer were injected at  $150 \mu\text{L}/\text{min}$  until the baseline was again stable, typically after 30 min; (3) the samples were rinsed with HEPES buffer at  $150 \mu\text{L}/\text{min}$  until the baseline was stable, typically after 5 min.

**Surface Plasmon Resonance (SPR) Measurements.** SPR experiments were performed using the SPR Navi200 (Bionavis, Finland) at  $23^\circ\text{C}$ . An increase in layer thickness adsorbed on the SPR sensor produces a shift in optical resonance properties of the sensor. This shift is detected as an increase in the SPR angle ( $\theta_{\text{peak}}$ ) where the reflected light intensity is minimized.<sup>35</sup> Reflected intensity as a function of incident angle was collected over the angular range of  $40^\circ$ – $80^\circ$  such that the SPR angle position and the angle of total internal reflectance ( $\theta_{\text{tir}}$ ) were both detected. The  $\theta_{\text{tir}}$  is related to the refractive index of the surrounding medium, and if the medium changes,  $\theta_{\text{tir}}$  shifts and the SPR angle shifts by the same amount. As such, it is important to subtract  $\theta_{\text{tir}}$  from the SPR peak angle to ensure that measured angular shifts are due to adsorbed material alone and not to media effects. SPR sensorgrams are presented as  $\Delta\theta_{\text{peak}} - \Delta\theta_{\text{tir}}$  as a function of adsorption time. All SPR measurements were performed using 670 and 785 nm wavelengths for the bare sensor surfaces and the CNC-coated sensor surface before and after polymer adsorption. Polysaccharide solutions were introduced at  $100 \mu\text{L}/\text{min}$ .

The SPR data (full angular scans from  $40^\circ$  to  $80^\circ$ ) were simulated using Winspall 3.02 (Max-Planck Institute for Polymer Research Mainz, Germany). This model treats the surface as a uniform slab and yields plots of slab thickness versus refractive index. By making independent measurements at two wavelengths, it is possible to estimate a unique combination of slab thickness and refractive index.<sup>36</sup> Details of the method and optical constants are given in the Supporting Information.

For polymer desorption experiments as a result of surfactant addition, the sequence of injections was identical: (1) an aqueous solution of HEPES buffer was injected at a constant flow rate of  $100 \mu\text{L}/\text{min}$  until the baseline  $\Delta\theta_{\text{peak}} - \Delta\theta_{\text{tir}}$  shift was less than 0.005 over 5 min; (2) the 1 g/L hydroxyethyl cellulose (HEC,  $M_w = 250$  kDa) was injected at  $100 \mu\text{L}/\text{min}$  until the baseline was again stable, typically after 20 min; (3) the samples were rinsed with HEPES buffer at  $100 \mu\text{L}/\text{min}$  until the baseline was stable, typically after 5 min; (4) SDS (10 mM in HEPES buffer), CTAB (2 mM in HEPES buffer), or Triton X-100 (2 mM in HEPES buffer) was injected at  $100 \mu\text{L}/\text{min}$  until the baseline was again stable, typically after 20 min; (5) the samples were rinsed with HEPES buffer at  $100 \mu\text{L}/\text{min}$  until the baseline was stable, typically after 10 min.

**Gelation Tests.** Equal volumes of CNC suspensions (ranging from 0.5 to 20 wt %) and each polysaccharide solution (in 300 mM HEPES buffer) with different concentrations were mixed together, and gelation was assessed by a modified test tube inversion method. Specifically, if no liquid accumulation was observed on the bottom of the inverted vial/tube 30 min after mixing of polymers and CNC suspensions, it was concluded that a gel had formed. Some HEC–CNC gels were treated with surfactants. Equal volumes of surfactant solution (SDS, CTAB, or Triton X-100) were combined and immediately vortexed. The tube inversion tests were repeated as before to determine the effects of surfactant addition on gelation. The final concentrations of SDS, CTAB, and Triton X-100 in the samples were kept to 10, 2, and 2 mM, respectively.

**Rheology.** Storage ( $G'$ ) and loss moduli ( $G''$ ) were measured using a CC25 concentric cylinder cell with a sample volume of 16 mL of an STRESSTECH HR ATS rheometer (Rheologica Instruments) at  $21^\circ\text{C}$ . A strain sweep was first performed to identify the linear viscoelastic range of each hydrogel composite, followed by a frequency sweep over the range of 0.01–10 rad/s to determine the shear-dependent complex viscosity,  $G'$ , and  $G''$  of the hydrogels. An example strain sweep is shown in Figure SI 13 of the Supporting Information.

**Polarized Optical Microscopy (POM).** Color micrographs were obtained using a Nikon Eclipse LV100POL microscope with a 530 nm phase retardation plate. With the retardation plate, isotropic areas appear dark pink and oriented regions, either blue or yellow, the

difference being a 90° in-plane rotation of the sample alignment direction. Digital images were taken of samples in rectangle hollow capillary tubes (VitroCom, Mountain Lakes, NJ).

## RESULTS

**Interactions of Water-Soluble Nonionic Polysaccharides with CNC Surfaces.** CNC dispersions were prepared by conventional sulfuric acid hydrolysis, yielding average crystal dimensions of 128 nm × 7 nm and a charge content of 0.16 ± 0.02 mequiv/g. For a few experiments, carboxylated cellulose nanocrystals (CNC-COOH) were also prepared,<sup>6</sup> producing particles with average dimensions of 119 nm × 8 nm and a charge content of 0.20 ± 0.04 mequiv/g. TEM micrographs and example conductometric titrations are shown in Figures SI-1 and SI-2, respectively. Many of the measurements reported in this paper were performed in 150 mM HEPES buffer at pH 7.2. Compared to the conditions used for many of the classic CNC studies, this is a high ionic strength that was chosen to more closely mimic conditions in commercial formulated aqueous products. Pristine sulfated CNC is electrostatically stabilized, and DLS measurements indicated some aggregation in HEPES buffer concentrations greater than 100 mM (see Figure SI-3).

The interactions of four polysaccharide types with CNC surfaces were probed by dynamic light scattering (DLS), microelectrophoresis, QCM-D, and SPR. In all cases the results suggest HEC, hydroxypropyl guar (HPG), and locust bean gum (LBG) adsorb onto cellulose in 150 mM HEPES buffer, whereas DEX does not. For example, Table 1 shows that DEX

**Table 1. Electrophoretic Mobility (EM) and Apparent Diameter of 0.04 wt % CNC Dispersions in the Presence of 0.1 g/L Polysaccharides and Surfactants<sup>a</sup>**

| additive               | CNC EM<br>10 <sup>-8</sup> m <sup>2</sup> /(V s) | apparent diameter<br>(nm) |
|------------------------|--|---------------------------|
| no additive            | -2.56 ± 0.21                                     | 113 ± 10                  |
| DEX                    | -2.29 ± 0.18                                     | 111 ± 10                  |
| HPG                    |  | 300 ± 28                  |
| LBG                    |  | 218 ± 20                  |
| HEC1300                |  | 269 ± 25                  |
| HEC720                 |  | 228 ± 20                  |
| HEC250                 | -0.11 ± 0.07                                     | 190 ± 18                  |
| HEC250 + SDS 10 mM     | -2.34 ± 0.06                                     |                           |
| HEC250 + CTAB 2 mM     | 0.19 ± 0.16                                      |                           |
| HEC250 + T. X-100 2 mM | -2.22 ± 0.19                                     |                           |

<sup>a</sup>Apparent diameters were based on the Stokes law conversion of diffusion coefficients obtained by DLS using the CONTIN analysis. The error estimates are the standard error of the mean apparent hydrodynamic diameter of three runs of each sample.

had little influence on CNC apparent diameter, whereas the other three polymers induced a substantial increase in the apparent size of the CNC crystals. Note the apparent diameters were based on sphere models that do not account for the particle shape. DLS measurements in the presence of the remaining polysaccharides and varying ionic strengths are shown in the Supporting Information (Figure SI-3), and these results are consistent with the adsorption of all polymers except DEX.

The electrophoretic mobilities of dilute CNC in 2 mM NaCl with and without polysaccharides are summarized in Table 1. Without polymers, the mobility is highly negative, reflecting the high surface charge density of sulfate half-ester groups. Again, we see that in the presence of DEX the mobility was slightly

decreased, whereas in HEC, LBG, and HPG, the mobility was substantially lower because adsorbed polymer shifted the shear plane away from the highly charged CNC surfaces.

Adsorption measurements were performed with a quartz crystal microbalance with dissipation (QCM-D) and surface plasmon resonance (SPR) spectroscopy using sensor surfaces spin-coated with CNC. Figure 2 shows QCM-D frequency shift

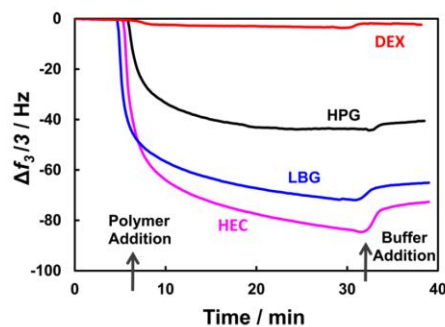


**Figure 2.**  $\Delta f_3/3$  versus time for QCM-D studies of sulfated CNC-coated silica sensors exposed to HEC1300, LBG, HPG, and DEX solutions (1 g/L in 150 mM HEPES buffer at pH 7.2).  $\Delta f_3/3$ , the frequency drop normalized by the overtone, is a measure of the adsorbed mass including bound water.

results from the introduction of the four polysaccharides. HEC, LBG, and HPG gave a large frequency drop, suggesting adsorption, whereas DEX did not. This series of experiments was repeated with QCM-D sensors coated with carboxylated cellulose nanocrystals, CNC-COOH, and the results in Figure SI-7 show similar results, but with slightly lower adsorbed masses.

The corresponding dissipation results (see Figure SI-6) show significant viscoelastic behavior, indicating highly associated water contents for the adsorbed polymers and thus precluding the use of the Sauerbrey model for predicting adsorbed amounts. Thus, it is not possible from these results to rank the relative adsorbed amounts of HPG, LBG, and HEC. On the other hand, it is clear that DEX did not adsorb; presumably, DEX adsorption onto cellulose is energetically unfavorable.

SPR adsorption measurements were performed to obtain adsorbed layer thickness values for the HEC samples. Our SPR instrument performed simultaneous measurements at two wavelengths, permitting the estimation of the adsorbed layer thickness values. The analyses, including the optical constants, are described in the Supporting Information. The resulting estimates of adsorbed layer thickness values are plotted as a function of the square root of the HEC molecular weight in Figure 3. In view of the complexity of the samples, we consider these thickness results to be semiquantitative. Nevertheless, the adsorbed layer thickness values, estimated from SPR measurements, were proportional to the square root of the molecular weight. Also shown in Figure 3 are adsorbed layer values from a model—these results are explained in the Discussion section.

**Influence of Water-Soluble Nonionic Polysaccharides on Gelation.** Initial experimentation showed that very low concentrations of some nonionic, water-soluble polysaccharides could induce CNC suspension gelation. CNC gelation was assessed by simple vial inversion tests. Gels that did not move when the vials were inverted are classified as “invertible gels”. Figure 4 shows that 3 wt % CNC suspensions formed gels

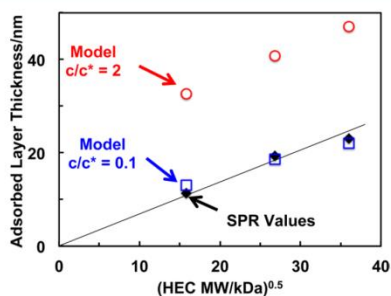


**Figure 3.** Influence of HEC molecular weight on the estimated adsorbed thickness on CNC-coated substrates in 150 mM HEPES buffer at pH 7.2. The model results are explained in the Discussion section.

when mixed with only 0.2 wt % LBG, HPG, or HEC. By contrast, DEX did not induce formation of an invertible gel.

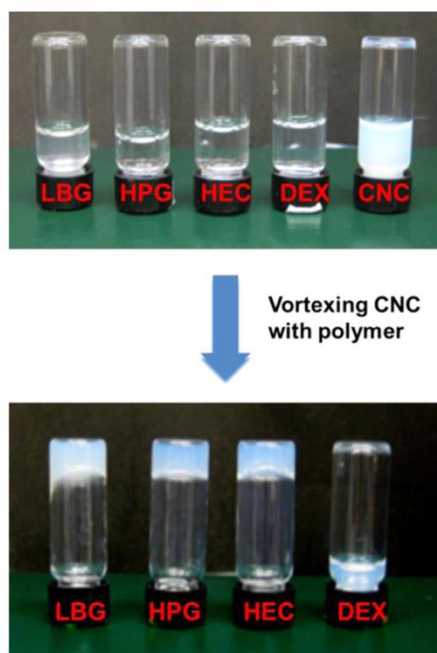


**Figure 4.** Photographs of polysaccharide solutions before and after vortex mixing with CNC suspensions. Only the dextran (DEX) did not induced gelation. The final suspensions were 3 wt % CNC + 0.2 wt % polysaccharide in 150 mM HEPES buffer at pH 7.2. The HEC was HEC1300 (see Table 1).

Gel formation was further demonstrated by rheological measurements. HEC–CNC mixtures showed classic gel behavior with  $G' > G''$  and a rather flat frequency response. HPG or LBG with CNC showed similar behaviors (Figure SI-4). By contrast, with DEX–CNC mixtures,  $G'' > G'$ , which is typical behavior for polymer solutions. The corresponding curves made with carboxylated CNC–COOH showed similar behavior (see Figure SI-5).

Polarized optical microscopy (POM) and transmission electron microscopy (TEM) images of polymer–CNC samples are shown in Figure 5. LBG–CNC, HPG–CNC, and HEC–

CNC samples demonstrated anisotropic regions in both POM and TEM images, whereas the DEX–CNC sample only showed random ordering of the CNC particles.

Figure 6 further illustrates the ability of HEC to induce CNC gelation. The Y-axis shows the minimum CNC volume fraction required to form a gel as judged by the vial inversion tests. The X-axis shows the polymer concentration divided by  $C^*$ , which is the polymer concentration corresponding to the dilute-to-semidilute transition (overlap concentration). At concentrations as low as 1/10th  $C^*$ , all three HEC molecular weights lowered the CNC gelation concentration by an order of magnitude. In addition, the higher the HEC molecular weight, the more dramatic the effect on gelation. Note that without polymer the CNC concentration for invertible gel formation was about 15 vol % and that none of the polymers gave invertible gels at the concentrations we evaluated. Therefore, gelation depended upon HEC/CNC interactions.

**Surfactant Interaction of CNC–HEC Gels.** In addition to water-soluble polymers, most formulated products contain surfactants. We mixed three typical surfactants, at concentrations slightly above their critical micelle concentrations, with HEC–CNC gels. Anionic SDS and nonionic Triton X-100 destroyed the uniform gels, giving visible CNC precipitates immediately after mixing. By contrast, cationic CTAB did not disrupt the gel. POM micrographs (Figure SI-12) indicated the presence of ordered domains in the samples after the addition of all three surfactants. The electrophoresis results in Table 1 show that addition of SDS or Triton X-100 to CNC–HEC mixtures increases the negative electrophoretic mobility back to values close to CNC without polymers. By contrast, CTAB absorption gives charge reversal. In the Discussion section we argue that that SDS and Triton disrupted the adsorbed HEC and thus led to gel breaking.

Further support for the proposal that SDS and Triton induce HEC desorption from CNC is given in Figure 7. SDS and Triton X-100 induced partial desorption ( $\sim 70\%$ ) of the adsorbed HEC with most desorption occurring during the final buffer rinse. This is a reproducible observation for which we have no explanation. In contrast to the behaviors in SDS and Triton X-100, exposure to cationic CTAB increased the amount of material adsorbed on the cellulose. We presume the additional adsorbed material is CTAB; however, this remains to be proven. These results highlight the complexities of mixing CNC with polymers and surfactants.

## DISCUSSION

In this work we have focused on factors influencing gelation of CNC suspensions with particular emphasis on whether or not the inverted gels flow. Without added polymer our CNC gels did not flow when inverted if the volume fraction of CNC was  $\geq 14\%$  (see Figure 6). A 14 vol % suspension corresponds to 19.6 wt % CNC, and a number concentration of  $\sim 14 \times 10^{-6} \text{ nm}^{-3}$ . This number concentration is within the range of CNC concentrations reported by Dong et al.<sup>17</sup> for suspensions with an anisotropic volume fraction of 100% (i.e., no coexisting isotropic phase).

Our results show that three of four nonionic, water-soluble polysaccharides greatly lower the CNC concentration required for invertible gel formation. On the other hand, two of three common surfactant types disrupt HEC–CNC gels. These sensitivities of CNC dispersions have serious implications for CNC formulation into water-based products because such polysaccharides are frequently used to control viscosity. The

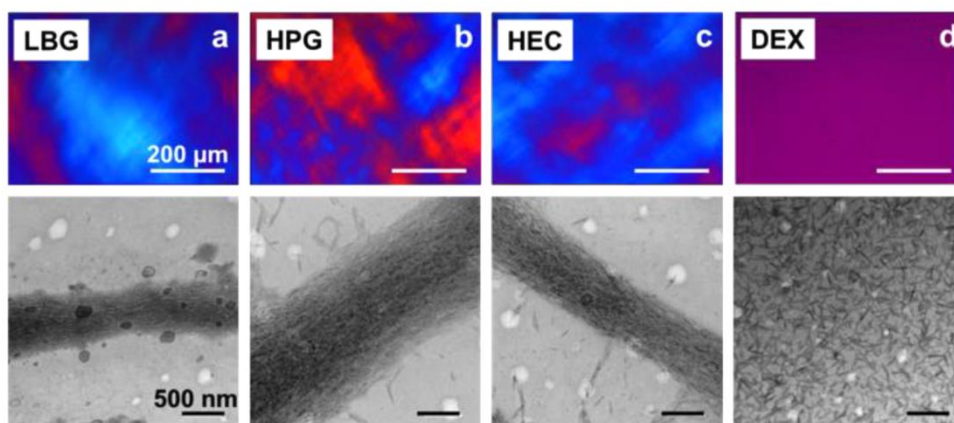


**Figure 5.** Polarized optical micrographs (POM; top panel) and transmission electron micrographs (TEM; bottom panel) of CNC (3 wt %) suspensions in the presence of polysaccharides (0.2 wt %) in 150 mM HEPES buffer at pH 7.2.

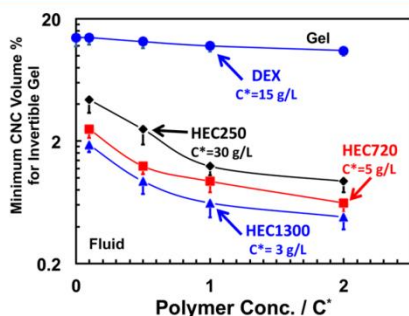


**Figure 6.** Minimum CNC volume percent for gelation (inversion test) as a function of the polysaccharide concentration in 150 mM HEPES buffer at pH 7.2.  $C^*$ , the overlap concentrations, were from the literature.<sup>28,37</sup>

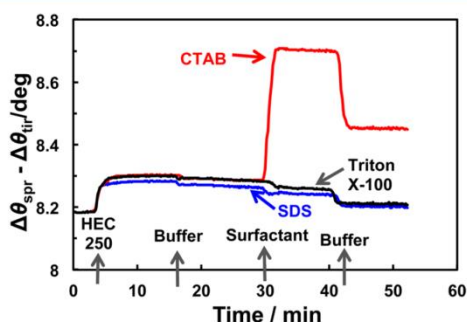


**Figure 7.** Influence of surfactants on HEC250 adsorbed from a 1 g/L solution onto a CNC-coated SPR sensor (data collected at 785 nm). The surfactant concentrations were SDS 10 mM, CTAB 2 mM, and Triton X-100 2 mM. All measurements were made in 150 mM HEPES buffer at pH 7.2.

ability of hydrophilic polysaccharides to influence rheology and colloidal stability has been discussed in many other systems, and generally most effects are explained by depletion flocculation.<sup>38</sup> The following paragraphs make the case that depletion effects (and bridging) are not dominant in our system.

Addition of HEC to CNC suspensions at concentrations as low as 1/10th  $C^*$ , the overlap concentration, induced gelation, whereas dextran had little influence (see Figure 6). The polymer concentrations were in the dilute regime (i.e.,  $<C^*$ ), suggesting that depletion forces were not responsible for the invertible gel formation.

The QCM-D, SPR, electrophoresis, and dynamic light scattering results showed HEC, HPG, and LBG adsorbed onto CNC surfaces, whereas DEX did not. Therefore, the ability of polymers to induce CNC gelation was correlated with the tendency of the polymers to adsorb onto CNC. These results were surprising to us as HEC is widely used as a thickener in aqueous dispersions because it does not adsorb onto many surfaces. There are few publications describing HEC interactions with cellulose. Boluk's isothermal titration calorimetry experiments failed to measure heat effects associated with HEC interaction with CNC.<sup>28</sup> Berglund's group has shown that nanocellulose/HEC blends form tough dry composites suggesting adhering interfaces between HEC and cellulose.<sup>39</sup> In summary, we are confident that HEC adsorption on our CNC-coated surfaces was not an artifact because the QCM-D and SPR coated sensors were prepared with different adhesive layers (polyvinylamine for the QCM-D and no adhesive layer on  $\text{TiO}_2$  for SPR) and the CNC layer was thick enough to avoid substrate effects. Furthermore, both the microelectrophoresis and DLS results suggest HEC adsorption onto CNC. Assuming that our adsorption measurements reflect adsorption onto dispersed CNC particles, the role of polysaccharide adsorption on CNC gelation is now considered.

The simultaneous adsorption of polymer molecules onto two or more particles gives bridging structures and thus could explain gelation. However, a common feature of bridging is that it is not operative at high polymer concentrations. Instead, at high polymer/surface area ratios, all surfaces are saturated with adsorbed polymer giving steric stabilization. Our gelation results in Figure 6 show no evidence of a bridging-to-steric stabilization transition at high polymer concentrations. Therefore, we do not believe bridging interactions explain the polysaccharide-induced gelation. Instead, we propose that HEC lowers the CNC concentration for gelation by adsorbing onto the particles, increasing the effective volume fraction of CNC particles. The following model illustrates the roles of polymer adsorption and volume fraction.

A gelation model requires a criterion for the onset of gelation. For example, Philippe's review discusses the criteria for gelation of nonadhering and adhering rod suspensions.<sup>40</sup> For simplicity, we assume that an invertible gel forms at the CNC concentration =  $C_2$  and  $\phi = \phi_a = 1$ , the lowest CNC concentration at which the suspension is entirely anisotropic (see Figure 1). Although reasonable, we emphasize this assumption is arbitrary. The effective volume fraction of a suspension of rectangular particles of width  $W = 7$  nm with an adsorbed polymer layer thickness  $\delta$  is given by eq 1, where  $c$  is the mass fraction of cellulose in the suspension,  $\rho_w$  is the density of water, and,  $\rho_{\text{CNC}} = 1600$  kg/m<sup>3</sup> is the density of cellulose. Note this expression ignores the contribution of polymer adsorbed on the ends of the particles.

$$\phi = \frac{\rho_w}{\left(\frac{1}{c} - 1\right)\rho_{\text{CNC}} + \rho_w} \frac{(W + 2\delta)^2}{W^2} \quad (1)$$

We applied eq 1 to the results in Figure 6 to estimate the corresponding  $\delta$  values. The experimental cellulose volume fractions in Figure 6 were converted to the corresponding mass fractions,  $c$ , and eq 1 was solved numerically for  $\delta$  values, setting  $\phi = 1$ . The calculations, performed with Mathcad, are listed in the Supporting Information. Polymer adsorbed layer thickness values,  $\delta$ , were calculated for  $c$  values corresponding to both the lowest and highest experimental HEC concentrations in Figure 6. The resulting thickness values are compared to the SPR experimental values in Figure 3. The computed thickness corresponding to the low polymer concentrations are very close to the experimental SPR values, whereas those for the high polymer concentration data are about 2 times greater than the experimental values. In summary, this simple model simulated the major features of gelation results, giving support to our proposal that HEC, HPG, and LBG induced gelation because the polymer adsorbed on the CNC surfaces, increasing the effective volume fraction.

If we accept that HEC adsorption explains enhanced gelation of CNC dispersions, it seems reasonable to propose that subsequent SDS or Triton X-100 addition induced HEC desorption. The literature teaches that the anionic surfactant SDS<sup>41</sup> and the nonionic Triton X-100<sup>42</sup> do not bind to HEC in solution. On the other hand, the adsorption of an anionic surfactant, sodium dodecylbenzenesulfonate (NaDBS), and a nonionic surfactant, Triton X-100, on cellulose surfaces with and without electrolytes has been reported.<sup>43</sup> Both our SPR (Figure 7) and microelectrophoresis (Table 1) results together with the literature support the proposition that SDS and Triton X-100 adsorb on CNC surfaces, displacing the adsorbed HEC layer. Furthermore, the photographs in Figure SI-12 of the Supporting Information show that SDS and Triton X-100 induced some aggregation, possibly because of depletion flocculation. By contrast, CTAB, the cationic surfactant, showed very different behavior.

The results in Figure 7 show a surface mass increase when HEC-treated cellulose is exposed to CTAB. It is not known whether CTAB simply adds to the layer or displaces some of the HEC. However, since there is no destruction of the invertible gel, we propose that CTAB penetrates the HEC layers, binding to the negatively charged CNC surfaces with little change to the effective volume fraction of the coated particles. In addition, electrophoretic mobility measurements (Table 1) of CNC suspensions that have been previously mixed with HEC were positively charged and colloiddally stable.

Though HEC-free CNC suspension in 2 mM CTAB was also positively charged ( $EM = (0.68 \pm 0.12) \times 10^{-8}$  m<sup>2</sup>/(V s)), the dispersion was unstable and aggregated 1 h after mixing CNC with CTAB. The sample of HEC–CNC–CTAB, on the other hand, showed no sign of aggregation three days after preparation, presumably because adsorbed HEC served as a steric stabilizer.

Finally, formulators have hundreds of water-soluble polymers and thousands of surfactants from which to choose. Obviously, this work involves a limited subset of the formulation landscape. Our nonionic polysaccharides are particularly benign because they are very hydrophilic and thus are weakly interacting in water both with surfaces and surfactants. Nevertheless, we have demonstrated a complex range of behaviors. More hydrophobic and/or charged polymers are likely to display more dramatic interactions with CNC and with any surfactants present.

## CONCLUSIONS

Gelation of dilute CNC suspensions was induced by the introduction of the nonionic polysaccharides HEC, HPG, and LBG, whereas DEX has no influence on gelation. The ability of a polysaccharide to induce gelation directly correlates with the tendency of the polymer to adsorb on the CNC surfaces. Absorbing polymers dramatically increase the effective volume fraction of CNC dispersions, driving them into a completely anisotropic phase with a sufficient yield stress to not flow when inverted. Addition of surfactants to HEC–CNC invertible gels gave a range of behaviors depending upon the nature of the surfactant. Anionic SDS and nonionic Triton X-100 decompose the gels inducing HEC desorption from CNC surfaces, whereas gels were preserved in the presence of CTAB. This work emphasizes that although CNC is potentially a potent ingredient for promoting weak gel formation in formulated chemical products, the detailed behaviors are very sensitive to the presence of water-soluble polymers and surfactants.

## ASSOCIATED CONTENT

### Supporting Information

Transmission electron microscopy (TEM), conductometric titration, dynamic light scattering (DLS), rheology data corresponding to the results in Figure 5, quartz crystal microbalance with dissipation monitoring (QCM-D) data corresponding to the results in Figure 2, surface plasmon resonance (SPR) data and simulation example corresponding to the results in Figure 3, atomic force microscopy (AFM) data, and a copy of the MathCad model used to perform the calculation of volume fraction increase due to the adsorption of polymer. This material is available free of charge via the Internet at <http://pubs.acs.org>.

## AUTHOR INFORMATION

### Corresponding Author

\*E-mail: [peltonrh@mcmaster.ca](mailto:peltonrh@mcmaster.ca) (R.P.).

### Notes

The authors declare no competing financial interest.

## ACKNOWLEDGMENTS

The authors thank Sarah Ballinger and Kevin Kan for CNC preparation, Elizabeth Takacs and Roozbeh Mafi for rheometry support, and Heera Marway for SPR support. Tiffany Abitbol is thanked for sample analysis with POM and AFM. The

McMaster Biointerfaces Institute is acknowledged for access to instrumentation. Hu thanks NSERC for funding this work through the CREATE Biointerfaces Training Program Grant. Pelton holds the Canada Research Chair in Interfacial Technologies.

## REFERENCES

- (1) Ranby, B. G. Aqueous Colloidal Solutions of Cellulose Micelles. *Acta Chem. Scand.* **1949**, *3*, 649–650.
- (2) Klemm, D.; Kramer, F.; Moritz, S.; Lindstrom, T.; Ankerfors, M.; Gray, D.; Dorris, A. Nanocelluloses: A New Family of Nature-Based Materials. *Angew. Chem., Int. Ed.* **2011**, *50*, 5438–5466.
- (3) Revol, J. F.; Bradford, H.; Giasson, J.; Marchessault, R. H.; Gray, D. G. Helicoidal Self-Ordering of Cellulose Microfibrils in Aqueous Suspension. *Int. J. Biol. Macromol.* **1992**, *14*, 170–172.
- (4) Espinosa, S. C.; Kuhnt, T.; Foster, E. J.; Weder, C. Isolation of Thermally Stable Cellulose Nanocrystals by Phosphoric Acid Hydrolysis. *Biomacromolecules* **2013**, *14*, 1223–1230.
- (5) Cao, X.; Dong, H.; Li, C. M. New Nanocomposite Materials Reinforced with Flax Cellulose Nanocrystals in Waterborne Polyurethane. *Biomacromolecules* **2007**, *8*, 899–904.
- (6) Kalashnikova, I.; Bizot, H.; Cathala, B.; Capron, I. New Pickering Emulsions Stabilized by Bacterial Cellulose Nanocrystals. *Langmuir* **2011**, *27*, 7471–7479.
- (7) Rincon-Torres, M. T.; Hall, L. J. Cellulose Nanowhiskers in Well Services. US Patent App. 13/561,158, 2012.
- (8) Kan, K. H. M.; Li, J.; Wijesekera, K.; Cranston, E. D. Polymer-Grafted Cellulose Nanocrystals as pH-Responsive Reversible Flocculants. *Biomacromolecules* **2013**, *14*, 3130–3139.
- (9) Boluk, Y.; Lahiji, R.; Zhao, L.; Mcdermott, M. T. Suspension Viscosities and Shape Parameter of Cellulose Nanocrystals (Cnc). *Colloids Surf., A* **2011**, *377*, 297–303.
- (10) Zhong, L.; Fu, S.; Peng, X.; Zhan, H.; Sun, R. Colloidal Stability of Negatively Charged Cellulose Nanocrystalline in Aqueous Systems. *Carbohydr. Polym.* **2012**, *90*, 644–649.
- (11) Revol, J. F.; Godbout, L.; Gray, D. G. Solid Self-Assembled Films of Cellulose with Chiral Nematic Order and Optically Variable Properties. *J. Pulp Paper Sci.* **1998**, *24*, 146–149.
- (12) Fall, A. B.; Lindstrom, S. B.; Sundman, O.; Odberg, L.; Wagberg, L. Colloidal Stability of Aqueous Nanofibrillated Cellulose Dispersions. *Langmuir* **2011**, *27*, 11332–11338.
- (13) Araki, J.; Wada, M.; Kuga, S. Steric Stabilization of a Cellulose Microcrystal Suspension by Poly(Ethylene Glycol) Grafting. *Langmuir* **2001**, *17*, 21–27.
- (14) Onsager, L. The Effects of Shape on the Interaction of Colloidal Particles. *Ann. N. Y. Acad. Sci.* **1949**, *51*, 627–659.
- (15) Flory, P. J. Statistical Thermodynamics of Mixtures of Rodlike Particles. 5. Mixtures with Random Coils. *Macromolecules* **1978**, *11*, 1138–1141.
- (16) Stroobants, A.; Lekkerkerker, H. N. W.; Odijk, T. Effect of Electrostatic Interaction on the Liquid Crystal Phase Transition in Solutions of Rodlike Polyelectrolytes. *Macromolecules* **1986**, *19*, 2232–2238.
- (17) Dong, X. M.; Kimura, T.; Revol, J. F.; Gray, D. G. Effects of Ionic Strength on the Isotropic-Chiral Nematic Phase Transition of Suspensions of Cellulose Crystallites. *Langmuir* **1996**, *12*, 2076–2082.
- (18) Dong, X. M.; Gray, D. G. Effect of Counterions on Ordered Phase Formation in Suspensions of Charged Rodlike Cellulose Crystallites. *Langmuir* **1997**, *13*, 2404–2409.
- (19) Odijk, T. Theory of Lyotropic Polymer Liquid Crystals. *Macromolecules* **1986**, *19*, 2313–2329.
- (20) Wierenga, A. M.; Philipse, A. P. Low-Shear Viscosity of Isotropic Dispersions of (Brownian) Rods and Fibres; a Review of Theory and Experiments. *Colloids Surf., A* **1998**, *137*, 355–372.
- (21) Araki, J.; Wada, M.; Kuga, S.; Okano, T. Flow Properties of Microcrystalline Cellulose Suspension Prepared by Acid Treatment of Native Cellulose. *Colloids Surf., A* **1998**, *142*, 75–82.
- (22) Bercea, M.; Navard, P. Shear Dynamics of Aqueous Suspensions of Cellulose Whiskers. *Macromolecules* **2000**, *33*, 6011–6016.
- (23) Liu, D.; Chen, X.; Yue, Y.; Chen, M.; Wu, Q. Structure and Rheology of Nanocrystalline Cellulose. *Carbohydr. Polym.* **2011**, *84*, 316–322.
- (24) Ureña-Benavides, E. E.; Ao, G.; Davis, V. A.; Kitchens, C. L. Rheology and Phase Behavior of Lyotropic Cellulose Nanocrystal Suspensions. *Macromolecules* **2011**, *44*, 8990–8998.
- (25) Edgar, C. D.; Gray, D. G. Influence of Dextran on the Phase Behavior of Suspensions of Cellulose Nanocrystals. *Macromolecules* **2002**, *35*, 7400–7406.
- (26) Beck-Candanedo, S.; Viet, D.; Gray, D. G. Induced Phase Separation in Low-Ionic-Strength Cellulose Nanocrystal Suspensions Containing High-Molecular-Weight Blue Dextran. *Langmuir* **2006**, *22*, 8690–8695.
- (27) Beck-Candanedo, S.; Viet, D.; Gray, D. G. Triphase Equilibria in Cellulose Nanocrystal Suspensions Containing Neutral and Charged Macromolecules. *Macromolecules* **2007**, *40*, 3429–3436.
- (28) Boluk, Y.; Zhao, L.; Incani, V. Dispersions of Nanocrystalline Cellulose in Aqueous Polymer Solutions: Structure Formation of Colloidal Rods. *Langmuir* **2012**, *28*, 6114–6123.
- (29) Persson, B.; Nilsson, S.; Sundelöf, L.-O. On the Characterization Principles of Some Technically Important Water-Soluble Nonionic Cellulose Derivatives. Part II: Surface Tension and Interaction with a Surfactant. *Carbohydr. Polym.* **1996**, *29*, 119–127.
- (30) Sperry, P. R. A Simple Quantitative Model for the Volume Restriction Flocculation of Latex by Water-Soluble Polymers. *J. Colloid Interface Sci.* **1982**, *87*, 375–384.
- (31) Beck-Candanedo, S.; Viet, D.; Gray, D. G. Induced Phase Separation in Cellulose Nanocrystal Suspensions Containing Ionic Dye Species. *Cellulose* **2006**, *13*, 629–635.
- (32) Dhar, N.; Au, D.; Berry, R. C.; Tam, K. C. Interactions of Nanocrystalline Cellulose with an Oppositely Charged Surfactant in Aqueous Medium. *Colloids Surf., A* **2012**, *415*, 310–319.
- (33) Peng, B.; Han, X.; Liu, H.; Berry, R. C.; Tam, K. C. Interactions between Surfactants and Polymer-Grafted Nanocrystalline Cellulose. *Colloids Surf., A* **2013**, *421*, 142–149.
- (34) Filpponen, L.; Argyropoulos, D. S. Regular Linking of Cellulose Nanocrystals via Click Chemistry: Synthesis and Formation of Cellulose Nanoplatelet Gels. *Biomacromolecules* **2010**, *11*, 1060–1066.
- (35) Liang, H.; Miranto, H.; Granqvist, N.; Sadowski, J. W.; Viitala, T.; Wang, B.; Yliperttula, M. Surface Plasmon Resonance Instrument as a Refractometer for Liquids and Ultrathin Films. *Sens. Actuators, B* **2010**, *149*, 212–220.
- (36) Grassi, J. H.; Geogiadis, R. M. Temperature-Dependent Refractive Index Determination from Critical Angle Measurements: Implications for Quantitative Spr Sensing. *Anal. Chem.* **1999**, *71*, 4392–4396.
- (37) Ioan, C. E.; Aberle, T.; Burchard, W. Light Scattering and Viscosity Behavior of Dextran in Semidilute Solution. *Macromolecules* **2001**, *34*, 326–336.
- (38) Kiratzis, N.; Faers, M.; Luckham, P. F. Depletion Flocculation of Particulate Systems Induced by Hydroxyethylcellulose. *Colloids Surf., A* **1999**, *151*, 461–471.
- (39) Sehaqui, H.; Zhou, Q.; Berglund, L. A. Nanostructured Biocomposites of High Toughness—a Wood Cellulose Nanofiber Network in Ductile Hydroxyethylcellulose Matrix. *Soft Matter* **2011**, *7*, 7342–7350.
- (40) Philipse, A. P.; Wierenga, A. M. On the Density and Structure Formation in Gels and Clusters of Colloidal Rods and Fibers. *Langmuir* **1998**, *14*, 49–54.
- (41) Yamanaka, Y.; Esumi, K. Adsorption of Hydroxyethylcellulose or Hydrophobically Modified Cellulose and Anionic Surfactant from Their Binary Mixtures on Particles. *Colloids Surf., A* **1997**, *122*, 121–133.
- (42) Zhao, G.; Chen, S. B. Clouding and Phase Behavior of Nonionic Surfactants in Hydrophobically Modified Hydroxyethyl Cellulose Solutions. *Langmuir* **2006**, *22*, 9129–9134.

(43) Paria, S.; Manohar, C.; Khilar, K. C. Adsorption of Anionic and Non-Ionic Surfactants on a Cellulosic Surface. *Colloids Surf, A* **2005**, 252, 221–229.

## Appendix: Supporting Information for Chapter 2

**Transmission Electron Microscopy (TEM).** The anionic (sulfate half-ester and carboxylic acid) functional groups on CNC particles were selectively stained by mixing a 0.05 mL aliquot of the CNC (0.5 wt%) with 0.5 mL of a 1 mM uranyl acetate solution and vortexing the mixture for 2 min. A single drop of the stained suspension was dropped on a Formvar-coated copper TEM grid and dried for 4 h. TEM images were acquired using a JEOL 1200 EX TEMSCAN microscope operating at 80 kV.

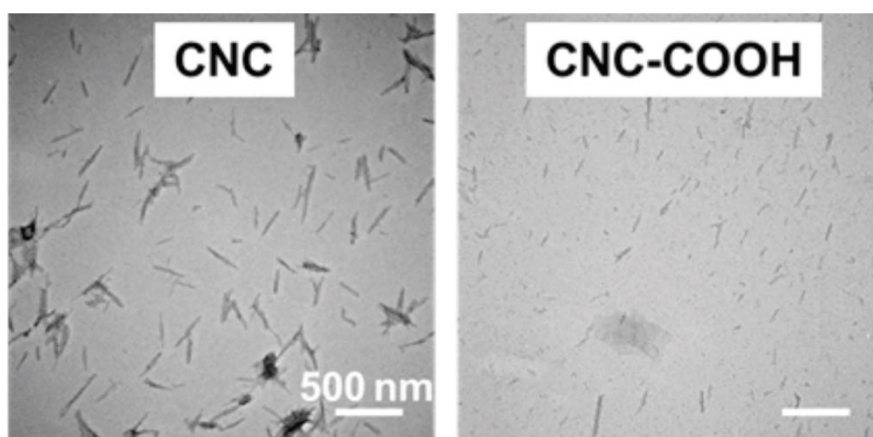


Figure SI- 1. TEM images of sulfated cellulose nanocrystals (CNC) and carboxylated cellulose nanocrystals (CNC-COOH).

TEM images of sulfated cellulose nanocrystals (CNC) and carboxylated cellulose nanocrystals (CNC-COOH) are presented in Figure SI-1 and show well-dispersed whisker-like nanoparticles with average lengths of  $128 \pm 7$  and  $119 \pm 8$  nm and heights of  $7 \pm 2$  and  $8 \pm 2$  nm, respectively.

The average dimensions of these nanocrystals were determined by measuring the sizes of about 100 individual nanocrystals.

**Conductometric Titration.** 100 mg CNC or 120 mg CNC-COOH suspended in 1 mM KCl was titrated by using slow base-into-acid titrations (30 min/unit pH) on a Burivar-I2 automatic buret (ManTech Associates) as described previously.<sup>1</sup> Sample titration curves are shown in Figure SI-2.

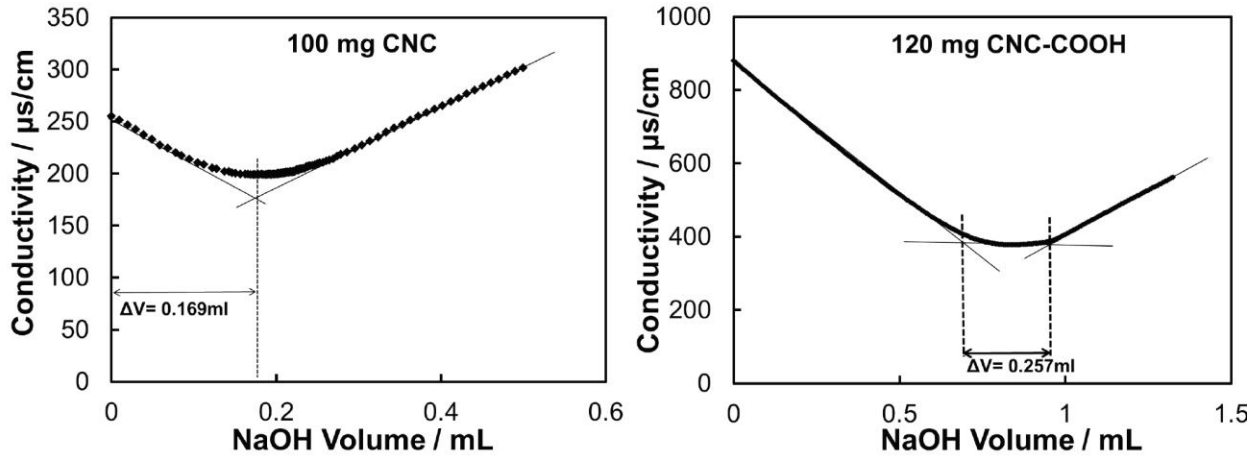


Figure SI- 2. Examples of conductometric titration curve of sulfated CNC (CNC) and carboxylated CNC (CNC-COOH) used to determine charged groups on CNC.

The surface charge density,  $\sigma$ , in meq/g was calculated from the titration results as

$$\sigma = \frac{C_{\text{NaOH}} V_{\text{NaOH}}}{C_{\text{CNC}} \alpha_{\text{CNC}}} \quad (1)$$

where  $c_{\text{NaOH}}$  is the concentration of the titrant,  $V_{\text{NaOH}}$  is the titrant volume at the equivalence point,  $c_{\text{CNC}}$  is the concentration of the CNC suspension, and  $\alpha_{\text{CNC}}$  is the amount of CNC suspension titrated. Charge densities of CNC and CNC-COOH were determined to be  $0.16 \pm 0.02$  and  $0.20 \pm 0.04$  meq/g, respectively.

**Dynamic Light Scattering (DLS).** Particle sizes of CNC only or in the presence of different polymers were determined by dynamic light scattering using a detector angle of  $90^\circ$ . A Melles Griot HeNe laser operating at a wavelength of 633 nm was used as the light source. The scattering intensity was between 100 and 250 kcps for all measurements. Each sample was measured for three runs with 3 min for each run and averages with error intervals are plotted in Figure SI-3.

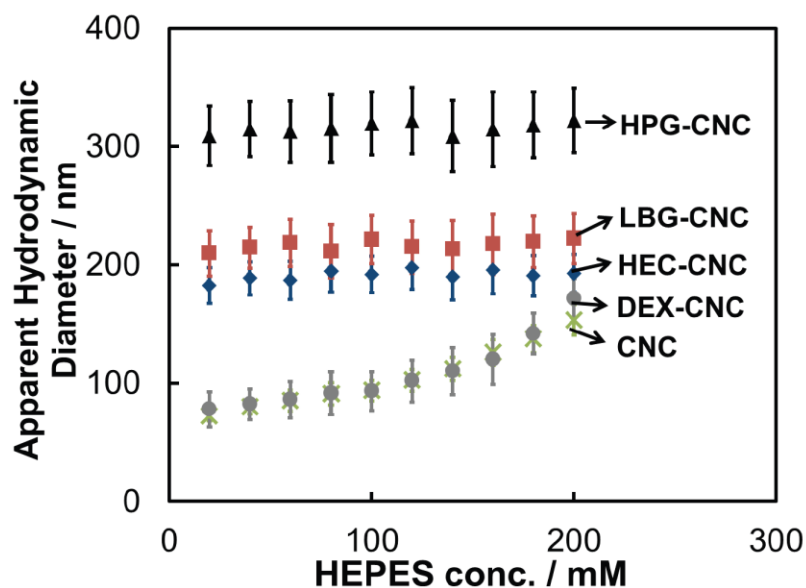


Figure SI- 3. Apparent hydrodynamic diameter of CNC suspensions (0.4 wt %) only and in the presence of HPG, LBG, HEC, or DEX versus concentration of HEPES buffer (pH=7.2). All the polysaccharide concentrations were fixed to be 1 g/L and  $M_w$  of HEC was 250 kDa.

Considering the fact that suspended particles are assumed to be spherical by using DLS, apparent hydrodynamic diameters of the suspensions were reported here for comparison purpose only. The salt concentration dependence of CNC and DEX-CNC hydrodynamic diameters suggests the absence of steric stabilization of polymer layer on CNC surface and agglomeration of the nanocrystals with increasing ionic strength. Conversely, for all other samples of HPG-CNC, LBG-CNC, and HEC-CNC suspensions hydrodynamic diameter does not change, implying steric stabilization induced by the adsorbed polymer layers. The average hydrodynamic diameters of HPG-CNC, LBG-CNC, HEC-CNC are at least 100 nm bigger than the ones of CNC and DEX-CNC, which again is due to the presence of an adsorbed polymer layer on CNC surfaces.

**Rheology.** Storage ( $G'$ ) and loss moduli ( $G''$ ) were measured using a CC25 concentric cylinder cell with a sample volume of 16 mL of an STRESSTECH HR ATS rheometer (Rheologica Instruments, USA) at  $21^\circ\text{C}$ . A stress sweep was first performed to identify the linear viscoelastic range of each hydrogel composite, followed by a frequency sweep over the range of 0.01–10 rad/s to determine the shear dependent complex viscosity,  $G'$ , and  $G''$  of the hydrogels.

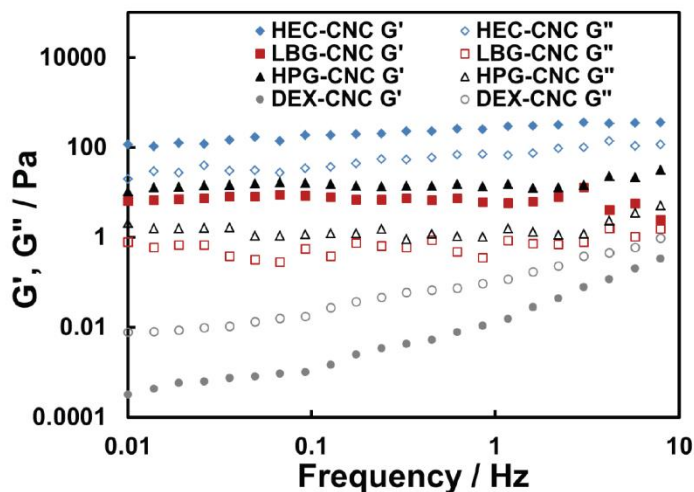


Figure SI- 4 Rheological behaviors of CNC (3 wt %)-polysaccharide (0.2 wt %) mixtures in 150 mM HEPES buffer at pH 7.2.  $M_w$  of HEC was 1300 kDa.

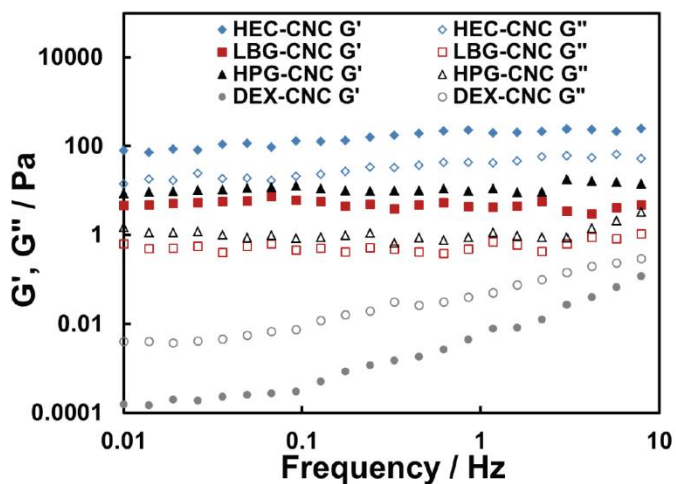


Figure SI- 5 Rheological behaviors of CNC-COOH (3 wt %)-polysaccharide (0.2 wt %) mixtures in 150 mM HEPES buffer at pH 7.2.  $M_w$  of HEC was 1300 kDa.

As shown in Figure SI-4, only DEX-CNC sample was found to be liquid, whereas other samples were gel displaying bigger  $G'$  values than  $G''$  ones. This was also observed for CNC-COOH samples (Figure SI-5), which showed slightly smaller  $G'$  values compared to their sulfated counterparts.

**Quartz Crystal Microbalance with Dissipation Monitoring (QCM-D).** Adsorption measurements were performed with an E4 QCM-D instrument from Q-Sense AB (Sweden) where the third, fifth, and seventh overtones were recorded. For each adsorption experiment the sequence of injections was identical: (1) an aqueous solution of HEPES buffer was injected at a constant flow rate of 150  $\mu\text{L}/\text{min}$  until the baseline frequency shift was less than 0.5 Hz over 1 min; (2) the 1 g/L hydroxyethyl cellulose (HEC), hydroxypropyl guar (HPG), locust bean gum (LBG), or dextran (DEX) in HEPES buffer were injected at 150  $\mu\text{L}/\text{min}$  until the baseline was again stable, typically after 30 min; (3) the samples were rinsed with HEPES buffer at 150  $\mu\text{L}/\text{min}$  until the baseline was stable, typically after 5 min.

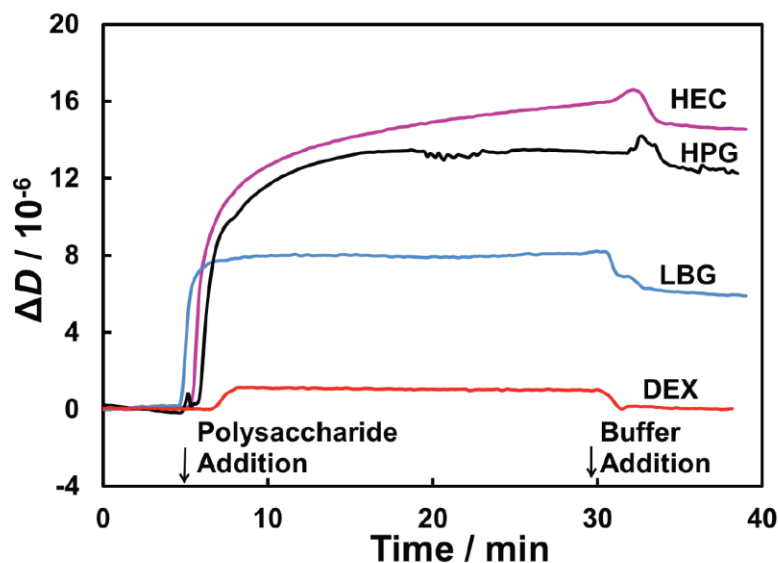


Figure SI- 6  $\Delta D$  versus time for QCM-D studies of sulfated CNC-coated sensors exposed to HEC, LBG, HPG, and DEX solutions (1 g/L in 150 mM HEPES buffer). Curves correspond to the third overtone.  $M_w$  of HEC was 1300 kDa.

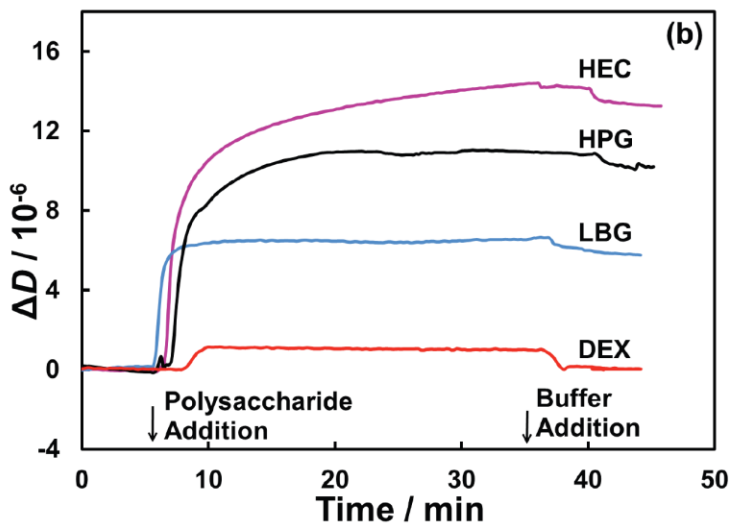


Figure SI-7  $\Delta f_3/3$  (a) and  $\Delta D$  (b) versus time for QCM-D studies of carboxylated CNC (CNC-COOH) coated sensors exposed to HEC, LBG, HPG, and DEX solutions (1g/L in 150 mM HEPES buffer).  $M_w$  of HEC was 1300 kDa.

In Figure 2 and SI-7, HEC, LBG and HPG gave a large frequency drop, suggesting adsorption on both sulfated CNC and carboxylated CNC whereas DEX did not. The corresponding dissipation results (see Figure SI-6 and SI-7) show significant viscoelastic behavior indicating high associated water contents, which makes Sauerbrey model for predicting adsorbed amounts unreliable.<sup>2</sup>

### Estimating Adsorbed Layer Thickness from SPR Measurements

The SPR data (full angular scans from 40° to 80°) were simulated using Winspall 3.02 (Max-Planck Institute for Polymer Research Mainz, Germany). This model treats the surface as a uniform slab and yields plots of slab thickness versus refractive index. By making independent measurements at two wavelengths it is possible to estimate a unique combination of slab thickness and refractive index.<sup>3</sup> Figure SI-8 shows two examples of the raw SPR data fitting of a CNC-coated TiO<sub>2</sub> sensor after HEC250 adsorption by using Winspall. The SPR signal of the bare TiO<sub>2</sub> sensor surface was simulated first to obtain the background for the subsequent simulation of the CNC layer. The starting parameters shown in the inset table of Figure SI-8 were either provided by BioNavis Ltd. or found in the online refractive index database (<http://refractiveindex.info/>). Minor tuning of the parameters was necessary to achieve the best fitting, which was determined by comparing the peak angles  $\Delta\theta$  of experiment data to simulation data and a difference smaller than 0.001° between these two was considered to be the best fit. The layers in the model correspond to the glass slide (layer 0), gold adhesive layer (layer 1), gold layer (layer 2), TiO<sub>2</sub> layer (layer 3), CNC layer (layer 4), HEC layer (layer 5), and medium layer (layer 6).

As the refractive index depends on the wavelength, analysis of results from two or more wavelength yield layer thickness,  $d$ , and refractive index,  $n$ , values using the following procedure:<sup>4</sup>

Chromatic dispersion ( $dn/d\lambda$ ) values of cellulose nanocrystals and hydroxyethyl cellulose (HEC) were assumed to equal that value of pure cellulose,  $-0.0271 \mu\text{m}^{-1}$ .<sup>4,5</sup> This is the averaged value of chromatic dispersion of cellulose at 670 and 785 nm, from <http://refractiveindex.info/>. The corresponding value for water is  $-0.0205 \mu\text{m}^{-1}$ .<sup>6</sup> The  $n$ - $d$  curves of the CNC layer obtained with two wavelengths were plotted on the same axis and the  $n$ - $d$  curve of the 785 nm measurement was shifted by the  $dn/d\lambda$  value of cellulose to obtain the intersection point of the curve of 670 nm and shifted curve of 785 nm (Figure SI-9). The volume fraction of CNC,  $\phi$ , in the CNC layer corresponding to the obtained  $n_{\text{CNC}}$  value, was estimated according to equation 2:

$$n_{\text{CNC}} = \phi n_{\text{cellulose}} + (1-\phi) n_{\text{medium}} \quad (2)$$

where  $n_{\text{cellulose}}$  is 1.466 and  $n_{\text{medium}}$  is 1.330.<sup>4,6</sup>

Based on  $\phi$ , the value of  $dn/d\lambda$  was re-estimated corresponding to equation 2. After this, the intersection point of the  $n$ - $d$  curve of 785 nm and the curve of 670 nm with the corrected  $dn/d\lambda$  was taken as the unique solution for both  $n$  and  $d$  of the CNC layer. The same procedures were repeated for adsorbed polymer layer on the top of CNC-coated substrates, assuming the  $n$  and  $d$  values of CNC layer were not affected with the adsorption of another layer of polymer. HEC with different molecular weights were chosen as model polymers that adsorb on CNC surfaces to investigate the relationship between polymer molecular weight and adsorbed layer thickness. The refractive index parameters of pure HEC,  $n_{\text{HEC}} = 1.466$  and  $dn/d\lambda = -0.0271 \mu\text{m}^{-1}$  were taken from the literature, assuming these values are the same as cellulose.<sup>4,5</sup> The final stage of the iterations of thickness ( $d$ ) and refractive index ( $n$ ) of a HEC250 layer on CNC-coated sensor is shown as an example in Figure SI-9. In the first stage of iteration, the starting values used for chromatic dispersion,  $dn/d\lambda$ , were the averaged value of pure cellulose,  $-0.0204 \mu\text{m}^{-1}$  at 785 nm, and  $-0.0338 \mu\text{m}^{-1}$  at 670 nm. Based on the intersection points obtained with the starting values and corresponding compositions of the film (equation 2), the more accurate values of  $dn/d\lambda$  were

re-estimated to be  $-0.023 \mu\text{m}^{-1}$ . The unique solution of the HEC250 layer properties were found to be  $n = 1.348$  and  $d = 11.0 \text{ nm}$ . The final values of  $\phi$  for CNC and HEC250 layer were found to be  $48 \pm 17\%$ , and  $14 \pm 6\%$ , respectively. It has been found out that in the swollen state adsorbed layer contained only  $\sim 15\text{-}30\%$  cellulose, which is slightly smaller than what we observed here.<sup>4, 7</sup> The same procedures were repeated for HEC720 and HEC1300 to obtain the corresponding adsorbed polymer layer thickness. Typically, two iteration cycles were enough to match the composition of the layer with the chosen value of chromatic dispersion.

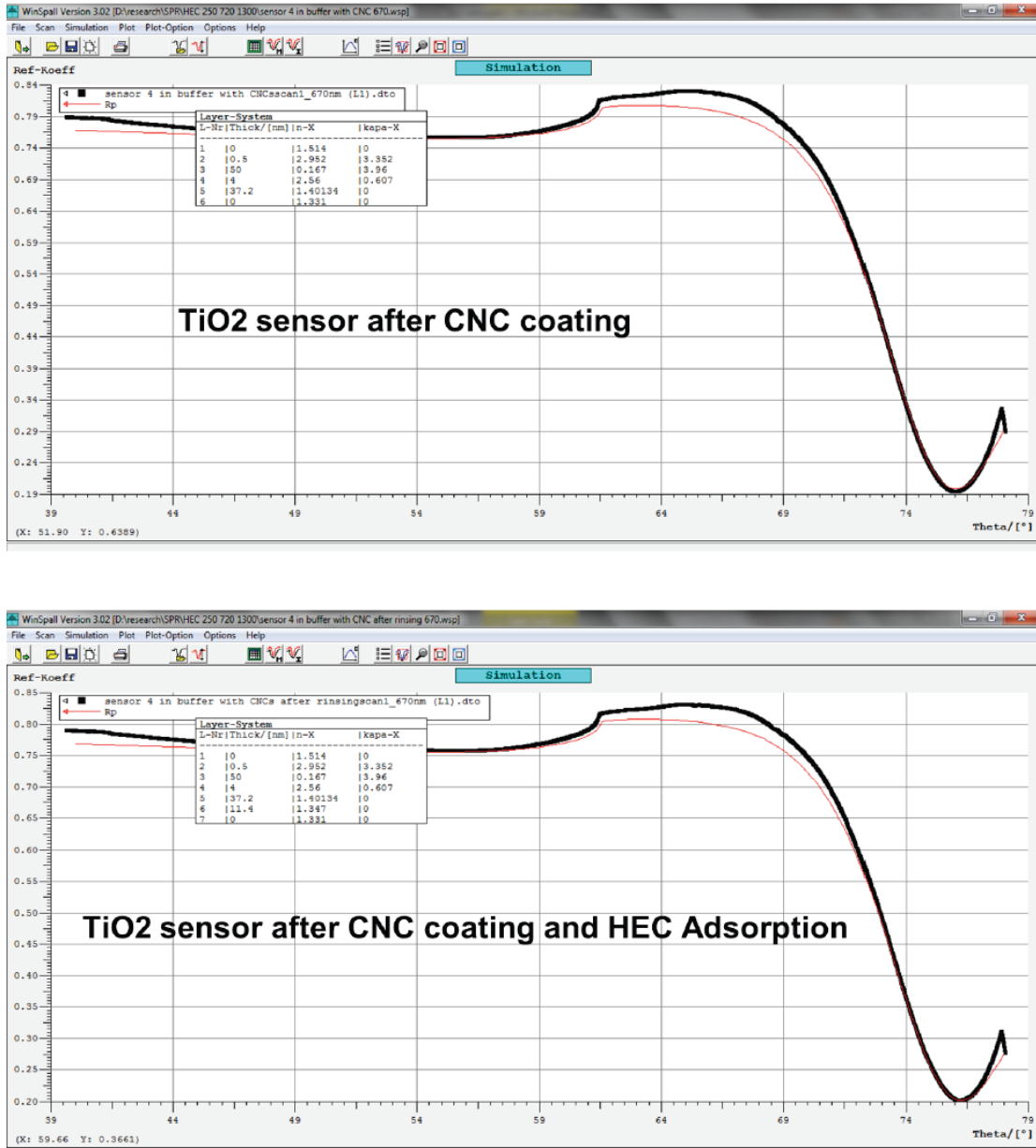


Figure SI- 8. Examples showing the raw SPR data fitting of a  $\text{TiO}_2$  sensor with spin-coated CNC layer (top) and after HEC250 adsorption (bottom) simulated using WinSpall version 3.02.

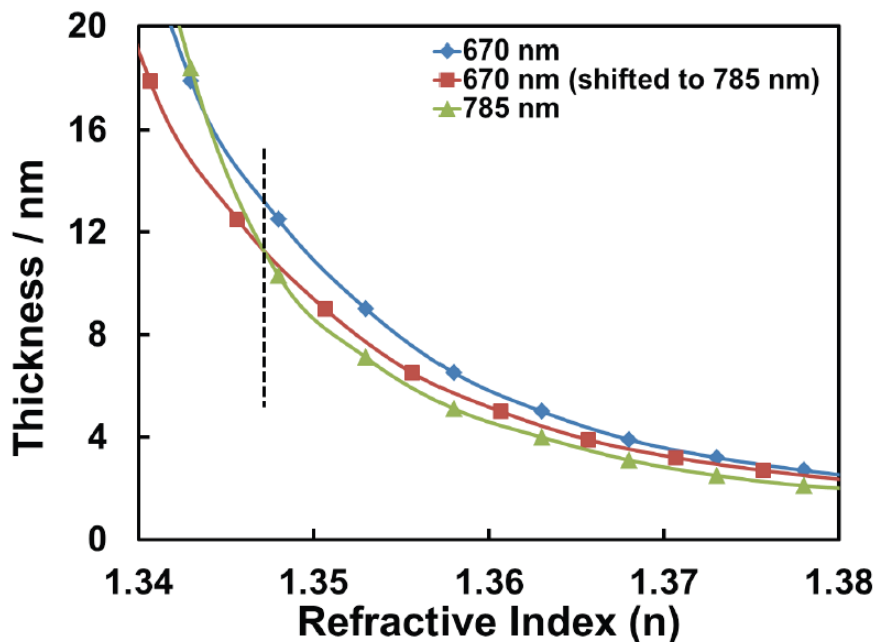


Figure SI- 9. Adsorbed HEC layer thickness versus refractive index measured with two wavelengths by SPR. The final stage of the iterations of thickness ( $d$ ) and refractive index ( $n$ ) of a HEC250 layer on CNC-coated sensor. In the first stage of iteration, the starting values used for chromatic dispersion,  $dn/d\lambda$ , were that of pure cellulose,  $-0.0204 \mu\text{m}^{-1}$  at 785 nm, and  $-0.0338 \mu\text{m}^{-1}$  at 670 nm. Based on the intersection points obtained with the starting values and corresponding compositions of the film (equation 2), the more accurate values of  $dn/d\lambda$  were re-estimated to be  $-0.023 \mu\text{m}^{-1}$ . The unique solution of the HEC250 layer properties were found to be  $n = 1.348$  and  $d = 11.0$  nm.

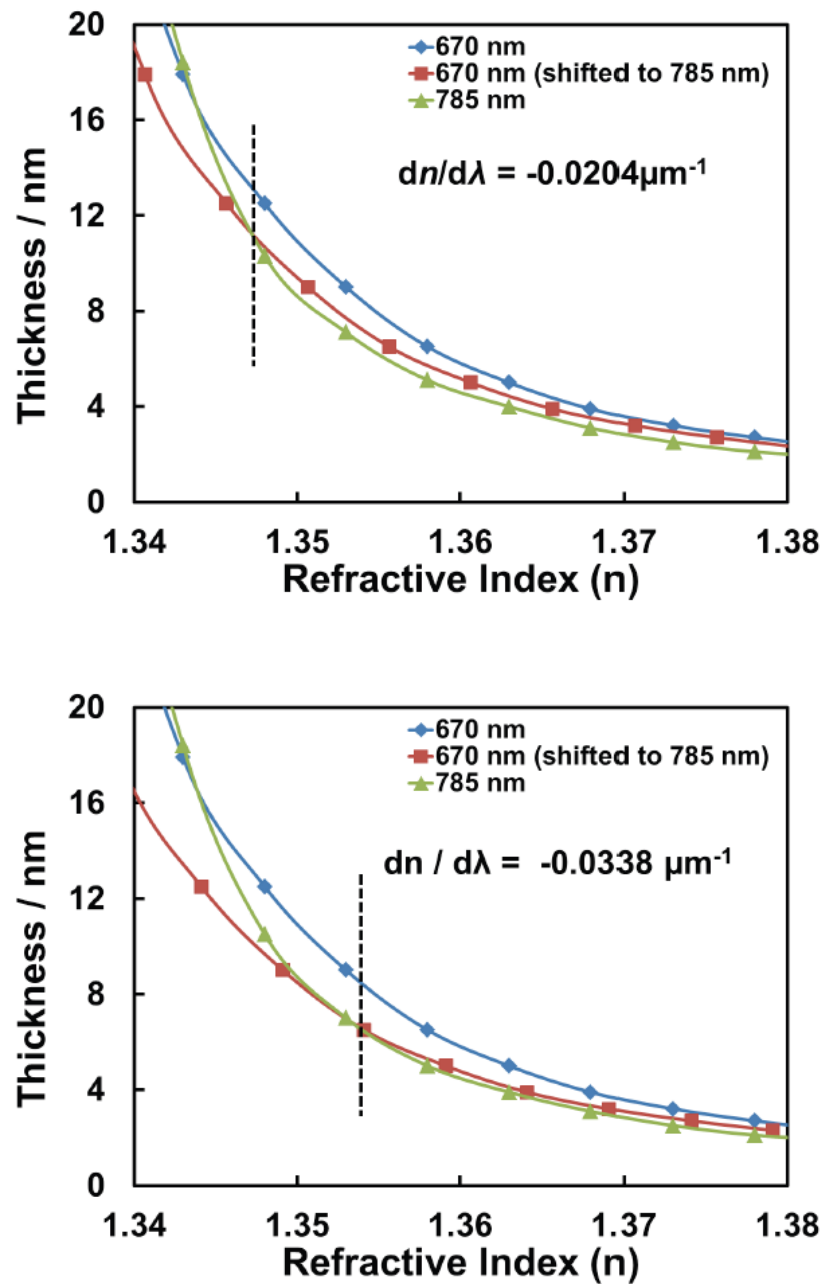


Figure SI- 10. Adsorbed HEC layer thickness versus refractive index measured with two wavelengths by SPR. In the first stage of iteration, the starting values used for chromatic dispersion,  $dn/d\lambda$ , were that of pure cellulose,  $-0.0204 \mu\text{m}^{-1}$  at 785 nm, and  $-0.0338 \mu\text{m}^{-1}$  at 670 nm. These two gave a unique thickness solution of 11.3 nm and 6.0 nm, respectively.

Table SI- 1. Refractive index  $n$ , thickness  $d$ , and CNC or HEC volume fraction  $\phi$  of each layer as determined by multiple iteration method in SPR measurements.

| layer   | $n$   | $d / \text{nm}$                               | $\phi$ |
|---------|-------|---|--------|
| CNC     | 1.401 | 37.2  | 51.8%  |
| HEC250  | 1.348 | 11.0 (6.0 <sup>a</sup> ~11.3 <sup>b</sup> )   | 12.1%  |
| HEC720  | 1.350 | 19.1 (11.5 <sup>a</sup> ~19.8 <sup>b</sup> )  | 13.5%  |
| HEC1300 | 1.347 | 23.1 (18.1 <sup>a</sup> ~ 24.0 <sup>b</sup> ) | 11.9%  |

a: thickness calculated by using  $-0.0338 \mu\text{m}^{-1}$  as the value for  $dn/d\lambda$ ;

b: thickness calculated by using  $-0.0204 \mu\text{m}^{-1}$  as the value for  $dn/d\lambda$ .

As the chromatic dispersion ( $dn/d\lambda$ ) value for HEC is assumed to be the same as pure cellulose as shown in Figure SI-9, sensitivity of thickness  $d$  to  $dn/d\lambda$  is investigated and shown in Table SI-1. Thickness values of the layers of HEC with different  $M_w$  are calculated by using  $-0.0338$  and  $-0.0204 \mu\text{m}^{-1}$  as the values for chromatic dispersion (Figure SI-10), which are the  $dn/d\lambda$  values of cellulose at 670 and 785 nm, respectively. The more accurate values for  $dn/d\lambda$  as determined by iteration method and equation 2 are shown in Figure SI-9 and also listed in Table SI-1. Generally,  $-0.0338 \mu\text{m}^{-1}$  gives smaller thickness values whereas  $-0.0204 \mu\text{m}^{-1}$  gives bigger ones. Iteration method provides values that are between the ones determined by using  $-0.0338 \mu\text{m}^{-1}$  and  $-0.0204 \mu\text{m}^{-1}$ . Though the exact values for thickness seem to be sensitive to chromatic dispersion, the general trend of increasing thickness with the increase of HEC  $M_w$  is well preserved. HEC volume fraction  $\phi$  is found to be much smaller than that of CNC layer, which is likely to be due to the hydration and molecular extending of HEC.

**Atomic Force Microscopy (AFM).** The topography of CNC-coated SPR sensors was characterized by AFM with a BioScope Catalyst™ BioAFM (Bruker AXS, Santa Barbara, CA) in contact mode, using probes from Bruker AFM Probes (SNL-10 type A, 0.35 N/m spring constant, and 65 kHz resonance frequency). The AFM height image in Figure SI-11 confirms the full coverage of CNC on the TiO<sub>2</sub> SPR sensor, which leads us to believe that the underneath TiO<sub>2</sub> surface plays a negligible role in polymer adsorption on CNC-coated sensors.

As shown in Figure SI-11, no overall alignment of the CNC was found in the AFM image of the CNC-coated SPR sensor, which implies that it is unlikely that the CNC film is significantly birefringent. If we simulate the SPR data in Winspall assuming isotropic refractive indices or use  $n_x$ ,  $n_y$  and  $n_z$  values that take into account the birefringence of cellulose ( $\Delta n = 0.06$ ), the SPR

peak angle changes by less than  $0.001^\circ$ . This small difference in signal between an isotropic or anisotropic cellulose film is within the error of the data fitting.

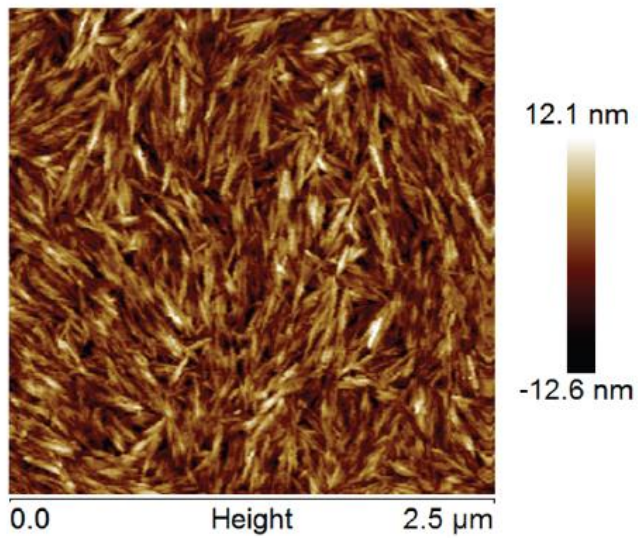


Figure SI- 11. AFM height image of CNC-coated SPR sensor.

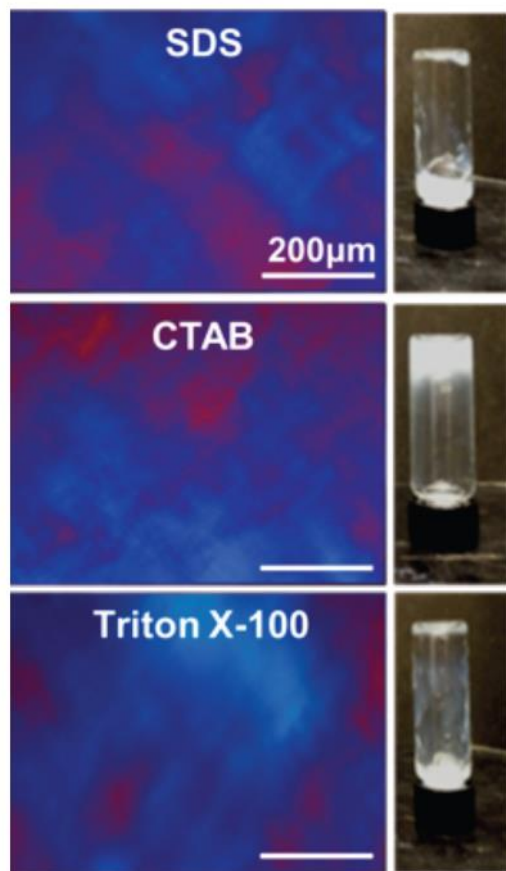


Figure SI 12 POM optical micrographs of HEC1300 (0.2 wt%) + CNC (3 wt%) gels after addition of 10 mM SDS, 2 mM CTAB, or 2 mM Triton X-100. 150 mM HEPES buffer maintained the pH at 7.2.

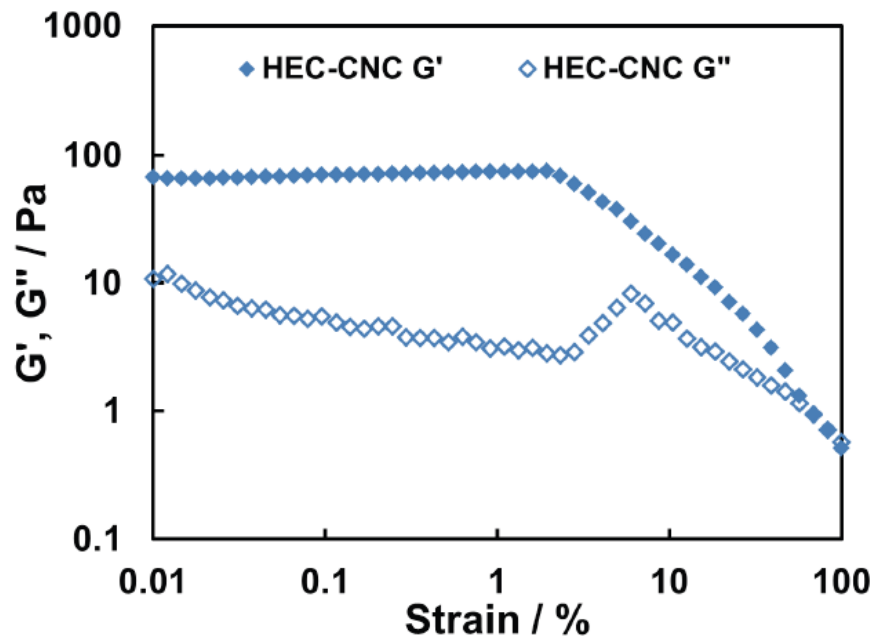


Figure SI-13 Strain sweep results for HEC1300(0.2 wt %)-CNC (3 wt %) mixture in 150 mM HEPES buffer at pH 7.2 at varying strain from 0.01 to 100% with a constant angular frequency of 1 rad/s. Our other gel samples showed similar behaviors and only HEC-CNC sample is plotted.

---

**REFERENCES**

1. Hoare, T.; Pelton, R., Highly pH and temperature responsive microgels functionalized with vinylacetic acid. *Macromolecules* 2004, *37* (7), 2544-2550.
2. Hook, F.; Kasemo, B.; Nylander, T.; Fant, C.; Sott, K.; Elwing, H., Variations in coupled water, viscoelastic properties, and film thickness of a Mefp-1 protein film during adsorption and cross-linking: A quartz crystal microbalance with dissipation monitoring, ellipsometry, and surface plasmon resonance study. *Analytical Chemistry* 2001, *73* (24), 5796-5804.
3. Grassi, J. H.; Georgiadis, R. M., Temperature-Dependent Refractive Index Determination from Critical Angle Measurements: Implications for Quantitative SPR Sensing. *Anal. Chem.* 1999, *71* (19), 4392-4396.
4. Kontturi, K. S.; Kontturi, E.; Laine, J., Specific water uptake of thin films from nanofibrillar cellulose. *Journal of Materials Chemistry A* 2013, *1* (43), 13655-13663.
5. Kasarova, S. N.; Sultanova, N. G.; Ivanov, C. D.; Nikolov, I. D., Analysis of the dispersion of optical plastic materials. *Optical Materials* 2007, *29* (11), 1481-1490.
6. Daimon, M.; Masumura, A., Measurement of the refractive index of distilled water from the near-infrared region to the ultraviolet region. *Applied Optics* 2007, *46* (18), 3811-3820.
7. Kittle, J. D.; Du, X.; Jiang, F.; Qian, C.; Heinze, T.; Roman, M.; Esker, A. R., Equilibrium Water Contents of Cellulose Films Determined via Solvent Exchange and Quartz Crystal Microbalance with Dissipation Monitoring. *Biomacromolecules* 2011, *12* (8), 2881-2887.

**Estimating adsorbed layer R. Pelton 2013****The physical picture**

We assume that polymer adsorbs uniformly on all of the cnc surfaces except the ends. The major assumption is that an invertible gel occurs when the dispersed phase volume fraction, including the contribution of the adsorbed polymer, =1.

**Nomenclature**

$\bar{m}$  or  $\bar{\delta}$  - thickness of saturated adsorbed polymer (nm)  
 $\lambda$  - a range variable (dimensionless 0-1)  
 $C$  - overall mass fraction of dry cnc  
 $c$  - mass fraction of dry cnc, individual phases  
 $d$  - nematic phase particle surface to surface separation without adsorbed polymer  
 $\phi$  - volume fraction  
 $W$  - width of cnc particles  
 $L$  - length length of cnc particles  
 $\rho$  - density

$$T_w := 298K \quad \eta_o := \eta_w(T) = 0.8935 \cdot \text{mPa}\cdot\text{s} \quad \text{Viscosity of water} \quad \rho_w := \frac{\text{gm}}{\text{mL}} \quad \text{Density of water}$$

**CNC Properties**

$$L_{\text{cnc}} := 128\text{nm} \quad \text{Length of CNC particle}$$

$$W_{\text{cnc}} := 7\text{nm} \quad \text{Width of cnc nano boards}$$

$$\rho_{\text{cnc}} := 1.6 \cdot \frac{\text{gm}}{\text{mL}} \quad \text{Density of crystalline cellulose}$$

**Relating Mass and Volume Fractions**

Herein we assume that cnc particles can have adsorbed layer of thickness  $\bar{\delta}$  which contributes to the dispersed phase volume fraction. The following three functions are frequently used in the following modeling.

$$\phi(c_g, \bar{\delta}) := \frac{\rho_w}{\left[ \left( \frac{1}{c_g + 10^{-9}} - 1 \right) \cdot \rho_{\text{cnc}} + \rho_w \right]} \cdot \frac{(W_{\text{cnc}} + 2\bar{\delta})^2}{W_{\text{cnc}}^2} \quad \text{Volume fraction of cnc suspension including adsorbed layer thickness, } \bar{\delta}. \text{ This function ignores the contribution of polymer adsorbed on the ends of the cnc particles - the E-9 term prevents division by zero errors if concentration is 0}$$

$$x_{\text{cnc}}(\bar{\delta}, \phi) := \frac{\rho_{\text{cnc}}}{\rho_{\text{cnc}} + \frac{\rho_w}{\phi} \cdot \frac{(W_{\text{cnc}} + 2\bar{\delta})^2}{W_{\text{cnc}}^2} - \rho_w} \quad \text{This is the mass fraction of pure cellulose as function of total volume fraction } \phi \text{ and adsorbed layer thickness } \bar{\delta}$$

$$N_{\text{cnc}}(c_g) := \frac{c_g}{(L_{\text{cnc}} \cdot W_{\text{cnc}}^2 \cdot \rho_{\text{cnc}}) \cdot \left( \frac{1 - c_g}{\rho_w} + \frac{c_g}{\rho_{\text{cnc}}} \right)} \quad \text{Corresponding number concentration}$$

**Minimum adsorbed layer thickness for gelation**

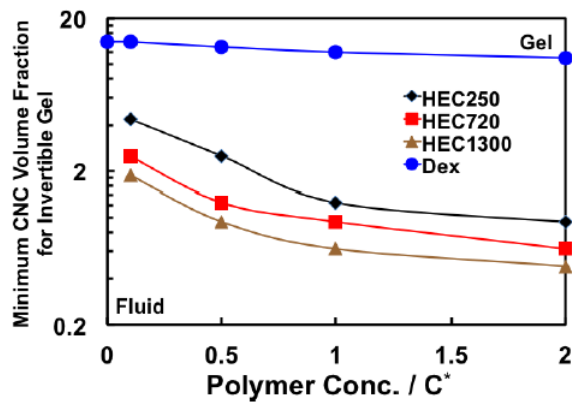
For a given cnc mass fraction of cellulose,  $C_t$ , the following function calculates the minimum adsorbed layer thickness required for gelation.

$$\bar{\delta}_w := \text{nm} \quad \text{adsorbed layer thickness, a variable}$$

$$\bar{\delta}_o := 0\text{nm} \quad \text{zero thickness}$$

$$\bar{\delta}_g(C_t) := \text{root}(\phi(C_t, \bar{\delta}) - 1, \bar{\delta}) \quad \text{Numerically finding } \bar{\delta} \text{ value that gives total volume fraction} = 1.$$

Experimental data



$$\delta_o = 0$$

HEC 250 kDa

HEC 770 kDa

HEC 1300 kDa

$$\phi_{250} := \begin{pmatrix} 4.471 \\ 2.5 \\ 1.25 \\ 0.94 \end{pmatrix} \%$$

$$\phi_{770} := \begin{pmatrix} 2.5 \\ 1.25 \\ 0.94 \\ 0.625 \end{pmatrix} \%$$

$$\phi_{1300} := \begin{pmatrix} 1.875 \\ 0.94 \\ 0.625 \\ 0.48 \end{pmatrix} \%$$

Experiment volume fraction of cellulose only corresponding to gelation

$$C_{250} := c(\delta_o, \phi_{250})$$

$$C_{770} := c(\delta_o, \phi_{770})$$

$$C_{1300} := c(\delta_o, \phi_{1300})$$

Corresponding total mass fraction of cellulose

$$C_{250} = \begin{pmatrix} 6.9667 \\ 3.9409 \\ 1.9851 \\ 1.4956 \end{pmatrix} \%$$

$$C_{770} = \begin{pmatrix} 3.9409 \\ 1.9851 \\ 1.4956 \\ 0.9963 \end{pmatrix} \%$$

$$C_{1300} = \begin{pmatrix} 2.9666 \\ 1.4956 \\ 0.9963 \\ 0.7658 \end{pmatrix} \%$$

$$\delta_{250} := \overrightarrow{\delta_g(C_{250})} \qquad \delta_{770} := \overrightarrow{\delta_g(C_{770})} \qquad \delta_{1300} := \overrightarrow{\delta_g(C_{1300})}$$

$$\delta_{250} = \begin{pmatrix} 13.0526 \\ 18.6359 \\ 27.805 \\ 32.5997 \end{pmatrix} \cdot \text{nm} \qquad \delta_{770} = \begin{pmatrix} 18.6359 \\ 27.805 \\ 32.5997 \\ 40.7719 \end{pmatrix} \cdot \text{nm} \qquad \delta_{1300} = \begin{pmatrix} 22.0604 \\ 32.5997 \\ 40.7719 \\ 47.0181 \end{pmatrix} \cdot \text{nm}$$

Calculating thickness values corresponding to  $\phi =$

**Thickness values as functions of MW**

$$\delta_{\text{sat}} := \begin{pmatrix} \delta_{250_3} \\ \delta_{770_3} \\ \delta_{1300_3} \end{pmatrix} \qquad \delta_{\text{sat}} = \begin{pmatrix} 32.5997 \\ 40.7719 \\ 47.0181 \end{pmatrix} \cdot \text{nm} \qquad \text{Model fit to highest HEC concentration}$$

$$\delta_{\text{low}} := \begin{pmatrix} \delta_{250_0} \\ \delta_{770_0} \\ \delta_{1300_0} \end{pmatrix} \qquad \delta_{\text{low}} = \begin{pmatrix} 13.0526 \\ 18.6359 \\ 22.0604 \end{pmatrix} \cdot \text{nm} \qquad \text{Model fit to lowest HEC concentration}$$

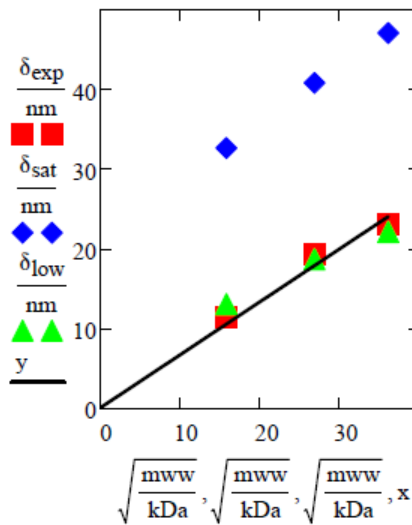
$$\delta_{\text{exp}} := \begin{pmatrix} 11.4 \\ 19.3 \\ 23.1 \end{pmatrix} \cdot \text{nm} \qquad \text{results from SPR}$$

$$kDa := 1000\text{Da}$$

Line

$$mww := \begin{pmatrix} 250 \\ 720 \\ 1300 \end{pmatrix} \text{kDa} \qquad y := \begin{pmatrix} 0 \\ 24 \end{pmatrix} \qquad x := \begin{pmatrix} 0 \\ \sqrt{1300} \end{pmatrix}$$

**Figure for paper**



**SLO model - Dong Gray 1996 - Pelton Dec 2013**

the goal is to extend Dong and Gray calculations to include the effects of cnc length. Number concentrations are converted to mass/L

$$T_w := 298\text{K}$$

$$\eta_o := \eta_w(T) = 0.8935 \cdot \text{mPa}\cdot\text{s} \quad \text{Viscosity of water}$$

$$\text{mM} := 0.001 \frac{\text{mole}}{\text{L}} \quad \epsilon_r := 78$$

$$\rho_w := \frac{\text{gm}}{\text{mL}} \quad \text{Density of water}$$

**CNC Properties**

$$L_{\text{cnc}} := 115\text{nm}$$

Length of CNC particle

Specific surface area

ignoring contributions of ends

$$W_{\text{cnc}} := 7\text{nm}$$

Width of cnc nano boards

$$\rho_{\text{cnc}} := 1.6 \cdot \frac{\text{gm}}{\text{mL}}$$

Density of crystalline cellulose

$$\sigma_{\text{cnc}} := \frac{(W_{\text{cnc}} \cdot L_{\text{cnc}} \cdot 4)}{(W_{\text{cnc}}^2 \cdot L_{\text{cnc}} \cdot \rho_{\text{cnc}})} = 357.1429 \cdot \frac{\text{m}^2}{\text{gm}}$$

**Relating Mass and Volume Fractions**

Herein we assume that cnc particles can have adsorbed layer of thickness  $\delta$  which contributes to the dispersed phase volume fraction. The following three functions are frequently used in the following modeling.

$$\phi(c_g, \delta) := \frac{\rho_w}{\left[ \left( \frac{1}{c_g + 10^{-9}} - 1 \right) \cdot \rho_{\text{cnc}} + \rho_w \right]} \cdot \frac{(W_{\text{cnc}} + 2\delta)^2}{W_{\text{cnc}}^2}$$

Volume fraction of cnc suspension including adsorbed layer thickness,  $\delta$ . This function ignores the contribution of polymer adsorbed on the ends of the cnc particles - the E-9 term prevents division by zero errors if concentration is 0

$$\epsilon(\delta, \phi) := \frac{\rho_{\text{cnc}}}{\rho_{\text{cnc}} + \frac{\rho_w}{\phi} \cdot \frac{(W_{\text{cnc}} + 2\delta)^2}{W_{\text{cnc}}^2} - \rho_w}$$

This is the inverse function  
Corresponding number concentration

$$N_{\text{cnc}}(c_g) := \frac{c_g}{(L_{\text{cnc}} \cdot W_{\text{cnc}}^2 \cdot \rho_{\text{cnc}}) \cdot \left( \frac{1 - c_g}{\rho_w} + \frac{c_g}{\rho_{\text{cnc}}} \right)}$$

Dong and Gray relating number conc. and mass fraction

$$C = \frac{w}{[w + (100 - w)\rho]LD^2}$$

**Solution properties**

$$\text{NaCl} := 0.7\text{mM}$$

$$Q := \frac{\epsilon_o^2}{(\epsilon_r \epsilon_o \cdot k_b \cdot T)} = 9.0339 \cdot \text{nm}$$

Bjerrum length value does not agree with Dong and Gray

$$\kappa(\text{NaCl}) := \left( \frac{\epsilon_o^2 \cdot N_{\text{av}}}{\epsilon_r \epsilon_o \cdot k_b \cdot T} \cdot 2 \cdot \text{NaCl} \right)^{0.5}$$

$$\kappa := \kappa(\text{NaCl})$$

$$\frac{1}{\kappa} = 11.4584 \cdot \text{nm}$$

Salt conc varied to give kappa value in first row of Table 2 Dong Gray

$$D_{\text{eff}} = D + \kappa^{-1}(\ln A' + 0.7704)$$

where

SLO theory uses electrostatic arguments to calculate the apparent diameter of cnc particles. The values in D&G are very large

$$A' = 2\pi\nu_{\text{eff}}^2 Q \kappa^{-1} \exp(-\kappa D)$$

In these equations,  $Q = e^2/\epsilon k_B T$  is the Bjerrum (7.14 Å for this aqueous system at 25 °C), .

$$C_1 = 3.290[(1 - 0.675h)b]^{-1} \quad (1)$$

$$C_2 = 4.191[(1 - 0.730h)b]^{-1}$$

SLO equations from Dong and Gray

where the concentrations are expressed as the number density of rods,  $b$  is the second virial coefficient of the system, and  $b$  and  $h$  are given by

$$b = \frac{\pi}{4} L^2 D_{\text{eff}} \quad (2)$$

$$h = (\kappa D_{\text{eff}})^{-1} \quad (3)$$

Here,  $D_{\text{eff}}$  is defined as

$$D_e := 86.6 \text{ nm}$$

$$N_{T1}(D_e, \kappa, L_{\text{cnc}}) := 3.290 \cdot \frac{1}{\left[1 - 0.675 \cdot (\kappa \cdot D_e)^{-1}\right] \cdot \frac{\pi}{4} \cdot L_{\text{cnc}}^2 \cdot D_e}$$

$$\kappa = 8.7272 \times 10^7 \text{ m}^{-1}$$

$$N_{T2}(D_e, \kappa, L_{\text{cnc}}) := 4.1910 \cdot \frac{1}{\left[1 - 0.730 \cdot (\kappa \cdot D_e)^{-1}\right] \cdot \frac{\pi}{4} \cdot L_{\text{cnc}}^2 \cdot D_e}$$

$$c_{\text{cnc}}(\phi) := \frac{\rho_{\text{cnc}}}{\rho_{\text{cnc}} + \frac{\rho_w}{\phi} - \rho_w}$$

Only valid if volume fraction is pure cellulose

Table from D&G

Table 2. Comparison of Theory and Experiment for Suspensions with Added Electrolyte

| $n_c$<br>(mM) | $\kappa^{-1}$<br>(nm) | $v_{\text{eff}}$<br>(e/nm) | $h$   | $D_{\text{eff}}$<br>(nm) | $b \times 10^5$<br>(nm <sup>3</sup> ) | $C_{\text{ic}} \times 10^{-6}$<br>(nm <sup>-3</sup> ) | $C_{\text{ac}} \times 10^{-6}$<br>(nm <sup>-3</sup> ) | $C_i \times 10^{-6}$<br>(nm <sup>-3</sup> ) | $C_a \times 10^{-6}$<br>(nm <sup>-3</sup> ) |
|---------------|-----------------------|----------------------------|-------|--------------------------|---------------------------------------|---|---|---|---|
| 0             | 11.76                 | 3.72                       | 0.136 | 86.6                     | 143.9                                 | 4.02  | 5.17  | 8.29  | 10.06                                       |
| 0.43          | 9.17                  | 3.87                       | 0.139 | 66.0                     | 109.7                                 | 5.30  | 6.80  | 8.31  | 10.10                                       |
| 0.53          | 8.77                  | 3.99                       | 0.140 | 62.8                     | 104.3                                 | 5.56  | 7.15  | 8.27  | 9.92  |
| 0.83          | 7.87                  | 4.00                       | 0.141 | 56.0                     | 93.1                                  | 6.25  | 8.03  | 8.48  | 10.20                                       |
| 1.05          | 7.35                  | 4.07                       | 0.141 | 52.0                     | 86.4                                  | 6.73  | 8.65  | 8.54  | 10.03                                       |
| 1.38          | 6.71                  | 4.17                       | 0.142 | 47.2                     | 78.4                                  | 7.42  | 9.54  | 8.77  | 10.31                                       |
| 1.65          | 6.32                  | 4.25                       | 0.143 | 44.4                     | 73.8                                  | 7.90  | 10.15   | 8.77  | 10.31                                       |
| 1.98          | 5.92                  | 4.34                       | 0.143 | 41.3                     | 68.6                                  | 8.48  | 10.90   | 9.03  | N.A.  |
| 2.37          | 5.55                  | 4.46                       | 0.143 | 38.5                     | 64.0                                  | 9.10  | 11.70   | 9.03  | N.A.  |

## Calculating transition concentrations

$$N_{T1}(86.6\text{nm}, \kappa, L_{\text{cnc}}) = 4.0163 \times 10^{-6} \cdot \text{nm}^{-3} \quad \text{These two values agree with table above}$$

$$N_{T2}(86.6\text{nm}, \kappa, L_{\text{cnc}}) = 5.1574 \times 10^{-6} \cdot \text{nm}^{-3}$$

$$N_{T1}(86.6\text{nm}, \kappa, L_{\text{cnc}} \cdot 1.5) = 1.785 \times 10^{-6} \cdot \text{nm}^{-3} \quad \text{These two are new values - longer cnc}$$

$$N_{T2}(86.6\text{nm}, \kappa, L_{\text{cnc}} \cdot 1.5) = 2.2922 \times 10^{-6} \cdot \text{nm}^{-3}$$

$$\frac{1}{\kappa \kappa(3.0\text{mM})} = 5.5349 \times 10^{-9} \text{ m} \quad \text{Finding a salt conc to give same kappa as table above}$$

## Converting number concentrations to wt percentages

$$m_c(N, L_{\text{cnc}}) := N \cdot W_{\text{cnc}}^2 \cdot L_{\text{cnc}} \cdot \rho_{\text{cnc}}$$

$$m_c\left(\frac{4.02 \cdot 10^{-6}}{\text{nm}^3}, L_{\text{cnc}}\right) = 36.2443 \cdot \frac{\text{gm}}{\text{L}} \quad m_c\left[\frac{(5.17 \cdot 10^{-6})}{\text{nm}^3}, L_{\text{cnc}}\right] = 46.6127 \cdot \frac{\text{gm}}{\text{L}}$$

## **Chapter 3 Surfactant-enhanced Cellulose Nanocrystal Pickering Emulsions**

In chapter 3, all experiments were conducted by myself with assistance from Sarah Ballinger (undergraduate student). The paper was initially drafted by Dr. Emily D. Cranston and myself, and edited later to final version by Dr. Robert Pelton and Dr. Emily D. Cranston. This work has been published in *Journal of Colloid and Interface Science*, 2015, 439 (10), pp 139-148. It is produced by permission of Elsevier.



Contents lists available at ScienceDirect

## Journal of Colloid and Interface Science

www.elsevier.com/locate/jcis



## Surfactant-enhanced cellulose nanocrystal Pickering emulsions



Zhen Hu, Sarah Ballinger, Robert Pelton, Emily D. Cranston\*

Department of Chemical Engineering, McMaster University, 1280 Main Street West, Hamilton, Ontario L8S 4L7, Canada

## ARTICLE INFO

## Article history:

Received 14 September 2014

Accepted 20 October 2014

Available online 29 October 2014

## Keywords:

Cellulose nanocrystals

Emulsions

Double phase inversion

Pickering

Surfactants

Confocal microscopy

Surface and interfacial tension

Fluorescent labeling

## ABSTRACT

The effect of surfactants on the properties of Pickering emulsions stabilized by cellulose nanocrystals (CNCs) was investigated. Electrophoretic mobility, interfacial tension, confocal microscopy and three-phase contact angle measurements were used to elucidate the interactions between anionic CNCs and cationic alkyl ammonium surfactants didecyltrimethylammonium bromide (DMAB) and cetyltrimethylammonium bromide (CTAB). Both surfactants were found to adsorb onto CNCs with concentration-dependent morphology. At low concentrations, individual surfactant molecules adsorbed with alkyl tails pointing outward leading to hydrophobic CNCs. At higher concentrations, above the surfactant's apparent critical micelle concentration, surfactant aggregate morphologies on CNCs were inferred and the hydrophobicity of CNCs decreased. DMAB, which has two alkyl tails, rendered the CNCs more hydrophobic than CTAB which has only a single alkyl tail, at all surfactant concentrations. The change in CNC wettability from surfactant adsorption was directly linked to emulsion properties; adding surfactant increased the emulsion stability, decreased the droplet size, and controlled the internal phase of CNC Pickering emulsions. More specifically, a double transitional phase inversion, from oil-in-water to water-in-oil and back to oil-in-water, was observed for emulsions with CNCs and increasing amounts of DMAB (the more hydrophobic surfactant). With CNCs and CTAB, no phase inversion was induced. This work represents the first report of CNC Pickering emulsions with surfactants as well as the first CNC Pickering emulsions that can be phase inverted. The ability to surface modify CNCs *in situ* and tailor emulsions by adding surfactants may extend the potential of CNCs to new liquid formulations and extruded/spray-dried materials.

© 2014 Elsevier Inc. All rights reserved.

## 1. Introduction

Cellulose nanocrystals (CNCs)<sup>1</sup> are new commercially available nanoparticles which are derived from natural cellulose sources and have recently been demonstrated to stabilize emulsions [1–5]. Due to their “green” nature and non-toxicity [6], CNCs show great promise as emulsifiers, stabilizers and gelation agents in formulated chemical products such as foods, pharmaceuticals, household cleaning agents and personal care products. The intermediate wettability and nanometric size of CNCs allows them to adsorb at oil–water interfaces, similar to the first particle-stabilized emulsions described by Ramsden [7] and Pickering [8]. So-called Pickering emulsions are ubiquitous in nature and have become more common in commercial

products because they are generally more stable to coalescence than emulsions stabilized by surfactants alone. The ability to control emulsion stability, the nature of an emulsion's continuous phase, and the internal phase droplet size, has important implications in both chemical processing and new product development.

Pickering emulsion stability is attributed to the formation of a densely packed particle layer at the oil–water interface, which prevents droplet coalescence through a mechanical barrier mechanism and slows creaming or sedimentation [9]. The magnitude of the mechanical barrier is determined by the energy required to remove a particle from the interface, which is a function of the three-phase contact angle of the particle ( $\theta_{ow}$ ) [10]. For contact angles around 90°, this energy is considerably large (on the order of  $10^5 k_B T$  for a 100 nm spherical particle) [11,12]. Therefore, once a partially wettable particle is at the oil–water interface, it will not leave spontaneously. Interestingly, small changes in the chemical composition of the particles or the oil and water phases, salt concentration [13], pH [14], temperature [15] and particle shape [16,17], lead to major changes in emulsion stability, and rich physicochemical phenomena overall.

\* Corresponding author.

E-mail addresses: huz7@mcmaster.ca (Z. Hu), ballinse@mcmaster.ca (S. Ballinger), peltonrh@mcmaster.ca (R. Pelton), ecranst@mcmaster.ca (E.D. Cranston).

<sup>1</sup> CMC = critical micelle concentration; CNCs = cellulose nanocrystals; CTAB = cetyltrimethylammonium bromide; DMAB = didecyltrimethylammonium bromide; DTAF = 5-(4,6-dichlorotriazinyl) aminofluorescein; o/w = oil-in-water; w/o = water-in-oil.

Inorganic or petrochemical-based particles of silica, clay, calcium carbonate, hematite, polystyrene, and microgels, ranging in size from nanometers to micrometers, can all stabilize Pickering emulsions [9,18]. In many applications, however, organic and biocompatible colloidal particles are preferred, making materials like starch [19–22] and cellulose more suitable. Previous work has examined Pickering emulsions with various types of small cellulose particles including cellulose nanocrystals [1–5,23,24], cellulose fibrils [25–30], microcrystalline cellulose [25,26,31], bacterial cellulose [32,33], and cellulose derivatives [34].

Cellulose nanocrystals are rod-shaped, highly crystalline nanoparticles which can be extracted from wood, cotton, bacteria, algae, tunicin and other plant sources. CNCs are most commonly prepared by sulfuric acid hydrolysis [35] which gives nanocrystals with anionic sulfate half-ester groups on their surface (approximately 1 sulfate half-ester per 3 nm<sup>2</sup> or 1 sulfate half-ester in every 6 surface hydroxyl groups). Typical dimensions of CNCs range from 5 to 20 nm in cross-section by hundreds of nanometers long, depending on the cellulose source and hydrolysis conditions (Fig. 1) [36]. CNCs form stable colloidal suspensions in water, above pH 2.5 and below ionic strengths of 100 mM [37,38], and exhibit lyotropic liquid crystalline behavior [39]. The main advantage of using CNCs in new formulations and composites stems from their favorable material properties including a large elastic modulus, high aspect-ratio, high surface-area-to-volume ratio, low density, and general chemical and thermal stability. CNCs and the “Nanocellulose family” are further discussed in a number of comprehensive review articles and books [40–43].

Recent results of Capron and co-workers have highlighted the use of CNCs as emulsion stabilizers [1–5]. They have established that despite the fact that cellulose and CNCs are normally considered hydrophilic (due to the high density of hydroxyl groups and an air–water contact angle around 20°) [44], the crystalline organization of polymer chains allows for a “hydrophobic edge” to the nanocrystals and thus amphiphilic properties overall [1]. The insolubility of cellulose in common solvents is also attributed to these hydrophobic interactions which contribute to the crystalline organization of cellulose chains, along with extensive hydrogen bonding [45]. Unmodified CNCs are effective at stabilizing emulsions when they have a low surface charge density, or when the surface charge is screened in the presence of salt [1–3]. Furthermore, lower concentrations of CNCs are needed for stable emulsions when nanocrystals with larger aspect ratios are used. For example, long bacterial cellulose-derived CNCs only need to cover 40% of the emulsion droplet surface area to impede droplet coalescence as the CNCs form an interconnected mesh-like structure, compared to 84% surface coverage required for shorter cotton-derived CNCs [3]. High-internal-phase emulsion “gels” have also been prepared by making CNC-stabilized emulsions with equal parts oil and water and then slowly increasing the oil content; this is possible because the high aspect ratio CNCs are close-packed in the original emulsion but are then separated into a diluted mesh network, without

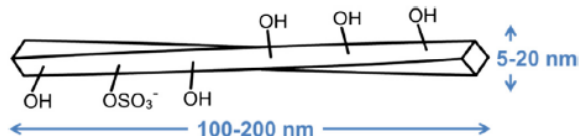


Fig. 1. Schematic representation of a cellulose nanocrystal which is composed of high molecular weight homopolymer chains of  $\beta$ -1,4 linked anhydro-D-glucose units. The cellulose chains are arranged parallel into the native cellulose I crystal structure where the hydroxyl groups are positioned in the equatorial plane and the hydrogen atoms are in the axial position. The sulfuric acid hydrolysis production method replaces some surface hydroxyl groups with anionic sulfate half-ester groups (not drawn to scale).

leaving the oil–water interface, as oil is added [4]. In another literature example, grafting thermo-responsive polymers to CNCs to control the hydrophobicity with temperature also led to successful stabilization of emulsions [24]. To the best of our knowledge all CNC Pickering emulsions described to-date have been oil-in-water type (o/w) emulsions [46].

The internal emulsion phase (oil or water) and the stability of Pickering emulsions can be controlled by combining surfactants with colloidal particles [47]. As a result of particle–surfactant synergy, relatively small amounts of both emulsifiers are needed and properties can be finely tuned by varying the ratio of the two components. Binks et al. [48–55], demonstrated that surfactant-containing Pickering emulsions may undergo single phase inversions (o/w to w/o) or double phase inversions (o/w to w/o [phase inversion 1], followed by w/o to o/w [phase inversion 2]) by increasing the surfactant concentration. Such transitional phase inversions have been observed for silica and calcium carbonate nanoparticles with oppositely charged surfactants, i.e., cationic alkyl-ammonium surfactants for silica, and anionic C<sub>6</sub>–C<sub>12</sub> sodium carboxylate fatty acids, sodium dodecylsulfate and sodium 2-ethylhexylsulfosuccinate for CaCO<sub>3</sub>. The phase inversions are attributed to the adsorption of oppositely charged surfactant at the particle surface which changes the particle's wettability. Surfactants that can pack densely on the particle surface or that have long (or multiple) alkyl tails easily lead to more hydrophobic particles at low surfactant concentration which then become hydrophilic again at high surfactant concentration due to surfactant bilayer adsorption (or perhaps more precisely, admicelle aggregates adsorbed on the nanoparticle surfaces).

This work aims to understand how surfactants influence the stability of CNC Pickering emulsions. Specifically, single C<sub>16</sub> alkyl tail cetyltrimethylammonium bromide (CTAB) and double C<sub>10</sub> alkyl tail didecyldimethylammonium bromide (DMAB) surfactants with lab-made sulfuric acid hydrolyzed CNCs (from cotton) are investigated. Particle–surfactant interactions are measured by electrophoretic mobility, interfacial tension and contact angle and correlated with CNC-stabilized water–dodecane emulsion properties. By adding surfactant, we demonstrate for the first time a double phase inversion in CNC Pickering emulsions, and as a result, obtain the first water-in-oil type emulsion with CNCs. Emulsions are characterized by confocal microscopy, conductivity and droplet sizing and the stability mechanism is elucidated using fluorescently labeled CNCs. To the best of our knowledge, this is the first report of tailored CNC Pickering emulsions enhanced with surfactants and represents progress towards developing related CNC-based products, such as CNC-containing emulsions, biphasic gels, foams and extruded/spray-dried materials.

## 2. Experimental

### 2.1. Materials

Cetyltrimethylammonium bromide (CTAB), didecyldimethylammonium bromide (DMAB), dodecane, Nile red and sulfuric acid were obtained from Sigma–Aldrich. All measurements were performed at room temperature unless otherwise specified.

### 2.2. Preparation of cellulose nanocrystals

A suspension of cellulose nanocrystals (CNCs) was prepared by sulfuric acid hydrolysis, as previously described [56]. 40 g of cotton (Whatman ashless filter aid) was treated with 700 mL of 64 wt.% sulfuric acid at 45 °C for 45 min with continuous stirring. Immediately after, the reaction was quenched with 4 °C purified water (Barnstead NANOpure Diamond system, ThermoScientific,

Asheville, NC) to a 10-fold dilution. The suspension was centrifuged at 6000 rpm to remove excess acid, and dialysed until neutral pH was achieved. The suspension was sonicated for 15 min three times (Sonifier 450, Branson Ultrasonics, Danbury, CT) at intensity level 6 and 60% pulses, in an ice bath to prevent overheating. Dowex Marathon C Hydrogen form resin (Sigma–Aldrich) was added to the suspension for 2 days and removed with glass filter paper (Whatman grade GF/B, WWR, Chicago, IL). The surface charge density of sulfate half-ester groups on CNCs was determined by conductometric titration to be  $0.33 \pm 0.02 \text{ e/nm}^2$  (equivalent to ca. 0.5% sulfur or  $0.16 \pm 0.02 \text{ meq/g}$  cellulose), with average crystal dimensions of  $128 \times 7 \text{ nm}$  from transmission electron microscopy (TEM) image analysis. A TEM micrograph of the CNCs is presented in Supporting Information Fig. S1.

Fluorescently labeled CNCs, dyed with 5-(4,6-dichlorotriazinyl)aminofluorescein (DTAF) were prepared as previously described in a facile, one-pot reaction under alkaline conditions [57]. The degree of labeling is estimated at 24 nmol of DTAF per g of cellulose, or 4 DTAF molecules per  $10^5$  anhydroglucose units, which is readily visible by fluorescence microscopy without significantly altering the surface chemistry or charge of the CNCs.

### 2.3. Preparation of the emulsions

Batch emulsions of 6 mL containing equal volumes of dodecane and aqueous dispersions (1:1 oil to water) were prepared by mixing 1.5 mL of 0.5 wt.% CNCs and 1.5 mL of CTAB or DMAB solution (concentrations ranging from 0.25 mM to 32 mM). The final concentration of CNCs in the emulsions is thus 0.25 wt.%. After combining the components, the mixture were immediately emulsified using a sonicator (Sonifier 450, Branson Ultrasonics, Danbury, CT) while in an ice bath for 1 min at an intensity level 6 and 50% pulses for every emulsion. This corresponds to an energy input of approximately 1371 J/g of emulsion. All measurements and photographs are taken approximately 3 h after emulsion preparation.

### 2.4. Electrophoretic mobility of CNCs with surfactants

The electrophoretic mobility was measured at 25 °C using a Zeta Potential ZetaPlus analyzer (Brookhaven, Holtsville, NY). CNCs (0.5 wt.%) were mixed with equal volume of surfactant solutions with various concentrations. All electrophoretic mobility data points were the average values of 10 measurements with 15 cycles per measurement. Error bars represent one standard deviation of the mean.

### 2.5. Interfacial and surface tension

Interfacial tension was measured by the pendant drop method using a Krüss Drop Shape Analysis System DSA10 instrument. Prior to the measurement, a sample (ca. 50 mL) of dodecane was added to a glass box of  $5.0 (L) \times 5.0 (W) \times 5.0 (H) \text{ cm}$ , and a pendant drop of surfactant aqueous solution of 20  $\mu\text{L}$ , with or without CNCs (0.25 wt.%), was formed on the end of a stainless steel needle immersed in the oil phase. The aging of the interface can be accurately monitored by measuring the dynamic interfacial tension of a drop having a constant interfacial area. Typically, the data collected after 20 min aging were used as the equilibrium interfacial tension values. Similarly, surface tension was also measured by the pendant drop method using air as the continuous phase instead of dodecane.

### 2.6. Contact angle at oil–water–CNC interface

The static contact angle measurements were performed using a Krüss Drop Shape Analysis System DSA10 (Hamburg, Germany)

instrument at room temperature ( $22 \pm 2 \text{ }^\circ\text{C}$ ). Uniform films for contact angle measurements were obtained by spin coating (Chemat Technology KW-4A, Northridge, CA)  $\sim 2 \text{ wt.}\%$  CNC suspension onto polyvinyl amine ( $M_w = 45 \text{ kDa}$ , BASF, Ludwigshafen, Germany) coated Si wafers at 3000 rpm for 60 s, followed by heat treatment for 12 h at 80 °C. The contact angles of 10  $\mu\text{L}$  aqueous surfactant solution on CNC films were measured under dodecane. A small piece of CNC-coated Si wafer was put in a glass box of  $5.0 (L) \times 5.0 (W) \times 5.0 (H) \text{ cm}$ , and a sessile drop of surfactant solution of 10  $\mu\text{L}$  was released, followed by adding the oil phase using a pipet along the wall of the box until the surfactant drop was totally immersed. The image of the sessile drop was recorded, and the contact angle was measured using ImageJ software. Error bars represent one standard deviation of the mean.

### 2.7. Confocal laser scanning microscopy (CLSM)

For CLSM visualization, the oil phase was stained with Nile red (492/520 nm). Images were acquired using a Zeiss LSM 510 Meta on a Axiovert 200M microscope (Zeiss, Gottingen, Germany) using a  $\times 63$  water-immersion laser technique. The freshly prepared emulsion was placed on the glass slide and a cover glass was placed over it. The microscope images were analyzed with the software ImageJ to determine the size distribution of the droplets and background color intensity.

### 2.8. Conductivity measurements

Immediately after emulsion sonication, the conductivity of the emulsions was measured using a CDM 83 conductivity meter (Radiometer, Copenhagen, Denmark). Generally, a high conductivity indicates an o/w emulsion and a low conductivity ( $< 5 \mu\text{S cm}^{-1}$ ) is indicative of a w/o emulsion.

### 2.9. Malvern Mastersizer

The emulsion droplet size was also measured using a Malvern Mastersizer 2000G instrument with a HeNe laser operating at 633 nm. A 300f lens was used, which enabled droplet diameters from 0.50 to 900  $\mu\text{m}$  to be measured. The diluted emulsion was placed in the cell using a plastic pipette. The mean droplet diameter was taken to be the volume mean diameter ( $D_{4/3}$ ) from 3 replicate measurements, which is mathematically expressed as  $D_{4/3} = \Sigma D_i^4 N_i / \Sigma D_i^3 N_i$ , where  $D_i$  is the droplet diameter for droplet fraction  $i$ , and  $N_i$  is the number of droplets with size  $D_i$ . The ‘span’ was taken as a measurement of the width of the particle size distribution (Table 1). It is calculated using  $\text{span} = (D(0.9) - D(0.1)) / D(0.5)$ , where  $D(0.9)$  is the droplet diameter for which 90% of the droplets lie below this size,  $D(0.5)$  is the droplet diameter for which 50% of the droplets are below this size, and  $D(0.1)$  is the diameter for which only 10% of the droplets are smaller than this size. The stability of emulsions was also evaluated by monitoring the emulsion droplet diameter over 200 h with the Malvern Mastersizer. Error bars represent one standard deviation of the mean.

## 3. Results and discussion

### 3.1. Electrophoretic mobility, interfacial tension and contact angle

To understand how surfactants affect CNC Pickering emulsions, the first step involved measuring CNC–surfactant interactions in water and at the water–dodecane interface. The surfactants tested were both quaternary ammonium salts: CTAB has a single alkyl tail that is 16 carbons long and a critical micelle concentration (CMC) of 1 mM [58], and DMAB has two alkyl tails that are each 10

**Table 1**

Conductivity, type of emulsion, mean droplet diameter and span (measured by Malvern Mastersizer) for 1:1 water–dodecane emulsions stabilized by 0.25 wt.% CNCs and CTAB or DMAB. (The span is calculated as described in the Experimental Section).

|                  | Conductivity of emulsion ( $\mu\text{S cm}^{-1}$ ) | Type of emulsion | Mean diameter ( $\mu\text{m}$ ) | Span |
|------------------|--|------------------|---------------------------------|------|
| <b>CTAB (mM)</b> |  |                  |                                 |      |
| 1                | 140  | o/w              | 32                              | 2.52 |
| 2                | 194  | o/w              | 25                              | 2.11 |
| 4                | 211  | o/w              | 14                              | 1.95 |
| 6                | 278  | o/w              | 11                              | 1.49 |
| 8                | 312  | o/w              | 7                               | 1.84 |
| <b>DMAB (mM)</b> |  |                  |                                 |      |
| 1                | 129  | o/w              | 33                              | 1.79 |
| 2                | 113  | o/w              | 31                              | 1.46 |
| 4                | 2  | w/o              | 44                              | 2.04 |
| 6                | 3  | w/o              | 51                              | 1.91 |
| 8                | 177  | o/w              | 8                               | 1.55 |

carbons long and a CMC of 1.8 mM [59]. While DMAB can form vesicles and other surfactant aggregate structures in water, and microemulsions in the presence of oil, we expect that micellar phases dominate at room temperature and in the low concentration range used in this study [60].

Fig. 2 shows the electrophoretic mobility, which is proportional to the surface charge, for CNCs in the presence of CTAB and DMAB. The CNCs have an anionic surface charge of  $0.33 \pm 0.02 \text{ e/nm}^2$  which leads to a negative electrophoretic mobility of  $-3 \times 10^{-8} \text{ m}^2 \text{ V}^{-1} \text{ s}^{-1}$  (or a zeta potential of approximately  $-40 \text{ mV}$ ). As the concentration of surfactant increases, the mobility approaches zero due to charge compensation of the sulfate half-ester groups with cetyltrimethylammonium (CTA<sup>+</sup>) or didecyldimethylammonium (DMA<sup>+</sup>) ions. At higher surfactant concentrations, CNCs become cationic with an electrophoretic mobility increasing up to  $+3 \times 10^{-8} \text{ m}^2 \text{ V}^{-1} \text{ s}^{-1}$ . This surface charge reversal is attributed to surfactant aggregates on CNCs with cationic heads facing outwards. A small decrease in electrophoretic mobility at high surfactant concentration is observed which may be due to a rearrangement of surfactant/micelles on the CNC surface, free micelles in solution and/or the overall increase in ionic strength.

These electrophoretic mobility results agree with previous studies which have characterized the interaction between quaternary ammonium surfactants and cellulose model films [61], cellulose fibers [62], and CNCs [63–67]. At low surfactant

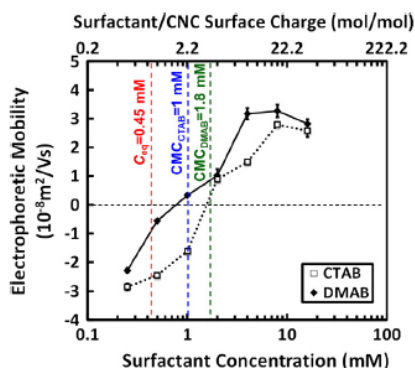


**Fig. 2.** Electrophoretic mobility of 0.25 wt.% CNCs in purified water with CTAB (single  $\text{C}_{16}$  alkyl tail, open squares) and DMAB (double  $\text{C}_{10}$  alkyl tails, closed diamonds) at room temperature. The dashed vertical lines indicate:  $C_{\text{eq}}$ , where the number of surfactant molecules and CNC sulfate half-ester groups are equal (red), the theoretical CMC of CTAB (blue) and the theoretical CMC of DMAB (green). Error bars represent one standard deviation of the mean.

concentrations the interaction is believed to be primarily electrostatic in nature, this is essentially an ion-exchange reaction where the bulky surfactant couples with the anionic sulfate half-ester groups on the surface of the CNCs [64]. At higher surfactant concentrations, alkyl tail interactions lead to cooperative binding and bilayer or admicelle adsorption morphologies [61,65].

The dotted red line in Fig. 2 is the concentration of surfactant required for CNC surface charge neutralization ( $C_{\text{eq}} \approx 0.45 \text{ mM}$  for both CTAB and DMAB). What is observed experimentally is that the isoelectric point occurs around 1.6 mM for CTAB and 0.8 mM for DMAB which is higher than  $C_{\text{eq}}$  because there is a balance of free and bound surfactant which governs the amount of surfactant needed for full charge neutralization. As such, an excess of surfactant is needed to reach the isoelectric point. We have observed a similar tendency in previous work, and further note that high ionic strength can push the required excess of surfactant for charge neutralization to even higher concentrations [64].

At all surfactant concentrations, CNCs in the presence of DMAB have higher electrophoretic mobility values than for the corresponding CNCs with CTAB. Accordingly, CNCs with DMAB reach charge neutralization at lower surfactant concentration. As adsorption is driven by a combination of electrostatics and hydrophobic interactions, the more hydrophobic surfactant (DMAB) is expected to have a stronger tendency to adsorb to CNCs, as observed experimentally. The isoelectric point does not appear correlated with the surfactant CMC. The electrophoretic mobility of CNCs with added surfactant corresponds directly to colloidal stability as shown in Fig. 3; suspensions flocculate near the isoelectric point.

Next, pendant drop experiments were undertaken to measure surface and interfacial tension of CNC suspensions, and mixtures of CNCs and surfactants. Fig. 4 demonstrates that CNCs alone do not reduce the surface tension at the air–water interface; however, they do reduce the interfacial tension at the dodecane–water interface due to their intermediate wettability. As dodecane is significantly less hydrophobic than air, this seems reasonable. However, for our emulsion experiments, only 0.25 wt.% of CNCs was used and thus the decrease in interfacial tension attributed to CNCs alone should be considered negligible. This result implies the need to modify the CNC surface to make them more likely to

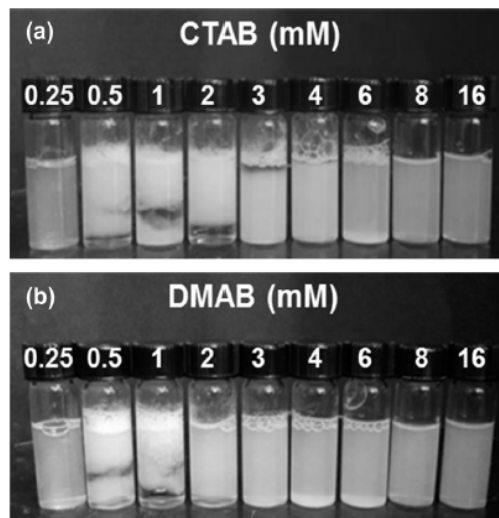


**Fig. 3.** Photographs of 0.25 wt.% CNCs and surfactant (a) CTAB and (b) DMAB in purified water. The suspensions do not appear colloiddally stable at concentrations of 0.5, 1 and 2 mM which correspond to electrophoretic mobilities close to zero (Fig. 2).

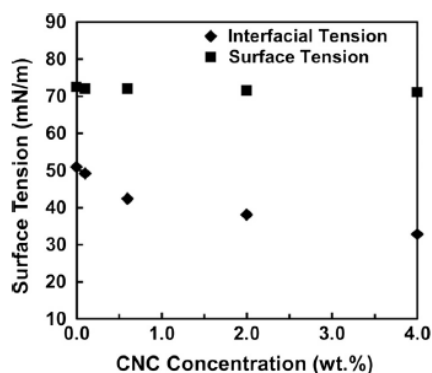


Fig. 4. Surface (air–water) and interfacial (dodecane–water) tension of CNC suspensions ranging from 0.25 to 4 wt.% CNCs at room temperature; square symbols are surface tension and diamonds represent interfacial tension.

partition at the dodecane–water interface. As mentioned previously, Kalashnikova et al. [2] modified CNCs by partially removing the sulfate half-ester groups, or by synthesizing un-charged CNCs, and Zoppe et al. [24] grafted polymers onto CNCs to achieve enhanced emulsion stability. Our electrophoretic mobility measurements imply that surfactant adsorption to CNCs is occurring, offering an *in situ* modification route for CNCs.

The effect of surfactant adsorption onto CNCs on the surface and interfacial tension is presented in Fig. 5. Mixtures of CNCs and surfactants have much lower surface/interfacial tension than CNCs alone. CMC values are taken as the intersection point between the region of the curve where the tension drops with increasing surfactant concentration and the lower region where the tension no longer changes. The CMC values for CTAB and DMAB without

CNCs agree with literature values (from open symbols in Fig. 5). The addition of CNCs to surfactants, however, caused an increase in surface/interfacial tension resulting in the entire curve shifting to the right. Similar behavior has been observed by Dhar et al. [65] with another quaternary ammonium surfactant. In the presence of CNCs and dodecane, the apparent CMC values increased to 3 mM and 4 mM for CTAB and DMAB, respectively (intersection of red-dotted lines in interfacial tension measurements, Fig. 5). Conceptually this means that CNCs are “using up” some of the surfactant, which keeps it from partitioning at the interface, and so the concentration of surfactant needed to have free micelles in solution is increased. The apparent CMC values measured here should only be taken as approximate as the ratio of CNC:water:dodecane interfaces will affect the overall partitioning of surfactant and the exact CMC.

CNCs’ hydrophobic–hydrophilic balance and wettability are also changed through surfactant adsorption as shown by three-phase contact angle measurements (Fig. 6). CNC–water–dodecane contact angles ( $\theta_{bw}$ ) were determined by placing a droplet of surfactant solution on a CNC film under dodecane, as done by Binks et al. [50,51] and supported by their SEM shadow method [55]. Fig. 6 shows that the three-phase contact angle increases with surfactant concentration, until a threshold value, and then decreases slightly and levels off. DMAB leads to higher contact angles and thus more hydrophobic CNCs due to its double alkyl tail and ability to pack tighter [50], compared to CTAB. Only in the case of DMAB does the three-phase contact angle surpass 90°.

Contact angle results mimic the trend in electrophoretic mobility which offers insight into the wettability changes. At low surfactant concentration, individual surfactant molecules adsorb onto CNCs with cationic heads pointing in and alkyl tails out, the surface charge density approaches the isoelectric point and the alkyl tails increase the surface hydrophobicity of the CNCs. At higher surfactant concentration, in fact, above the apparent CMC for these

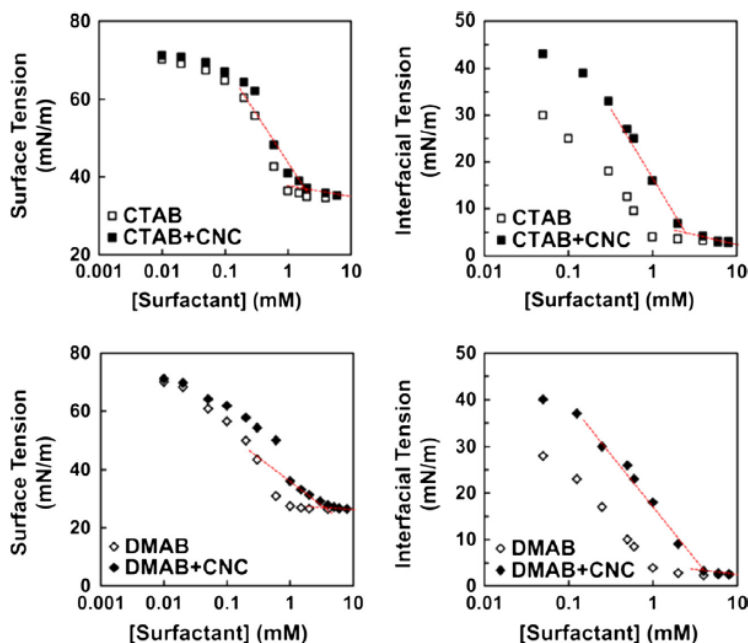


Fig. 5. Surface (air–water) and interfacial (dodecane–water) tension of CTAB (top) and DMAB (bottom) at room temperature; open symbols are without CNCs and closed symbols are with 0.25 wt.% CNCs added. The addition of CNCs increases the surface/interfacial tension below the CMC. Red dotted lines intersect at the apparent CMC values for CTAB and DMAB in the presence of CNCs.

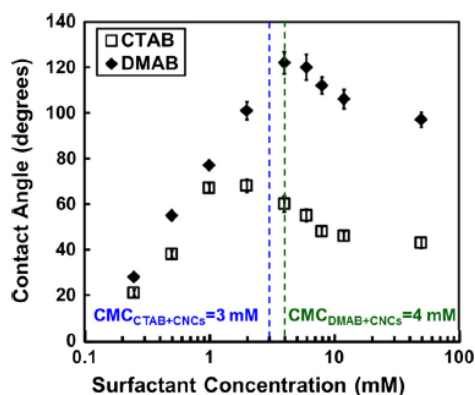


Fig. 6. Three-phase contact angle of a 10  $\mu\text{L}$  drop of surfactant solution on a spin-coated CNC surface measured under dodecane for CTAB solutions (open squares) and DMAB solutions (closed diamonds). Dotted vertical lines indicate the apparent CMC of CTAB in the presence of CNCs and dodecane (blue) and the apparent CMC of DMAB in the presence of CNCs and dodecane (green) determined from Fig. 5 data. Above the apparent CMC, the contact angle values decrease. Error bars represent one standard deviation of the mean.

surfactants in the presence of CNCs and dodecane (determined from Fig. 5 and shown as dotted lines in Fig. 6), adsorbed surfactant aggregates (likely admicelles) with cationic heads pointing outward lead to cationic CNCs which are more hydrophilic but still more hydrophobic than the starting CNCs. It is this change in CNC wettability that dictates the type of emulsion formed, either oil-in-water or water-in-oil, and the size and stability of emulsion droplets, as described in the following sections.

### 3.2. Emulsions, phase inversion and droplet size

Emulsions consisting of equal parts water and dodecane were prepared with 0.25 wt.% CNCs and varying concentrations of CTAB or DMAB. As shown in Fig. 7, CNCs with both CTAB and DMAB lead to stable emulsions. It is important to note that the photographs in Fig. 7 were taken 3 h after emulsion preparation, where all emulsions were stable to coalescence; however, emulsions containing only CNCs, with no surfactant, were unstable over longer time periods as discussed extensively in Section 3.4. This result, that highly charged CNCs alone cannot stabilize oil–water emulsions is consistent with the work of Kalashnikova et al. [2].

All CTAB-CNC-stabilized emulsions have oil as the internal droplet phase and water as the external phase, termed oil-in-water emulsions, whereas with DMAB, a double phase inversion from o/w to w/o [phase inversion 1] and back to o/w [phase inversion 2] is observed with increasing DMAB concentration. (Note that all other parameters are held constant and only the surfactant concentration is being altered). Fig. 7 also shows that oil-in-water emulsions exhibit slight creaming with an aqueous serum below, whereas water-in-oil emulsions tend to sediment leaving a top oil phase (density of dodecane is 0.78 g/mL), as expected. Emulsions with the least creaming were formed above 6 mM CTAB and above 8 mM DMAB which is significantly above the apparent CMC values for both surfactants; this is desirable in commercial products because it indicates an emulsion which is more stable to coalescence and generally contains smaller droplets.

The change in emulsion type is explicitly shown by confocal microscopy in Fig. 8 where dodecane is stained with Nile red (and appears green) and confirms that the internal phase for CTAB-CNC-stabilized emulsions is oil. However, for DMAB-CNC-stabilized emulsions, dodecane is the internal phase below 2 mM

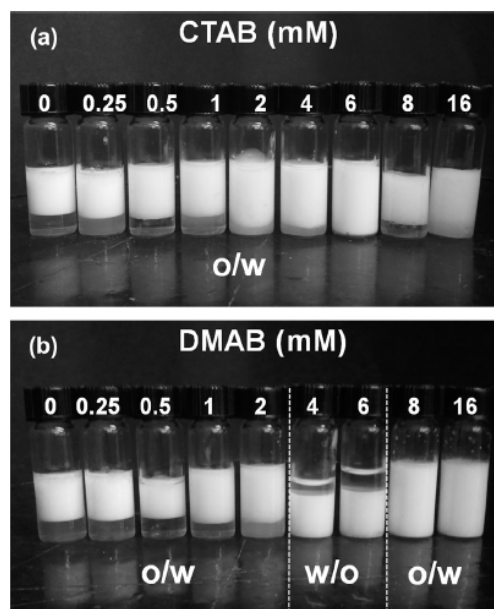


Fig. 7. Water–dodecane emulsions (1:1 by volume) stabilized by 0.25 wt.% CNCs and surfactant (a) CTAB and (b) DMAB with concentrations from 0 to 16 mM (left to right, as indicated). All emulsions with CTAB are oil-in-water, whereas two phase inversions are seen in emulsions with DMAB; from o/w to w/o and back to o/w, with increasing surfactant concentration.

and above 8 mM, yet is the external phase at 4 and 6 mM. The type of emulsion is also supported by conductivity measurements, whereby emulsions with water as the external phase have a high conductivity (hundreds of  $\mu\text{S}$ ) and emulsions with dodecane as the external phase have a near-zero conductivity (Supporting Information Fig. S2). On the other hand, emulsions without CNCs (surfactant-only emulsions) are all oil-in-water type and do not exhibit phase inversion (Supporting Information Fig. S3). The type of emulsion, conductivity and average internal phase droplet diameter are summarized in Table 1.

The emulsions produced herein can be classified as macroemulsions where droplets are generally larger than 10  $\mu\text{m}$ . For CTAB-CNC-stabilized emulsions the average oil droplet size decreases steadily from 32 to 7  $\mu\text{m}$  with increasing CTAB concentration (Fig. 8 and Table 1), which is consistent with the ability of more surfactant and surfactant-coated CNCs to lower the interfacial tension between water and dodecane. For the DMAB-CNC-stabilized emulsions, the oil droplets are also  $\sim 30 \mu\text{m}$  below 2 mM, but after the first phase inversion, the water droplets are almost double the size (at 4 and 6 mM). This implies that there are less surfactant-coated CNCs with the appropriate wettability to lower the interfacial tension for the w/o emulsions, than then were in the o/w emulsions below 4 mM. This is likely because not all CNCs have exactly the same amount of bound surfactants and a combination of monolayer, bilayer and admicellar morphologies may be present. Above 8 mM for the DMAB-CNC-stabilized emulsions, the phase inversion leads back to oil droplets which are significantly smaller and less uniform (8  $\mu\text{m}$ ). The droplet sizes observed in this work are similar to Kalashnikova et al. [1,2] who measured oil droplets ranging from 3 to 19  $\mu\text{m}$  for hexadecane-water emulsions stabilized with 0.2 wt.% CNCs, but with no surfactant; however, their CNCs were modified to reduce the surface charge density below 0.03 e/nm<sup>2</sup>. In contrast, our CNCs have a normal charge density of 0.33 e/nm<sup>2</sup> but are modified *in situ* with small amounts of surfactant, to effectively stabilize emulsions.

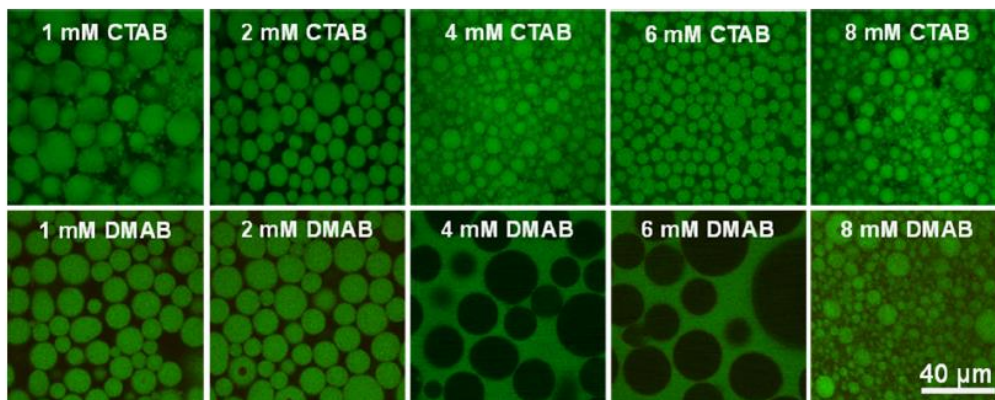


Fig. 8. Confocal laser scanning micrographs of 1:1 water–dodecane emulsions stabilized by 0.25 wt.% CNCs with surfactant, CTAB (top) and DMAB (bottom). The dodecane (oil) phase is dyed and appears green in the images showing the double phase inversion in the DMAB–CNC-stabilized emulsions.

The visual observations and confocal microscopy images of surfactant-enhanced CNC Pickering emulsions are perfectly in-line with the three phase contact angle measurements (Fig. 6). The change in emulsions properties are attributed to the adsorption of surfactants onto CNCs as described above. Specifically, the phase inversions in DMAB–CNC-stabilized emulsions are predicted by Bancroft's rule which states that if  $\theta_{ow}$  is slightly less than  $90^\circ$ , the interface bends towards the oil phase and the "hydrophilic" particles stabilize o/w emulsions. Conversely if  $\theta_{ow}$  is slightly more than  $90^\circ$ , the interface bends towards the water phase and such 'hydrophobic' particles stabilize w/o emulsions. According to Fig. 6, only DMAB systems exhibit  $\theta_{ow} > 90^\circ$  and the two highest contact angle points correspond to the surfactant concentrations where w/o emulsions were observed (i.e., 4 and 6 mM). The second phase inversion back to o/w at higher DMAB concentrations is associated with the decrease in hydrophobicity when surfactant aggregates with cationic heads pointing outward are adsorbed onto CNCs. Despite the similar trend in surface charge density for CTAB and DMAB, the wettability of CNCs in the presence of CTAB is never sufficient to achieve w/o emulsions as  $\theta_{ow}$  is less than  $70^\circ$  and thus no phase inversions are seen for CTAB systems.

Binks and co-workers have extensively studied similar double phase inversions in emulsions with nanoparticles (silica and  $\text{CaCO}_3$ ) and surfactants [48–55]. Both of these nanoparticles in their native form are too hydrophilic to stabilize emulsions alone, however, with oppositely charged surfactants that adsorb and can pack tightly on the particle surfaces, emulsions have been formed with droplet sizes generally over  $> 30 \mu\text{m}$  [50]. Because such double phase inversions have been observed in various particle–surfactant systems, and particle wettability has been extensively documented, it is believed that surfactant adsorption is the driving force and that these phenomena are not specific to only a few anomalous surfactants. In our case, the use of CNCs which are larger high-aspect ratio particles, appears to have some advantages over previously tested particles: less CNCs were needed (0.25 wt.% CNCs compared to 2 wt.% silica) because only an interconnected mesh coverage was required instead of multiple layers of densely packed spherical nanoparticles; and less surfactant was needed to induce the first and second phase inversions (4 and 8 mM with CNCs and 7 and 20 mM with silica) because the surface area was smaller with CNCs and the wettability was already suitable for emulsion stabilization. In general, CNC Pickering emulsions have smaller droplet sizes as well. The reduction in the amount of surfactant needed to control emulsion properties, compared with other nanoparticle systems, is beneficial as using

less surfactant is considered favorable due to rising environmental, health and safety concerns regarding a number of synthetic surfactants.

### 3.3. Role of CNCs in emulsion stabilization

We used fluorescent CNCs (f-CNCs), covalently labeled with DTAF [57], to track the location of particles within the DMAB–CNC-stabilized emulsions (Fig. 9). As expected, with no surfactant added, CNCs were observed at the oil–water interface of the o/w emulsion, agreeing with previously acquired electron microscopy images of CNC Pickering emulsions [1]. With 4 mM DMAB added, CNCs again coated the oil–water interface, however, in this case

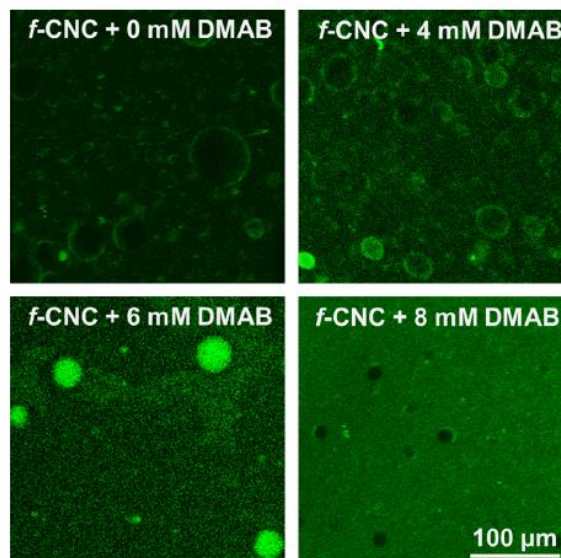


Fig. 9. Confocal laser scanning micrographs of 1:1 water–dodecane emulsions stabilized by 0.25 wt.% fluorescently labeled CNCs (f-CNC) with DMAB. At low DMAB concentrations CNCs are found primarily at the oil–water interface, for medium DMAB concentrations CNCs are found at the interface and within the water droplets, and upon the second phase inversion at high DMAB concentrations the CNCs are no longer primarily at the interface and the emulsion is stabilized mainly by DMAB.

the droplet internal phase is water (based on Fig. 8) and so it is inferred that the CNCs are in their most hydrophobic state. At 6 mM DMAB, which is above the apparent CMC for DMAB with CNCs and dodecane (i.e.,  $CMC_{DMAB+CNCs} = 4$  mM as determined from Fig. 5) it appears there are hydrophobic CNCs stabilizing the interface but also some more hydrophilic CNCs which are dispersed in the water phase droplets. Clearly, in the 4–6 mM DMAB concentration range, the amount of CNCs available to stabilize the interface is lower than at other concentrations tested, leading to the formation of larger w/o emulsion droplets as discussed above. At 8 mM DMAB, after the second phase inversion back to o/w, there is no enhancement of green at the oil–water interface and the continuous water phase is uniformly light green. Supporting Information Fig. S4 shows that the fluorescent color intensity of the water phase increases with increasing DMAB concentration which means the CNCs are less concentrated at the interface.

While CNCs may still contribute partially to the droplet stabilization at high surfactant concentration, the implication is that as there is more free surfactant, the CNCs are less responsible for emulsion stabilization. Additionally, we speculate that CNCs with large amounts of adsorbed surfactant may not have the intermediate wettability needed to stabilize emulsions as the (200) hydrophobic edge [2] of the cellulose crystal is likely masked by surfactant. This result is in contrast to previous work that indicated that silica particles with adsorbed surfactant bilayers were responsible for stabilizing o/w emulsions after the second phase inversion [50,55], and we attribute the differences to the inherent wettability of the nanoparticles.

An approximate calculation of interfacial area and CNC surface area also tells us that free surfactant is essential for the second phase inversion. We estimate that 1 mL of 0.25 wt.% CNCs can cover an interfacial area of  $0.2 \text{ m}^2$ , which could fully cover droplets that are  $30 \mu\text{m}$  in diameter. This is based on similar calculations to Kalashnikova et al. where it was shown that emulsion droplets required about 84% surface coverage, i.e., a fairly dense layer of particles, to be stabilized by cotton-derived CNCs [1,3]. This implies that in all our emulsions we have sufficient CNCs to cover droplets as small as  $\sim 25 \mu\text{m}$  but that smaller droplets must be stabilized by surfactants as well. For  $10 \mu\text{m}$  emulsion droplets, if all CNCs were at the interface, the surface coverage would only be about 33% which is not predicted to give stable emulsions and furthermore, the *f*-CNCs indicate that not all CNCs are at the interface. Figs. 7 and 8 tell us that the emulsions are stable and above 6 mM CTAB in CTAB-CNC-stabilized emulsions, and 8 mM DMAB in DMAB-CNC-stabilized emulsions, the emulsion droplets look more like the surfactant-only stabilized system (Supporting Information Fig. S3) in terms of size and uniformity. This leads us to conclude that in this case, surfactants play a significant role in stabilizing droplets in addition to modifying the CNC wettability.

### 3.4. Emulsion stability

Finally, the long-term stability of water–dodecane emulsions stabilized by CNCs and surfactants was assessed by measuring the change in average internal phase droplet size over time using a Malvern Mastersizer. Fig. 10 shows that both CTAB and DMAB-enhanced CNC Pickering emulsions are extremely stable to coalescence, with minimal increase in droplet size over 200 h. The emulsions which have the smallest droplet sizes at the beginning exhibit the least coalescence. On the other hand, extensive coalescence occurs in less than 10 h for emulsions stabilized by CNCs without surfactants (i.e., Fig. 10, square data sets for 0 mM CTAB and 0 mM DMAB). Likewise, surfactant-only emulsions are relatively unstable both above and below their CMC, as shown in Supporting Information Fig. S5. Without CNCs, the droplet sizes increase quickly indicating significant coalescence. Mastersizer

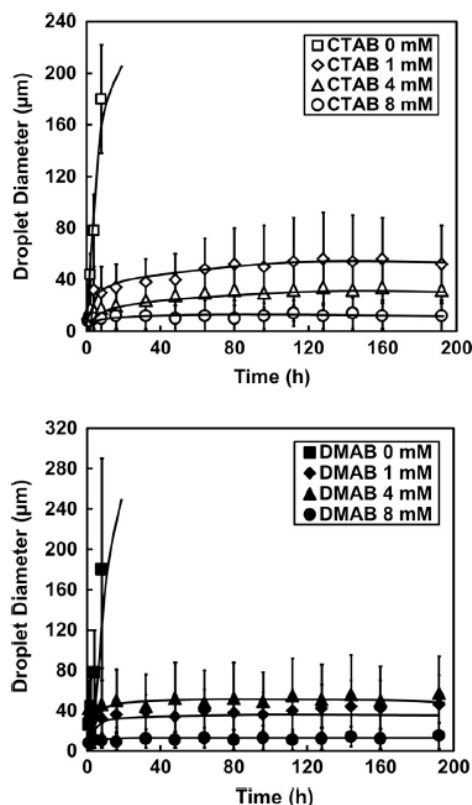


Fig. 10. Average droplet diameter in 1:1 water–dodecane emulsions stabilized by 0.25 wt.% CNCs and CTAB (top) and DMAB (bottom) over 200 h, as measured by a Malvern Mastersizer. Coalescence occurs quickly in emulsions stabilized by CNCs alone, otherwise, the emulsions and droplet diameters are stable over long time scales. Error bars represent one standard deviation of the mean (3 repeats).

measurements of CNC-only and surfactant-only emulsions for longer periods of time were not possible because either macroscopic phase separation occurred or the emulsion size was beyond the instrument's detection limit.

The minimum surfactant concentration needed to stabilize CNC emulsions long-term can be inferred from surface charge, colloidal stability and wettability data of CNCs in the presence of surfactants. In our CNC plus CTAB/DMAB mixtures, the isoelectric point occurs between 0.5 and 2 surfactant (Fig. 2) and the most flocculation occurs at 1 (Fig. 3) which corresponds to systems with similar wettabilities (Fig. 5). Thus, in this case, a surfactant concentration of approximately 1 represents the onset of the formation of emulsions which are extremely stable over long time periods.

Minor creaming, but no phase separation was visible for CNC Pickering emulsions with CTAB or DMAB after being stored in the lab for over 1 year, making them highly desirable in potential emulsion formulation applications. The stability over similar time scales for other surfactant–particle systems or other CNC-stabilized emulsions has not been reported. Clearly, the combination of CNCs and surfactants leads to more stable emulsions than either emulsifier can provide alone.

## 4. Conclusions

Cellulose nanocrystals are not significantly surface active, however, their intermediate wettability is key to stabilizing emulsions

[1] and the hydrophilicity/hydrophobicity can be tailored through *in situ* surfactant adsorption, as shown here. Emulsion properties are dependent on the chemical nature of the surfactant and the adsorbed surfactant structure on CNCs. This work highlights that interfacial properties of CNCs are very sensitive to the presence of surfactants and the major conclusions are as follows:

1. CNC Pickering emulsions are more stable in the presence of small amounts of CTAB or DMAB because surfactant adsorption onto CNCs increases the nanoparticles' hydrophobicity and makes them better emulsifiers.
2. The surfactant type and concentration can be used to control whether the continuous phase of the emulsion is oil or water which extends the potential use of CNCs in emulsified products. With increasing concentrations of DMAB, CNC Pickering emulsions exhibit a double phase inversion (o/w to w/o [phase inversion 1], followed by w/o to o/w [phase inversion 2]), whereas with CTAB, all emulsions are oil-in-water. Water-in-oil emulsions have not been demonstrated for CNC Pickering emulsions previously. Emulsion phase inversions correlate directly to CNC wettability; adsorbed DMAB gives more hydrophobic CNCs because it has two alkyl tails compared to CTAB's one, and the highest three-phase contact angles above 90° correspond to water-in-oil emulsions.
3. The smallest emulsion droplets are obtained above the apparent CMC for CTAB and DMAB, and at high surfactant concentrations, surfactants preferentially take over stabilizing the oil-water interface as CTAB and DMAB have a higher affinity to the interface than surfactant-treated CNCs.

The emulsion behavior documented here mirrors the work of Binks and co-workers which uses silica nanoparticles [48–55], however, the dimensions of CNCs offer advantages such as requiring less nanoparticles and less surfactant overall. Furthermore we have elucidated that surfactant is primarily responsible for emulsion stability above the apparent CMC by tracking the location of labeled CNCs in the emulsions. Although, DMAB and CTAB are not green, we believe this work shows that suitable mixtures of phospholipids, fatty acids or other biological surfactants could lead to exceptionally stable CNC Pickering emulsions with tunable properties that are low-cost, green and potentially edible.

#### Acknowledgments

The authors thank M. Timleck and M. Reid (Electron Microscopy Facility, Faculty of Health Sciences McMaster University) for sample analysis and training. Dr. T. Abitbol is gratefully acknowledged for providing fluorescently labeled CNCs and for useful discussions. Hu thanks NSERC for funding this work through the CREATE Biointerfaces Training Program Grant and the McMaster Biointerfaces Institute for access to equipment. Cranston thanks NSERC and the Faculty of Engineering at McMaster University for financial support. Pelton holds the Canada Research Chair in Interfacial Technologies.

#### Appendix A. Supplementary material

Transmission electron microscopy of CNCs, conductivity of emulsion continuous phase, confocal laser scanning microscopy images and stability of surfactant-only emulsions (no CNCs), background color intensity of confocal microscopy images of emulsions with f-CNCs. This material is available free of charge via the Internet. Supplementary data associated with this article can be found,

in the online version, at <http://dx.doi.org/10.1016/j.jcis.2014.10.034>.

#### References

- [1] I. Kalashnikova, H. Bizot, B. Cathala, I. Capron, *Langmuir* 27 (2011) 7471.
- [2] I. Kalashnikova, H. Bizot, B. Cathala, I. Capron, *Biomacromolecules* 13 (2012) 267.
- [3] I. Kalashnikova, H. Bizot, P. Bertoncini, B. Cathala, I. Capron, *Soft Matter* 9 (2013) 952.
- [4] I. Capron, B. Cathala, *Biomacromolecules* 14 (2013) 291.
- [5] S. Tasset, B. Cathala, H. Bizot, I. Capron, *RSC Adv.* 4 (2014) 893.
- [6] T. Kovacs, V. Naish, B. O'Connor, C. Vlais, F. Gagne, L. Hall, V. Trudeau, P. Martel, *Nanotoxicology* 4 (2010) 255.
- [7] W. Ramsden, *Proc. Roy. Soc. (London)* 72 (1903) 156.
- [8] S.U. Pickering, *J. Chem. Soc.* 91 (1907) 2001.
- [9] B.P. Binks, T.S. Horozov, L. Bergström, J.C. Fernández-Toledano, A. Moncho-Jordá, F. Martínez-López, R. Hidalgo-Álvarez, W.A. Goedel, G.G. Fuller, E.J. Stancik, S. Melle, R.J.G. Lopeťinsky, J.H. Masliyah, Z. Xu, K.P. Velikov, O.D. Velev, E. Dickinson, A.V. Nguyen, G.J. Jameson, R.J. Pugh, N.D. Denkov, K.G. Marinova, N. Babcsán, J. Banhart, *Colloidal Particles at Liquid Interfaces*, Cambridge University Press, Cambridge, 2008.
- [10] S. Levine, B.D. Bowen, S.J. Partridge, *Colloids Surf.* 38 (1989) 325.
- [11] H. Katepalli, V.T. John, A. Bose, *Langmuir* 29 (2013) 6790.
- [12] B.P. Binks, S.O. Lumsdon, *Langmuir* 16 (2000) 8622.
- [13] J.C. Zhang, L. Li, J. Wang, H.G. Sun, J. Xu, D.J. Sun, *Langmuir* 28 (2012) 6769.
- [14] B.P. Binks, B. Duncumb, R. Murakami, *Langmuir* 23 (2007) 9143.
- [15] K. Shinoda, N. Moriyama, K. Hattori, *J. Colloid Interface Sci.* 30 (1969) 270.
- [16] B. Madivala, S. Vandebriel, J. Franssaerb, J. Vermant, *Soft Matter* 5 (2009) 1717.
- [17] W.J. de Folter Julius, M. Hutter Eline, I.R. Castillo Sonja, E. Klop Kira, P. Philipse Albert, K. Kegel Willem, *Langmuir* 30 (2014) 955.
- [18] R. Aveyard, B.P. Binks, J.H. Clint, *Adv. Colloid Interface Sci.* 100–102 (2003) 503.
- [19] L. Nilsson, B. Bergenstahl, *J. Agric. Food Chem.* 55 (2007) 1469.
- [20] Y. Tan, K. Xu, C. Niu, C. Liu, Y. Li, P. Wang, B.P. Binks, *Food Hydrocolloids* 36 (2014) 70.
- [21] C. Li, P. Sun, C. Yang, *Starch-Stärke* 64 (2012) 497.
- [22] M. Rayner, M. Sjöö, A. Timgren, P. Dejmek, *Faraday Discuss.* 158 (2012) 139.
- [23] M. Pereda, A. Dufresne, M.I. Aranguren, N.E. Marcovich, *Carbohydr. Polym.* 101 (2014) 1018.
- [24] J.O. Zoppe, R.A. Venditti, O.J. Rojas, *J. Colloid Interface Sci.* 369 (2012) 202.
- [25] K.P. Oza, S.G. Frank, *J. Dispersion Sci. Technol.* 7 (1986) 543.
- [26] K.P. Oza, S.G. Frank, *J. Dispersion Sci. Technol.* 10 (1989) 163185.
- [27] M. Anderson, P. Stenius, *J. Dispersion Sci. Technol.* 28 (2007) 837.
- [28] A. Lif, P. Stensrad, K. Syverud, M. Nyden, K. Holmberg, *J. Colloid Interface Sci.* 352 (2010) 585.
- [29] K. Xhandari, K. Syverud, G. Chinga-Carrasco, K. Paso, P. Stenius, *J. Colloid Interface Sci.* 356 (2011) 58.
- [30] K. Xhandari, K. Syverud, P. Stenius, *J. Dispersion Sci. Technol.* 32 (2011) 447.
- [31] M. Kargar, K. Fayakmanesh, M. Alavi, F. Spyropoulos, I.T. Norton, *J. Colloid Interface Sci.* 366 (2012) 209.
- [32] J.J. Blaker, K.-Y. Lee, X. Li, A. Menner, A. Bismarck, *Green Chem.* 11 (2009) 1321.
- [33] H. Ougiya, K. Watanabe, Y. Morinaga, F. Yoshinaga, *Biosci. Biotech. Biochem.* 61 (1997) 1541.
- [34] H.A. Wege, S. Kim, V.N. Paunv, Q. Zhong, O.D. Velev, *Langmuir* 24 (2008) 9245.
- [35] B.G. Rånby, *Acta Chem. Scand.* 3 (1949) 649.
- [36] S. Beck-Candanedo, M. Roman, D.G. Gray, *Biomacromolecules* 6 (2005) 1048.
- [37] H. Wang, C. Qian, M. Roman, *Biomacromolecules* 12 (2011) 3708.
- [38] L. Zhong, S. Fu, X. Peng, H. Zhan, R. Sun, *Carbohydr. Polym.* 90 (2012) 644.
- [39] J.-F. Revol, H. Bradford, J. Giasson, R.H. Marchessault, D.G. Gray, *Int. J. Biol. Macromol.* 14 (1992) 170.
- [40] Y. Habibi, L.A. Lucia, O.J. Rojas, *Chem. Rev.* 110 (2010) 3479.
- [41] B.L. Peng, N. Dhar, H.L. Liu, K.C. Tam, *Can. J. Chem. Eng.* 89 (2011) 1191.
- [42] D. Klemm, F. Kramer, S. Moritz, T. Lindstrom, M. Ankerfors, D. Gray, A. Dorris, *Angew. Chem. Int. Ed.* 50 (2011) 5438.
- [43] A. Dufresne, *Nanocellulose from Nature to High Performance Tailored Materials*, Walter de Gruyter GmbH, Berlin, 2012.
- [44] T.A. Dankovich, D.G. Gray, *J. Adhesion Sci. Technol.* 25 (2011) 699.
- [45] B. Lindman, G. Karlström, L. Stigsson, *J. Mol. Liq.* 156 (2010) 76.
- [46] K.-Y. Lee, A. Bismarck, in: K. Okman, O. Rojas, P. Qvintus (Eds.), *Handbook of Green Materials*, World Scientific, 2014, pp. 11.
- [47] B.P. Binks, A. Desforges, D.G. Duff, *Langmuir* 23 (2006) 1098.
- [48] B.P. Binks, J.A. Rodrigues, *Langmuir* 23 (2007) 7436.
- [49] B.P. Binks, J.A. Rodrigues, W.J. Frith, *Langmuir* 23 (2007) 3626.
- [50] B.P. Binks, J.A. Rodrigues, *Angew. Chem. Int. Ed.* 46 (2007) 5389.
- [51] Z.G. Cui, K.Z. Shi, Y.Z. Cui, B.P. Binks, *Colloids Surf. A* 329 (2008) 67.
- [52] B.P. Binks, J.A. Rodrigues, *Colloids Surf. A* 345 (2009) 195.
- [53] Z.G. Cui, L.L. Yang, Y.Z. Cui, B.P. Binks, *Langmuir* 26 (2010) 4717.
- [54] Z.G. Cui, C.F. Cui, Y. Zhu, B.P. Binks, *Langmuir* 28 (2012) 314.
- [55] B.P. Binks, L. Isa, A.T. Tyowua, *Langmuir* 29 (2013) 4923.
- [56] E.D. Cranston, D.G. Gray, *Biomacromolecules* 7 (2006) 2522.
- [57] T. Abitbol, A. Palermo, J.M. Moran-Mirabal, E.D. Cranston, *Biomacromolecules* 14 (2013) 3278.

- [58] D.C. McDermott, D. Kanelleas, R.K. Thomas, A.R. Rennie, S.K. Satija, C.F. Majkrzak, *Langmuir* 9 (1993) 2404.
- [59] P. Lianos, J. Lang, R. Zana, *J. Colloid Interface Sci.* 91 (1983) 276.
- [60] G.G. Warr, R. Sen, D.F. Evans, *J. Phys. Chem.* 92 (1988) 774.
- [61] J. Penfold, I. Tucker, J. Petkov, R.K. Thomas, *Langmuir* 23 (2007) 8357.
- [62] S. Alila, S. Boufi, M.N. Belgacem, D. Beneventi, *Langmuir* 21 (2005) 8106.
- [63] M. Salajková, L.A. Berglund, Q. Zhou, *J. Mater. Chem.* 22 (2012) 19798.
- [64] T. Abitbol, H. Marway, E.D. Cranston, *Nord. Pulp Pap. Res. J.* 29 (2014) 46.
- [65] N. Dhar, D. Au, R.C. Berry, K.C. Tam, *Colloids Surf. A* 415 (2012) 310.
- [66] B. Peng, X. Han, H. Liu, R.C. Berry, K.C. Tam, *Colloids Surf. A* 421 (2013) 124.
- [67] Z. Hu, E.D. Cranston, R. Ng, R. Pelton, *Langmuir* 30 (2014) 2684.

## Appendix: Supporting Information for Chapter 3

**Transmission Electron Microscopy (TEM).** CNC particles were selectively stained by mixing a 0.05 mL aliquot of the CNC (0.5 wt.%) with 0.5 mL of a 1 mM uranyl acetate solution and vortexing the mixture for 2 min. A single drop of the stained suspension was dropped on a Formvar-coated copper TEM grid and dried for 4 h. TEM images were acquired using a JEOL 1200 EX TEMSCAN microscope operating at 80 kV.

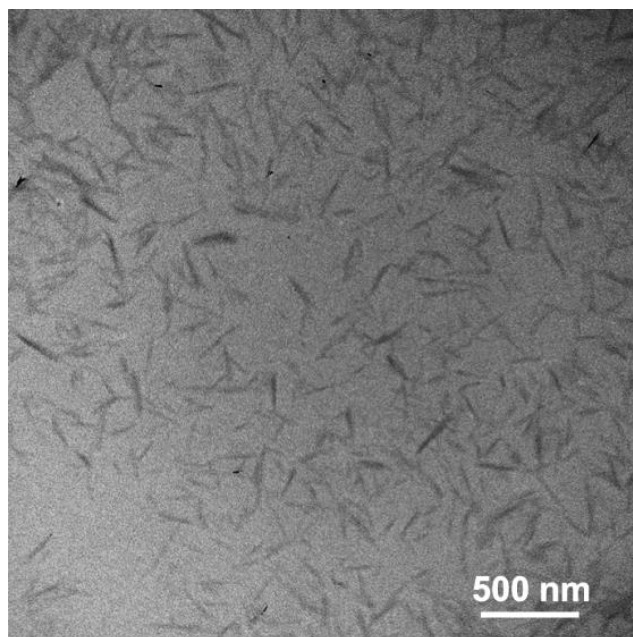


Figure S1. TEM image of cellulose nanocrystals (CNCs) prepared by sulfuric acid hydrolysis.

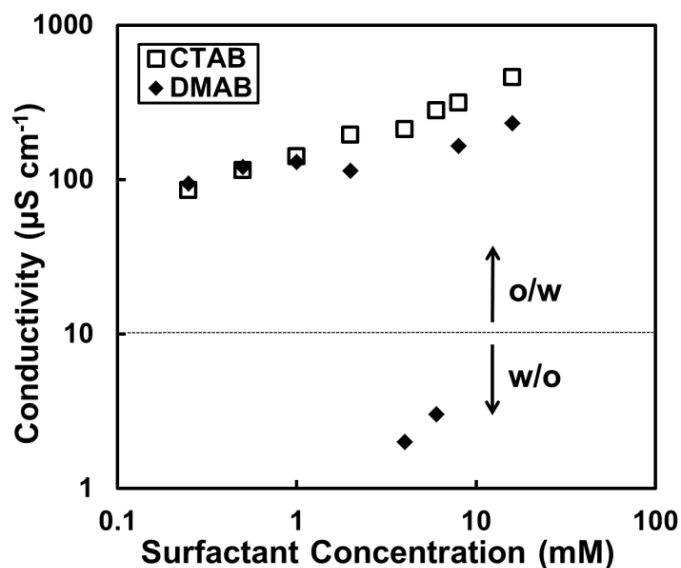


Figure S2. Conductivity of 1:1 water-dodecane emulsions stabilized by 0.25 wt. % CNCs and surfactant for CTAB (open squares) and DMAB (closed diamonds). Large conductivity values indicate that the continuous phase is water, whereas the low conductivity at 4 and 6 mM DMAB, results from a water-in-oil (w/o) emulsion.

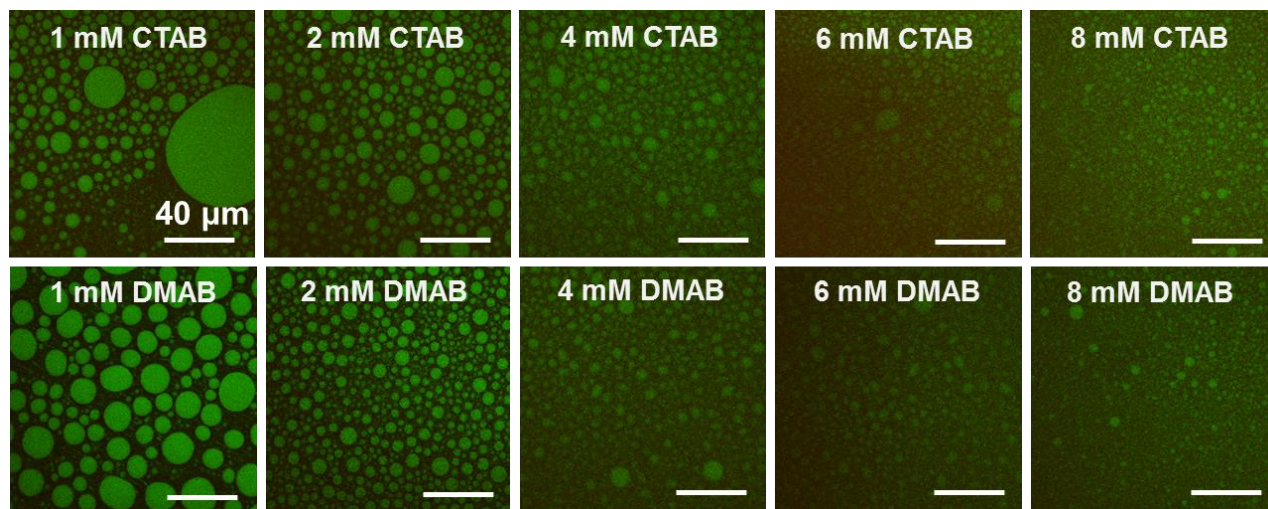


Figure S3. Confocal laser scanning micrographs of surfactant-only-stabilized 1:1 water-dodecane emulsions (no CNCs) showing of CTAB (top) and DMAB (bottom). The dodecane oil phase is dyed and appears green in the images showing no phase inversion in either surfactant system. Images collected at room temperature.

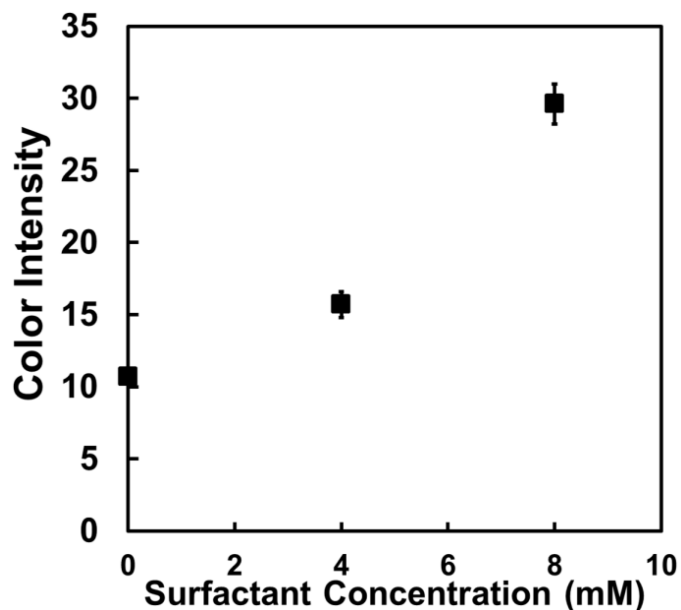


Figure S4. Background color intensity increase in confocal laser scanning microscopy images as a function of DMAB concentration for 1:1 water-dodecane emulsions stabilized by 0.25 wt. % fluorescently labeled CNCs. Error bars represent one standard deviation of the mean.

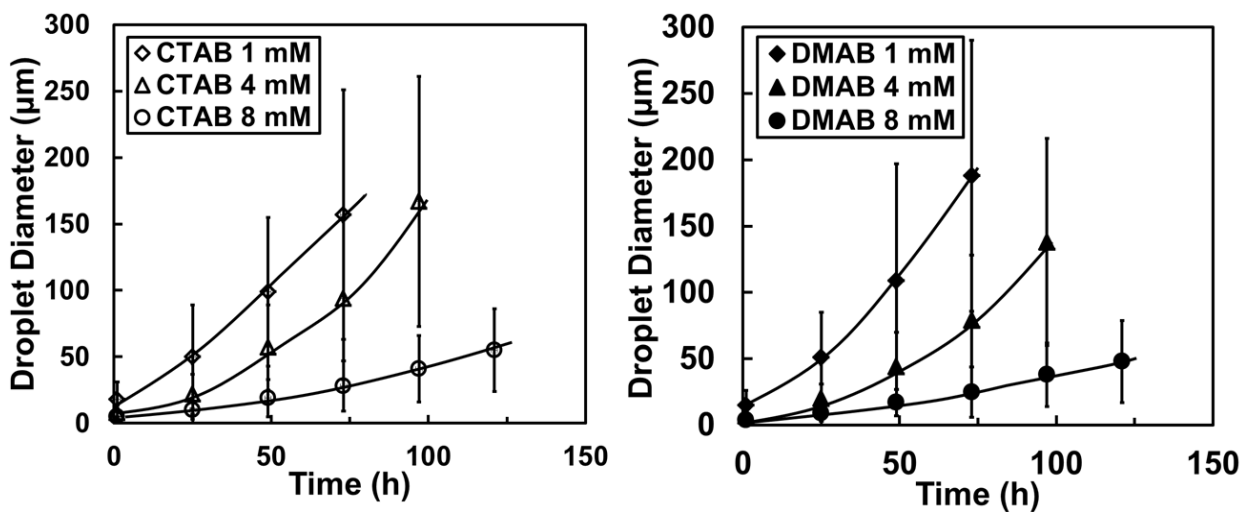


Figure S5. Emulsion stability as evidenced by average droplet diameter in 1:1 water-dodecane emulsions with no CNCs, stabilized by CTAB (left) and DMAB (right) over 150 hours, as measured by a Malvern Mastersizer. Error bars represent one standard deviation of the mean (3 repeats).

## **Chapter 4 Synergistic Stabilization of Emulsions and Emulsion Gels with Water-soluble Polymers and Cellulose Nanocrystals**

In chapter 4, all experiments were conducted by myself with assistance from Tyler Patten (undergraduate student). The chapter was initially drafted by myself, and edited later by Dr. Robert Pelton and Dr. Emily D. Cranston.

# Synergistic Stabilization of Emulsions and Emulsion Gels with Water-soluble Polymers and Cellulose Nanocrystals

Zhen Hu,<sup>†</sup> Tyler Patten,<sup>†</sup> Emily D. Cranston,<sup>†</sup> and Robert Pelton <sup>\*,†</sup>

<sup>†</sup> Department of Chemical Engineering, McMaster University, Hamilton, Canada L8S 4L7

## Abstract

The effect of water-soluble polymers on the properties of Pickering emulsions stabilized by cellulose nanocrystals (CNCs) was investigated. Addition of hydroxyethyl cellulose (HEC) or methyl cellulose (MC) proved to be beneficial in stabilizing the dodecane-water interface, whereas dextran did not. The emulsion droplet size can be readily tuned by varying the concentration of CNCs and polymers. CNCs in the presence of HEC or MC produce oil-in-water (o/w) emulsion (denoted CNC-HEC and CNC-MC emulsions) droplets around 3  $\mu\text{m}$  in diameter stable for several months. Interfacial tension measurements and confocal laser scanning microscopy images indicate that both HEC and MC are surface active and are capable of stabilizing o/w emulsions together with CNCs in a synergistic fashion. Calculated surface coverage for CNCs on CNC-HEC and CNC-MC emulsions indicated that a coverage of 20 % was surprisingly effective in producing stable emulsions, which was attributed to the co-stabilization effect of the polymers. Rheological measurements of CNC-HEC emulsions with additional MC added to the water phase showed that viscoelastic emulsion gels could be readily produced at 70 °C. This thermogelation was reversible and multiple cycles of heating/cooling treatments did not lead to coalescence of the emulsion. The use of CNC-HEC emulsion as a template for the preparation of corn oil dry powders by freeze-drying and air-drying was demonstrated. Additional carriers such as HEC and MC were required to produce oil powders containing oil content as high as 94 wt. %. It was shown that stable emulsions, emulsion gels, and dry oil powders can be readily prepared with tuned properties by using both CNCs and cellulose-based polymers as the emulsifying and gelling agents. This work will enable broad applications of CNCs and cellulose derivatives to stabilize emulsions for food, pharmaceutical, and cosmetic products.

## 4.1 Introduction

Emulsions consist of dispersed droplets of one immiscible liquid in another immiscible liquid. They are of great practical interest due to their widespread use in the formulation of food, pharmaceutical, cosmetic, paint, and ink products. In many of these applications the stability of emulsions is of utmost importance to keep their properties over long periods of time. Addition of surface-active molecules like surfactants, amphiphilic polymers, lipids, and proteins allows the formulation of stable emulsions thanks to the formulation of structured interfacial films.

Alternatively, Ramsden<sup>1</sup> and Pickering<sup>2</sup> demonstrated that solid colloidal particles may adsorb at interfaces to form “Pickering emulsions”. It is believed that the partitioning of colloidal particles at the oil-water interface produces a densely packed particle layer and thus prevents both emulsion flocculation and coalescence by inducing a steric barrier. Various inorganic and organic colloidal particles with different sizes, shapes and surface chemistries have been employed to prepare Pickering emulsions, including silica,<sup>3</sup> clay,<sup>4</sup> carbon nanotubes,<sup>5</sup> magnetic particles,<sup>6</sup> gold nanoparticles,<sup>7</sup> polymeric microgel particles,<sup>8</sup> and cellulose nanocrystals.<sup>9</sup>

Cellulose nanocrystals from cotton and wood are highly crystalline rigid rod-shaped nanoparticles that are 5-10 nm in cross-section and 100-200 nm long.<sup>10</sup> CNCs are entering the marketplace in commercial scale quantities in Canada, United States, and Europe.<sup>11</sup> They are most commonly prepared by sulfuric acid hydrolysis which gives nanocrystals with anionic sulfate half-ester groups on their surface.<sup>10</sup> Capron and co-workers have established the groundwork of using of CNCs as emulsion stabilizers.<sup>9, 12-14</sup> They found that unmodified CNCs are effective at stabilizing emulsions when they have a low surface charge density, or when the surface charge is screened in the presence of salt. In their work, a minimum of 84% of the emulsion droplet surface area required to be covered with cotton-derived CNCs to impede droplet coalescence.<sup>13</sup> The same research group also prepared high-internal-phase emulsion “gels” by making CNC-stabilized emulsions with equal parts oil and water and then slowly increasing the oil content.<sup>14</sup>

Many commercial emulsion-based products contain polymers, surfactants, and particles, hence the characterization of emulsions prepared with all these components is of great importance. Studying the interfacial properties of cellulose nanocrystals in the presence of interacting surfactants and polymers can provide useful insight into the mechanistic origin of some emulsion properties. In our previous work, we investigated *in situ* surface modification of CNCs with cationic surfactants and its effect on the properties of Pickering emulsion.<sup>15</sup> In another literature example, thermo-responsive poly(N-isopropylacrylamide) (poly(NIPAM)) brushes were grafted onto CNCs to control the hydrophobicity with temperature to tune the emulsion stability.<sup>16</sup> The emulsions stabilized by poly(NIPAM)-g-CNCs broke after heating at a temperature above the LCST of poly(NIPAM), which was attributed to the temperature responsiveness of the brushes installed on the particles and thus the responsiveness of the Pickering emulsions. Similarly, a weak polyelectrolyte poly[2-(dimethylamino)ethyl methacrylate] (PDMAEMA) was grafted onto the surface of CNCs and imparted pH and temperature sensitiveness to the emulsions stabilized with these modified CNCs.<sup>17</sup> Unlike pristine cellulose nanocrystals, modified CNCs significantly reduced the surface and interfacial tensions. The PDMAEMA chains on CNC surface promoted the stability of emulsion droplets and their chain conformation varied with pH and temperature to trigger the emulsification and demulsification of oil droplets.

Compared to chemically modify surface properties of particles through polymer grafting, physically adsorbing polymers onto particle surface to tune surface hydrophobicity and interfacial tension may be relatively simpler and easier to achieve. Saleh et al.<sup>18</sup> found that physisorbed layers of amphiphilic triblock copolymers not only improved the colloidal stability of iron nanoparticles in water but also drove them to adsorb at the oil/water interface, forming a highly stable emulsion. Adsorbing surface-active copolymers onto nanoparticles makes the nanoparticles extremely efficient emulsifiers, with their concentrations of as low as 0.04 wt. % being sufficient to stabilize emulsions for many months. Similarly, Feng et al.<sup>19</sup> used the salt-

bridge interactions between carboxylic acid groups of single-walled carbon nanotubes (SWCNTs) and amine groups of amine-terminated polystyrene to facilitate the assembly of SWCNTs at the oil/water interface and produce stable emulsions. To the best of our knowledge, however, no CNC Pickering emulsions described to-date has reported using physically adsorbed water-soluble polymers to control the emulsion properties via a simple mixing and emulsification method.

Formulated food, pharmaceutical, and cosmetic products are often structured oil-in-water (o/w) Pickering emulsions that are gel-like soft solids. These viscoelastic products are mostly water continuous emulsions using protein and/or polysaccharides as emulsifiers as well as gelling agents or concentrated emulsions where enhanced viscosity comes from the close crowding of dispersed oil droplets in high internal phase emulsions (HIPEs).<sup>20</sup> HIPEs are defined as emulsions with an internal phase volume fraction ( $\phi$ ) of 0.74 or greater. However, HIPEs using solid particles as stabilizers either require tedious processes to prepare or involve particulate emulsifiers with defined hydrophobicity, which makes them undesirable in industrial productions.<sup>14, 21</sup> Centrifugation can be sufficient to force all the droplets closer together and generate a concentrated emulsion phase with gel-like behavior.<sup>22</sup> However, centrifugation can be detrimental to the stability of emulsions and it is a nontrivial process at industrial scale.<sup>9</sup> Therefore, we envision that using CNCs and/or polymers as emulsion stabilizers as well as thickening agents to prepare emulsion gels is more industry-relevant and likely to lead to many interesting applications, where using raw bio-based materials is advantageous.

It is common in the food, pharmaceutical, and cosmetic industries to reduce a liquid oil base, for example, an o/w emulsion, to a solid-like powder.<sup>23-25</sup> Two widely used methods to evaporate the water continuous phase rapidly are spray-drying and freeze-drying.<sup>26</sup> To prevent oil droplets from collapsing into a macrophase-separated liquid state either during these drying processes or during the shelf life of the powder, a solid hydrophilic carrier is often added to the aqueous phase. This hydrophilic carrier, together with the emulsifiers used to stabilize the liquid emulsion, constitutes the continuous phase of the powder after water evaporation, whereas the oil droplets are kept intact and trapped in the continuous phase. The minimum amount of carrier required varies depending on the system but typically ranges between 30 and 80 wt % of the total final powder.<sup>26</sup> Typical examples of the constituents of the solid dry base are lactose, glucose, maltodextrin, starch, and cellulose. Although the presence of carrier in the formulation alters the composition of the powder, its role in the formulation is necessary to prevent oil leakage. In this paper, we present the first fabrication of oil powder with high oil content using CNCs and water-soluble cellulose derivatives via freeze-drying process.

## 4.2 Experimental Section

**Materials.** Methyl cellulose (MC, 40 kDa, degree of substitution (DS) of 1.6~1.9), 2-hydroxyethyl cellulose (HEC, 90 kDa, molar substitution (MS) = 2.5), dextran (DEX, 70 kDa), dodecane, corn oil, Nile Red, Nile Blue, 5-(4, 6-dichlorotriazinyl) aminofluorescein (DTAF), azobisisobutyronitrile (AIBN), and sodium chloride were all purchased from Sigma-Aldrich Inc. The water used in all solutions was deionized and further purified with a Barnstead Nanopure Diamond system (Thermo Scientific, Asheville, NC).

**Preparation of Cellulose Nanocrystals.** CNCs were prepared by sulfuric acid hydrolysis of cotton from cotton filter aid (Whatman ashless filter aid, GE Healthcare Canada, Mississauga, Canada), as described previously.<sup>27</sup> The filter aid was first torn into small squares and blended into a fluffy, white powder in a standard household blender (Magic Bullet brand). The powder was dried at 80°C for 1 h prior to the reaction. 40 g of the filter aid was treated with 700 mL of 64 wt. % sulfuric acid (Fischer Scientific) for 45 min at 45 °C with constant mechanical stirring. The hydrolysis reaction was quenched by adding 10-fold cold water. The acid removal was achieved by extensive dialysis against purified water until the pH of the external reservoir was stable over the last few water changes (~2 weeks). The surface charge density of sulfate half-ester groups on CNCs was determined by conductometric titration to be  $0.33 \pm 0.02$  e/nm<sup>2</sup>, with average crystal dimensions of 128 x 7 nm from transmission electron microscopy (TEM) image analysis. A TEM micrograph of the CNCs is provided in the Supporting Information Figure S1.

**Preparation of the Emulsions.** A emulsion of 6 mL containing equal volumes of dodecane and aqueous dispersions (1:1 oil to water) was obtained by mixing 1.5 mL of 0.6 wt. % CNCs and 1.5 mL of 0.4 wt. % polymer solution, making the final concentration of CNCs and polymer in the emulsions 0.3 wt. % and 0.2 wt. %, respectively. After mixing the components, the mixture was immediately emulsified using a sonicator (Sonifier 450, Branson Ultrasonics, Danbury, CT) while in an ice bath for 1 minute at an intensity level 6 and 50% pulses for every emulsion, which corresponds to an energy input of approximately 1371 J/g of emulsion. The polymer solutions tested were MC, HEC, and DEX. The emulsions using both CNCs and polymers were denoted as CNC-MC, CNC-HEC, and CNC-DEX emulsion, respectively. Other emulsions samples were prepared using either CNCs or polymers as the sole emulsifier. A salt concentration of 50 mM was maintained by adding NaCl to the water phase. For some emulsions used for freeze-drying, dodecane was replaced with corn oil whereas every other components were the same unless noted otherwise.

**Polymerization.** The CNCs could stabilize the styrene/water interface and form a stable emulsion. Following the work of Kalashnikova et al<sup>9</sup> we polymerized the internal emulsion oil phase as a way to visualize the emulsions under scanning electron microscopy. Solid polystyrene particles were prepared through polymerization of styrene emulsion droplets stabilized CNCs alone or in the presence of polymers. Aqueous suspensions containing 0.3 wt. % CNC were sonicated for 1 min and degassed with nitrogen for 3 min. Styrene was mixed with AIBN, an oil-soluble initiator, to obtain a styrene/AIBN ratio of 100/1 (w/w). A total volume of 3 mL of this mixture was added to equal volume of the CNC suspension, and an emulsion was produced by sonication for 1 min. In some samples, 0.2 wt. % HEC or MC was used together with 0.3 wt. % CNC in stabilizing the emulsions. The emulsions were placed in oven at 65 °C, without stirring, for 8 h. The dried polystyrene particles were metallized with 5 nm platinum and visualized with a JEOL 7000F scanning electron microscopy (JEOL Ltd., Japan).

**Fluorescent Labeling.** The CNCs were labeled with Nile blue. Nile blue (10 mg) was added to 50 mL 1 wt. % CNC suspension (pH 3) and mixed for 24 h in the dark. Unbound Nile blue was removed by extensive dialysis for a week against purified water. The polymers were labeled with DTAF using an approach that has been previously applied to CNCs.<sup>28</sup> HEC or MC (500 mg) was reacted with DTAF (7.5 mg) under alkaline conditions (0.2 M NaOH) for 24 h, in the dark, with mechanical stirring. To remove unreacted DTAF and the bulk of the NaOH, extensive dialysis against purified water was employed. Purified reaction products were freeze-dried and stored in

the dark. The labeled CNCs and polymers are denoted as CNCs-Nile blue, HEC-DTAF, and MC-DTAF, respectively.

**Confocal Laser Scanning Microscopy (CLSM).** For CLSM visualization of the microstructure of the emulsions, the oil phase was stained with Nile red (492/520 nm). For some samples, the CNCs and polymers were labeled with Nile blue (630/660 nm) and DTAF (495/517 nm), respectively. Images were obtained with a Zeiss LSM 510 Meta on an Axiovert 200M microscope (Zeiss, Gottingen, Germany). For high resolution images, a x63 water-immersion laser technique was used.

**Scanning Electron Microscopy (SEM).** Morphology characterization of polystyrene particles stabilized by CNCs alone or CNCs together with polymers was done by using a JEOL 7000F SEM (JEOL Ltd., Japan). A 3 nm thick gold coating was applied before SEM imaging. Micrographs were taken at several magnifications at 6 mm working distance and at 20 kV acceleration voltage.

**Malvern Mastersizer.** A Malvern Mastersizer 2000G instrument with a HeNe laser operating at 633 nm was used to measure the emulsion droplet size. The mean droplet diameter was taken to be the volume mean diameter ( $D_{4/3}$ ) from 3 replicate measurements. It is mathematically expressed as  $D_{4/3} = \sum D_i^4 N_i / \sum D_i^3 N_i$ , where  $D_i$  is the droplet diameter for droplet fraction  $i$ , and  $N_i$  is the number of droplets with size  $D_i$ . The ‘span’ was reported as a measurement of the emulsion droplet diameter size distribution and calculated using  $\text{span} = (D(0.9) - D(0.1)) / D(0.5)$ , where  $D(0.9)$  is the droplet diameter for which 90% of the droplets are below this size,  $D(0.5)$  is the droplet diameter for which 50% of the droplets are smaller than this size, and  $D(0.1)$  is the diameter for which only 10% of the droplets lie below this size. The stability of emulsions was determined by following the emulsion droplet diameter over 150 hours with the Malvern Mastersizer.

**Surface Coverage Determination.** The percentage of emulsion droplet surface area covered by CNCs was calculated. The surface coverage  $C$  is given by the ratio of the theoretical maximum surface of the particles available for stabilizing the emulsion and the total surface displayed by the emulsion droplets as derived in an earlier work.<sup>9</sup> The total coverage can be expressed as

$$C = \frac{mD}{6h\rho V} \quad [1]$$

Where  $m$  is the mass of CNCs,  $D$  is the  $D_{4/3}$  mean diameter of the emulsion droplets,  $h$  is the CNC thickness (7 nm as determined from TEM images of CNCs),  $\rho$  is the CNC density (1.59 g/cm<sup>3</sup>), and  $V$  is the volume of oil used in the emulsion.

**Dynamic Interfacial Tension.** Interfacial tension was measured by the pendant drop method with a Krüss Drop Shape Analysis System DSA10 instrument. Prior to the measurement, a sample (ca. 50 mL) of dodecane was added to a glass box of 5.0 (L) × 5.0 (W) × 5.0 (H) cm, and a pendant drop of CNC suspension or polymer aqueous solution of about 20 μL, was formed on the end of a stainless steel needle immersed in the dodecane oil phase. The aging of the interface can be accurately monitored by measuring the dynamic interfacial tension of a drop having a constant interfacial area over 20 min.

**Rheology.** Oscillatory rheological measurements of emulsions were performed using an ARES rheometer (TA Instruments) with parallel-plate geometry. In all experiments, a 7 mm diameter parallel plate geometry and 1.5 mm gap distance were used. Dynamic frequency sweeps were performed at 1% strains, which were confirmed to be in the linear viscoelastic range for each emulsion sample, from 0.1 to 100 rad/s to determine the storage modulus ( $G'$ ) and loss modulus ( $G''$ ) of the emulsions. Measurements were done at temperatures of 25 °C and 70 °C. The evaporation of water from the samples was avoided by covering the sides of the plate with low viscosity mineral oil. After heating samples to 70°C, they were allowed to thermally equilibrate for 3 min before the measurements.

**Freeze-Drying.** CNC-HEC emulsions with 0.3 wt. % CNCs and 0.2 wt. % HEC were used as stock emulsion samples and mixed with equal volume of 1 wt. % HEC or MC solution. Corn oil is used as the oil phase instead of dodecane as elsewhere in this study. Freeze-drying over 24 h of the emulsions was carried out on a Millrock Technology freeze-dryer (Kingston, NY) at -40 °C and a vacuum of  $10^{-2}$  mbar.

### 4.3 Results

**Droplet Size.** As most formulated chemical products, including food and cosmetics, are complex mixtures of surfactants, polymers, and particles in relatively high ionic strength solutions, we herein report our work of producing CNC-stabilized Pickering emulsion in the presence of water-soluble polysaccharides. We previously investigated the effect of surfactants on the properties of Pickering emulsions stabilized by cellulose nanocrystals.<sup>15</sup>

Various polymers were first mixed with CNCs and then emulsified upon addition of equal volume of oil through ultrasonication. To investigate the emulsion morphology and droplet size with the addition of polymers, the oil phase (dodecane) was stained with an oil-soluble fluorophore Nile red and visualized by confocal laser scanning microscopy (CLSM) as shown in Figure 1. Nile red stained the dispersed phase and showed as green, which allows the determination of emulsion droplet size. The continuous phase was not stained and appears black in the images. CNCs partitioned into the oil-water interface and stabilize o/w emulsions. NaCl at 50 mM was added in all emulsions to screen electrostatic repulsion between the particles at oil-water interface, increase surface coverage, and thus improve the emulsion stability.<sup>9</sup> The mean diameter of emulsions stabilized by CNCs alone is 12  $\mu\text{m}$ , whereas the emulsions stabilized by various water-soluble polymers alone show different mean diameter values (Figure 1 and Table 1). For the samples prepared with hydroxyethyl cellulose (HEC) or methyl cellulose (MC) as the only emulsifier at 0.2 wt %, emulsion droplets with mean diameter values around 6  $\mu\text{m}$  were obtained. Dextran (DEX), on the other hand, displayed poor emulsifying capability as the emulsion droplets stabilized by dextran alone at 0.2 wt % have a mean diameter of around 28  $\mu\text{m}$ .

The effect of polymer addition on CNC emulsifying behavior was studied by mixing polymers with CNCs prior to emulsification. Our previous work showed that HEC adsorbs on CNC surfaces and increases the viscosity of the mixture due to an increase in the particle volume fraction.<sup>29</sup> Adsorption of MC on CNC surfaces was also studied and similar adsorption behavior was observed (Supporting Information, Figure S2). As shown in Figure 1, by adding HEC or MC to CNC suspensions before emulsification and using CNC-HEC or CNCs-MC as the emulsifier produced smaller emulsion droplets with mean diameters of about 3  $\mu\text{m}$ . Dextran and CNCs

together, on the other hand, produced relatively larger emulsion droplets than the ones stabilized by CNCs alone with mean diameters of about 21  $\mu\text{m}$ .

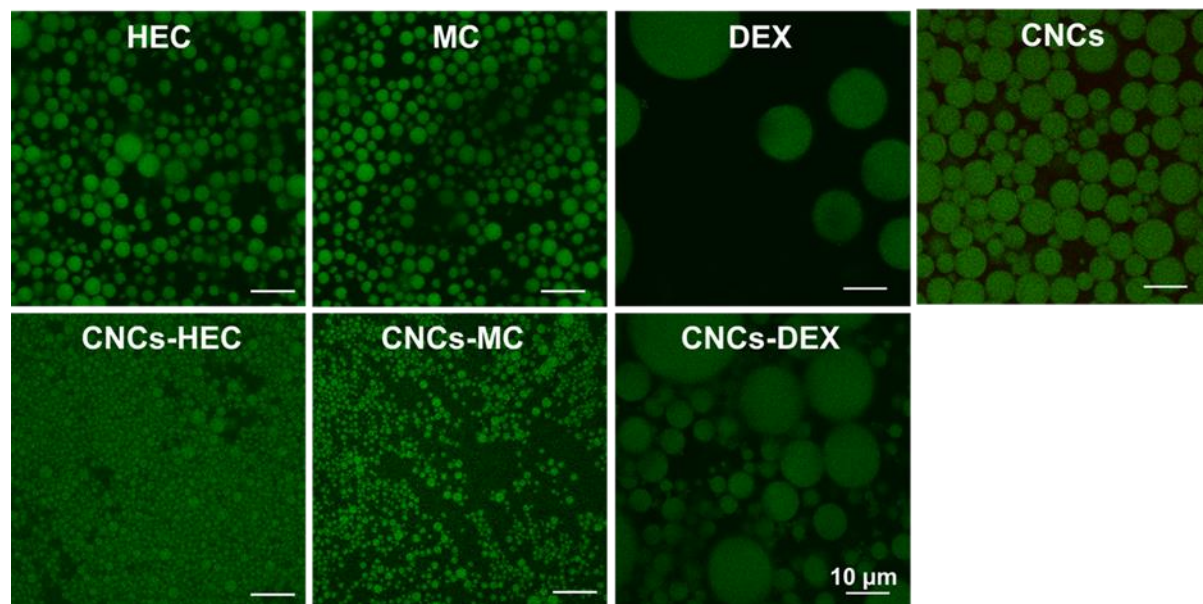


Figure 1. Confocal laser scanning microscopy images of 1:1 dodecane-water emulsions stabilized by 0.3 wt. % CNCs, 0.2 wt. % polymers individually and together. The oil phase is dyed with Nile red and appears green in the images.

Because of dodecane volatility, the emulsions formed could not be introduced in the SEM chamber. CNCs showed the same ability to stabilize styrene and dodecane droplets, and therefore, styrene was selected to allow polymerization of the oil phase and thus imaging under SEM. The reduction of emulsion droplet size was also observed by visualizing polystyrene particles prepared via polymerization of styrene emulsion droplets stabilized by CNCs alone or in the presence of polymers (Figure 2). CNCs (0.3 wt.%) alone led to production of polystyrene particles with average diameter of  $\sim 20 \mu\text{m}$ . The addition of HEC or MC greatly reduced the diameters of polystyrene particles to  $2\sim 3 \mu\text{m}$  as shown in Figure 2, which confirms the influence of polymers on producing smaller emulsion droplets as already demonstrated in Figure 1.

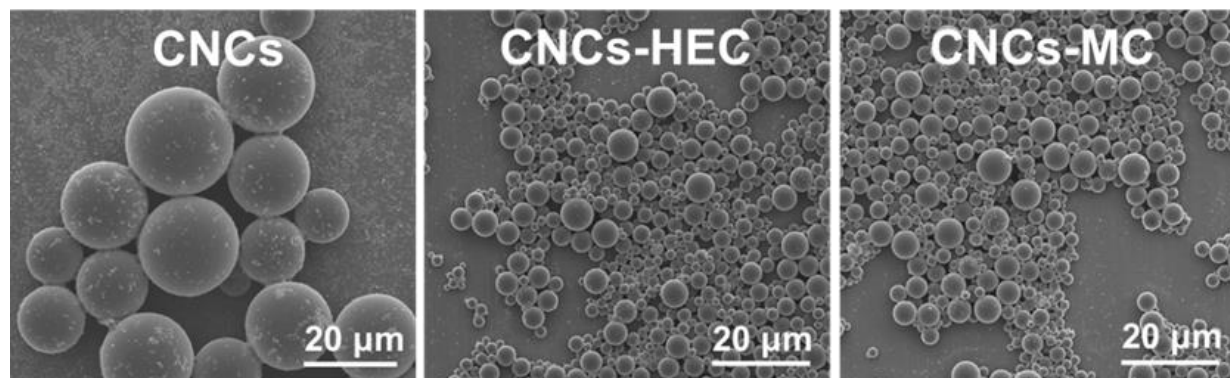


Figure 2. Scanning electron microscopy images of polymerized styrene/water emulsion stabilized by CNCs suspensions alone (CNCs: 0.3 wt. %) or in the presence of HEC (CNCs: 0.3 wt. %, HEC: 0.2 wt. %) or MC (CNCs: 0.3 wt. %, MC: 0.2 wt. %).

Table 1. Summary of the Mean Emulsion Droplet Diameter and Span for 1:1 Dodecane-Water Emulsions Prepared with Increasing Amount of CNCs.<sup>a</sup> (The span is calculated as described in the Experimental Section.)

| CNCs<br>Conc.<br>(wt. %) | CNCs Emulsion                         |      | CNC-HEC Emulsion                      |      | CNC-MC Emulsion                       |      | CNC-DEX Emulsion                      |      |
|--------------------------|---------------------------------------|------|---------------------------------------|------|---------------------------------------|------|---------------------------------------|------|
|                          | Mean<br>Diameter<br>( $\mu\text{m}$ ) | Span |
| 0.05                     | 58                                    | 2.6  | 15                                    | 2.2  | 12                                    | 2.3  | 102                                   | 3.7  |
| 0.1                      | 27                                    | 2.3  | 7.2                                   | 2.0  | 6.2                                   | 1.9  | 52                                    | 3.5  |
| 0.2                      | 18                                    | 2.1  | 4.5                                   | 1.9  | 3.3                                   | 1.7  | 29                                    | 3.3  |
| 0.3                      | 13                                    | 1.8  | 3.3                                   | 1.5  | 2.4                                   | 1.6  | 18                                    | 3.4  |
| 0.4                      | 11                                    | 1.9  | 3.1                                   | 1.7  | 2.2                                   | 1.6  | 15                                    | 3.5  |
| 0.5                      | 10                                    | 1.7  | 2.8                                   | 1.5  | 1.9                                   | 1.5  | 13                                    | 3.3  |

<sup>a</sup> A mass ratio of CNCs over polymer was fixed to 3:2 when the polymer was used in combination with CNCs. The polymers tested were MC, HEC, and DEX. The emulsions using both CNCs and polymers were denoted as CNC-MC, CNC-HEC, and CNC-DEX emulsion, respectively. A salt concentration of 50 mM was maintained by adding NaCl to the water phase.

Emulsion droplet size variations were monitored by measuring the volume mean diameter ( $D_{4/3}$ ) with a Malvern Mastersizer 2000G instrument and varying concentrations of CNCs in the water phase for a fixed oil-water volume ratio of 1:1. Results of emulsions stabilized by CNCs alone

and together with each polymer are given in Table 1. For the emulsions using both CNCs and polymer as emulsifiers, mass ratio of CNCs over polymer is fixed at 3:2. For CNCs emulsion, the increasing amount of CNC particles resulted in decreasing droplet mean diameter before a plateau value of about 11  $\mu\text{m}$  was reached for all emulsions containing more than 0.4 wt % in the water phase. Higher concentrations of CNCs provide larger interfacial areas which leads to the decreasing of droplet size. Similar trend is also observed for other types of Pickering emulsions stabilized by both CNCs and polymers. CNC-HEC and CNC-MC emulsion droplets displayed smaller mean diameter values than CNCs emulsion. However, CNCs produced larger emulsion droplets with a broader size distribution in the presence of dextran.

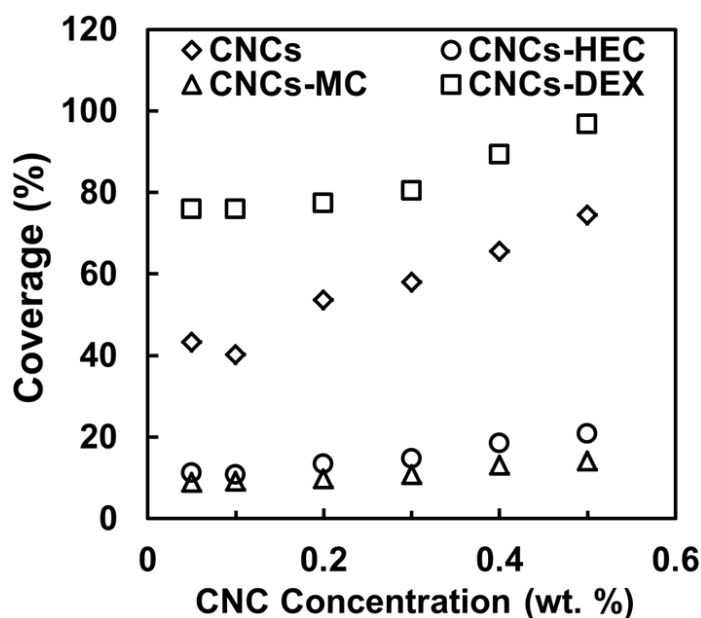


Figure 3. Evolution of surface coverage vs the amount of CNC particles included in the water phase for 1:1 dodecane-water emulsions of CNCs, CNC-HEC, CNC-MC, and CNC-DEX.

**Surface Coverage of Oil Droplets by CNCs.** Packing density of the CNCs at the interface was investigated by calculating the surface coverage according to eq 1, for emulsions prepared with different CNC concentrations. These values are plotted against  $m$ , that is, the mass of CNCs in the aqueous phase, as shown in Figure 3, to characterize the variation of surface coverage at different CNC concentrations. For emulsions stabilized by CNCs alone, surface coverage is increased at higher CNC concentrations, reaching a maximum coverage of about 74 % at 0.5 wt. % CNCs. Similar trend of increasing surface coverage as more CNC particles are used for emulsion stabilization along with different polymers were observed as well. The presence of HEC and MC seems to greatly reduce surface coverage to values below 20%, which is believed to be not

enough for effectively stabilizing emulsions as a minimum of approximately 84% of covered surface is required according to works from Capron et al.<sup>13</sup> On the contrary, surface coverage of CNCs at all concentrations in the presence of dextran is relatively higher than the ones of CNCs emulsion. All the values for CNC-DEX emulsion are close to or even higher than 84% (above 0.4 wt. % CNCs), which implies that CNC-DEX emulsion should be stable.

**Emulsion Stability.** The stability of dodecane/water emulsions stabilized by CNCs and polymers was assessed by monitoring the change of emulsion droplet mean diameter over time using a Malvern Mastersizer. CNC and polymer concentration were fixed to 0.3 wt. % and 0.2 wt. %, respectively. Figure 4 shows that the addition of HEC or MC enables the production of emulsions with minimal droplet size change over about 6 days, suggesting the beneficial effects of HEC and MC have on stabilizing emulsions. On the other hand, emulsion droplet size increase is observed one day after emulsion preparation for samples using CNCs as the sole emulsifier, suggesting the occurrence of coalescence. The addition of DEX does not seem to enhance the emulsion stability as the CNC-DEX emulsion displays fast and large increase of droplet size in the first two days after emulsion preparation. Mastersizer measurements of CNC-DEX emulsion for longer periods of time were not possible because either the emulsion size was beyond the instrument's detection limit or macroscopic phase separation occurred. Emulsions stabilized by the polymers alone were not stable to coalescence as the droplet diameters of those emulsion increased extensively over 6 days (Supporting Information, Figure S3).

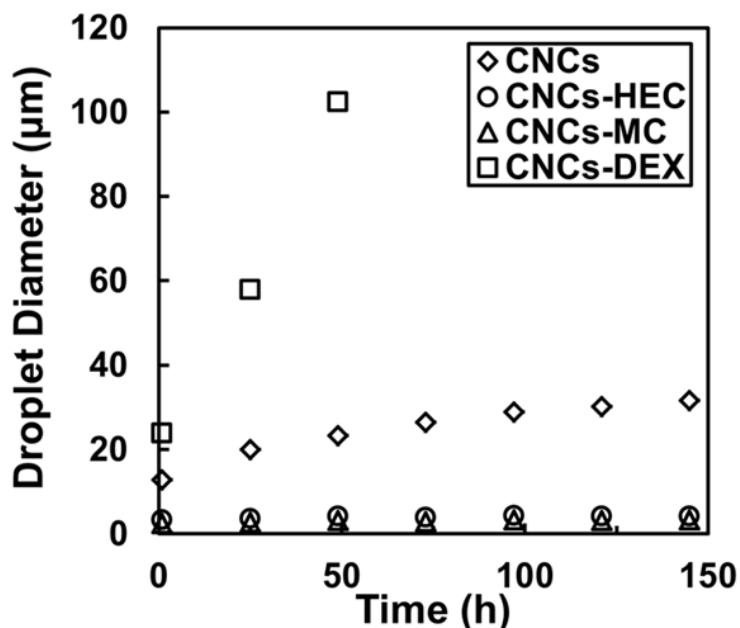


Figure 4. Mean droplet diameter of 1:1 dodecane-water emulsions stabilized by 0.3 wt. % CNCs alone and in the presence of 0.2 wt. % polymer over 150 hours, as measured by a Malvern

Mastersizer instrument. The mean droplet diameter was taken to be the volume mean diameter ( $D_{4/3}$ ) from 3 replicate measurements.

The long-term stability of o/w emulsions stabilized by CNCs and polymers was determined by visual check of emulsion appearance 30 days after emulsion preparation (Supporting Information, Figure S4). Emulsions stabilized by either CNCs or HEC show extensive creaming and mild color intensity decrease which imply the occurrence of coalescence. MC seems to be an effective emulsifier that enables the production of stable emulsion with mild creaming. DEX, on the other hand, could not provide long term stability to the emulsion stabilized by DEX alone and macroscopic phase separation is observed after 1 month storage. Using both DEX and CNCs to prepare emulsion does not lead to production of emulsion with enhanced stability either. However, both HEC and MC seem to greatly improve the stability of Pickering emulsions stabilized with CNCs and each one of these two polymers. Only mild creaming was found in CNC-HEC and CNC-MC emulsions.

**Interfacial Properties.** Dynamic interfacial tension was conducted to assess the adsorption of polymers as well as CNCs at the oil-interface. As shown in Figure 5, dodecane-water interfacial tension was measured over the course of 20 min. CNCs are able to lower the oil-water interfacial tension but even after 20 min the interfacial tension value still has not reached the equilibrium yet, implying that the slow partition of CNC particles to the oil-water interface, possibly due to their large hydrodynamic size. HEC can reduce the oil-water interfacial tension and equilibrium value of 32 mN/m is reached in about 5 min, which indicates that HEC can adsorb at the interface and can form a polymer layer to stabilize the emulsion. MC is more effective in reducing oil-water interfacial tension and an equilibrium value of about 20 mN/m could be achieved in less than 5 min, meaning that MC is more surface active than HEC. However, the interfacial tension values of DEX at dodecane-water interface display only a small reduction of about 1~2 mN/m. Therefore, DEX is not surface active and not an effective emulsifier for stabilizing o/w emulsions.

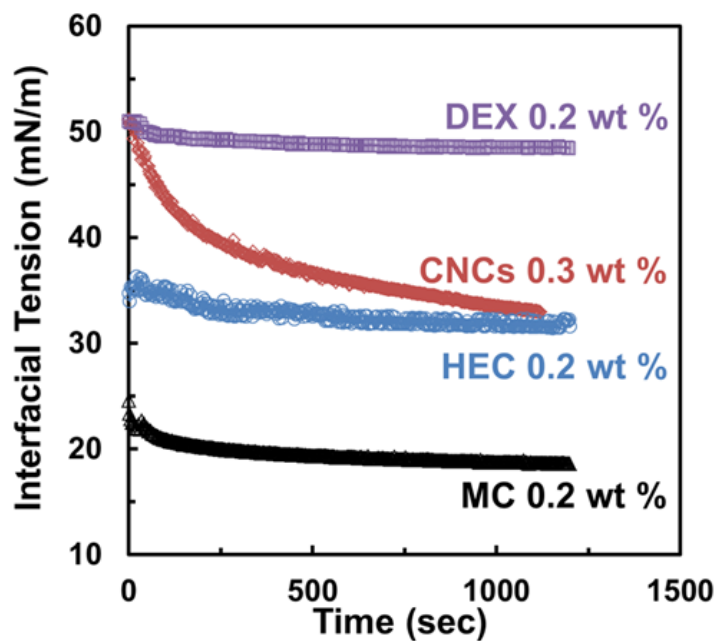


Figure 5. Time dependence of dodecane-water interfacial tension  $\gamma$  in the presence of CNCs (0.3 wt. %) or various polymers (0.2 wt. %).

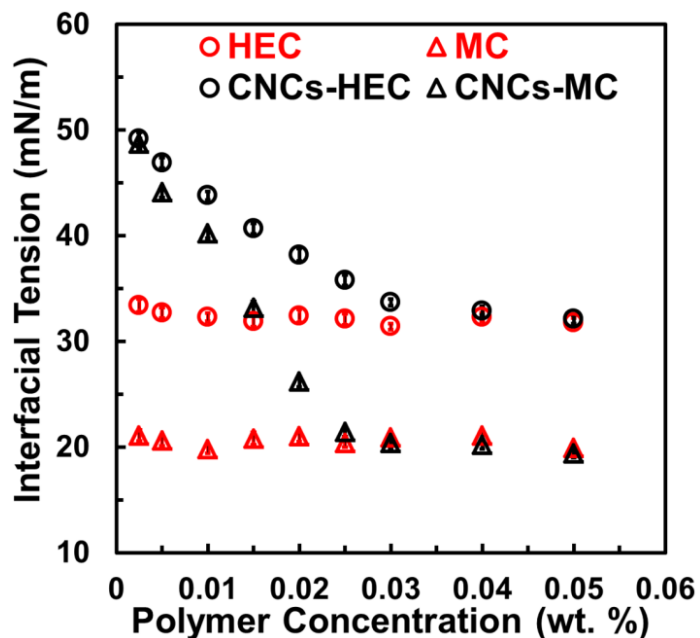


Figure 6. Interfacial tension of increasing amount of HEC or MC alone and in the presence of 0.5 wt. % CNCs.

Interfacial tension measurements were used to determine the maximum surface coverage of polymers on CNC surfaces. The critical points where the CNC particles have been fully covered with polymers and additional polymers start to partition to oil-water interface in Figure 6 were calculated based on the linear fitting of first 6 and last 3 black data points of each sample that is a mixture of polymers and CNCs. The maximum surface coverage of HEC and MC on CNC surfaces is found to be 0.16 and 0.14 mg/m<sup>2</sup>, respectively. According to this calculation, CNC surfaces are fully covered when mass ratio of CNCs:HEC and CNCs:MC is smaller than about 20:1. Since the mass ratio of CNCs over polymers was fixed to 3:2 in this work, we believe that all CNC particles have been coated with a polymer layer and there is a large amount of additional free polymer in the mixture. Therefore, it is expected that both polymer-coated CNCs and free polymers are present at the oil-water interface, stabilizing emulsion droplets together.

**Location of CNCs and Polymers in the Emulsions.** To further confirm the localization of CNCs and polymers at the oil-water interface, CNC particles and polymers were labelled with Nile blue and DTAF, respectively, and the emulsion samples were imaged under CLSM (Figure 7). Labeled CNCs and polymers are denoted as CNC-Nile blue, HEC-DTAF, and MC-DTAF and the labelling was confirmed with UV/Visible spectrometer (Supporting Information, Figure S5). This double staining of CNCs and polymers allows one to clearly determine the partition of CNCs and polymers at the interface. CNC-Nile Blue appears as red color in original CLSM images (Figure S6) and the ring structure suggests CNC particles are preferentially localized at the oil-water interface. On the other hand, HEC-DTAF and MC-DTAF appear as green color in original CLSM images (Figure S6) and display similar ring structure, which implies the partition of both HEC and MC to the interface. To obtain more visible distinction between the fluorescent area and blank area, the original images have been inverted using Adobe Photoshop software and shown in Figure 7. The presence of similar ring structures suggests the co-localization of both CNCs and polymer at the oil-water interface of each individual emulsion droplets.

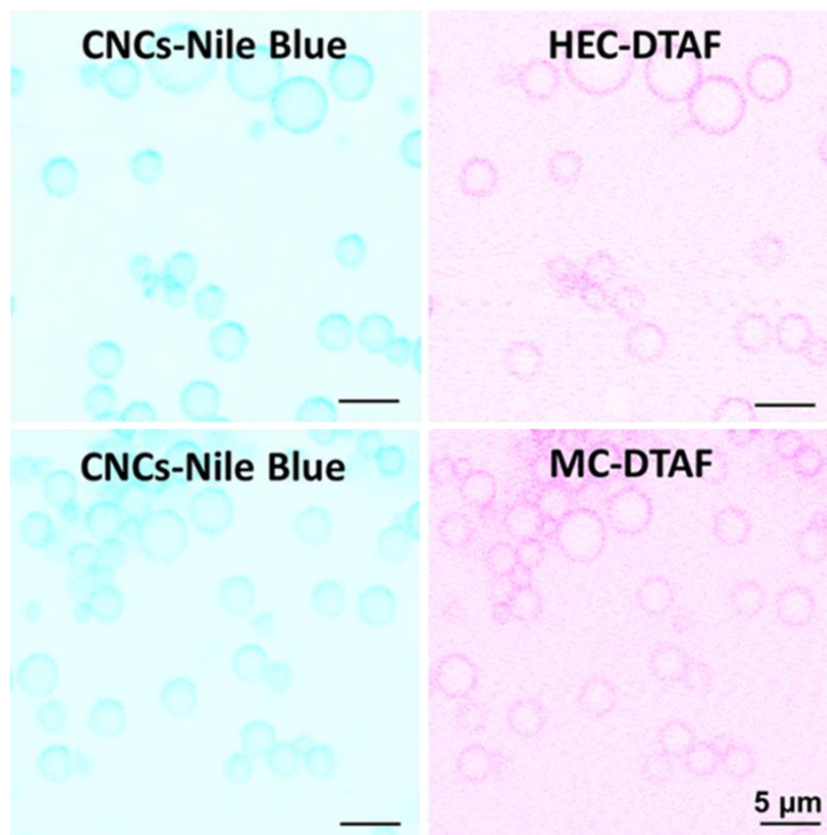


Figure 7. Confocal laser scanning micrographs of 1:1 dodecane-water emulsion droplets stabilized by CNCs labeled with Nile Blue and polymers labeled with DTAF (Top: CNCs-Nile Blue and HEC-DTAF; bottom: CNCs-Nile blue and MC-DTAF, the images have been inverted using Adobe Photoshop software).

**Emulsion Gels.** Many of the food and pharmaceutical products are emulsion-based soft solids that display gel-like behavior (structured emulsions).<sup>20</sup> The expression ‘emulsion gel’ is used to denote this class of soft-solid-like material that is essentially emulsion-based viscoelastic material. The oscillation test was performed at 25 °C and 70 °C to characterize the viscoelastic properties of the emulsion samples at different temperatures. CNC-HEC emulsion made with 0.3 wt. % CNCs and 0.2 wt. % HEC at oil volume fraction of 0.5 was used as the stock emulsion sample and equal volume of 2 wt. % of HEC or MC solution was added to the stock emulsion, which resulted in the reduction of oil volume fraction to 0.25. For CNC-HEC emulsion added with equal volume of 2 wt. % HEC (denoted as CNC-HEC+HEC), the overall behavior remains reminiscent of viscous liquids at both 25 °C and 70 °C (Figure 8) where the loss modulus ( $G''$ ) dominates over elastic modulus ( $G'$ ). There is no noticeable difference of rheological behaviors between difference temperatures. Figure 8a inset shows emulsion samples at 25 °C and 70 °C confirm that emulsion flows similarly at high temperature to room temperature. However, CNC-

HEC emulsion added with equal volume of 2 wt. % MC (denoted as CNC-HEC+MC), show classic gel behavior with  $G' > G''$  and a rather flat frequency response at 70 °C, implying the emulsion gel formation. Figure 8b inset shows that the emulsion does not move when the vial is inverted at high temperature, which means that the emulsion gels when temperature is increased. This gelation behavior of CNC-HEC emulsion with equal volume of MC at 25 °C was not observed. Stock CNCs-HEC emulsion without any additional MC at 70 °C does not display viscoelastic behavior either. Unlike MC, HEC could not induce gel formation of the emulsion when additional HEC is added to CNCs-HEC emulsion at 70 °C due to its lack of thermogelation property.

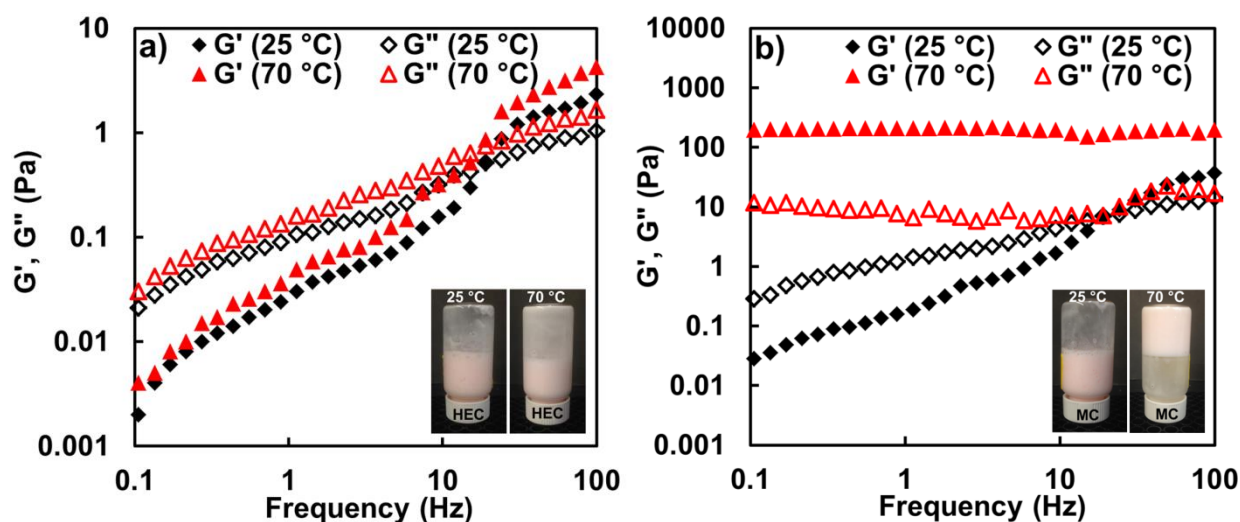


Figure 8. The storage modulus,  $G'$ , and loss modulus,  $G''$ , of (a) CNC-HEC+HEC emulsion, (CNCs: 0.15 wt. %, HEC: 1.1 wt. %, 25 vol % o/w emulsion ) (b) CNC-HEC+MC emulsion (CNCs: 0.15 wt. %, HEC: 0.1 wt. %, MC: 1 wt. %, 25 vol % o/w emulsion) at 25 °C (black diamonds) and 70 °C (red triangles). Inset images show that gel formation was achieved only in sample of CNC-HEC+MC emulsion at 70 °C.

Temperature affects the physical properties of oil, water, and interfacial films. These, in turn, affect the stability of the emulsion.<sup>30</sup> Temperature increases the thermal energy of the emulsion droplets, leading to the increase of frequency of droplet collisions. It generally reduces the interfacial viscosity and increases the film-drainage rate, which results in faster droplet coalescence. However, our emulsion gel samples subjected to multiple cycles of heat treatment did not display any noticeable change of emulsion droplet morphology ( Supporting Information, Figure S6), suggesting the emulsions are stable to coalescence in heating and cooling processes.

**Oil Solids.** In food, cosmetics, and pharmaceutical industries, reducing an o/w emulsion with encapsulated hydrophobic compounds in oil droplets to a dried solid is often required.<sup>26, 31</sup> In this work, we are interested in using a CNC-HEC corn oil-water emulsion with 25 % oil volume fraction as a template to produce structured dry oil powder with high oil content trapped in the matrix of cellulose-based only materials via freeze-drying.

The appearance of the materials resulting from freeze-drying of CNC-HEC, CNC-HEC+HEC, and CNC-HEC+MC emulsions is shown in Figure 9. CNC-HEC emulsion without second-step addition of HEC or MC yields a turbid flowing liquid, indicating that freeze-drying did not produce an encapsulated oil solid due to extensive oil leakage. In this work, we tested HEC and MC as the hydrophilic carrier to prevent emulsion droplets from collapsing into macrophase-separated liquid state during drying processing. By contrast the CNC-HEC emulsion with a second-step addition of HEC or MC formed pink solids without any oil leakage. No evidence of oil leakage of any kind is found even after 3 months of storage. Only upon pressing with fingers is oil partially released, revealing the nature of high oil content in the dried oil powders and the efficiency of oil encapsulation.

CLSM was used to assess the microstructure of the resulting oil powder better. Images of the freeze-dried CNC-HEC+MC emulsion sample produced with 0.15 wt. % CNCs, 0.1 wt. % HEC, 0.5 wt. % MC and stained with Nile Red are given in Figure 10. The oil powder exhibits macroporous structures where the pore size of about 20 to 200  $\mu\text{m}$  was dependent on the size of the ice crystals formed during the freezing procedure. As a result of the viscoelastic continuous phase impeding the coalescence of oil droplets, some individual deformed emulsion droplets can be seen by zooming in on the “walls” that form the macropores under CLSM (Figure 10b). However, the fluorescent phase seems to cover the entire oil powder, meaning the oil droplets undergo at least partial coalescence after freeze-drying. In this work, solid corn oil with an oil weight content of as high as 94% was successfully produced by freeze-drying CNC-HEC+MC emulsions, meaning only about 6 wt. % of the total final oil powders was from the emulsifiers and hydrophilic carriers. In addition, air-drying the same emulsion sample in oven at 60 °C for two days also produced solid oil but with a translucent look (Figure S8).

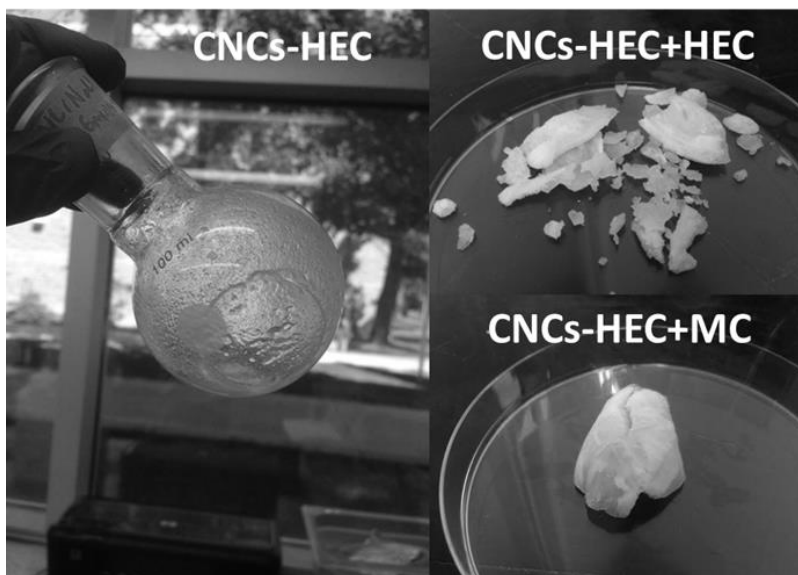


Figure 9. Appearance of CNC-HEC, CNC-HEC+HEC, and CNC-HEC+MC emulsions after freeze-drying. All samples are 25 vol % o/w emulsion before freeze-drying and the concentrations of all the components in the emulsions are:  $C_{\text{CNCs}} = 0.15$  wt. %,  $C_{\text{HEC}} = 0.1$  wt. % (CNC-HEC);  $C_{\text{CNCs}} = 0.15$  wt. %,  $C_{\text{HEC}} = 0.6$  wt. % (CNC-HEC+HEC);  $C_{\text{CNCs}} = 0.15$  wt. %,  $C_{\text{HEC}} = 0.1$  wt. %,  $C_{\text{MC}} = 0.5$  wt. % (CNC-HEC+MC). The oil phase is corn oil.

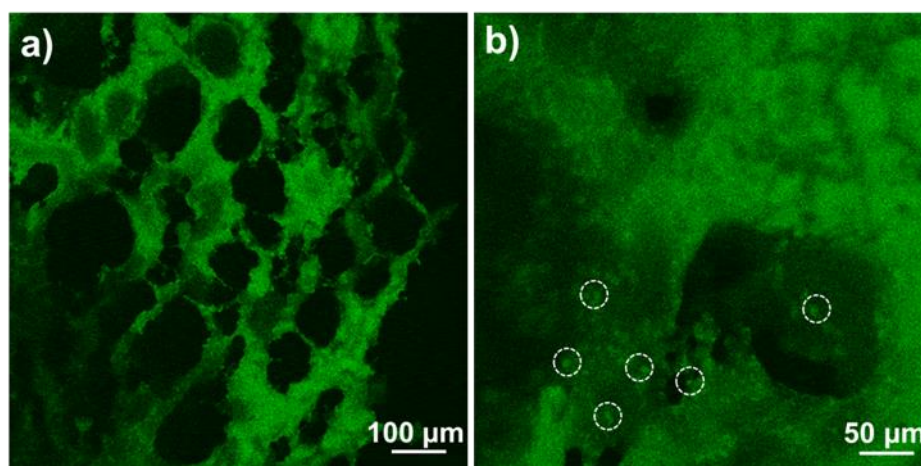


Figure 10. Confocal laser scanning micrographs of freeze-dried CNC-HEC+MC emulsion sample produced with 0.15 wt. % CNCs, 0.1 wt. % HEC, 0.5 wt. % MC at low magnification (a) and higher magnification (b). The oil phase is corn oil and labeled with Nile red. Individual emulsion droplets are highlighted in the dotted circles in (b).

## 4.4 Discussion

The surface coverage of the CNCs at the oil-water interface is a function of CNC concentration and emulsion droplet size according to eq 1. Capron et al.<sup>9, 13</sup> found that CNC-stabilized emulsion showed a clear tendency to coalescence when CNC concentration and surface coverage was low. Similar trend of emulsion droplet size reduction as a result of increasing CNC concentration was also observed in this work as demonstrated in Table 1. As a minimum of approximately 84% of oil-water interface area is required to be covered by CNCs for the emulsion to be stable to coalescence, CNCs-HEC and CNCs-MC emulsions should be extremely susceptible to coalescence and obviously unstable due to their low surface coverage (below 20%) according to Figure 3. However, both Figure 4 and Figure S4 suggest that CNCs-HEC and CNCs-MC emulsions are more stable than the emulsions stabilized by each individual stabilizers. This leads us to believe that both the CNCs and polymers contribute to the stabilization of oil-water interface, likely in a synergistic manner.

Dynamic interfacial tension was conducted to assess the interactions between polymers and CNCs when oil phase is present. As shown in Figure 5, CNC particles displayed small interfacial tension reduction, which agrees with the literature that particulate emulsifiers normally do not lower interfacial tension significantly. HEC and MC, on the other hand, can reduce the oil-water interfacial tension to equilibrium values of 32 and 20 mN/m, respectively, in about 5 min. As the polymers and CNCs were vigorously mixed before oil addition and emulsification, we expect that CNC particles were already covered with polymers due to the fast adsorption of polymer on CNC surface according to our earlier work and Figure S2.<sup>29</sup>

To determine whether the surface of CNC particles has been fully coated with a layer of adsorbed polymers, interfacial tension of increasing amount of HEC or MC in the presence of 0.5 wt. % CNCs was measured. As demonstrated in Figure 6, the introduction of CNCs greatly increased interfacial tension values of the mixture at low polymer concentrations, likely due to the preferential adsorption of polymers on CNC surfaces over partition to oil-water interface. The maximum surface coverage of HEC and MC on CNC surfaces was found to be 0.16 and 0.14 mg/m<sup>2</sup>, respectively. Based on these calculations, we believe that all CNC particles have been coated with a polymer layer and there was also a large amount of additional free polymer in the mixture.

Though the surface coverage of CNCs at the oil-water interface of CNCs-HEC and CNCs-MC emulsions was calculated to be below 20%, the adsorbed polymer layer on CNCs and free polymers should play a role in increasing the apparent surface coverage of the interface and thus stabilizing the emulsion droplets. This was confirmed by staining of CNCs and polymers with different dyes and imaging the CNCs-HEC and CNCs-MC emulsions at different wavelengths. The presence of similar ring structures suggests the co-localization of both CNCs and polymer at the oil-water interface of each individual emulsion droplets.

The emulsion gels discussed in literature are mostly for protein-coated emulsion droplets. They are typically produced by inducing gelation through various methods such as heating, high-pressure treatment, acidification, and enzymatic cross-linking.<sup>32-33</sup> Gels made of Pickering emulsions using CNCs and biopolymers as the emulsifiers and thickening agents was reported for the first time herein. MC is a widely available nontoxic commercial cellulose derivative that undergoes thermoreversible gelation in aqueous solutions in the range 50-60 °C. Upon heating, MC molecules lose part of their affinity to the surrounding water and thus start to bundle up into about 14 nm thick fibrils.<sup>34</sup> The fibrillation leads to the sol-to-gel transition of continuous phase and dramatic increase of  $G'$ . As shown in Figure 8, thermogelation was observed at 70 °C when additional MC was used as the gelling agent. The addition of HEC, on the other hand, showed no gelation behavior at increased temperature as the HEC does not display sol-to-gel transition. We believe that this finding may offer various industries a new route of producing CNC-based emulsion gels. More interestingly, our emulsion gel samples subjected to multiple cycles of heat treatment did not display any noticeable change of emulsion droplet morphology (Supporting Information, Figure S7), suggesting the emulsions are stable to coalescence in heating and cooling processes. Though emulsions stabilized by MC alone also showed thermogelation at high temperature, macroscopic coalescence and phase separation was obtained. This highlights the vast potential application of using both CNCs and MC to produce stable emulsion gels with homogenous distribution of emulsion droplets throughout the sample.

CNCs-HEC emulsion without second-step addition of HEC or MC failed to produce an encapsulated oil powder due to extensive oil leakage. As hydrophilic carriers are normally added to the water phase to prevent the emulsion droplets from collapsing into a macrophase-separated liquid state during drying processing, HEC and MC were tested as the hydrophilic carrier in our work. The CNCs-HEC emulsion with a second-step addition of HEC or MC formed corn oil solids without any oil leakage. This stresses the need to introduce a hydrophilic carrier before drying the samples. Typical examples of hydrophilic carriers used in oil powder production are lactose, glucose, maltodextrin, starch, and cellulose.<sup>26, 35-37</sup> In the absence of this carrier, the emulsion droplets easily coalesce during drying process, leading to the oil leaking and collapse of the oil powder. It is believed that the increase of continuous phase viscosity upon introduction of additional more polymers to the water phase might protect the emulsion droplets from extensive breaking when water is drained from the interfacial areas in drying process. Though some individual deformed emulsion droplets can be seen by zooming in on the “walls” that form the macropores under CLSM (Figure 10b), the whole solid oil piece displayed fluorescence except the pores due to the freeze-drying, meaning the oil droplets undergo at least partial coalescence upon drying. This is consistent with the observation on dry oil powder by freeze-drying silica-stabilized emulsions as precursors.<sup>26</sup>

The minimum amount of these hydrophilic carriers needed ranges from 30 to 80 wt. % of the total final oil powder.<sup>26</sup> In this work, oil powders with an oil weight content of as high as 94% was successfully produced by freeze-drying CNCs-HEC+MC emulsions, meaning only about 6

wt. % of the total final oil powders was from the emulsifiers and hydrophilic carriers. Similar work on using silica particle-stabilized o/w emulsions as a template for the preparation of oil powders by freeze-drying obtained oil content as high as 98 wt. %. However, we believe that a dry solid oil powder comprising a very high percentage of oily compounds that are usually liquid at room temperature by using CNCs and cellulose-based biopolymers have never been reported. Due to the simplicity and versatility of the proposed pathway, the present method is of particular interests to food, pharmaceutical, and cosmetic industries, where converting any type of hydrophobic liquid into the corresponding solid powder using bio-based materials is highly desirable.

## 4.5 Conclusions

1. We have presented a simple method of preparing stable emulsion with tunable size by using CNCs and cellulose-based polymers. The emulsion stability was substantially enhanced when CNCs were first mixed with surface-active water-soluble cellulose polymers (HEC or MC) before oil addition and emulsification.
2. HEC or MC-coated CNC particles and free polymers partition to the oil-water interface giving increased emulsion stability with no change in interfacial tension.
3. Robust and reversible thermogelation was obtained with CNCs-HEC emulsions upon addition of extra thermosensitive polymer MC with 1.0 wt.% MC in the aqueous phase. Multiple cycles of heating and cooling treatment does not induce any noticeable emulsion coalescence, indicating the ultrastable nature of the emulsions gels.
4. We have also shown that solid oils containing up to 94 wt. % corn oil (which is a liquid under ambient conditions) can be prepared by freeze-drying or air-drying emulsions stabilized by CNCs and polymers when additional cellulose-based polymers are introduced. It is reasonable to expect that, by following the procedure presented above, the transformation of other types of non-volatile oil into dry oil powders should be achievable. Since only cellulose-based materials are used, and considering the affordable process and precursor, stable emulsions, viscoelastic emulsion gels, and dry oil powders may serve in a broad range of industrial applications.

## References

- (1) Ramsden, W. Separation of Solids in the Surface-Layers of Solutions and 'Suspensions' (Observations on Surface-Membranes, Bubbles, Emulsions, and Mechanical Coagulation). -- Preliminary Account. *Proceedings of the Royal Society of London* **1903**, 72 (477-486), 156-164.
- (2) Pickering, S. U. CXCVI.-Emulsions. *Journal of the Chemical Society, Transactions* **1907**, 91 (0), 2001-2021.
- (3) Binks, B. P.; Whitby, C. P. Nanoparticle silica-stabilised oil-in-water emulsions: improving emulsion stability. *Colloids and Surfaces a-Physicochemical and Engineering Aspects* **2005**, 253 (1-3), 105-115.
- (4) Ashby, N. P.; Binks, B. P. Pickering emulsions stabilised by Laponite clay particles. *Physical Chemistry Chemical Physics* **2000**, 2 (24), 5640-5646.
- (5) Shen, M.; Resasco, D. E. Emulsions Stabilized by Carbon Nanotube-Silica Nanohybrids. *Langmuir* **2009**, 25 (18), 10843-10851.
- (6) Zhou, J.; Qiao, X. Y.; Binks, B. P.; Sun, K.; Bai, M. W.; Li, Y. L.; Liu, Y. Magnetic Pickering Emulsions Stabilized by Fe<sub>3</sub>O<sub>4</sub> Nanoparticles. *Langmuir* **2011**, 27 (7), 3308-3316.
- (7) Larson-Smith, K.; Pozzo, D. C. Pickering Emulsions Stabilized by Nanoparticle Surfactants. *Langmuir* **2012**, 28 (32), 11734-11741.
- (8) Ngai, T.; Behrens, S. H.; Auweter, H. Novel emulsions stabilized by pH and temperature sensitive microgels. *Chemical Communications* **2005**, (3), 331-333.
- (9) Kalashnikova, I.; Bizot, H.; Cathala, B.; Capron, I. New Pickering Emulsions Stabilized by Bacterial Cellulose Nanocrystals. *Langmuir* **2011**, 27 (12), 7471-7479.
- (10) Habibi, Y.; Lucia, L. A.; Rojas, O. J. Cellulose Nanocrystals: Chemistry, Self-Assembly, and Applications. *Chemical Reviews* **2010**, 110 (6), 3479-3500.
- (11) *The Global Market for Nanocellulose to 2020*. Future Markets Inc.: Edinburgh, United Kingdom, **2012**.
- (12) Kalashnikova, I.; Bizot, H.; Cathala, B.; Capron, I. Modulation of Cellulose Nanocrystals Amphiphilic Properties to Stabilize Oil/Water Interface. *Biomacromolecules* **2011**, 13 (1), 267-275.
- (13) Kalashnikova, I.; Bizot, H.; Bertoncini, P.; Cathala, B.; Capron, I. Cellulosic Nanorods of Various Aspect Ratios for Oil in Water Pickering Emulsions. *Soft Matter* **2013**, 9 (3), 952-959.
- (14) Capron, I.; Cathala, B. Surfactant-Free High Internal Phase Emulsions Stabilized by Cellulose Nanocrystals. *Biomacromolecules* **2013**, 14 (2), 291-296.
- (15) Hu, Z.; Ballinger, S.; Pelton, R.; Cranston, E. D. Surfactant-enhanced cellulose nanocrystal Pickering emulsions. *Journal of Colloid and Interface Science* **2015**, 439 (0), 139-148.
- (16) Zoppe, J. O.; Venditti, R. A.; Rojas, O. J. Pickering emulsions stabilized by cellulose nanocrystals grafted with thermo-responsive polymer brushes. *Journal of Colloid and Interface Science* **2012**, 369 (1), 202-209.
- (17) Tang, J.; Lee, M. F. X.; Zhang, W.; Zhao, B.; Berry, R. M.; Tam, K. C. Dual Responsive Pickering Emulsion Stabilized by Poly[2-(dimethylamino)ethyl methacrylate] Grafted Cellulose Nanocrystals. *Biomacromolecules* **2014**, 15 (8), 3052-3060.

- (18) Saleh, N.; Phenrat, T.; Sirk, K.; Dufour, B.; Ok, J.; Sarbu, T.; Matyjaszewski, K.; Tilton, R. D.; Lowry, G. V. Adsorbed Triblock Copolymers Deliver Reactive Iron Nanoparticles to the Oil/Water Interface. *Nano Letters* **2005**, *5* (12), 2489-2494.
- (19) Feng, T.; Hoagland, D. A.; Russell, T. P. Assembly of Acid-Functionalized Single-Walled Carbon Nanotubes at Oil/Water Interfaces. *Langmuir* **2014**, *30* (4), 1072-1079.
- (20) Dickinson, E. Emulsion gels: The structuring of soft solids with protein-stabilized oil droplets. *Food Hydrocolloids* **2012**, *28* (1), 224-241.
- (21) Menner, A.; Ikem, V.; Salgueiro, M.; Shaffer, M. S. P.; Bismarck, A. High internal phase emulsion templates solely stabilised by functionalised titania nanoparticles. *Chemical Communications* **2007**, (41), 4274-4276.
- (22) Tasset, S.; Cathala, B.; Bizot, H.; Capron, I. Versatile cellular foams derived from CNC-stabilized Pickering emulsions. *RSC Adv.* **2014**, *4* (2), 893-898.
- (23) Jayasundera, M.; Adhikari, B.; Aldred, P.; Ghandi, A. Surface modification of spray dried food and emulsion powders with surface-active proteins: A review. *Journal of Food Engineering* **2009**, *93* (3), 266-277.
- (24) Fuchs, M.; Turchiuli, C.; Bohin, M.; Cuvelier, M. E.; Ordonnaud, C.; Peyrat-Maillard, M. N.; Dumoulin, E. Encapsulation of oil in powder using spray drying and fluidised bed agglomeration. *Journal of Food Engineering* **2006**, *75* (1), 27-35.
- (25) Mezzenga, R.; Ulrich, S. Spray-Dried Oil Powder with Ultrahigh Oil Content. *Langmuir* **2010**, *26* (22), 16658-16661.
- (26) Adelman, H.; Binks, B. P.; Mezzenga, R. Oil Powders and Gels from Particle-Stabilized Emulsions. *Langmuir* **2012**, *28* (3), 1694-1697.
- (27) Beck-Candanedo, S.; Roman, M.; Gray, D. G. Effect of Reaction Conditions on the Properties and Behavior of Wood Cellulose Nanocrystal Suspensions. *Biomacromolecules* **2005**, *6* (2), 1048-1054.
- (28) Abitbol, T.; Palermo, A.; Moran-Mirabal, J. M.; Cranston, E. D. Fluorescent Labeling and Characterization of Cellulose Nanocrystals with Varying Charge Contents. *Biomacromolecules* **2013**, *14* (9), 3278-3284.
- (29) Hu, Z.; Cranston, E. D.; Ng, R.; Pelton, R. Tuning Cellulose Nanocrystal Gelation with Polysaccharides and Surfactants. *Langmuir* **2014**, *30* (10), 2684-2692.
- (30) Ghosh, S.; Rousseau, D. Fat crystals and water-in-oil emulsion stability. *Current Opinion in Colloid & Interface Science* **2011**, *16* (5), 421-431.
- (31) Patel, A. R.; Rajarethinam, P. S.; Cludts, N.; Lewille, B.; De Vos, W. H.; Lesaffer, A.; Dewettinck, K. Biopolymer-Based Structuring of Liquid Oil into Soft Solids and Oleogels Using Water-Continuous Emulsions as Templates. *Langmuir* **2014**.
- (32) van Vliet, T.; Lakemond, C. M. M.; Visschers, R. W. Rheology and structure of milk protein gels. *Current Opinion in Colloid & Interface Science* **2004**, *9* (5), 298-304.
- (33) Rodríguez-Abreu, C.; Lazzari, M. Emulsions with structured continuous phases. *Current Opinion in Colloid & Interface Science* **2008**, *13* (4), 198-205.
- (34) Lott, J. R.; McAllister, J. W.; Arvidson, S. A.; Bates, F. S.; Lodge, T. P. Fibrillar Structure of Methylcellulose Hydrogels. *Biomacromolecules* **2013**, *14* (8), 2484-2488.
- (35) Christensen, K. L.; Pedersen, G. P.; Kristensen, H. G. Technical optimisation of redispersible dry emulsions. *International Journal of Pharmaceutics* **2001**, *212* (2), 195-202.

- (36) Christensen, K. L.; Pedersen, G. P.; Kristensen, H. G. Preparation of redispersible dry emulsions by spray drying. *International Journal of Pharmaceutics* **2001**, *212* (2), 187-194.
- (37) Heinzelmann, K.; Franke, K. Using freezing and drying techniques of emulsions for the microencapsulation of fish oil to improve oxidation stability. *Colloids and Surfaces B: Biointerfaces* **1999**, *12* (3–6), 223-229.

## Appendix: Supporting Information for Chapter 4

**Transmission Electron Microscopy (TEM).** The anionic functional groups on CNC particles were selectively stained by mixing a 0.05 mL aliquot of the CNC (0.5 wt%) with 0.5 mL of a 1 mM uranyl acetate solution and vortexing the mixture for 2 min. A single drop of the stained suspension was dropped on a Formvar-coated copper TEM grid and dried for 4 h. TEM images were acquired using a JEOL 1200 EX TEMSCAN microscope operating at 80 kV.

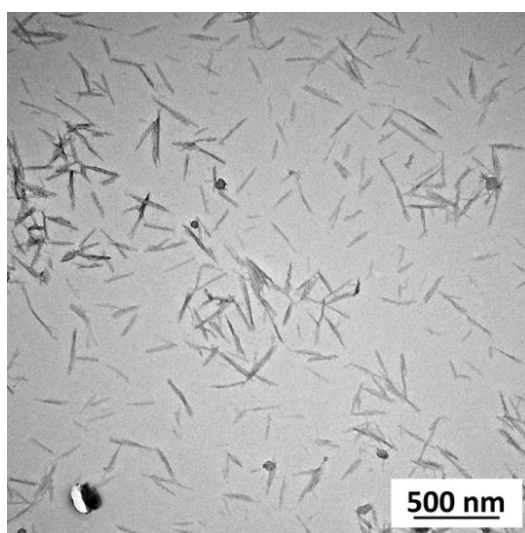


Figure S1. TEM image of sulfated cellulose nanocrystals (CNCs).

TEM image of CNCs is presented in Figure S1 and shows well-dispersed rod-shaped nanoparticles with average crystal dimensions of 128 x 7 nm. The average dimensions of these CNCs were determined by measuring the sizes of about 100 individual nanocrystals.

**Quartz Crystal Microbalance with Dissipation Monitoring (QCM-D).** CNCs-coated sensors were prepared using an approach that has been previously used in a similar work. Methyl cellulose (MC) adsorption on CNC surface was measured with an E4 QCM-D instrument from Q-Sense AB (Sweden) where the third, fifth, and seventh overtones were recorded. An aqueous solution of HEPES buffer was injected at a constant flow rate of 150  $\mu\text{L}/\text{min}$  until the baseline frequency shift was less than 0.5 Hz over 10 min. Then 1 g/L MC in HEPES buffer was injected at 150  $\mu\text{L}/\text{min}$  until the baseline was again stable, typically after 60 min. The sensor was rinsed with HEPES buffer at 150  $\mu\text{L}/\text{min}$  until the baseline was stable, typically after 5 min.

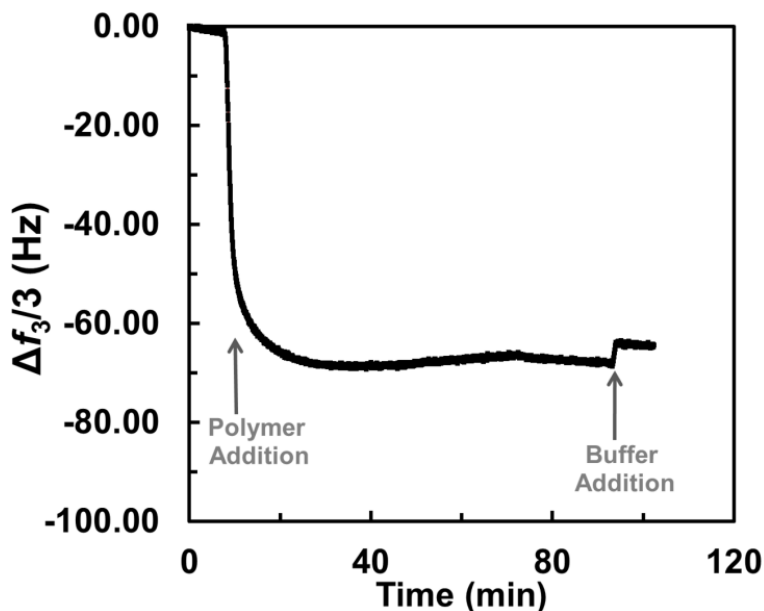


Figure S2.  $\Delta f_3/3$  versus time for QCM-D study of CNCs-coated QCM sensors exposed to MC (1g/L in 150 mM HEPES buffer).

In Figure S2, MC gave a large frequency drop, indicating adsorption of MC on CNC surfaces.

**Malvern Mastersizer.** The stability of emulsions stabilized with polymers at 0.2 wt. % was investigated by monitoring the emulsion droplet mean diameter change over about 6 days using a Malvern Mastersizer instrument. DEX emulsions displayed extensive coalescence in less than 2 days after being prepared, whereas both HEC and MC showed slow coalescence with MC emulsion being more stable. The emulsion droplet diameter increased by about 270% and 390% for MC emulsion and HEC emulsion, respectively.

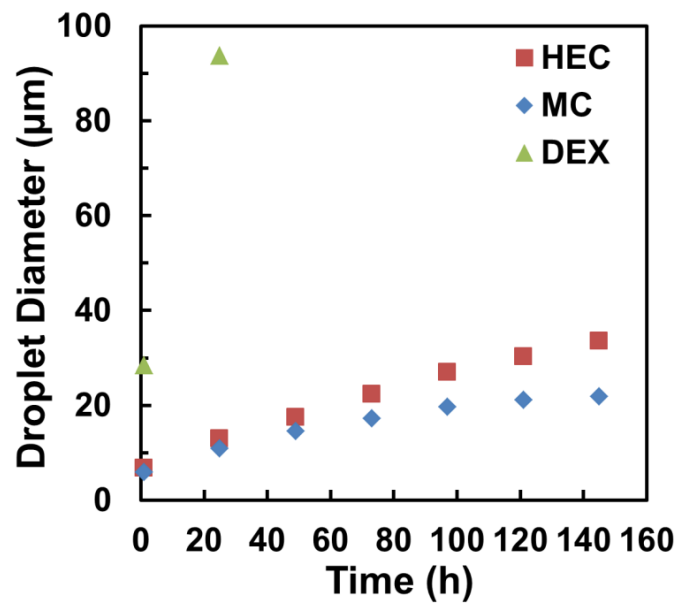


Figure S3. Mean droplet diameter of 1:1 dodecane-water emulsion stabilized by 0.2 wt. % polymer alone over 150 hours, as measured by a Malvern Mastersizer instrument. The mean droplet diameter was taken to be the volume mean diameter ( $D_{4/3}$ ) from 3 replicate measurements.

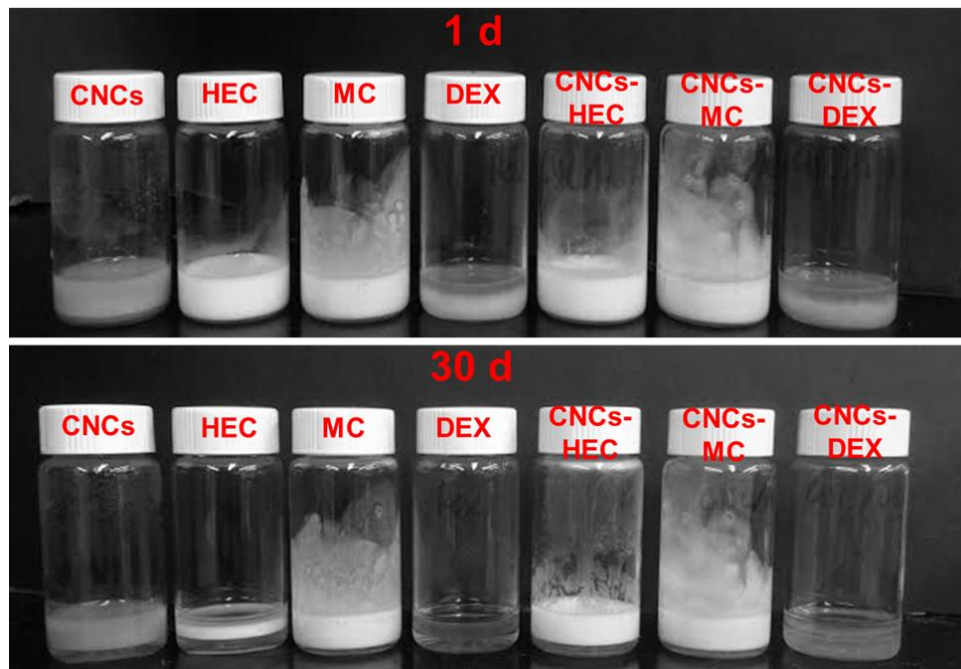


Figure S4. Appearance of emulsions stabilized by CNCs, polymers, or CNCs with polymers in 1 day and 30 days after emulsification.

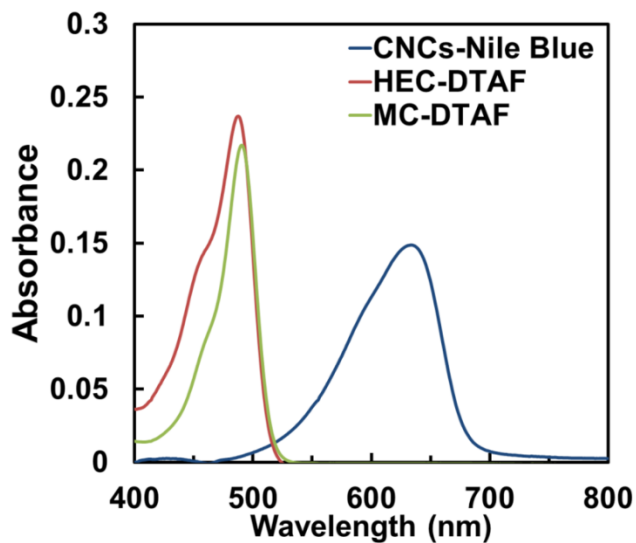


Figure S5. UV-vis absorbance spectrum of CNCs-Nile Blue, HEC-DTAF, and MC-DTAF.

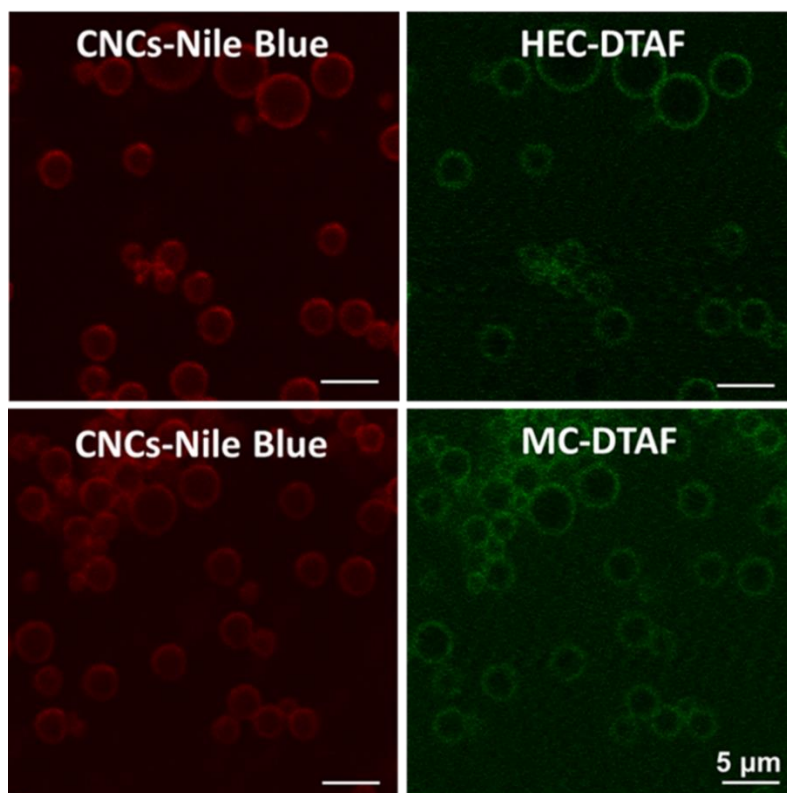


Figure S6. Confocal laser scanning micrographs of 1:1 dodecane-water emulsion droplets stabilized by CNCs labeled with Nile Blue and polymers labeled with DTAF (Top: CNCs-Nile Blue and HEC-DTAF; bottom: CNCs-Nile Blue and MC-DTAF).

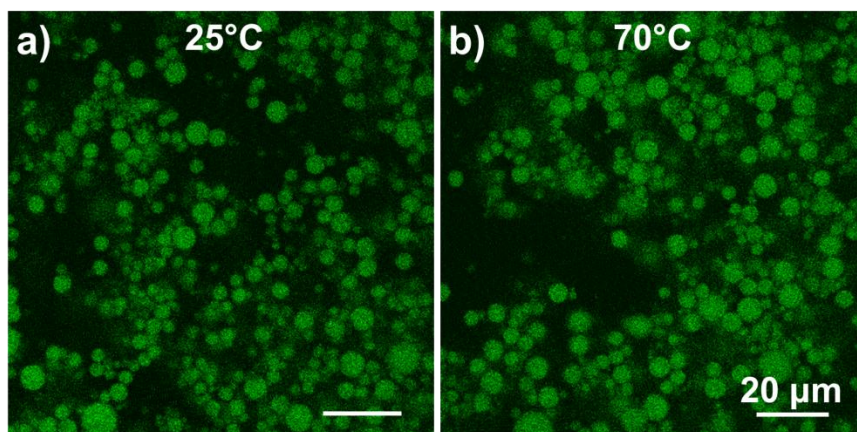


Figure S7. CLSM images of CNCs-HEC+MC emulsion at a) 25 °C and b) 70 °C (CNCs: 0.15 wt. %, HEC: 0.1 wt. %, MC: 1 wt. %, 25 vol % o/w emulsion).



Figure S8. Appearance of CNCs-HEC+MC emulsion after air-drying in oven at 60 °C for two days. The concentrations of all the components in the emulsions are:  $C_{\text{CNCs}} = 0.15$  wt. %,  $C_{\text{HEC}} = 0.1$  wt. %,  $C_{\text{MC}} = 0.5$  wt. %. The oil phase is corn oil.

## **Chapter 5 Preparation and Templating Properties of Stable Foams of Cellulose Nanocrystals and Methyl Cellulose**

In chapter 5, all experiments were conducted by myself with assistance from Richard Xu (undergraduate student). The chapter was initially drafted by myself, and revised later by Dr. Robert Pelton and Dr. Emily D. Cranston.

# Preparation and Templating Properties of Stable Wet Foams of Cellulose Nanocrystals and Methyl Cellulose

Zhen Hu,<sup>†</sup> Richard Xu,<sup>†</sup> Emily D. Cranston,<sup>†</sup> and Robert Pelton<sup>\*,†</sup>

<sup>†</sup> Department of Chemical Engineering, McMaster University, Hamilton, Canada L8S 4L7

## Abstract

Stable aqueous foams based on cellulose nanocrystals (CNCs) and methyl cellulose (MC) were prepared and characterized. No surface modification of the CNCs was required to produce the aqueous foams. To our knowledge, our study provides the first experimental evidence of making stable aqueous foams with unmodified CNCs. The foamability, foam stability, and water drainage of foams with CNCs at various loadings were examined. Surface tension measurements and confocal laser scanning microscopy imaging were conducted to determine the interfacial properties of CNCs and MC. 15 g/L CNCs in the presence of 5 g/L MC were able to produce foams with about 80 vol% of air, which are stable to coalescence for at least a week. Macroporous polymers with tailored microstructures and properties were produced by using CNC-MC foams as the templates. By varying the composition of CNC-MC foams, porous materials with porosities between 70 and 83% and pore sizes between 100 and 500  $\mu\text{m}$  were obtained. This foaming process is also applicable to a wide range of hydrophilic monomers of acrylamide (AM), 2-hydroxyethyl methacrylate (HEMA), and polyethylene glycol diacrylate (PEGDA). The foaming and templating process developed here presents a new way to design macroporous structures for potential applications in biomedical, food, personal care, and oil recovery industries.

## 5.1 Introduction

Aqueous foams are dispersions of gas bubbles in a continuous aqueous phase. They have been a subject of much research in colloid science due to their wide practical applications in chemical, food, and cosmetic industries. They are thermodynamically unstable or metastable systems that their bubble size increases with time and they will eventually separate into two distinct phases.<sup>1</sup> The average bubble size increase is mainly driven by two processes, coarsening and coalescence. Coarsening involves gas diffusion from a small bubble to a larger one due to the higher Laplace pressure inside the small bubble. Coalescence, on the other hand, occurs when two bubbles merge due to the rupture of the liquid film between them during the drainage of the liquid.<sup>2</sup> Most conventional foams are stabilized by surfactants, proteins, or polymers. However, these surface-active molecules are not able to completely avoid bubble growth due to their low energy of attachment to the gas-liquid interface, which is only a few  $kT$ 's for a single molecule ( $k$  being the Boltzmann constant and  $T$  the temperature).<sup>3</sup> Therefore, there is constant adsorption and

desorption of these molecules at the interface. Though these stabilizers are well studied and widely applied in various industries, the interest in particulate stabilizers of bio-based source especially has been surging in academia as well as industry due to their remarkable stability and novel functionalities.

The particle-stabilized foams, or Pickering foams, have been fully investigated during the last decades.<sup>4-13</sup> As opposed to surfactants, the energy of attachment of a particle at a gas-liquid interface can reach thousands of  $kT$ 's, meaning particles can irreversibly adsorb at gas-liquid interfaces.<sup>6-7, 12</sup> Particles adsorbed at the interface hinder bubble coalescence due to steric repulsion and form an interfacial armor with increased mechanical rigidity that resists shrinkage/expansion of bubbles and impedes Ostwald ripening.<sup>10</sup> Another mechanism by which particles can induce high foam stability is through an increase in the viscosity of the bulk aqueous phase via aggregation of particles and jamming of the bubbles.<sup>14</sup> As a result, Pickering foams exhibit enhanced stability in comparison to foams stabilized by surface-active molecules.

Pickering foams have been obtained with clay platelets,<sup>15</sup> silica spheres,<sup>11-13</sup> iron particles,<sup>16</sup> metal oxide nanoparticles,<sup>17-18</sup> polymer latex,<sup>19-21</sup>  $\text{CaCO}_3$  rods,<sup>22</sup> and cellulose particles,<sup>14, 23-24</sup> among others. Although solid particles produce long-lasting stable foams, there are some particular conditions that need to be satisfied for effective stabilization of the gas-water interface, such as hydrophobicity, size, shape, aspect ratio, and concentration.<sup>13, 25-26</sup> For instance, surface modification of the particles is normally required to tune the hydrophobicity by chemical functionalization of the surface or adding surface-active molecules.<sup>12, 24, 27-28</sup> In addition, though solid particles are capable of producing foams with enhanced stability, they can be disadvantageous due to their relatively low foamability.<sup>14</sup> Mass transport and partition at the air-water interface may not be as fast as surface-active molecules to stabilize the bubbles as a result of their large size and aggregation in the aqueous phase for particles with high hydrophobicity. Furthermore, particles with large aspect ratio are likely to form intertwined networks of high mechanical stability in the bulk aqueous phase and thus increase the bulk viscosity, which hinders the formation of air bubbles in the first place.<sup>14, 20</sup>

The formation of Pickering foams opens many opportunities in a number of areas where foams are used either as an intermediate or end product, including food, pharmaceuticals, cosmetics, oil recovery, mineral flotation, and materials fabrication.<sup>4, 9, 29-33</sup> In these applications, microstructural features of the aqueous foam such as the air content, average bubble size, the bubble size distribution, and bubble stability are of major importance, since they determine the rheological behavior and functional properties of the aqueous foam as the final product. In addition, these foam properties also have a substantial influence on the final mechanical and physical properties of the materials when these aqueous foams are used as templates to produce porous materials.<sup>31-33</sup>

Most particles presently used to form foams with long-term stability are not of biological origin and are not desirable for formulations in food, pharmaceutical, and cosmetic industries.<sup>7</sup>

Therefore, one needs to identify low-cost, natural origin particles of intermediate hydrophobicity and develop techniques to produce foams from them. Cellulose materials, the most abundant renewable natural polymer on earth, have displayed a particularly good potential in stabilizing foams.<sup>14, 23-24</sup> Hydrophobic cellulose microparticles of hypromellose phthalate have been formed *in situ* by a liquid-liquid dispersion technique and used to create foams that were stable for months.<sup>23</sup> Micron sized hydrophobic cellulose particles were also made through precipitation of ethyl cellulose onto Tencel and combined with caseins or whey proteins to give significant improvements in stability of bubbles.<sup>14</sup> Super stable aqueous foams with various bubble sizes stabilized by food grade colloidal ethyl cellulose particles were reported.<sup>34</sup> Surface-modified nanofibrillated cellulose (NFC) has been used to prepare stable wet foams. Careful removal of the water led to a lightweight and strong porous cellulose material suitable for insulation, absorption, and packaging applications.<sup>24</sup> Cellulose nanocrystals (CNCs), highly crystalline rigid rod-shaped nanoparticles that are 5-10 nm in cross-section and 100-200 nm long, are entering the marketplace in commercial scale quantities in Canada, United States, and Europe.<sup>35-36</sup> They are most commonly prepared by sulfuric acid hydrolysis of cotton which gives nanocrystals with anionic sulfate half-ester groups on their surface. Capron and co-workers have established the groundwork of using of CNCs as emulsion stabilizers.<sup>37</sup> To the best of our knowledge, no example of aqueous foams comprised of CNCs exists yet in the literature. This work focuses on using CNCs as stabilizing agents for bubbles and foams because of their small size, commercial availability, general biocompatibility, and outstanding stiffness. Tedious surface modification using potentially toxic chemicals is also avoided in this work by using a water-soluble cellulose derivative polymer.

Recently, Pickering foams and emulsions have been identified as promising precursors for the fabrication of novel porous materials because of their exceptional stability.<sup>4, 31-33</sup> Reactive monomers were incorporated in these Pickering foams and they solidified upon polymerization.<sup>38-39</sup> Polymerization-free methods for producing porous materials directly from ceramic and thermoplastic polymers have also been developed.<sup>31, 33, 40</sup> In this work, we present for the first time a process for producing porous composite materials with tunable properties based on Pickering foams made from CNCs and methyl cellulose (MC). The development of cellulose-based Pickering foams, and the ability to prepare functional porous materials using these foams as templates (denoted as polyFoams), may open new application potential for CNCs in personal care, construction and insulation, energy storage, and tissue engineering, to name just a few.

## 5.2 Experimental Section

**Materials.** Methyl cellulose (MC, 40 kDa, degree of substitution (DS) of 1.6~1.9), Nile Blue, 5-(4, 6-dichlorotriazinyl) aminofluorescein (DTAF), potassium persulfate (PP), 2-hydroxyethyl methacrylate (HEMA), acrylamide (AM), polyethylene glycol diacrylate (PEGDA), N,N'-Methylenebisacrylamide (MBA), and 2-[4-(2-hydroxyethyl)piperazin-1-yl]ethanesulfonic acid

(HEPES) were all purchased from Sigma-Aldrich Inc., USA. The water used in all solutions was deionized and further purified with a Barnstead Nanopure Diamond system (Thermo Scientific, Asheville, NC). All the chemicals are used as received, unless otherwise noted.

**Preparation of Cellulose Nanocrystals.** CNCs were prepared by sulfuric acid hydrolysis of cotton from cotton filter aid (Whatman ashless filter aid, GE healthcare Canada, Mississauga, Canada), as described previously.<sup>41</sup> The filter aid was first torn into small squares and blended into a fluffy, white powder in a standard household blender (Magic Bullet brand). The powder was dried at 80°C for 1 h prior to the reaction. 40 g of the filter aid was treated with 700 mL of 64 wt. % sulfuric acid (Fischer Scientific) for 45 min at 45 °C with constant mechanical stirring. The hydrolysis reaction was quenched by adding 10-fold water. The acid removal was achieved by extensive dialysis against purified water until the pH of the external reservoir was stable over the last few water changes (~2 weeks). The surface charge density of sulfate half-ester groups on CNCs was determined by conductometric titration to be  $0.33 \pm 0.02$  e/nm<sup>2</sup>, with average crystal dimensions of 128 x 7 nm from transmission electron microscopy (TEM) image analysis. A TEM micrograph of the CNCs is provided in the Supporting Information Figure S1.

**Foam Generation.** MC solutions (0.5 wt. %) with increasing amount of CNCs (0 – 1.5 wt. %) was subjected to high shearing and mixing by using an Ultra-Turrax homogenizer IKA T25 (Wilmington, NC) with an 18 mm diameter dispersion head. For a CNCs-MC mixture of 4 mL, foams were generated by having the dispersion head centered and placed well below the surface of the mixture at a shearing rating of 10,000 rpm for 1 min. 50 mM HEPES were added to the solutions used for foam formation, unless otherwise noted.

**Foamability and Foam Stability.** The normalized foamability ( $\phi$ ) was assessed by measuring the ratio of the foam volume ( $V_0$ ) immediately after preparation to the initial liquid volume ( $V_i$ ). Aging foams in an airtight container at room temperature prevents water evaporation from the foam. The foam stability was estimated by monitoring foam volume (total volume minus the volume of drained liquid) and bubble size over time at ambient temperature. The normalized foam volume ( $\phi_t$ ) was calculated as the ratio of foam volume ( $V_t$ ) to the initial liquid volume ( $V_i$ ). The fraction of liquid in the foam was represented by the expression:  $\varepsilon = V_{\text{liq}}/V_t$ , where  $V_{\text{liq}}$  is the volume of liquid dispersed/remaining in the foam, and  $V_t$  represents the volume of foam. Liquid drained out from the foam was collected by using a syringe and needle. Water remaining in the foam was removed by drying the sample in an oven at 90 °C. The fraction of liquid in the foam was then calculated through a mass balance.

**Fluorescent Labeling.** The CNCs were labeled with Nile Blue. Nile Blue (10 mg) was added to 50 mL 1 wt. % CNC suspension (pH 3) and mixed for 24 h in the dark. Unbound Nile Blue was removed by extensive dialysis for a week against purified water. The polymers were labeled with DTAF using an approach that has been previously applied to CNCs.<sup>42</sup> HEC or MC (500 mg) was reacted with DTAF (7.5 mg) under alkaline conditions (0.2 M NaOH) for 24 h, in the dark, with mechanical stirring. To remove unreacted DTAF and the bulk of the NaOH, extensive dialysis

against purified water was employed. Purified reaction products were freeze-dried and stored in the dark. The labeled CNCs and polymers are denoted as CNC-Nile Blue, HEC-DTAF, and MC-DTAF, respectively.

**Confocal Laser Scanning Microscopy (CLSM).** For CLSM visualization of the microstructure of the foams, the CNCs and polymers were labeled with Nile Blue (630/660 nm) and DTAF (495/517 nm), respectively. Images were obtained with a Zeiss LSM 510 Meta on an Axiovert 200M microscope (Zeiss, Gottingen, Germany). Optical microscopy images of foam were obtained by using the same microscopy at transmission mode. About 100 individual bubbles were measured to determine the average bubble diameter of each sample.

**Dynamic Surface Tension.** Surface tension of 0.5 wt. % CNCs alone and in the presence of various amount of MC was measured by a Krüss Drop Shape Analysis System DSA10 instrument based on the pendant drop method. The aging of the air-water interface can be accurately monitored by measuring the dynamic surface tension of a drop having a constant interfacial area over 20 min.

**Rheology.** Oscillatory rheological measurements of emulsions were performed using an ARES rheometer (TA Instruments) with parallel-plate geometry. In all experiments, a 7 mm diameter parallel plate geometry and 1.5 mm gap distance were used. Dynamic frequency sweeps were performed at 1% strains, which were confirmed to be in the linear viscoelastic range for each emulsion sample, from 0.1 to 100 rad/s to determine the storage modulus ( $G'$ ) and loss modulus ( $G''$ ) of the emulsions. Measurements were done at temperatures of 25 °C.

**Polymerization.** For the macroporous structure preparation using CNC-MC aqueous foam as templating material (denoted as polyFoam), three monomers, acrylamide (AM), 2-hydroxyethyl methacrylate (HEMA), and polyethylene glycol diacrylate (PEGDA), were used as received, and the initiator was potassium persulfate. The crosslinker used for AM and HEMA polyFoam samples was N,N'-Methylenebisacrylamide (MBA), whereas no crosslinker was used for PEGDA polyFoam samples. All the components used for polyFoam sample preparation are listed in Table 1. The mixture with all components was stirred in a 20 mL vial for 1 h and then purged for 5 min with nitrogen to remove dissolved oxygen. The vial was sealed and kept in 70 °C oil bath for polymerization. After 6 h, the vial was broken and the resulting wet hydrogel foam was cut into small pieces for rheological measurements and freeze-drying.

**Scanning Electron Microscopy (SEM).** Morphology characterization of freeze-dried foams after polymerization were done by using a JEOL 7000F SEM (JEOL Ltd., Japan). Foams were immersed in liquid nitrogen and fractured to image the inner sections. A 3 nm thick gold coating was applied before SEM imaging. Micrographs were taken at several magnifications at 6 mm working distance and at 20 kV acceleration voltage.

Table 1. Summary of components used to prepare PolyFoam materials.

| PolyFoam           | Monomer (g) | MBA <sup>a</sup> (g) | PP <sup>b</sup> (g) | CNCs (g) | MC (g) | Salt (g) | Water (g) |
|--------------------|-------------|----------------------|---------------------|----------|--------|----------|-----------|
| AM1 <sup>c</sup>   | 0.80        | 0.16                 | 0.02                | 0.03     | 0.03   | 0.07     | 5.87      |
| AM2                | 0.80        | 0.16                 | 0.02                | 0.06     | 0.03   | 0.07     | 5.84      |
| AM3                | 0.80        | 0.16                 | 0.02                | 0.09     | 0.03   | 0.07     | 5.81      |
| AM4                | 0.40        | 0.08                 | 0.01                | 0.09     | 0.03   | 0.07     | 5.81      |
| AM5                | 1.20        | 0.24                 | 0.03                | 0.09     | 0.03   | 0.07     | 5.81      |
| HEMA <sup>d</sup>  | 0.80        | 0.16                 | 0.02                | 0.09     | 0.03   | 0.07     | 5.81      |
| PEGDA <sup>e</sup> | 0.80        | NA                   | 0.02                | 0.09     | 0.03   | 0.07     | 5.81      |

<sup>a</sup>MBA: methylenebisacrylamide as the crosslinker; <sup>b</sup>PP: potassium persulfate as the initiator; <sup>c</sup>Acrylamide (AM) was used in the preparation of PolyFoam materials of AM1-AM5; <sup>d</sup>HEMA: 2-hydroxyethyl methacrylate; <sup>e</sup>PEGDA: polyethylene glycol diacrylate.

**Porosity.** The porosity ( $P$ ) of freeze-dried foams after polymerization was measured according to a literature protocol.<sup>43</sup> Samples were cut into pieces with dimensions of about  $1 \times 0.5 \times 0.5$  cm, weighed and immersed into 1-pentanol for 24 h. Then the samples were removed from the alcohol and weighed again after the surfaces being dried. The porosity was calculated using the following equation:

$$P (\%) = \frac{w_t - w_0}{\rho V} \times 100 \quad [1]$$

Where  $V$  is the apparent volume of the foam,  $\rho$  is the density of 1-pentanol, and  $w_t$  and  $w_0$  are the weights of the wet and dry foams, respectively.

**Freeze-Drying.** Freeze-drying over 24 h of the polyFoams was carried out on a Millrock Technology freeze-dryer (Kingston, NY) at  $-40$  °C and a vacuum of  $10^{-2}$  mbar.

### 5.3 Results

**Macroscopic Observation of the Foams.** Typically, unmodified CNCs are too hydrophilic to stabilize air-water interfaces. Methyl cellulose (MC), on the other hand, has been successfully used to aid in foam formation in food industry.<sup>44</sup> To analyze the effect of adding CNC to MC solution on the aqueous foam stabilization, we created a set of MC solutions of 5 g/L with increasing amount of CNCs. Initially, after homogenization using an Ultra-Turrax, the stabilized air bubbles were present throughout the entire sample for all the samples. Air bubble rapidly started to accumulate at the top of the container for some samples, leaving a liquid phase on the bottom as shown in Figure 1. As the CNC concentration increased, a growing trend in the total foam volume ( $V_0$ ) was observed. For the MC sample without CNCs, foaming occurred though the foam volume was less than the samples with CNCs. As the CNC concentration increases to

15 g/L, more air-water interface can be stabilized and the sample is completely filled with foams with no noticeable liquid phase on the bottom. When 5 or 10 g/L of CNCs was used with 5 g/L MC to produce the foams, a turbid bottom liquid phase was observed for both samples, which is clearly from the CNC suspension and means not all the CNC particles in the samples were consumed in preparing the foams. Additionally, it is observed that the turbidity of bottom water phase of the sample with 5 g/L CNCs is higher than the one with 10 g/L. This confirms again that CNCs do not prefer the air-water interface because only when extra CNCs are used in the sample will the particles be in the bottom water phase if they are surface-active. We believe that the viscosity of was greatly increased due to the addition of increasing amount of CNCs (Figure S2) and this increasing viscosity helped the stabilization of the foam by inhibiting the drainage and bubble coalescence.

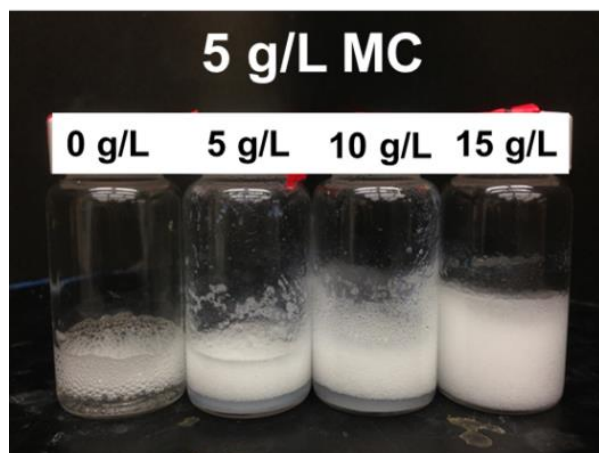


Figure 1. Aqueous CNC-MC foams immediately after preparation using various amount of CNCs.

**Foamability.** The normalized foamability ( $\phi$ ) was assessed by measuring the ratio of the foam volume immediately after preparation ( $V_0$ ) to the initial liquid volume ( $V_i$ ). The foamability of the MC solutions with added CNCs was measured as a function of CNCs/MC. The obtained results are shown in Figure 2. For all the MC solutions with different concentrations, the addition of increasing amount of CNCs all seem to lead to higher foamability values except the MC sample of 20 g/L. This suggests that the presence of CNCs in the sample favors the production of air bubbles. Overall, 5 and 10 g/L MC samples provide more foamed volume than MC samples with lower and higher concentrations. Since MC is surface-active, it is reasonable that MC solution with lower concentration (2 g/L) produces less foam. As to the one with higher MC concentration (20 g/L), it was observed that the addition of CNCs resulted in substantial viscosity increase of the mixture and eventually viscoelastic gel formed.

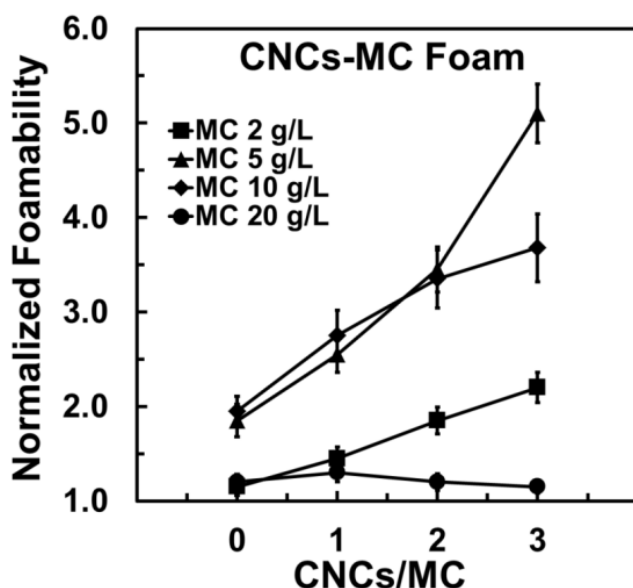


Figure 2. Normalized foamability as a function of CNC/MC at different MC concentrations. Squares, triangles, diamonds, and circles correspond to 2, 5, 10, and 20 g/L, respectively. Lines are a guide to the eye.

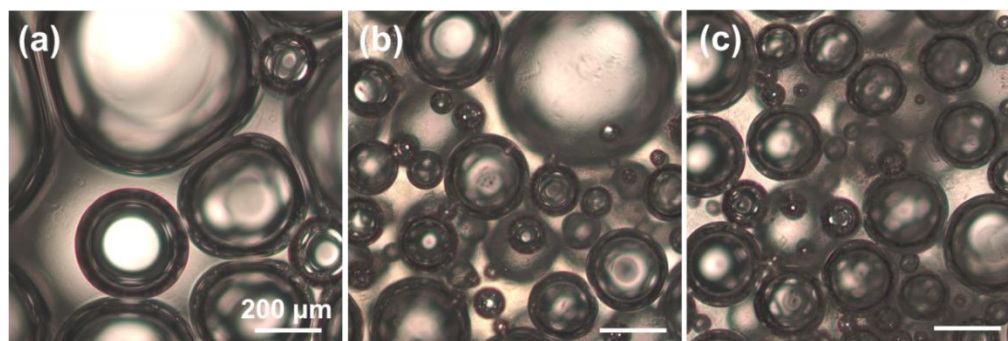


Figure 3. Optical micrographs of bubbles taken 1 h after foam stabilization. The aqueous foams were obtained by using (a) 5 g/L, (b) 10 g/L, and (c) 15 g/L of CNCs, in addition to 5 g/L MC. The scale bar is 200  $\mu\text{m}$ .

**Microscopic Analysis of the Aqueous Foams.** The optical micrographs in Figure 3 reveal the variation of the bubble size as a function of the CNC concentration in 5 g/L MC solutions. As the concentration of CNCs is increased, smaller air bubbles are produced. Average bubble diameter

decreases from about 500  $\mu\text{m}$  to 200  $\mu\text{m}$  as CNC concentration is increased from 5 to 15 g/L (Figure S3), indicating the potential of tuning bubble sizes by adjusting CNC concentration in the foam preparation.

**Interfacial Characterization.** The change of interfacial property of CNC particles through the surface adsorption of MC was investigated with the help of surface tension measurements. The dynamic surface tension of suspensions containing 5 g/L CNCs and different initial concentrations of MC is shown in Figure 4. A decrease in surface tension over time upon increasing the initial polymer concentration in solution is observed for samples with 0.25 g/L MC or higher. On the other hand, no noticeable reduction in surface tension is found for samples with 0.025 and 0.1 g/L MC. The surface tension of MC alone at concentrations of 0.025 and 0.1 g/L showed fast reduction to about 50 mN/m (Figure S4), implying MC molecules are prohibited from partitioning to air-water interface in the presence of CNCs. To determine the localization of CNC particles and MC molecules in the CNC-MC aqueous foams, confocal laser scanning microscopy (CLSM) images as shown in Figure 5 were taken of foams stabilized by CNCs and MC. The fluorescently labeled CNC-Nile Blue (red) can be seen at the surfaces of the bubbles, whereas MC that has been labeled with DTAF (green) is also present at the air-water interfaces. Therefore, it is reasonable to conclude that both MC and CNCs are localizing at the bubble surfaces.

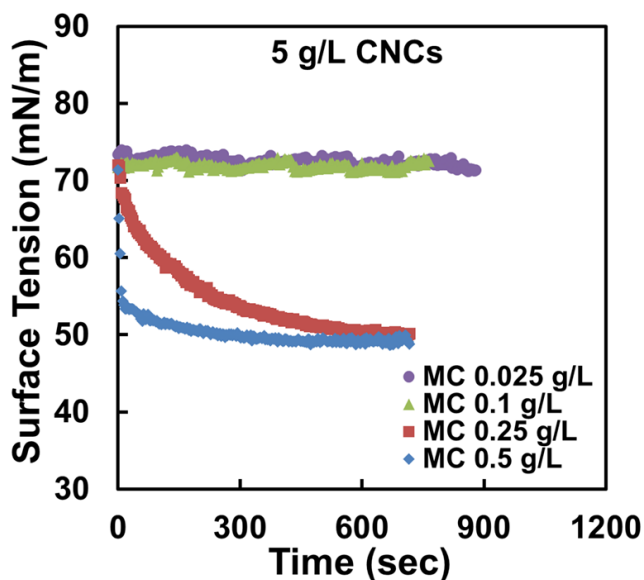


Figure 4. Time dependence of MC surface tension at different concentrations in the presence of 5 g/L CNCs. Purple circles, green triangles, red squares, and blue diamonds correspond to 0.025, 0.1, 0.25, and 0.5 g/L, respectively.

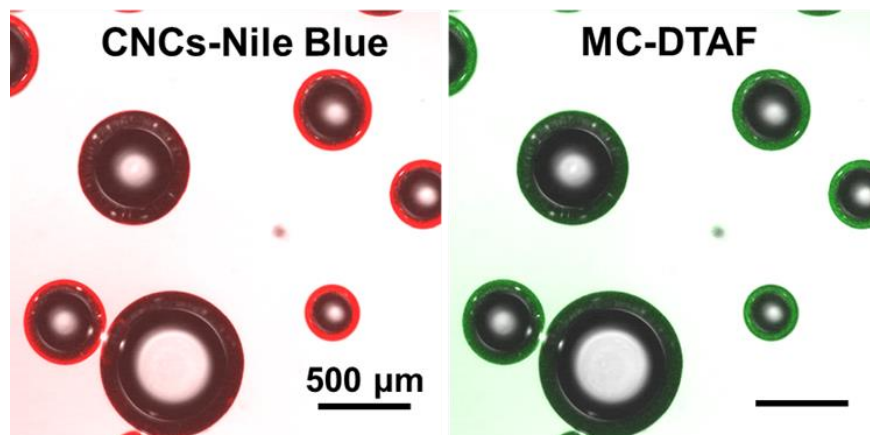


Figure 5. Confocal laser scanning micrographs (transmission mode) of air bubbles stabilized by CNCs (labeled with Nile Blue) and MC (labeled with DTAF). The scale bar is 500  $\mu\text{m}$ .

**Foam Stability.** To analyze the stability of the aqueous foam, we tracked the foam volume (total volume minus the volume of drained liquid) as a function of time at ambient temperature, as shown in Figure 6. The foam volume was normalized ( $\phi_t$ ) and calculated as the ratio of foam volume ( $V_t$ ) to the initial liquid volume used for foam preparation ( $V_i$ ). The graph shows that the most stable foams were achieved when 10 g/L CNCs were added to 10 g/L MC solution. In comparison, the foam volume decreased faster for the sample with 5 g/L CNCs, though the initial foam volume immediately after preparation (foamability) was higher than the sample with 10 g/L CNCs. We believe the increase of continuous phase viscosity and air-water interface elasticity due to the addition of increasing amount of CNCs lead to the enhanced foam stability. When CNC concentration was increased to 20 g/L, minimal foam volume change over time was observed because the mixture was so viscous that effective foaming as well as foam volume reduction once some foams were generated was hindered. The effect of CNC addition on foam stability was also investigated by monitoring foam structure using CLSM (Figure S5). After 6 h of drying at room temperature, most of the air bubbles almost completely collapsed as the films between bubbles ruptured for the foam stabilized with MC alone, whereas closely packed air bubbles with random network of plateau borders were observed. This again clearly points out the beneficial effect of stabilizing foams with the addition of CNCs to MC solutions.

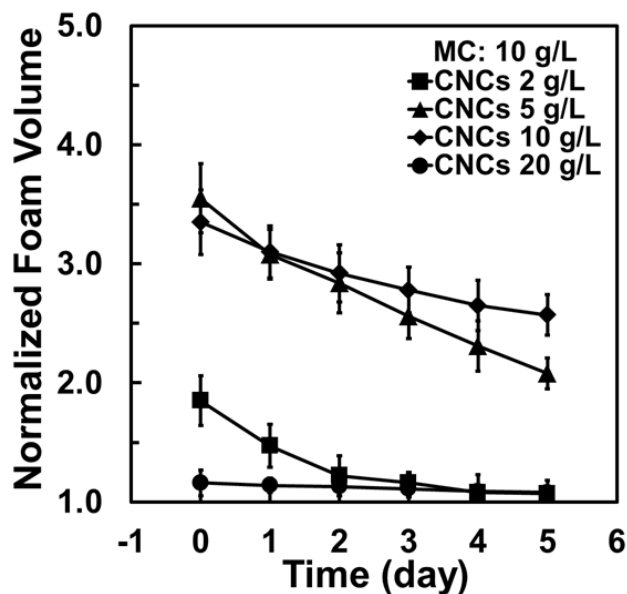


Figure 6. Normalized foam volume as a function of time at different CNC concentrations. The MC concentration was fixed to 10 g/L in all samples. Squares, triangles, diamonds, and circles correspond to 2, 5, 10, and 20 g/L, respectively. Lines are a guide to the eye.

We also investigated the water drainage process of CNC-MC foams. Draining is the free flow of water driven by gravity through the random network of plateau borders of the foam, leading to formation of dryer foam. Water drainage leads to the thinning of liquid borders between adjacent bubbles and eventually coalescence.<sup>45</sup> The fraction of liquid in the foam, represented by the expression:  $\varepsilon = V_{\text{liq}}/V_t$ , is directly correlated to the water drainage and thus used herein to assess water draining.<sup>46</sup>  $V_{\text{liq}}$  is the volume of liquid dispersed in the foam, and  $V_t$  represents the volume of foam. The foam water fraction  $\varepsilon$  as a function of time is reported in Figure 7a. The decay of water fraction can be approximated by an exponential expression  $\varepsilon \sim t^{-\beta}$ , where  $\beta$  is an exponent which correlates to the rate of water drainage from the foam and  $t$  is time. For the CNC-MC foams with increasing amount of CNCs, the value of  $\beta$  decreases from 0.24 to 0.10. In addition, it appears that the more CNCs added into MC solutions, the smaller value for  $\beta$  and thus the slower draining is. The dependence of average bubble sizes on time was also evaluated (Figure 7b). Mathematical fits of our data show that the average size of bubbles scale as  $R \sim t^{0.14}$ .

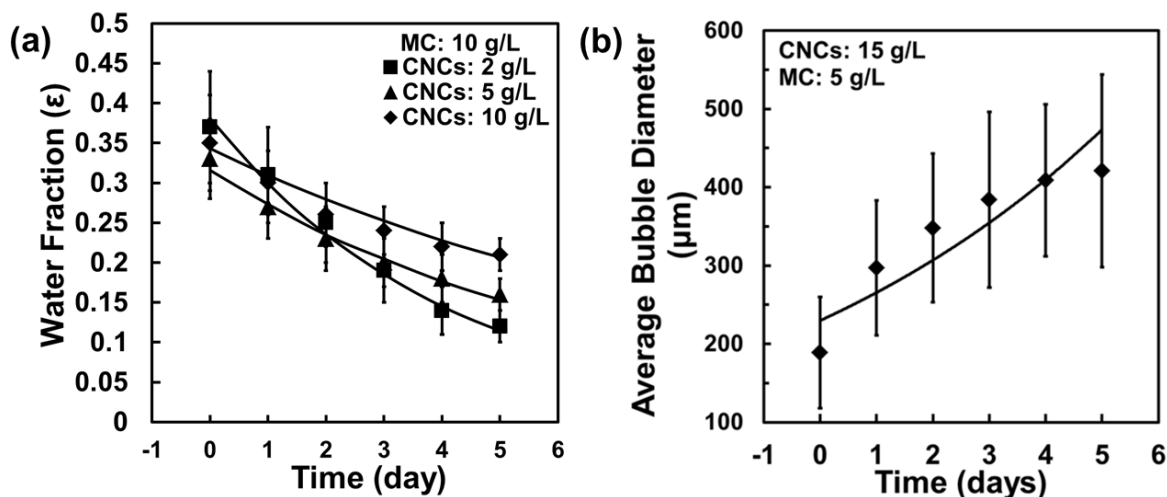


Figure 7 (a) Foam water fraction  $\epsilon$  as a function of time at different CNC concentrations. The MC concentration was fixed to 10 g/L in all samples. Squares, triangles, and diamonds correspond to 2, 5, and 10 g/L, respectively. (b) Average bubble diameter as a function of time for CNC-MC foam. The concentration of CNCs and MC was fixed to 15 and 5 g/L, respectively. Lines are a guide to the eye.

**Foam Templated Macroporous Structures.** Due to their enhanced stability, Particle-stabilized aqueous foams provide a general route for producing low-density macroporous materials.<sup>4, 31-33</sup> To demonstrate the effectiveness of processing macroporous polymers by using CNC-MC foams as templates (Figure 8), various monomers were individually added to mixture of CNCs and MC followed by homogenization to form the foams. The foamed samples were reacted at 70 °C to induce the polymerization of monomers and lock the foam structures (Figure S6a). No noticeable defoaming was observed during the reaction, which is probably due to the thermal gelation property of MC at high temperature and thus impeded foam breaking.<sup>47</sup> The samples were also freeze-dried to produce dry macroporous polymers (Figure S6b).

The compositions of the foams were systematically changed to determine the effects of composition on microstructures and properties of the polymerized wet and dry foams. Figure 9 shows optical images of three CNC-MC aqueous foams with different bubble size distributions and SEM images of the macroporous materials obtained from them by using acrylamide (AM) as the monomer. The MC concentration was 5 g/L and amount of AM added to each sample was kept the same (Table 1). The bubble size distribution of each sample as displayed in top panel in Figure 9 was tuned by varying the concentration of CNCs in the aqueous phase. As demonstrated in Figure 3, an increase in the amount of CNCs incorporated to prepare the foam facilitates the formation of smaller bubbles. As the starting CNC concentration increases, aqueous CNC-MC

foams added with the same amount of AM tend to produce smaller bubbles (Figure 9, top) and dry macroporous polyacrylamide materials using CNC-MC foams as the templates also display more macropores with smaller sizes (Figure 9, bottom). The top panel in Figure 9 displays the microstructures of wet foams with air contents of 47%, 71%, and 68%. After polymerizing and freeze-drying, these CNC-MC foams resulted in the porous materials seen on the bottom panel that have porosities of 70%, 87%, and 83%, respectively. The interconnectivity of the foam and porosity were greatly improved by the formation of numerous pore throats as a larger amount of CNCs are added (Figure 9e and Figure 9f). To emphasize the necessity of using CNC-MC foam at the template to prepare macroporous materials, no CNCs or MC were used but with other components the same as polyFoam AM2 in Table 1. As shown in Figure S7, only dense structures with some pores about 20  $\mu\text{m}$  were obtained, which confirms the critical role CNCs and MC play in generating macroporous materials.

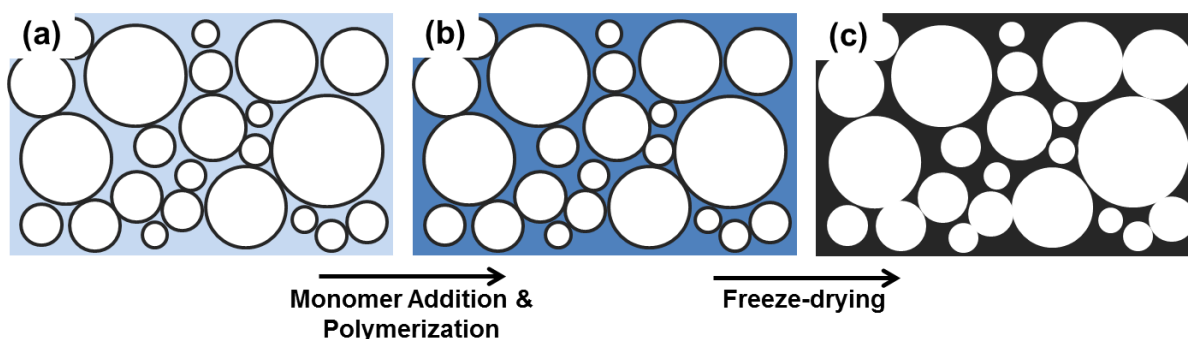


Figure 8. Schematic description of the different steps for the preparation of dry foams using CNC-MC wet foams as the templates: (a) CNC-MC foam (MC: 5 g/L; CNCs: 5~15 g/L) added with monomer (including initiator and crosslinker) and mixed using an Ultra Turrax mixer; (b) The monomer in the foam is polymerized at 70 °C for 6 h; (c) the polymerized foam is freeze-dried and a macroporous materials is formed, as shown in Figure S6.

In addition to polyacrylamide, biocompatible polymers, such as poly (2-hydroxyethyl methacrylate) (polyHEMA) and polyethylene glycol diacrylate (PEGDA), were also used as the matrix materials. HEMA or PEGDA were added to CNCs-MC foams and polymerized at 70 °C, resulting in macroporous structures composed of polyHEMA and PEGDA (Figure S8). Therefore, we believe that CNC-MC wet foams can be used as versatile templates to design macroporous polymers with tailored chemistry and structures.

The viscoelastic behavior of polymerized wet foam using CNC-MC as the template and AM as the monomer was investigated using frequency-sweep dynamic rheological measurements and

the data are shown in Figure 10a. A weak dependence of both storage ( $G'$ ) and loss ( $G''$ ) moduli on frequency for all the samples and  $G'$  moduli of each sample are approximately 1 order of magnitude higher than their  $G''$  indicates that our foams behave as elastic, gel-like materials. Variation of modulus with CNC content for polymerized foams is shown in Figure 10b. Though as more CNC particles are added to prepare the foam, more elastic polymerized foam sample was produced, a linear relationship of  $G'$  vs CNC concentration is not achieved.

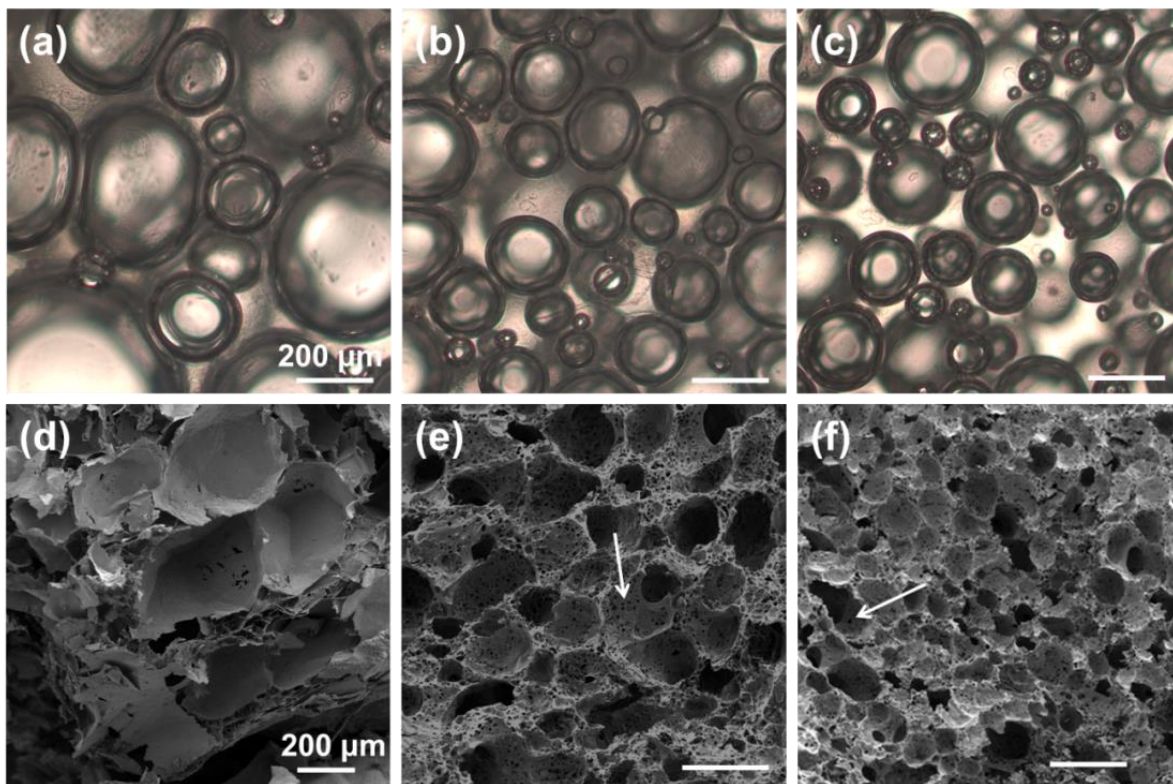


Figure 9. The congruencies between the microstructures of CNC-MC wet foams (a-c) and those of the dry macroporous materials derived from them (d-f) are corroborated by comparing optical transmission images and SEM images of the foams. The materials are denoted as (a, d) AM1, (b, e) AM2, and (c, f) AM3, respectively. The concentration of MC is 5 g/L for all samples, whereas various amounts of CNCs are used (a: 5 g/L; b: 10 g/L; c: 15 g/L). Composition details are provided in Table 1. Arrows in (e) and (f) highlight the presence of pore throats.

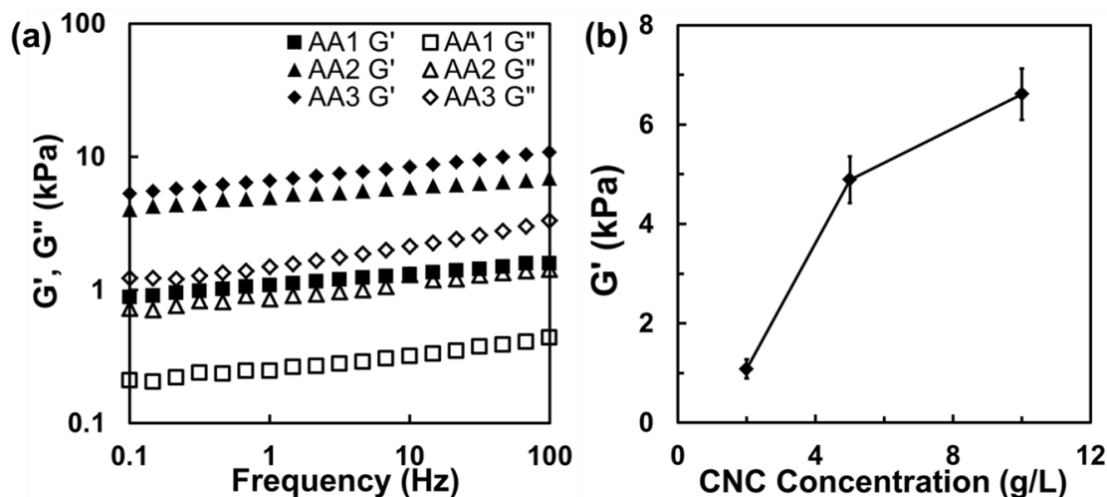


Figure 10. (a) Frequency-sweep data for various polymerized wet foams containing increasing amount of CNCs. The variation of storage modulus  $G'$  (closed symbols) and loss modulus  $G''$  (open symbols) with frequency is shown for AM1 (squares), AM2 (triangles), and AM3 (diamonds). (b) Variation of modulus with CNC concentration for polymerized wet foams that use CNC-MC foams as the templates and acrylamide as the monomer. Composition details are provided in Table 1.

## 5.4 Discussion

As demonstrated in Chapter 4, MC is surface-active and it has been used as a foaming agent.<sup>44</sup> Enhanced foaming capability was observed upon addition of CNCs into MC solutions as shown in both Figure 1 and Figure 2. Our previous work and Chapter 4 found that MC can readily adsorb onto CNC surfaces, leading to changes of rheological and interfacial properties of MC-coated CNC particles. It should also be noted that the foaming behavior of CNC-MC investigated in this study involves several processes, including the adsorption of MC on the CNC surface, the adsorption of MC-coated particles on the gas bubbles, and the adsorption of free MC on the gas bubbles. Therefore, changes in the initial foam composition often influence more than one parameter that is relevant for foam formation and stabilization. Figure 1 and Figure S2 showed that viscous foams could be produced when CNCs were added to MC solutions, indicating the change of rheology upon addition of CNCs. Figure 4, on the other hand, evidenced the influence of CNCs on the surface tension of MC solutions. At lower MC concentrations, the polymer molecules are hindered from transferring to the air-water interface, likely due to the preferential adsorption of MC on CNC surfaces instead of the air-water interface.

According to the calculation in Chapter 4, CNC surfaces are fully covered with polymers when the mass ratio of MC:CNCs is larger than about 1:20. Surprisingly, no noticeable surface tension reduction was observed when mass ratio of MC:CNCs is smaller than 1:20, implying that the CNC surfaces have been saturated with adsorbed MC polymer chains when MC concentration was higher than 0.25 g/L. The MC-coated CNCs are not as surface-active as the free MC molecules because surface tension values of 0.025 and 0.1 g/L MC in the presence of 5 g/L CNCs would have shown some reduction over time. The equilibrium surface tension values of 0.025 and 0.1 g/L MC in the presence of 5 g/L CNCs in Figure 4 are close to the values for free polymer solutions, indicating that MC-coated CNCs are not likely to partition to air-water interface and lower surface tension as effectively as free MC molecules. This may be due to the significant size increase of MC-coated CNC particles as opposed to individual MC polymer chains.

As the concentration of CNCs is increased, smaller air bubbles are produced (Figure 3). Other studies using particles such as modified silica, layered double hydroxide platelets, and  $\alpha$ -zirconium phosphate (ZrP) crystals also found that smaller average bubble sizes were observed at high surface-modifying agent concentrations, mainly as a result of a reduction in the suspension surface tension along with an increase in the foam viscosity.<sup>15, 48-49</sup> Since neither CNCs nor MC-coated CNCs are surface-active, the decrease in average bubble diameter should not be due to a reduction in the surface tension.<sup>50</sup> When 5 or 10 g/L of CNCs was used with 5 g/L MC to produce the foams, a turbid bottom liquid phase was observed in Figure 1 for both samples, which is clearly from the CNC suspension and means not all the CNC particles in the samples were consumed in preparing the foams.

According to our calculation, the CNCs should be fully covered with MC polymer chains and these MC-coated CNCs should display similar surface tension to free MC solution with the same concentration. However, both foamability and air bubble size values are substantially different from the ones of free polymer solutions. It should be noted that these samples also experience foam coalescence and breaking as the foams are generated in foaming process. In the absence of CNCs, foamed MC samples display small viscosities and therefore are prone to foam breaking. We believe that the viscosity of was greatly increased due to the addition of increasing amount of CNCs (Figure S2) and this increasing viscosity helped the stabilization of the foam by inhibiting the drainage and bubble coalescence. The increase of continuous phase viscosity and possibly air-water interface elasticity due to the addition of increasing amount of CNCs also lead to the enhanced foam stability as shown in Figure 6.

Confocal laser scanning microscopy (CLSM) images in Figure 5 reveal that both MC and CNCs are localizing at the bubble surfaces and stabilizing the air-water interface. Though surface tension data in Figure 4 does not suggest that MC-coated CNC particles are surface-active, we believe vigorous mixing used to prepare the foams should facilitate the contact of MC-coated CNC particles with air phase. Once in contact with air, those MC molecules adsorbed on CNC surface are likely to reorientate their methyl groups toward the more hydrophobic air phase and

thus help stabilize the air-water phase. Though the addition of CNCs and thus viscosity increase of the sample is beneficial to foam stabilization, excessive CNC addition tends to lower the foamability of the sample, likely due to the loss of MC flexibility to reorganize itself to stabilize air-water phase as a result of viscosity increase. It appears that the addition of CNCs generally is beneficial for the stabilization of air bubbles as long as the concentrations of CNCs and MC are not so high that the mixture turns to viscoelastic gels.

The decay of water fraction of the foam was approximated by the exponential expression  $\varepsilon \sim t^\beta$ . The value of  $\beta$  for surfactant foams is usually between 2/3 and 2.<sup>45-46</sup> For the CNCs-MC foams with increasing amount of CNCs, the value of  $\beta$  decreases from 0.24 to 0.10, all of which are significantly smaller than the values for surfactant foams. This demonstrates that our foams drain much slower than conventional foams that are stabilized by surfactants. This is common for particle stabilized foams. In addition, it appears that the more CNCs added into MC solutions, the smaller value for  $\beta$  and thus the slower draining is. We believe that hydrophilic CNC particles interact with MC molecules, stay at the plateau borders, and prevent water drainage by increasing the interfacial viscosity without limiting the ability of MC molecules to freely assemble at the air-water interface. Therefore, slower draining was observed when relatively more CNC particles are present in the foams. The relatively higher initial liquid fraction of our foams than that of conventional surfactant systems suggests the higher liquid retention capability of CNCs-MC, which may be attributed to the thick films sustained due to the presence of hydrophilic CNC particles at the surfaces of adjacent bubbles. It is likely that these CNC particles help retain water in the thick liquid films of the foam because of their hydrophilic nature, high aspect ratio, and interactions with MC molecules.

The bulk and interfacial viscosity are increased due to the percolating network formation as CNC particles are added, leading to a reduction of fluid drainage from the foams. A foam also evolves by gas diffusion through the thin films from bubble to bubble, which is called foam coarsening. Foams coarsen due to pressure differences between bubbles of different sizes. Coarsening therefore tends to increase the volume of certain bubbles at the expense of others. On average, this process leads to an increase of the average bubble size with time. Both coarsening and draining can occur on the same timescale and can thus be coupled.<sup>45</sup> As shown in Figure 7b, the average bubble sizes scale as  $R \sim t^{0.14}$ , whereas the average size of bubbles in foams stabilized by surfactants scale as  $R \sim t^{0.5}$ .<sup>46</sup> Thus, the evolution of average bubble size in our system occurs at a significantly slower rate than in surfactant stabilized foams, probably due to the larger film thickness and bulk and interfacial viscosity of CNCs-MC foams.<sup>46</sup>

Due to their enhanced stability, CNCs-MC foams were used to produce low-density macroporous materials. Similar behavior was previously reported in high internal phase emulsion templating materials (polyHIPEs).<sup>51</sup> The structure of polyFoams in this work resembles that of a typical polyHIPE, which involves the using of oil as the dispersed phase. In comparison, air is used in this work as the dispersed phase and thus more advantageous from the perspective of cost and safety. A wide range of other hydrophobic particles have been used to produce low-density

macroporous materials with tailored microstructures and properties through a similar foaming process.<sup>31</sup> However, we believe that it is the first time CNC particles are used in combination with water-soluble polysaccharides to produce macroporous hydrophilic materials through the foaming and templating method described here.

The value for  $G'$  can be considered as a measure of network connectivity. In this work, elasticity of the wet foams after polymerization results from the springlike nature of the foam films and polymerization and crosslinking of the acrylamide monomers in the continuous phase. The former depends upon the extent of bubble packing, porosity, and interactions between CNCs and MC, whereas the latter is directly influenced by the concentration of monomers and crosslinking density in the continuous phase. Variation of modulus with CNC content for polymerized foams is shown in Figure 10b. Though as more CNC particles are added to prepare the foam, more elastic polymerized foam sample was produced, a linear relationship of  $G'$  vs CNC concentration is not achieved. Introducing more CNC particles into the foam leads to the formation of more percolating networks, which therefore increases the elasticity. However, the presence of increasing amount CNCs also leads to larger foam volume increase and thus produces foams with higher porosity, which reduces the foam elasticity. In conclusion, the rheological properties of the polymerized foam can be tailored by changing the composition of the foam. The presence of air bubbles, however, imparts complexity to the analysis of influence of foam compositions on its mechanical properties.

## 5.5 Conclusions

1. We have presented a simple method of preparing highly stable foams using CNCs and water-soluble methyl cellulose. Both foamability and foam stability can be greatly improved by adding CNCs to MC solutions. However, excessive amount of CNCs can be detrimental for producing foams with high air content due to the high viscosity of the mixture.
2. Both CNCs and MC are present at the air-water interface. The CNC particles help retain fluid in the films and plateau borders between bubbles, increase bulk viscosity, and impede water drainage. Since the layers between bubbles determine foam stability by influencing drainage and coarsening, a more detailed study about their internal configuration is in progress and will be presented in the future.
3. Adding various types of monomers to CNC-MC wet foams did not lead to noticeable foam breaking. The successful production of macroporous polymeric structures with tailored chemistry and properties was achieved by subsequent polymerization of the monomers added to the foam. Due to the ubiquitous nature of macroporous materials and the green nature of foaming agents, this new foaming process has the potential to broaden the range of high performance materials in applications such as health care, thermal and electrical insulation, filters, catalyst supports, and sensors and actuators.

## References

- (1) Pugh, R. J. Foaming, foam films, antifoaming and defoaming. *Advances in Colloid and Interface Science* **1996**, *64* (0), 67-142.
- (2) Colin, A. *Foam Engineering*. John Wiley & Sons, Ltd: **2012**; p 75-99.
- (3) Dickinson, E. *An Introduction to Food Colloids; Chapters 1 and 4*. Oxford University Press: New York, **1992**.
- (4) Studart, A. R.; Gonzenbach, U. T.; Akartuna, I.; Tervoort, E.; Gauckler, L. J. Materials from foams and emulsions stabilized by colloidal particles. *Journal of Materials Chemistry* **2007**, *17* (31), 3283-3289.
- (5) Binks, B. P.; Murakami, R.; Armes, S. P.; Fujii, S.; Schmid, A. pH-Responsive Aqueous Foams Stabilized by Ionizable Latex Particles. *Langmuir* **2007**, *23* (17), 8691-8694.
- (6) Murray, B. S.; Ettelaie, R. Foam stability: proteins and nanoparticles. *Current Opinion in Colloid & Interface Science* **2004**, *9* (5), 314-320.
- (7) Binks, B. P. Particles as surfactants—similarities and differences. *Current Opinion in Colloid & Interface Science* **2002**, *7* (1–2), 21-41.
- (8) Koehler, S. A.; Hilgenfeldt, S.; Stone, H. A. A Generalized View of Foam Drainage: Experiment and Theory. *Langmuir* **2000**, *16* (15), 6327-6341.
- (9) Dickinson, E. Food emulsions and foams: Stabilization by particles. *Current Opinion in Colloid & Interface Science* **2010**, *15* (1–2), 40-49.
- (10) Du, Z.; Bilbao-Montoya, M. P.; Binks, B. P.; Dickinson, E.; Ettelaie, R.; Murray, B. S. Outstanding Stability of Particle-Stabilized Bubbles. *Langmuir* **2003**, *19* (8), 3106-3108.
- (11) Dickinson, E.; Ettelaie, R.; Kostakis, T.; Murray, B. S. Factors Controlling the Formation and Stability of Air Bubbles Stabilized by Partially Hydrophobic Silica Nanoparticles. *Langmuir* **2004**, *20* (20), 8517-8525.
- (12) Gonzenbach, U. T.; Studart, A. R.; Tervoort, E.; Gauckler, L. J. Ultrastable Particle-Stabilized Foams. *Angewandte Chemie International Edition* **2006**, *45* (21), 3526-3530.
- (13) Stocco, A.; Rio, E.; Binks, B. P.; Langevin, D. Aqueous foams stabilized solely by particles. *Soft Matter* **2011**, *7* (4), 1260-1267.
- (14) Murray, B. S.; Durga, K.; de Groot, P. W. N.; Kakoulli, A.; Stoyanov, S. D. Preparation and Characterization of the Foam-Stabilizing Properties of Cellulose–Ethyl Cellulose Complexes for Use in Foods. *Journal of Agricultural and Food Chemistry* **2011**, *59* (24), 13277-13288.
- (15) Guevara, J. S.; Mejia, A. F.; Shuai, M.; Chang, Y.-W.; Mannan, M. S.; Cheng, Z. Stabilization of Pickering foams by high-aspect-ratio nano-sheets. *Soft Matter* **2013**, *9* (4), 1327-1336.
- (16) Lam, S.; Blanco, E.; Smoukov, S. K.; Velikov, K. P.; Veleev, O. D. Magnetically Responsive Pickering Foams. *Journal of the American Chemical Society* **2011**, *133* (35), 13856-13859.
- (17) Gonzenbach, U. T.; Studart, A. R.; Tervoort, E.; Gauckler, L. J. Stabilization of Foams with Inorganic Colloidal Particles. *Langmuir* **2006**, *22* (26), 10983-10988.
- (18) Pugh, R. J. Foaming in Chemical Surfactant Free Aqueous Dispersions of Anatase (Titanium Dioxide) Particles. *Langmuir* **2007**, *23* (15), 7972-7980.
- (19) Fujii, S.; Iddon, P. D.; Ryan, A. J.; Armes, S. P. Aqueous Particulate Foams Stabilized Solely with Polymer Latex Particles. *Langmuir* **2006**, *22* (18), 7512-7520.

- 
- (20) Alargova, R. G.; Warhadpande, D. S.; Paunov, V. N.; Velev, O. D. Foam Superstabilization by Polymer Microrods. *Langmuir* **2004**, *20* (24), 10371-10374.
- (21) Somosvári, B. M.; Babcsán, N.; Bárczy, P.; Berthold, A. PVC particles stabilized water-ethanol compound foams. *Colloids and Surfaces A: Physicochemical and Engineering Aspects* **2007**, *309* (1-3), 240-245.
- (22) Zhou, W.; Cao, J.; Liu, W.; Stoyanov, S. How Rigid Rods Self-Assemble at Curved Surfaces. *Angewandte Chemie International Edition* **2009**, *48* (2), 378-381.
- (23) Wege, H. A.; Kim, S.; Paunov, V. N.; Zhong, Q.; Velev, O. D. Long-term stabilization of foams and emulsions with in-situ formed microparticles from hydrophobic cellulose. *Langmuir* **2008**, *24*, 9245-9253.
- (24) Cervin, N. T.; Andersson, L.; Ng, J. B. S.; Olin, P.; Bergström, L.; Wågberg, L. Lightweight and Strong Cellulose Materials Made from Aqueous Foams Stabilized by Nanofibrillated Cellulose. *Biomacromolecules* **2012**, *14* (2), 503-511.
- (25) Kruglyakov, P. M.; Elaneva, S. I.; Vilkova, N. G. About mechanism of foam stabilization by solid particles. *Advances in Colloid and Interface Science* **2011**, *165* (2), 108-116.
- (26) Johansson, G.; Pugh, R. J. The influence of particle size and hydrophobicity on the stability of mineralized froths. *International Journal of Mineral Processing* **1992**, *34* (1-2), 1-21.
- (27) Binks, B. P.; Horozov, T. S. Aqueous Foams Stabilized Solely by Silica Nanoparticles. *Angewandte Chemie International Edition* **2005**, *44* (24), 3722-3725.
- (28) Zhang, S.; Lan, Q.; Liu, Q.; Xu, J.; Sun, D. Aqueous foams stabilized by Laponite and CTAB. *Colloids and Surfaces A: Physicochemical and Engineering Aspects* **2008**, *317* (1-3), 406-413.
- (29) Ata, S.; Yates, P. D. Stability and flotation behaviour of silica in the presence of a non-polar oil and cationic surfactant. *Colloids and Surfaces A: Physicochemical and Engineering Aspects* **2006**, *277* (1-3), 1-7.
- (30) Binks, B. P.; Rocher, A.; Kirkland, M. Oil foams stabilised solely by particles. *Soft Matter* **2011**, *7* (5), 1800-1808.
- (31) Wong, J. C. H.; Tervoort, E.; Busato, S.; Gonzenbach, U. T.; Studart, A. R.; Ermanni, P.; Gauckler, L. J. Designing macroporous polymers from particle-stabilized foams. *Journal of Materials Chemistry* **2010**, *20* (27), 5628-5640.
- (32) Wong, J. C. H.; Tervoort, E.; Busato, S.; Gauckler, L. J.; Ermanni, P. Controlling Phase Distributions in Macroporous Composite Materials through Particle-Stabilized Foams. *Langmuir* **2011**, *27* (7), 3254-3260.
- (33) Wong, J. C. H.; Tervoort, E.; Busato, S.; Gonzenbach, U. T.; Studart, A. R.; Ermanni, P.; Gauckler, L. J. Macroporous polymers from particle-stabilized foams. *Journal of Materials Chemistry* **2009**, *19* (29), 5129-5133.
- (34) Jin, H.; Zhou, W.; Cao, J.; Stoyanov, S. D.; Blijdenstein, T. B. J.; de Groot, P. W. N.; Arnaudov, L. N.; Pelan, E. G. Super stable foams stabilized by colloidal ethyl cellulose particles. *Soft Matter* **2012**, *8* (7), 2194-2205.
- (35) Habibi, Y.; Lucia, L. A.; Rojas, O. J. Cellulose Nanocrystals: Chemistry, Self-Assembly, and Applications. *Chemical Reviews* **2010**, *110* (6), 3479-3500.
- (36) *The Global Market for Nanocellulose to 2020*. Future Markets Inc.: Edinburgh, United Kingdom, **2012**.
- (37) Kalashnikova, I.; Bizot, H.; Cathala, B.; Capron, I. New Pickering Emulsions Stabilized by Bacterial Cellulose Nanocrystals. *Langmuir* **2011**, *27* (12), 7471-7479.

- 
- (38) Murakami, R.; Bismarck, A. Particle-Stabilized Materials: Dry Oils and (Polymerized) Non-Aqueous Foams. *Advanced Functional Materials* **2010**, *20* (5), 732-737.
- (39) Ikem, V. O.; Menner, A.; Bismarck, A. High-Porosity Macroporous Polymers Synthesized from Titania-Particle-Stabilized Medium and High Internal Phase Emulsions. *Langmuir* **2010**, *26* (11), 8836-8841.
- (40) Gonzenbach, U. T.; Studart, A. R.; Tervoort, E.; Gauckler, L. J. Macroporous Ceramics from Particle-Stabilized Wet Foams. *Journal of the American Ceramic Society* **2007**, *90* (1), 16-22.
- (41) Beck-Candanedo, S.; Roman, M.; Gray, D. G. Effect of Reaction Conditions on the Properties and Behavior of Wood Cellulose Nanocrystal Suspensions. *Biomacromolecules* **2005**, *6* (2), 1048-1054.
- (42) Abitbol, T.; Palermo, A.; Moran-Mirabal, J. M.; Cranston, E. D. Fluorescent Labeling and Characterization of Cellulose Nanocrystals with Varying Charge Contents. *Biomacromolecules* **2013**, *14* (9), 3278-3284.
- (43) Kovacic, S.; Matsko, N. B.; Ferk, G.; Slugovc, C. Macroporous poly(dicyclopentadiene) [ $\gamma$ ]Fe<sub>2</sub>O<sub>3</sub>/Fe<sub>3</sub>O<sub>4</sub> nanocomposite foams by high internal phase emulsion templating. *Journal of Materials Chemistry A* **2013**, *1* (27), 7971-7978.
- (44) Karim, A. A.; Wai, C. C. Characteristics of foam prepared from starfruit (*Averrhoa carambola* L.) puree by using methyl cellulose. *Food Hydrocolloids* **1999**, *13* (3), 203-210.
- (45) Saint-Jalmes, A. Physical chemistry in foam drainage and coarsening. *Soft Matter* **2006**, *2* (10), 836-849.
- (46) Blanco, E.; Lam, S.; Smoukov, S. K.; Velikov, K. P.; Khan, S. A.; Velev, O. D. Stability and Viscoelasticity of Magneto-Pickering Foams. *Langmuir* **2013**, *29* (32), 10019-10027.
- (47) McKee, J. R.; Hietala, S.; Seitsonen, J.; Laine, J.; Kontturi, E.; Ikkala, O. Thermoresponsive Nanocellulose Hydrogels with Tunable Mechanical Properties. *ACS Macro Letters* **2014**, *3* (3), 266-270.
- (48) Gonzenbach, U. T.; Studart, A. R.; Tervoort, E.; Gauckler, L. J. Tailoring the Microstructure of Particle-Stabilized Wet Foams. *Langmuir* **2006**, *23* (3), 1025-1032.
- (49) Liu, Q.; Luan, L.; Sun, D.; Xu, J. Aqueous foam stabilized by plate-like particles in the presence of sodium butyrate. *Journal of Colloid and Interface Science* **2010**, *343* (1), 87-93.
- (50) Hu, Z.; Ballinger, S.; Pelton, R.; Cranston, E. D. Surfactant-enhanced cellulose nanocrystal Pickering emulsions. *Journal of Colloid and Interface Science* **2015**, *439* (0), 139-148.
- (51) Oh, B. H. L.; Bismarck, A.; Chan-Park, M. B. High Internal Phase Emulsion Templating with Self-Emulsifying and Thermoresponsive Chitosan-graft-PNIPAM-graft-Oligoproline. *Biomacromolecules* **2014**, *15* (5), 1777-1787.

## Appendix: Supporting Information for Chapter 5

**Transmission Electron Microscopy (TEM).** One drop of CNC suspension (0.001 wt. %) was placed onto a Formvar-coated copper TEM grid (Canemco Inc., Canada), air dried for 4 h, and stained using 5 mM uranyl acetate solution for 5 min before removing the remaining liquid by absorption with filter paper. TEM images were acquired using a JEOL 1200 EX TEMSCAN microscope operating at 80 kV.

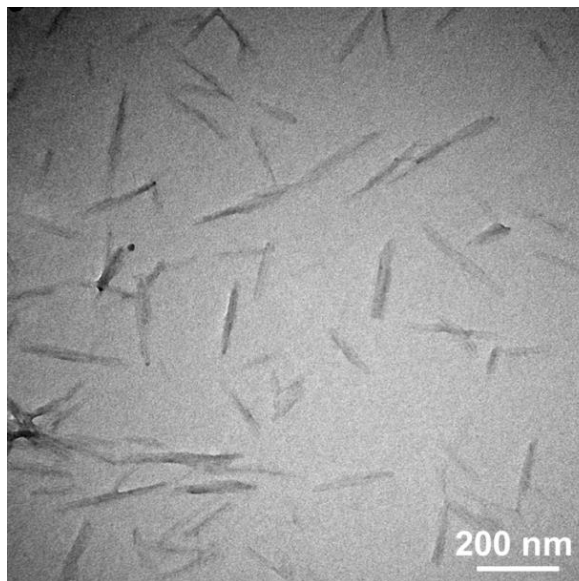


Figure S1. TEM image of sulfated cellulose nanocrystals (CNCs).

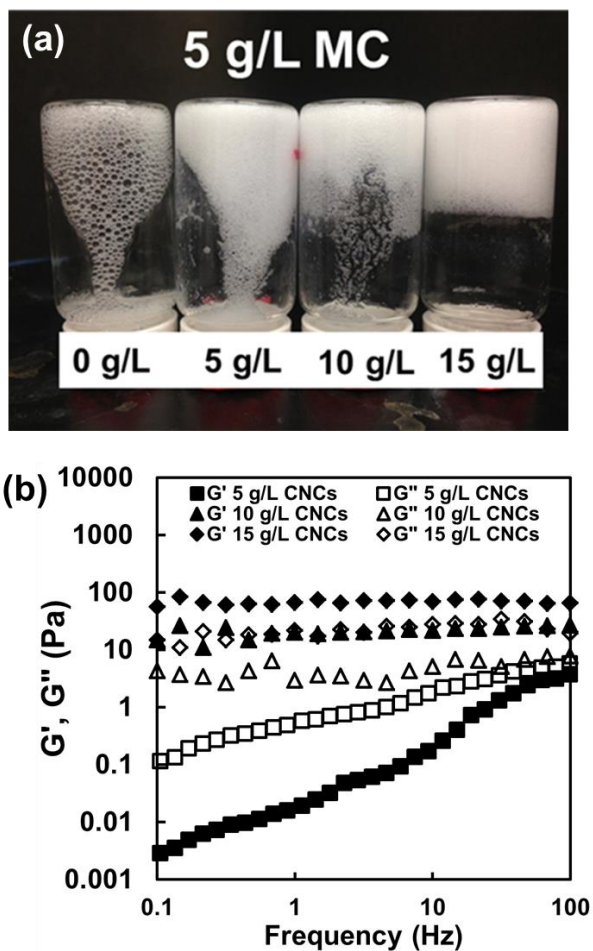


Figure S2. (a) Inverted vials with CNCs-MC foams immediately after preparation using increasing amount of CNCs. (b) Frequency-sweep data for aqueous foams containing increasing amount of CNCs. The MC concentration in all samples was fixed to be 5 g/L.

With the introduction of more CNCs into MC solutions, the rheological behavior of CNCs-MC foams turns from being viscous (5 g/L CNCs) to elastic gel-like (10 and 15 g/L CNCs) materials. The sample with 15 g/L of CNCs, especially, is able to hold its own weight, suggesting the foam bulk completely turns to viscoelastic gel-like material.

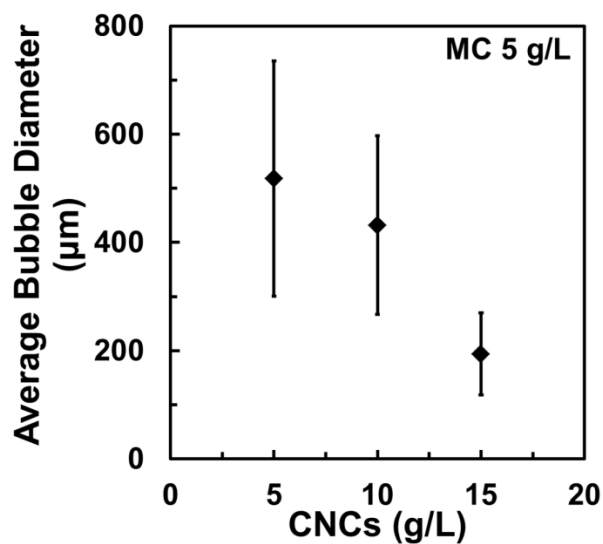


Figure S3. Average bubble diameter of CNCs-MC foam as a function of CNC concentration in MC 5 g/L solutions.

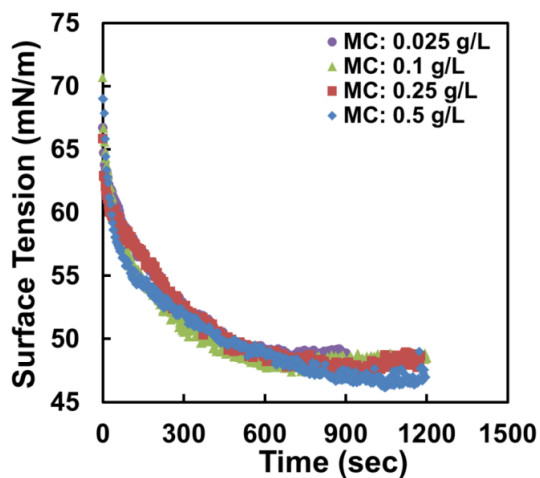


Figure S4. Time dependence of MC surface tension at different concentrations. Purple circles, green triangles, red squares, and blue diamonds correspond to 0.025, 0.1, 0.25, and 0.5 g/L, respectively.

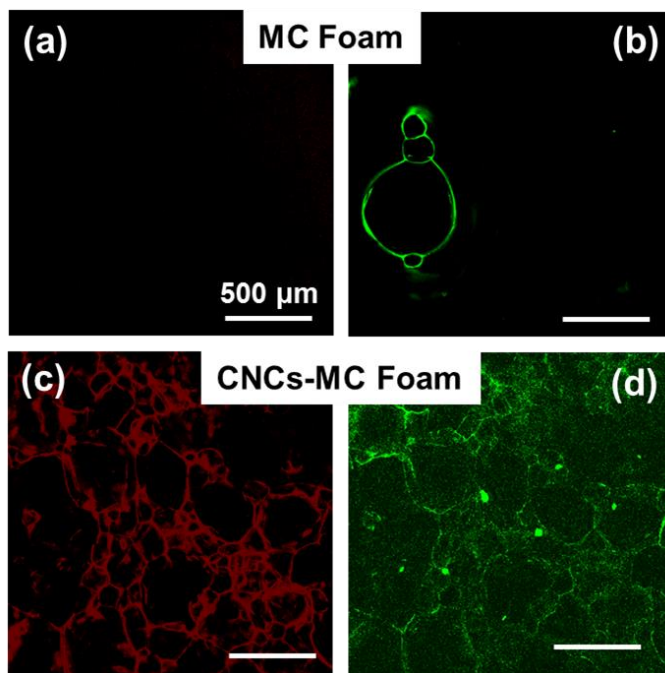


Figure S5. Confocal laser scanning micrographs of air bubbles stabilized by MC alone (a, b) or CNCs and MC (c, d). CNCs were labeled with Nile Blue and MC molecules were labeled with DTAF. The images were taken 6 h after foam preparation. The scale bar is 500  $\mu\text{m}$ .

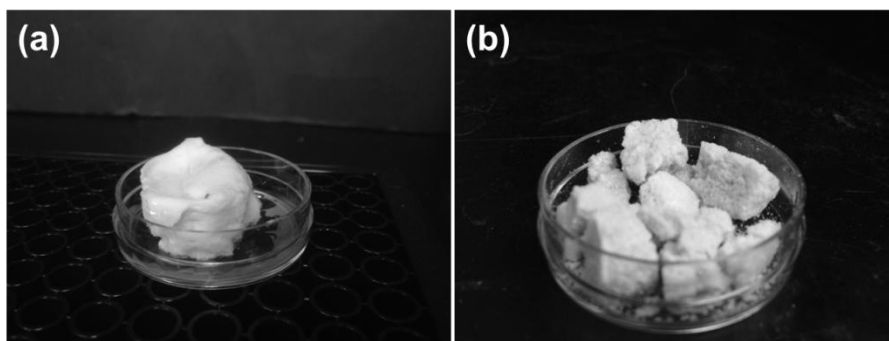


Figure S6. Photographs of AM2 polyFoam before (a) and after (b) freeze-drying. CNCs-MC wet foam was used as the template and acrylamide was the monomer. Composition details are provided in Table 1.

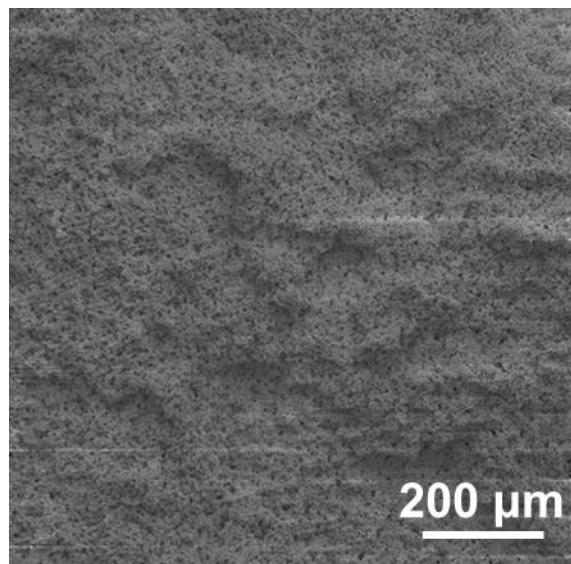


Figure S7. SEM image of polymerized materials using acrylamide as the monomer but no CNCs or MC. The recipe is the same as AM2 in Table 1 except for CNCs and MC.

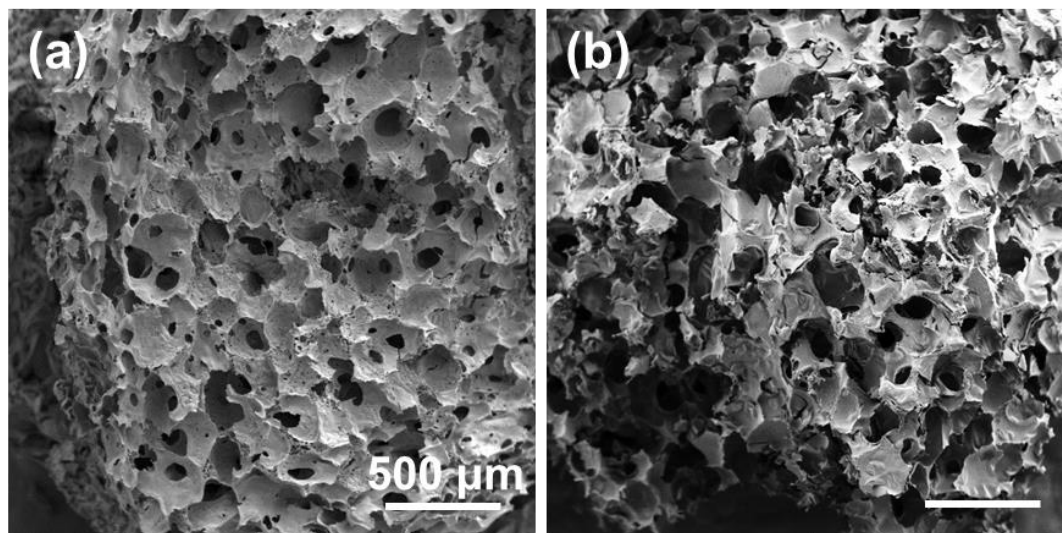


Figure S8. SEM images of polymerized materials using (a) 2-hydroxyethyl methacrylate or (b) polyethylene glycol diacrylate as the monomer. Composition details are provided in Table 1.

## Chapter 6 Concluding Remarks

This work focuses on the study of properties of cellulose nanocrystals (CNCs) in water and at interfaces in the presence of polysaccharides and/or surfactants. The work has yielded many remarkable outcomes and innovative discoveries, paving the way for the utilization of cellulose nanocrystals in producing hydrogels, emulsions, and foams. The results provide a better understanding of structure and mechanisms of the formation of cellulose nanocrystals-based hydrogels, emulsions, and foams and the role of CNCs at interfaces. The roles of various components such as polysaccharides and surfactants in formulating CNC products are extensively investigated. The research objectives proposed in Chapter 1 were fully achieved and the major contributions of this work are given as follows:

1. CNCs in water:
  - a) Addition of hydroxyethyl cellulose (HEC), hydroxypropyl guar (HPG), or locust bean gum (LBG) to CNC dispersions induced the gelation of dilute CNC dispersions, whereas dextran (DEX) did not. These behaviors correlated with adsorption tendencies as demonstrated in quartz crystal microbalance with dissipation monitoring measurements; HEC, HPG, and LBG adsorbed onto CNC-coated quartz crystal microbalance sensors, whereas DEX did not adsorb.
  - b) Adsorption measurements and gelation tests in this work led us to believe that neither depletion nor bridging effects were dominant in our system. Instead, the increase of effective volume fraction of dilute CNC dispersions due to polysaccharide adsorption was proposed to be the driving force for anisotropic domain formation and CNC gelation at dilute particle concentrations.
  - c) Negative surfactant SDS and non-ionic surfactant Triton X-100 addition disrupted HEC-CNC gels whereas cationic CTAB did not. Surface plasmon resonance measurements with CNC-coated sensors showed that SDS and Triton X-100 partially removed adsorbed HEC, whereas CTAB did not. This reveals the complexities associated with including CNC dispersions in formulated products where water-soluble polymers and surfactants are also used.
2. CNCs at oil-water interface:
  - a) CNC Pickering emulsions were more stable in the presence of small amounts of single-tailed cationic surfactant CTAB or double-tailed cationic surfactant DMAB because surfactant adsorption onto CNCs increased the nanoparticles' hydrophobicity and made them better emulsifiers than pristine CNCs.
  - b) With increasing concentrations of DMAB, CNC Pickering emulsions exhibited a double phase inversion (o/w to w/o [phase inversion 1], followed by w/o to o/w

- [phase inversion 2]), whereas with CTAB, all emulsions were oil-in-water. Emulsion phase inversions correlated directly to CNC wettability; adsorbed DMAB gave more hydrophobic CNCs because it has two alkyl tails compared to CTAB's one, and the highest three-phase contact angles above  $90^\circ$  correspond to water-in-oil emulsions.
- c) A simple method of preparing stable emulsion with tunable size by using both CNCs and cellulose-based polymers was presented. Adsorbing polymers on CNC surface before oil addition and emulsification appeared beneficial for the production of stable emulsions. Polymers that do not adsorb to CNCs did not aid in stabilizing emulsions.
  - d) Water-soluble surface active polymers HEC and methyl cellulose (MC) preferentially adsorb onto CNCs before partitioning to the oil-water interface. Both polymer-coated CNCs and the extra polymers partitioned to the interface and worked as the emulsifiers in a synergistic manner, leading to a reduction in CNC coverage on the emulsion droplet surface.
  - e) Reversible thermogelation of emulsions was obtained when MC was introduced to emulsions that were previously stabilized by CNCs and HEC. Heating and cooling treatment did not induce any noticeable emulsion coalescence, indicating the ultrastable nature of emulsions made with CNCs and water-soluble cellulose-based polymers.
  - f) Oil solids containing oil contents as high as 94 wt. % can be prepared by freeze-drying and air-drying emulsions stabilized with CNCs and polymers, when additional cellulose-based polymers were introduced to the emulsions to impart the high viscosity required to impede emulsion coalescence and breaking during drying. However, extensive oil leakage occurred if no additional polymers were added to the CNCs-polymer emulsions before drying.
3. CNCs at air-water interface:
- a) A simple method of preparing highly stable foams using CNCs and water-soluble MC was developed. Both foamability and foam stability were greatly improved by adding CNCs to MC solutions. Although MC-coated CNC particles are not surface-active, both CNCs and MC are present at the air-water interface. The CNC particles help retain fluid in the films and plateau borders between bubbles, increase bulk viscosity, and impede water drainage.
  - b) Adding various types of monomers to CNCs-MC wet foams did not lead to noticeable foam breaking and the monomers could be further polymerized to produce macroporous polymeric structures with tailored chemistry, morphology, and mechanical properties.